ATS-1/ATS-3 DUAL SATELLITE NAVIGATION STUDY

Project Engineer: W. M. Hoover
Texas Instruments Incorporated
13500 North Central Expressway
Dallas, Texas 75222

January 1971
(Published)

FINAL REPORT
April 1970 - October 1970

Prepared for
National Aeronautics and Space Administration
Goddard Space Flight Center
Greenbelt, Maryland 20771

1 Report No	2 Government Accession No	3 Recipient's Catalog No
4 Title and Subtitle ATS-1/ATS-3 DUAL SATELLITE NAVIGATION STUDY		5 Report Date January 1971 6 Performing Organization Code
7 Author(s) Project Engineer - W. M. Hoover		8 Performing Organization Report No U-03-835300-F
9 Performing Organization Name and Address Texas Instruments Incorporated 13500 North Central Expressway Dallas, Texas 75222		10 Work Unit No 11 Contract or Grant No NAS 5-21163 13 Type of Report and Period Covered Type III Final Report April 1970-October 1970
12 Sponsoring Agency Name and Address National Aeronautics & Space Administration Goddard Space Flight Center Greenbelt, Maryland 20771 Technical Officer: Charles N. Smith, Code 752		14 Sponsoring Agency Code
15 Supplementary Notes		

16 Abstract This report documents a study which illustrated the feasibility of implementing an on-board aircraft navigation system based on using the ATS-1 and ATS-3 satellites, the modified Omega Position Location Equipment (OPLE) Control Center, and a suitable aircraft terminal. The report provides: (1) a consideration of the problems of satellite navigation and an objective definition of the optimum system under the constraints of its specified components, (2) a description of the necessary modifications to the OPLE Control Center, the design of an aircraft terminal, and the design of ground reference terminals, and (3) an outline of an experiment plan and an estimate of the cost to be expected in conducting the program.

17 Key Words	18 Distribution Statement
Satellite Air Traffic Control Satellite Navigation Side-Tone Ranging Phase Measurement Range/Range Navigation	

19 Security Classif (of this report)	20 Security Classif (of this page)	21 No of Pages	22 Price
UNCLASSIFIED	UNCLASSIFIED	219	

Page Intentionally Left Blank

PREFACE

The objective of this study was to investigate the feasibility of implementing an on-board aircraft navigation system based on using the ATS-I and ATS-III satellites, the Omega Position Location Equipment (OPLE) Control Center (NASA/GSFC Contract NAS 5-10248) as modified for an aircraft surveillance function in the VHF Satellite Navigation Experiment (NASA/GSFC Contract NAS 5-21079), and a suitable aircraft terminal.

The study was performed by first considering the problems associated with satellite navigation and how the specified components could be employed effectively in that context. From this effort the optimum system was defined. Next, the modifications of the OPLE Control Center were described, which were necessary to configure a low-cost experimental system. In addition, an aircraft terminal and stationary ground reference terminals were designed. Although the resulting system was not optimum, the expected performance was sufficient to demonstrate at relatively low cost the principles developed in the study. The final task was to outline an experiment plan designed to demonstrate the navigational performance of the system, and an estimate of the cost of conducting the program was established.

It was concluded that the on-board navigation system was feasible. With relatively minor OPLE Control Center modifications it is expected that the system would provide aircraft navigation accuracy to approximately 1600 meters in a controlled experiment. With additional modifications the system would provide approximately 1500-meter accuracy over the continental United States in a configuration approximating an operational system.

TABLE OF CONTENTS

TABLE OF CONTENTS (Cont'd)

LIST OF ILLUSTRATIONS

LIST OF ILLUSTRATION (Cont'd)

LIST OF ILLUSTRATIONS (Cont'd)

LIST OF ILLUSTRATIONS (Cont'd)

LIST OF TABLES

LIST OF TABLES (Cont'd)

TEXAS INSTRUMENTS INCORPORATED
Equipment Group
13500 North Central Expressway
Dallas, Texas 75231

January 1971

FINAL PROJECT REPORT
FOR
ATS-1/ATS-3 DUAL SATELLITE NAVIGATION STUDY
U-03-835300-F

Reference: NASA/Goddard Space Flight Center Contract NAS 5-21163

SECTION I

INTRODUCTION

Texas Instruments was selected by NASA Goddard Space Flight Center to conduct a study of the feasibility of implementing an on-board navigation system based on using both ATS-I and ATS-III satellites, the Omega Position Location Equipment (OPLE) Control Center as modified for the VHF Satellite Navigation Experiment, an aircraft terminal, and other existing navigational aids. This report documents the results of the study.

It was concluded that an on-board satellite navigation system comprised of the specified components is feasible. With relatively minor OPLE Control Center modifications such a system will provide aircraft navigation accuracy to approximately 1600 meters in a controlled experiment. With additional modification the system will provide approximately 1500-meter accuracy over the continental United States in a configuration approximating an operational system.

The content of this report is divided into three main sections. The first of these sections, which is the study report, considers the problem of satellite navigation and objectively defines the optimum system. Constraints imposed by the ATS-I, ATS-III, and the modified OPLE Control Center preclude implementation of the optimum system; however, the study clearly delineates the problems and error sources that arise in implementing an experimental system using recommended minor modification to the OPLE Control Center.

The second section describes modifications to the existing OPLE Control Center, the design of the aircraft terminal, and the design of ground reference terminals which would be used in an experiment intended to demonstrate the conclusions reached in the study. The final section outlines an experiment plan to effect the demonstration, and provides an estimation of the costs to be expected in conducting the program.

SECTION II

NAVIGATION SYSTEM ANALYSIS

1. REQUIREMENTS FOR A NAVIGATION SYSTEM

The ideal satellite navigation system will be accurate, have a wide coverage area, and be economically accessible to a large number of users. The last constraint is the most difficult to achieve technologically, as illustrated by the fact that the bare minimum of user equipment required in a system such as the one developed in this report is a sophisticated VHF receiver system with a high stability clock synchronized to a ground control center (GCC). The receiver and clock are necessary to determine the satellite(s)-to-aircraft ranges. Since the receiver and clock must be carried by all users, the dream of providing an inexpensive satellite navigation service to the private pilot is still unrealized. For commercial users, however, a satellite navigation system is potentially cheaper than, and of comparable accuracy to, existing inertial navigation systems.

Wide coverage is essential to a satellite navigation system to make it economical. This follows from the fact that a major equipment cost is the cost of the ground control equipment, an expense that will most likely be shared among the users; therefore, more users result in a lower cost per aircraft. Clearly, the maximum usage is obtained when the navigation service is provided in all areas frequented by commercial air traffic.

Navigation accuracy is a function of equipment design. Categories of errors are thoroughly discussed and analyzed in this report. The results of the error study which are presented in Section II-3, along with cost considerations, dictate the design of the recommended system. In addition to the above listed considerations, desirable features of a satellite navigation system are: ease of maintenance, reliability, and aircraft in-flight independence from ground equipment. This last feature refers to the need of an aircraft to remain in time synchronization with the ground control station without the necessity of ground interrogation of the aircraft. Texas Instruments believes that the system recommended in the following pages meets these requirements.

1.1 Alternative Concepts

There are 16 general configuration classifications for satellite navigation systems. A tree of the various combinations is shown in Figure 2-1. In the following paragraphs the trade-offs involved in making each choice are briefly described and analyzed.

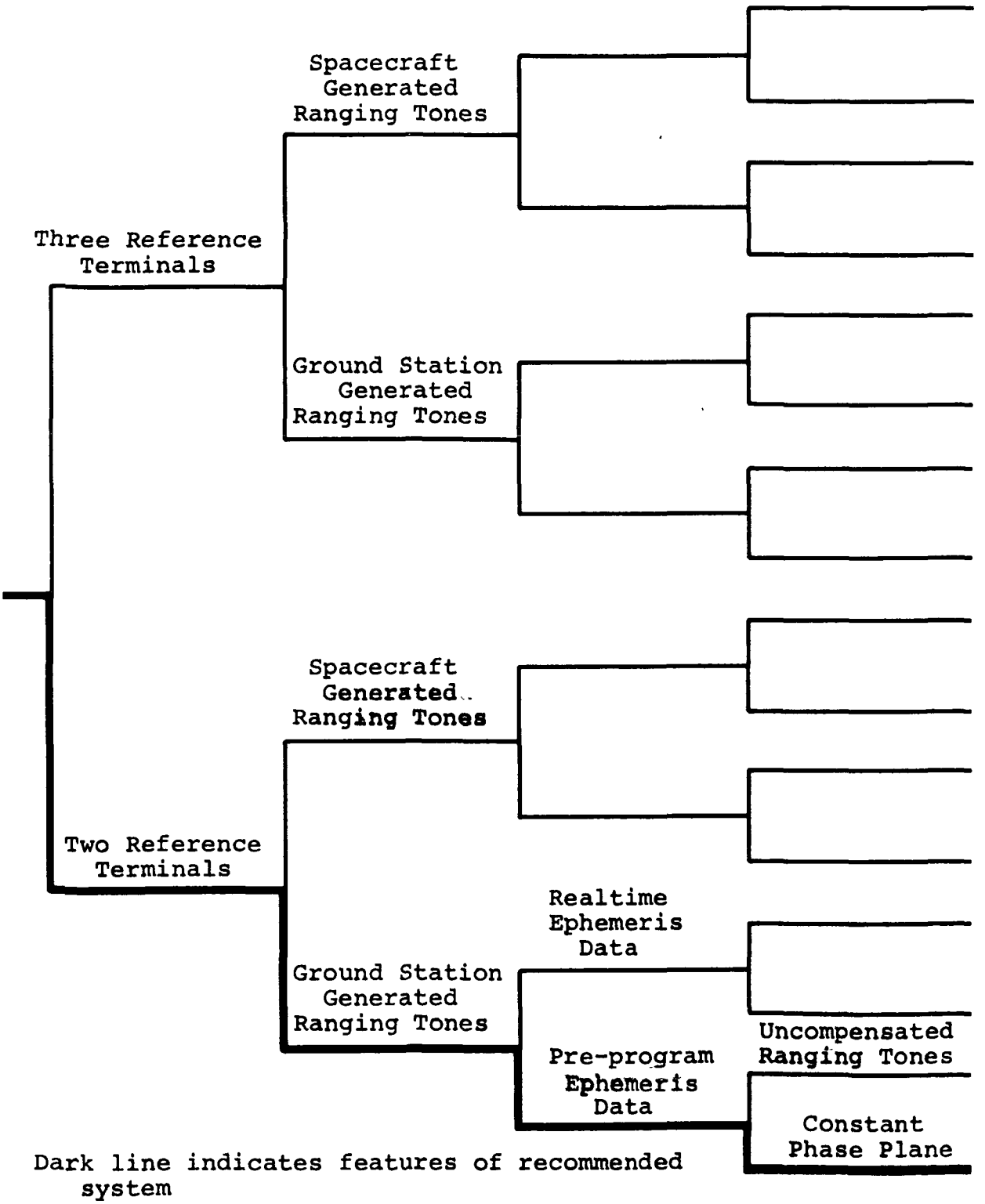

Figure 2-1. Tree of Possible Satellite Navigation Configurations

1.1.1 Two vs. Three Reference Terminal Configuration

Aside from the constraint that only two satellites will be available for the Dual Satellite Navigation Experiment, thus requiring that a third ranging tone source be ground based, the three reference terminal concept has been extensively studied and tested in the OPLE program in which Texas Instruments was a major contributor [1,2]. The technical advantage of the three reference terminal concept is that user position may be determined without allusion to altimeter data, whereas the two reference terminal configuration requires an external input, such as aircraft altitude data, to obtain a position location for the aircraft. Placement of a third reference station on the ground, while enabling implementation of the three reference terminal navigation concept, is impractical because all three references are simultaneously in view only over a small sector of the earth. In fact, the area of coverage is limited to a circle with a radius of no more than approximately 100 km for the 50°W and 150°W longitude placement of the ATS-I and ATS-III satellites. For this reason range measurements will be obtained from just two satellite references and combined with on-board aircraft altitude data to determine position from one of the two points of intersection of the three spheres centered at the two satellites and the center of the earth. The second intersection will be in the southern hemisphere - sufficiently far away for the derived user position to be non-ambiguous.

1.1.2 Ranging Tone Source Trade-Offs

Ranging tones are the tones emitted from each reference at a constant and known phase which are used to obtain range information. They may be generated on the ground and transponded to users by the satellites or they may be generated at the satellites themselves. The advantage of placement of the source of ranging signals in the satellite is that the system becomes very difficult to jam because the satellite becomes an autonomous source, and therefore intentional jammers are forced to jam individual users. Anti-jamming features, however, are not a major advantage to non-military navigation systems, and consequently the additional cost and lower reliability are not warranted. It is, therefore, recommended that ranging tones be generated at a ground control center and relayed to the aircraft users via satellite

1.1.3 Real-time Ephemeris Data vs. Pre-programmed Ephemeris Data

The ATS-I and ATS-III synchronous satellite reference stations are not adequately stable in position to be used as absolute reference points. The earth-referenced position of each satellite varies in a daily cycle because of the orbital

inclinations of each satellite with respect to the axis of earth rotation. This causes the subsatellite point, which is that point where the radius vector joining the center of the earth and the satellite intersects the earth surface, to trace out a figure "eight" during the course of one complete rotation of the earth. This movement may be predicted and compiled in some form as ephemeris data. Two data formats are available for use in a satellite navigation system: (1) listing such as available in R204 Operational Predicts and World Map Routine, published by NASA, and (2) the simplified set of equations such as derived in Section II-3.1.1.2 of this study report.

Ephemeris data is necessary for accurate position location because it provides the user with satellite position information of sufficient accuracy to utilize the range data derived from the GCC-transmitted ranging tones. The list format implies a need for a real-time ephemeris update via data-link through the satellite to the aircraft because the on-board data processor envisioned for the aircraft terminal will not have sufficient data storage capability to store the number of satellite coordinates compatible with the aircraft position location accuracy constraint and the aircraft ground independence constraint. On the other hand, the simplified equation format does not require a large data storage facility. As shown in Section II-3.1.1.2, the ephemeris of each satellite can be approximated by two simple sinusoids with eight adjustable constants to describe the phase relationships, amplitudes, bias, and frequencies of the latitude and longitude components of satellite movement. The lissajou pattern created by the equations is sufficiently accurate over a twenty-four hour period to eliminate any need for in-flight updating of the ephemeris. It will be shown later in this report that satellite altitude movement need not be considered. For all these reasons, pre-programmed ephemeris data is the recommended technique.

1.1.4 Compensated vs. Uncompensated Ranging Signal

The last alternative in the satellite navigation implementation tree concerns the choice between ranging tone compensation with its associated equipment complexity and expense and the uncompensated ranging tone technique which is less complicated to implement, but is also less accurate. Ranging tone compensation means that the phases of the ranging side tones are adjusted according to some criteria at the source so the user may obtain a more accurate position location. It is effected by adding one or more ground-based reference terminals which transpond ranging signals back to the GCC via the satellites according to a pre-determined sequence. The GCC then advances or retards the phases of the transmitted ranging tones according to how the measured phases of the returned signals compare with the expected phases as calculated for the particular

sector of the transponding reference, and knowledge of the approximate ephemeris information used at the aircraft in performing the position calculations.

The compensated ranging signal, or constant phase plane technique, enables the ground control center to partially cancel the effects of ionospheric bias and undetected variations in satellite-GCC-aircraft geometry. Changes in the electron density distribution of the ionosphere cause a variation of the index of refraction of this layer, which in turn changes the effective path length of VHF radio signals traveling through it. Without a constant phase plane technique to pre-distort the phase of the ranging signals to accommodate the variable delay introduced by propagation through the ionosphere, user aircraft will derive inaccurate position locations. Although the rate of change of the ionospheric index of refraction is relatively slow, the path length of a VHF signal traveling through it may vary by as much as a kilometer in a six-hour period. Since a one-km error in range translates to approximately 1.3 kilometers of aircraft position error, as shown in Section II-3, the effect cannot be neglected.

In similar manner, variations in the system geometry impact the accuracy of the aircraft position location. While the major diurnal satellite excursions will be largely accounted for by the use of ephemeris data (both on the ground to pre-distort the phase of the ranging tones, and in the air to calculate position), the approximate form of the data to be used in this system makes it impossible to locate the satellite closer than within 35 km of its true position. Using the same ratio of range error to aircraft position error as calculated in Section II-3 (and used above in assessing the impact of ionospheric bias) this implies a worst-case aircraft position error of 47 kilometers. The results of computer analysis of a ranging system with a constant phase plane indicate that this worst-case error can be reduced to less than 1300 meters when located as far as 1000 kilometers from the nearest reference station (see Figure 2-11). Moreover, the typical error at this distance for a 35-kilometer satellite error is only 900 meters. As the aircraft moves closer to the reference station, this error decreases and becomes zero when the aircraft and the reference terminal are collocated. The need for the constant phase plane technique is clear. Although this feature entails more equipment complexity, it is a feasible method of obtaining the necessary position location accuracy over a large area.

1.2 Selected Approach

1.2.1 Summary of System Characteristics

The recommended navigation system configuration which

the Dual Satellite Navigation Experiment will approximate will enable any aircraft with the proper on-board equipment to determine its own latitude and longitude to within 1500 meters of the true coordinates independent of external ground control equipment. The position computations will be handled by an on-board data processor which may be a separate unit or a small portion of a computer that is already on-board (as in the case of the larger commercial aircraft). The problem of keeping the aircraft synchronized with the ground control center which generates the ranging tones has been resolved by the choice of an inexpensive, but highly stable, on-board oscillator. This oscillator may be set before leaving the ground and is sufficiently stable so that no in-flight clock update is required for the duration of the flight.

The ground-based grid which enables the GCC to transmit ranging tones of the proper phase to all sections of the continental United States shall consist of one ground control center located in the South Central U.S. and a network of 10 to 20 inexpensive reference terminals. The exact number of reference terminals will depend on satellite elevation angles, and the desired accuracy of the position location at all points on the grid when the proposed system is implemented. Since the expense of the reference terminal is minimal compared to the cost of the ground control center, severe restrictions need not be placed on their total number.

1.2.2 Surveillance Compatibility

Aircraft position determination can be effected using the range data to a pair of satellites in conjunction with the altitude of the aircraft. Position determination on-board the aircraft is considered part of the navigation function while position determination at a ground station is commonly classified as surveillance. In a broader sense, the surveillance function also includes provisions for a data link between the aircraft and the ground station.

In both surveillance and navigation systems utilizing satellites, the aircraft receives the ranging tones transmitted from the ground station and relayed by the satellites. Because the transmitted tone package is common to both systems the two are compatible. For the recommended system, compatibility is further enhanced by the use of a 600-Hz ambiguity resolving tone which is ideally suited to the transmission of digital data (see Section II-2.1).

Addition of the surveillance function to the navigation system would require that each cooperating aircraft be equipped with a transponder to relay the received ranging tones back to the satellite. The ground station would require the down-link receivers, and appropriate hardware and software for position

determination and digital data processing. While the GCC function would be slightly more complex the additional aircraft equipment to provide for surveillance would be minimal.

1.2.3 Extension to Three Satellites

Two satellites in synchronous equatorial orbits have several limitations. They cannot be used to derive altitude information; they do not provide coverage in the polar regions; and while they derive excellent longitude information, latitude information is very poor in equatorial regions. In the North Atlantic region two satellites provide good coverage and reasonable accuracies (on the order of one nautical mile).

The addition of a third satellite can be used to improve coverage at higher latitudes while simultaneously improving accuracies at the low latitudes, or it can be used to extend coverage in a longitudinal direction.

If a third satellite is placed in a synchronous inclined elliptical orbit to improve coverage at higher latitudes and to enhance position location accuracies at the lower latitudes it must be remembered that the satellite will only be visible in the northern latitudes for twelve to eighteen hours a day depending on the orbit eccentricity. For example, with an eccentricity of 0.35, the satellite will be in the northern hemisphere approximately 18 hours while for an eccentricity of zero it will only be in the northern hemisphere for 12 hours. The addition of a fourth synchronous inclined elliptical orbit satellite gives twenty-four hour coverage for the same area of the northern hemisphere if properly spaced. The third and fourth satellites will not be available during the time span of the Dual Satellite Navigation Experiment, therefore their usefulness cannot be demonstrated by this experiment. For an operational system, however, added satellites are recommended because of the increased operational reliability and redundancy they provide in addition to the accuracy improvements achievable with inclined orbits.

If the third satellite is placed in a synchronous equatorial orbit, redundancy is obtained for the same longitudinal coverage by placing the satellite at a longitude between that of the other two satellites. The third satellite could otherwise be placed at a longitude east of the eastern most satellite (or west of the western most satellite) to increase the area of coverage that would be realized by using any two satellites. Position accuracies in the case of using three satellites are not significantly improved over that obtained with the original two satellites.

The system consisting of two equatorial synchronous satellites and one inclined synchronous satellite can also be used to obtain altitude information during the time the third satellite is in the higher latitudes. If the satellite is at 25°N or higher, altitude accuracies will be reasonable good. Altitude measurement error is a function of range error multiplied by a geometry factor. The best altitude accuracies are obtained when the aircraft is at a subsatellite point. It is necessary for this system to use satellite orbit and ephemeris in calculation of position and altitude; for the Dual Satellite Navigation system this correction is simply taken care of in the ground station data processor.

It is important to recognize that extending the proposed two-satellite configuration to three or more satellites in order to extend the coverage area or improve accuracy and increase capabilities does not require significant changes to the Dual Satellite Navigation System concepts.

2. POSITION LOCATION STUDY

2.1 Range Measurement

The time taken by a signal to propagate from a satellite to an aircraft is directly proportional to the range between them. Measurement of one way propagation delay, however, is not possible unless the time of transmission is known. Typical techniques that avoid this problem either measure the round trip signal delay that occurs for transponded signals or measure the time-of-arrival difference between the signals from two reference terminals at known locations.

The measurement of time delay of ranging signals is common for essentially all range measurement techniques. Therefore, the following paragraph discusses alternate approaches used to measure time delay.

2.1.1 Alternate Measurement Approaches

Three basic approaches have been used to measure time delay by appropriate measurement of the parameters of a general ranging signal. The approaches, discussed below, are concerned with measurement of time, phase and frequency.

2.1.1.1 Time Measurement

The measurement of time (as time-of-arrival) of a signal implies that the corresponding range is nonambiguous. This is true for a digital coded signal of appropriate code length, as for a pulse system when the period between pulses is long enough to be essentially nonambiguous.

2.1.1.2 Phase Measurement

Measurement of phase implies that the measurement is made on the phase of a sinusoidal or tone signal. Phase measurements are inherently ambiguous as the identical answer is obtained for every cycle of the tone. Ambiguities can be resolved by using other tone phase measurements to obtain range information. Time delay is determined from the phase measurement by dividing by the tone frequency.

Phase will be computed from quadrature samples of each ranging tone. Two quadrature samples of a sinusoidal signal of known frequency may be used to measure the phase of the location of the samples with respect to the zero crossing of the tone. For convenience, the in-phase sample is usually generated by the positive going zero crossing of the reference. To illustrate the principle, consider the sampling of the tone as shown in Figure 2-2. The samples shown are spaced 90 degrees apart. The location of the positive going zero crossing of the tone with respect to the sample S_I (taken at the positive going zero crossing of the reference) is the angle θ which is arbitrary and unknown. For the signal shown, with arbitrary amplitude A, the sample values are:

$$S_I = A \sin \theta \qquad (2\text{-}1)$$

$$S_Q = A \sin (\theta + 90°) = A \cos \theta \qquad (2\text{-}2)$$

The angle θ can then be calculated as follows:

$$\theta = \tan^{-1} \frac{S_I}{S_Q} \qquad (2\text{-}3)$$

This technique therefore provides a measure of the phase of the sinusoid at the instant of S_I with respect to the reference.

2.1.1.3 Frequency Measurement

Measurement of the frequency of a received signal can be used to calculate the desired range. Since the desired range (R) can be represented as the integral of the range rate ($\dot{R}$) plus an initial value of the range (R_o) it can be calculated using the following equation:

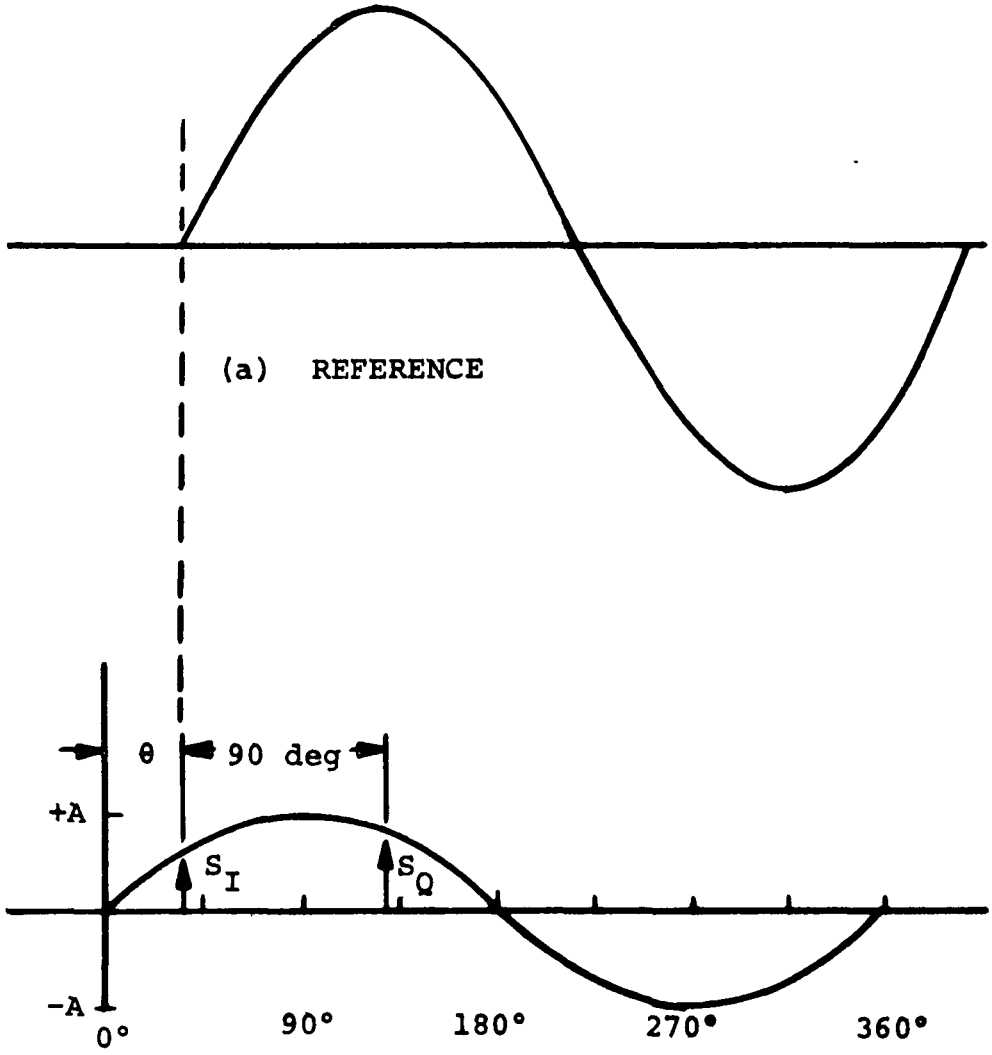

NOTE: S_I and S_Q are quadrature samples

θ is an arbitrary phase angle

Figure 2-2. Quadrature Sampling of a Sinusoid

$$R = \int \dot{R}\, dt + R_o \qquad (2\text{-}4)$$

where

$$\dot{R} = c\left(\frac{\omega_r}{\omega_t} - 1\right) = c\left(\frac{\omega_r - \omega_t}{\omega_t}\right) \qquad (2\text{-}5)$$

and c is the speed of light

ω_r is the angular frequency of the received signal

ω_t is the angular frequency of the transmitted signal.

The difference in the frequency transmitted by the spacecraft and that received by the aircraft is the doppler frequency. Measurement of this parameter is discussed in Section II-2.4.

2.1.2 *Range Measurement Accuracy*

The theory of ranging signal measurement can be used to directly compare alternate ranging techniques if the measurement accuracy is expressed in terms of time delay. The basic theory of range measurement considers the concept of signal time measurement from the view of a maximum likelihood process which expresses ultimate measurement limitations in terms of signal and noise characteristics alone. Generally the value of noise considered in the analysis is a composite of many effects of which thermal noise is but one. Other "noise-like" effects are due to propagation disturbances and equipment implementations. The maximum likelihood approach was chosen because it is optimum in the sense that it minimizes the mean square measurement error. The theory of ranging signal measurement has been well covered in the literature. Woodard [3] did much of the original work, and Skolnik [4], Wainstein and Zubakov [5] develop the theory further and present several interesting applications; the results presented here are based primarily on these developments.

Given a demodulated received signal f(t) contaminated by additive white Gaussian noise,

$$f(t) = S(t - \tau_o) + n(t) \qquad (2\text{-}6)$$

the problem is to determine the true time of arrival (τ_o) which represents the propagation delay from the transmitter to the receiver. The optimum (minimum mean square error) estimate τ of (τ_o) is found from the matched filter or cross-correlation receiver that maximizes the message-signal cross-correlation function

$$C(\tau) = \int f(t)\ S(t - \tau)\ dt \quad . \tag{2-7}$$

From the cross-correlation function the variance (σ_τ^2) in the estimation of τ of (τ_o) can be shown to be

$$\sigma_\tau^2 = \frac{1}{\beta^2 (2E/N_o)} \text{ (seconds)}^2 \tag{2-8}$$

where N_o is the one-sided noise power spectral density and E is the signal energy given by

$$E = \int_o^T |S(t)|^2\ dt \tag{2-9}$$

and

$$\beta^2 = \frac{\int_{-\infty}^{\infty} \omega^2\ |S(\omega)|^2\ d\omega}{\int_{-\infty}^{\infty} |S(\omega)|^2\ d\omega} \tag{2-10}$$

where $S(\omega)$ is the Fourier Transform of $S(t)$.

The parameter β is the second moment of the normalized signal energy and is thus a measure of bandwidth of the signal. For a general bandpass signal of the form

$$S(t) = g(t) \cos \omega_o t \tag{2-11}$$

where g(t) is slowly varying with respect to ω_o, the Fourier transform pair is

$$g(t) \cos \omega_o t \longleftrightarrow \frac{G(\omega - \omega_o) + G(\omega + \omega_o)}{2} = S(\omega) \quad (2\text{-}12)$$

Then,

$$\beta^2 = \frac{\int_{-\infty}^{\infty} \omega^2 |G(\omega)|^2 \, d\omega}{\int_{-\infty}^{\infty} S(\omega)^2 \, d\omega} = \beta_\nu^2 + \omega_o^2 \quad (2\text{-}13)$$

where

$$\beta_\nu^2 = \frac{\int_{-\infty}^{\infty} \omega^2 |G(\omega)|^2 \, d\omega}{\int_{-\infty}^{\infty} |G(\omega)|^2 \, d\omega} << \omega_o^2 \quad (2\text{-}14)$$

Then, for bandpass and tone signals of the form of equation (2-11) the value of β^2, to a very close approximation is ω_o^2.

2.1.3 Accuracy of Alternate Techniques

It is instructive to compare the fine range accuracies attainable with digital code ranging and with a fixed tone. The fine range measurement of a digital code is obtained from the measurement of phase of the clock frequency. The accuracy of the fine range measurement is given by equation (2-8) using the appropriate value of β^2. To make a meaningful comparison, the signal energy and the baseband bandwidth must be the same for both cases.

The digital code ranging signal will have a minimum baseband bandwidth (B) requirement of twice the clock frequency. The value of β^2 will therefore equal the squared value of clock frequency (ω_c^2), where $\omega_c \doteq B/2$. The minimum variance (σ_c^2)

attainable for a digital code ranging system constrained to a signal energy (E) and a bandwidth (B) can then be found from equation (2-8), and the above value for the clock frequency to be

$$\sigma_c^2 \geq \frac{4}{\beta^2 (2E/N_o)} \qquad (2\text{-}15)$$

The tone approach used for fine range measurement requires that the baseband bandwidth (B), be approximately equal to the radian frequency of the ranging tone (ω_o). The minimum variance (σ_t^2) attainable for a tone ranging system constrained to a signal energy (E) and a bandwidth (B) can then be found from equation (2-8) to be

$$\sigma_t^2 \geq \frac{1}{\beta^2 (2E/N_o)} \qquad (2\text{-}16)$$

The measurement of ranging tones in a given bandwidth yields four times better fine range accuracy than is obtainable with a digital code of the same energy in the same bandwidth. The ranging tone concentrates all its available signal energy at the edge of the frequency band which gives a higher value of β^2 than can be obtained for a signal with a distributed power spectrum.

This suggests that a ranging tone be used for best resolution at a given signal-to-noise ratio. Choosing an appropriate ranging tone is the next step. The choice involves several trade-off factors. The energy-to-noise power density ratio of the link between the satellite and the aircraft is the first constraint on the tone frequency. From Appendix A the worst cast effective carrier-to-noise power density of this link (ATS-I to A/C) is calculated to be 30.5 dB-Hz as shown in Table A-4. This includes the effect of all error sources. As the tone package will have three ranging tones (this choice is

justified by probability of ambiguity resolution as discussed below) and a carrier for a total of four tones among which the power must be shared, the amount of signal energy available to one tone will be approximately one-fourth of the total or 24.5 dB-Hz. The next step is to determine an acceptable value for rms range error (σ_R). Figure 2-3 shows the relationship between rms phase deviation (σ_ϕ) and energy-to-noise ratio for a one-second integration time.

A phase detector integration time of one second will be used since this interval is a good compromise between obtaining a good phase value average and minimizing the effects of satellite movement on phase measurements. From the approximation for σ_ϕ in the linear region of the curve, the equation relating σ_θ to σ_R is

$$\sigma_R = \frac{c}{\omega} \sigma_\phi \tag{2-17}$$

From this expression, the equation relating the ranging tone frequency to E/N_o and σ_R may be derived as

$$f = \frac{c}{2\pi \sigma_R (2E/N_o)^{1/2}} \tag{2-18}$$

where c = velocity of light

Substitution of 24.5 dB-Hz for the worst-case E/N_o and 200 meters as the worst case rms range deviation results in the selection of 10 kHz as a desirable frequency for the fine ranging tone.

2.1.4 Ambiguity Resolution

Ambiguity resolution is a lower accuracy range measurement that is necessary to obtain a measure of the <u>total</u> delay experienced by the ranging signal. It was shown in Section II-2.1 that the optimum ranging signal is a tone. Consequently,

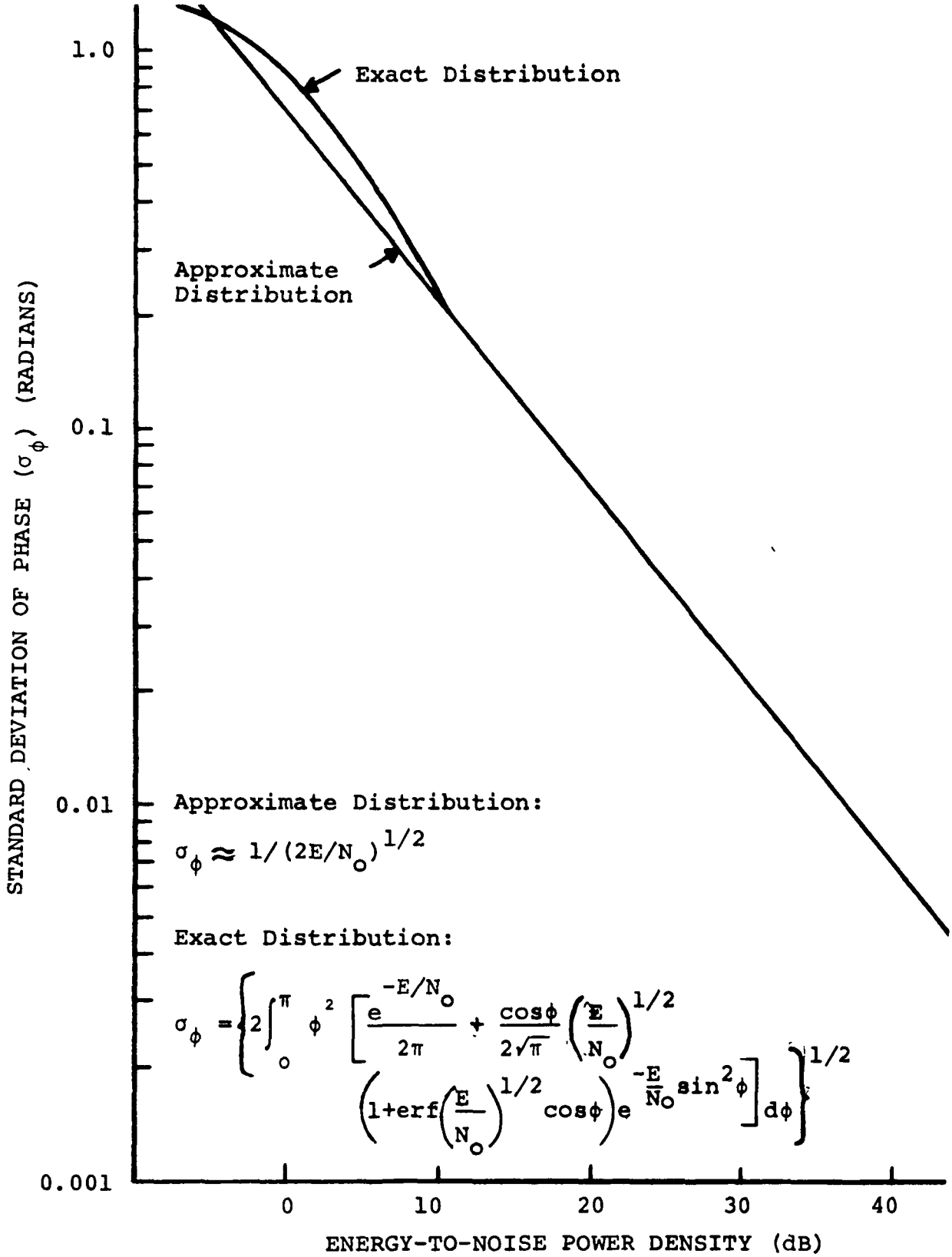

Figure 2-3. Standard Deviation of Phase Measurement vs. Energy-To-Noise Power Density

the optimum ranging signal for ambiguity resolution of the fine ranging tone is a tone of lower frequency. The accuracy required of the ambiguity resolving ranging system must be adequate to resolve, with high probability, the ambiguity inherent in the fine range measurement.

If the highest tone frequency required for accurate range measurement is f_h, then the next lowest tone frequency f_{h-1} is determined by a number of factors. For example, if the minimum total transmitted power is the primary criterion, it can be shown that a tone frequency ratio R, defined by

$$R = f_h/f_{h-1} \tag{2-19}$$

is approximately two for maximum probability of correctly resolving range ambiguity. If the lowest frequency tone required for the coarsest ambiguity resolution is f_ℓ, then the total number of tones required (N) to meet this criterion is given by

$$N = 1 + \frac{\log[f_h/f_\ell]}{\log R} \tag{2-20}$$

where R is 2. The difficulty with this method is that a large number of tones are required which complicates the equipment design.

To minimize receiver complexity it is desirable to reduce the number of tones required. This can usually be done while incurring only a very small penalty in the total power required. In the non-optimum case in which N tones are used from the lowest tone (f_ℓ) to the highest tone (f_h), the phase measurement variance allowed per tone can be determined once the probability (P) of the error in resolving all of the ambiguities is specified. In this case, the probability of error in the resolution (P_s) of each of the (N-1) ambiguity steps is

$$P_s \doteq \frac{P}{N-1} \tag{2-21}$$

For each step, the probability of error in resolution is

$$P_s = \text{Probability} \left[\left(\sigma_{f_i}^2 R^2 + \sigma_{f_{i+1}}^2 \right)^{1/2} < \pi \right] \tag{2-22}$$

where $\sigma_{f_i}^2$ = variance of the phase measurement of the i^{th} frequency tone

$\sigma_{f_{i+1}}^2$ = variance of the phase measurement of the $(i+1)^{th}$ frequency tone

and the probability distribution is approximately gaussian. The variance of the phase measurements for each ambiguity tone are essentially equal and hence equation (2-22) can be written as

$$P_s = \text{Probability} \left[\sigma_f (R^2 + 1)^{1/2} < \pi \right] \tag{2-23}$$

or

$$\frac{P}{N-1} = \text{Probability} \left[\sigma_f (R^2 + 1)^{1/2} < \pi \right] \tag{2-24}$$

Once the phase measurement variance σ_f^2 due to all effects is known, and the error probability P and number of tones have been selected, then the tone ratio can be determined using tables of the normal probability function.

A final factor that impacts the choice of the ambiguity resolving signal for the coarsest range measurements is that processing of low frequency tones introduces practical disadvantages. The most significant of these is the narrow bandwidth filter required to demultiplex the low frequency tones in the frequency domain. These filters are limited in response and have considerable time delay. As a result, it is desirable

to utilize an alternative technique other than tones for the resolution of the coarsest range measurements.

In a satellite navigation system, the choice of ambiguity resolving tone frequencies is dictated by the phase measuring technique, and the desire to minimize equipment complexity by maximizing equipment commonality. Because such a navigation system would also be compatible with a satellite surveillance system, as discussed in Section II-1.2, one ambiguity resolving tone will be recovered from a 600-Hz digital data channel which is incorporated in the system to satisfy this constraint. Ambiguity resolution of the 600-Hz tone would be provided by measuring the time of arrival of the data frame synchronization pulse with respect to the on-board frequency standard. This technique makes maximum use of the accurate on-board oscillator, yet eliminates the need to process low frequency tones.

The need for additional ambiguity resolving tones between 600 Hz and the fine ranging tone near 10 kHz can be determined from the results of equation (2-24). This equation can be expressed by requiring that

$$\sigma_f [R^2 + 1]^{1/2} \leq \frac{\pi}{F} \qquad (2\text{-}25)$$

where F is a confidence factor used to meet the allowable probability error for each ambiguity resolution. If a total probability of error (P) of 10^{-4} is chosen, then in a three-tone system, the probability of error at each ambiguity resolving step is 5×10^{-5}. The F factor in this case can be obtained from tables of the normal probability function [6] to be 4.06. The tone ratio R in this case is approximately 4. Hence the allowable phase measurement variance for ambiguity resolution is approximately 10 degrees on the 600-Hz tone, the fine ranging tone

near 10 kHz, and the intermediate tone near 2.5 kHz. In fact, the phase measurement variance on the fine ranging tone and the 600-Hz data channel will be appreciably better than this. This, therefore, represents the requirement for the intermediate tone.

The exact frequency of the fine ranging tone near 10 kHz and the intermediate tone needed to insure that the fine ranging tone ambiguity can be resolved will be determined from the constraints of the sampling system used in the phase measurement. A number of constraints apply to the choice of the sampling frequency. First, the sampling frequency (f_s) must be of a high enough rate to provide two quadrature samples of each ranging tone. Second, f_s must be greater than twice the bandwidth of the filters used to present a band limited signal to the sampler (in order to prevent aliasing as described in Section II-2.1.5).

These requirements may be met by choosing an intermediate tone frequency of 2.4 kHz and a sampling frequency of 9.6 kHz. The sample rate of 9.6 kHz has the added advantage that it is possible to derive sample pulses from this frequency which will provide two quadrature samples of a frequency which is nine times the fundamental frequency of 600 Hz or 10.2 kHz. Hence, the three ranging tone frequencies are 600 Hz, 2.4 kHz, and 10.2 kHz.

The fine grain tone at 10.2 kHz generates ambiguities in phase measurement every 98 μsec or every 29.9 km for a one-way range measurement. The 2.4 kHz tone increases the distance between one-way range ambiguities to 416 μsec or 126.8 km. The data subcarrier at 600 Hz further increases the distance between ambiguities to 1.66 ms or 507.0 km. The resolution of range provided by the period between successive frame sync pulses on the digital data channel will be on the order of 300,000 km between ambiguities as the message period is designed to be 1 second. Together, the four time intervals provided by three ranging tone frequencies and the repetition rate of the digital

code will be more than adequate to resolve any range ambiguities that the navigation experiment will encounter.

2.1.5 Implementation

The demodulated orderwire signal spectrum containing ranging tones and digital data is reproduced in Figure 2-4.

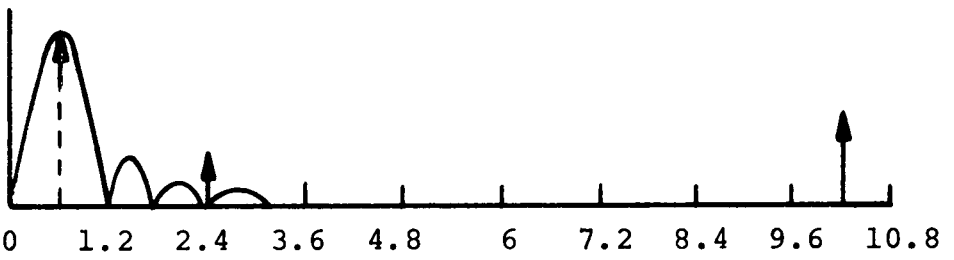

Figure 2-4. Demodulator Orderwire Signal Spectrum

The dotted line at 600 Hz represents the phantom data subcarrier that is recovered by processing of the digital data signal. The 600-Hz signal is used both as a range ambiguity resolution tone and also for bit synchronization for the digital data. Prime emphasis, however, will be on the use of the 600-Hz tone for ambiguity resolution. Measurement of the phase of the 10.2-kHz, 2.4-kHz and the 600-Hz tones will be done by accumulating binary samples of individually filtered signals, for each signal burst, as shown by the block diagram of Figure 2-5. The values of the accumulated quadrature samples will serve as inputs to the computer to determine the phase of each tone. The range will then be calculated by resolution of ambiguitites. The ambiguities in the 600-Hz signal will be resolved by the computer by the successive knowledge of bit synchronization, message framing and system timing.

The filters shown in Figure 2-5 are necessary to present a band-limited signal to the sampler and analog-to-digital converter. Band limiting is required since sampled data systems operating at a sampling rate less than twice the band-limited bandwidth can be contaminated by a phenomenon termed aliasing. Signals and noise outside a frequency band that is half the actual sampling rate (termed the Nyquist bandwidth) will be folded (aliased) into the Nyquist band and cause distortion. As filter bandwidths are reduced, however, the filter time delay

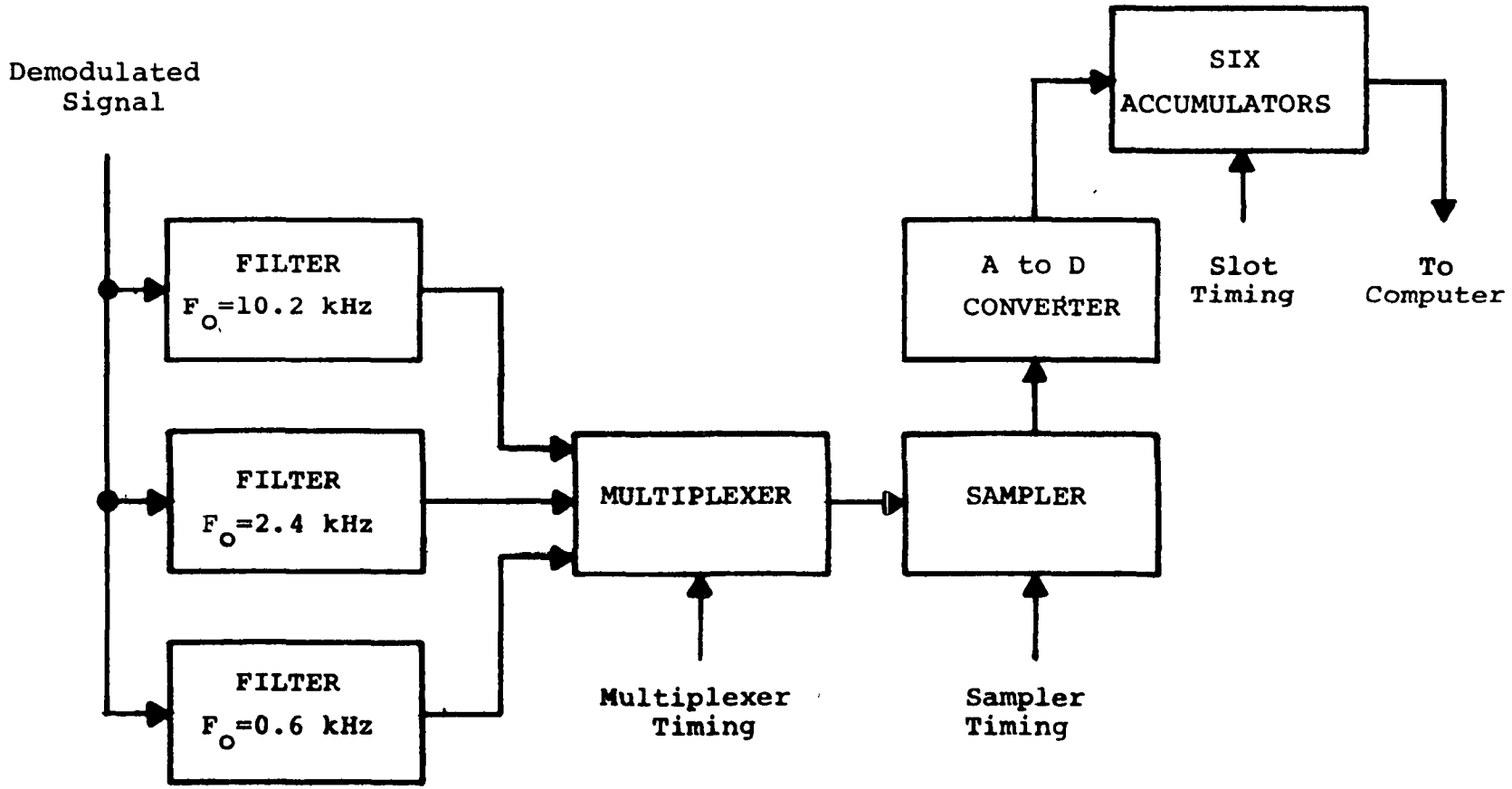

Figure 2-5. Block Diagram of Phase Measuring Equipment

increases. The filter time delay causes a delay in acquisition of the signals because of filter transient effects.

A good compromise between sampling rate requirements and acquisition delay is made by selecting a 500-Hz filter bandwidth. The filter time constant, to a first approximation, is 2 milliseconds which permits the attenuation of essentially all significant transient effects within six to ten milliseconds. The sampling rate required for a 500-Hz noise bandwidth filter is 1000 samples per second. Since the 500-Hz filters will not totally reject all unwanted signals, the sampling technique was configured to assure that the accumulated samples taken for measurement of each tone did not contain other undesired signals from the orderwire spectrum. This can be assured if the tone frequencies and integration periods are selected such that:

1. Harmonics of the sampling frequency do not beat (hetrodyne) other tones or data to dc (frequency equals zero)

2. Beat frequencies which do occur fall at zeros of the integrator sync function.

The measurement technique chosen for implementation generates periodic samples at a 9.6-kHz rate. The following paragraphs describe the process in which the signals are sampled, converted, and accumulated. Ranging tone sample timing and sample identification is shown in Figure 2-6 to aid the following discussion.

10.2-kHz Tone

Every fourth sample taken at the 9.6-kHz rate is used to integrate the 10.2-kHz signal. If the first sample chosen is arbitrarily designated sample S_1, the sample sequence to be used for the 10.2-kHz tone phase measurement is (S_1, S_5, S_9, S_{13} . . S_{357}). Samples (S_1, S_9, S_{17}, . . .) constitute the set of in-phase samples, while samples (S_5, S_{13}, S_{21}, . . .) are the set of quadrature samples.

The sense (sign) of adjacent samples is negative. Accumulation therefore requires that the magnitude of in-phase samples be added in the 10.2-kHz in-phase accumulator. Quadrature sample magnitudes will likewise be added in the 10.2-kHz quadrature accumulator. The sum of the samples in the in-phase accumulator for 10.2-kHz signals is A_{1I} and the sum of the

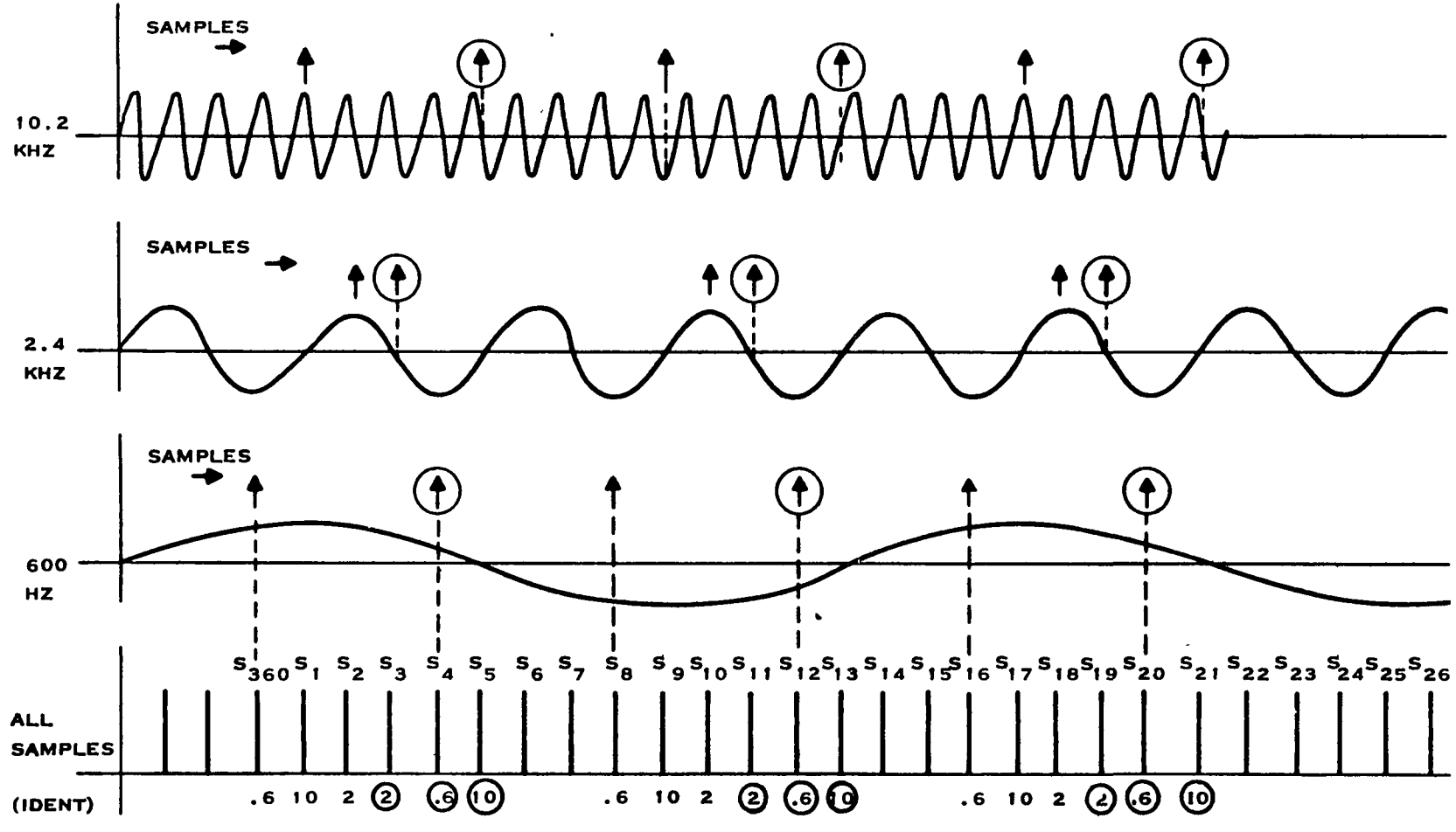

NOTE: (IDENT.) REFERS TO TONES SAMPLED
. 6 ~ 600 HZ
2 ~ 2.4 KHZ
10 ~ 10.2KHZ

CIRCLED IDENTIFIERS AND SAMPLES ARE FOR QUADRATURE SAMPLES
UNCIRCLED IDENTIFIERS AND SAMPLES ARE FOR IN PHASE SAMPLES

Figure 2-6. Ranging Tone Sampling

samples in the quadrature accumulator is A_{1Q}, where

$$A_{1I} = \sum_{n=1}^{45} |S_{[1+8(n-1)]}|$$

and

$$A_{1Q} = \sum_{n=1}^{45} |S_{[5+8(n-1)]}|$$

2.4-kHz Tone

The sample sequence to be used for the 2.4-kHz tone phase measurement is (S_2, S_3, S_{10}, S_{11}, S_{18}, S_{19}, . . . S_{354}, S_{355}).

Samples with even numbered subscripts constitute the set of in-phase samples while samples with odd numbered subscripts are the set of quadrature samples. The 2.4-kHz in-phase accumulator will contain the sum A_{2I} and the quadrature accumulator will contain the sum A_{2Q}, where

$$A_{2I} = \sum_{n=1}^{45} |S_{[2+8(n-1)]}|$$

and

$$A_{2Q} = \sum_{n=1}^{45} |S_{[3+8(n-1)]}|$$

600-Hz Tone

The sample sequence used to measure the phase of the 600-Hz tone is (S_4, S_8, S_{12}, . . . S_{360}). The in-phase sample set is (S_8, S_{16}, S_{24}, . . . S_{356}). Alternate sample values are negatives of each other which then requires that the accumulator

sum magnitudes of samples. Alternatively the first sample can be added, the second subtracted, the third added, and so on. The 600-Hz in-phase accumulator will contain the sum A_{6I}, and the quadrature accumulator will contain the sum A_{6Q}, where

$$A_{6I} = \sum_{n=1}^{45} |S_{[8+8(n-1)]}|$$

and

$$A_{6Q} = \sum_{n=1}^{45} |S_{[4+8(n-1)]}|$$

The values of the approximate sums contained in each accumulator determine the phase of the three tones. Once the phase of the 600-Hz tone is measured the phase of the 2.4-kHz tone will be measured such that ambiguities involving whole cycles are removed. That is, the zero crossing of the 2.4-kHz tone nearest the zero crossing of the 600-Hz tone is selected. The same process is effected with the 10.2-kHz signal. The correct epoch is determined by the 600-Hz tone zero crossing and the accurate measure of that time is given by the measured zero crossing of the 10.2-kHz tone. If the zero crossing of the 600-Hz tone corresponding to the end of the last bit of the last character of the digital message is chosen, the time delay of the signal with respect to the transmitted signal (and hence range) can be calculated.

2.2 Position Location Calculation

There exists several coordinate systems, each with its own set of equations describing the satellites and aircraft geometry, which can be used in computing the position of the aircraft. The set of coordinates which is most convenient, however, in the sense that the associated equations can be solved in a straightforward manner is the orthogonal earth-centered set oriented as shown in Figure 2-7. In this configuration three parameter measurements are required: the range from each of two satellites to the aircraft and the aircraft altitude above the surface of the earth. Additionally, the input parameters defining the position of both satellites and the distance from the center of the earth to the surface are required in the solution for aircraft position. Although the aircraft position solution is developed using two satellite reference locations, the solution technique is applicable in determining aircraft position location utilizing any pair of

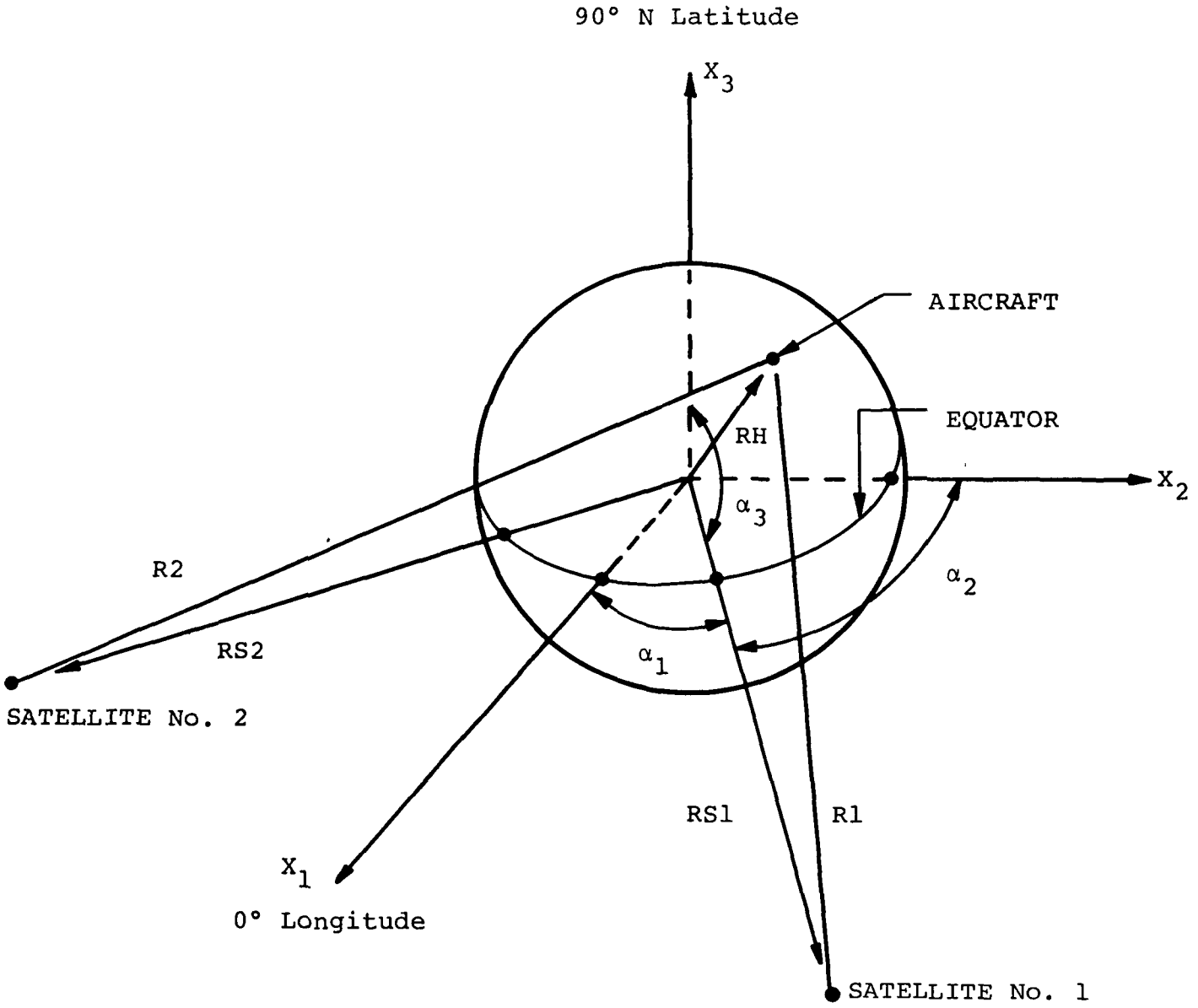

Figure 2-7. Two-Satellite Navigation Configuration

known reference locations from which straight-line range measurements to the aircraft have been made. For example, one reference location could be on the ground within line of sight of the aircraft while the other location could be a single satellite. The problem may be concisely stated as follows:

GIVEN: R1 = measured range between aircraft and satellite 1

R2 = measured range between aircraft and satellite 2

RS1 = distance from earth center to satellite 1

RS2 = distance from earth center to satellite 2

RH = distance from earth center to aircraft

B1 = direction cosine vector to satellite 1

$$= \begin{vmatrix} B11 \\ B12 \\ B13 \end{vmatrix}$$

B2 = direction cosine vector to satellite 2

$$= \begin{vmatrix} B21 \\ B22 \\ B23 \end{vmatrix}$$

FIND: BA = direction cosine vector to the aircraft

$$= \begin{vmatrix} BA1 \\ BA2 \\ BA3 \end{vmatrix}$$

SOLUTION: The components in B1 (the direction cosine column vector) are defined as shown in Figure 2-7 to be:

B11 = cosine α_1

B12 = cosine α_2

B13 = cosine α_3

If the orthogonal coordinate system X_1, X_2, X_3 is aligned such that the X_3 axis corresponds with the North/South axis of the earth and the X_1 axis passes through the Greenwich meridian (0° longitude), then the vector B1 is expressed in terms of satellite latitude and longitude as

$$B11 = \text{cosine (Latitude) cosine (Longitude)}$$
$$B12 = \text{cosine (Latitude) sine (Longitude)}$$
$$B13 = \text{sine (Latitude)}.$$

Vector B2 is defined in a similar manner with respect to satellite 2, and vector BA is similarly defined with respect to the aircraft. Once the components of the vector BA are found, the latitude and longitude are calculated by substitution in the equations

$$LAT = \text{arc sin (BA3)} \qquad (2\text{-}26)$$

$$L\emptyset N = \text{arc tan (BA2/BA1)} \qquad (2\text{-}27)$$

The derivation of the equations necessary to find the components of the direction cosine vector BA begins with the application of the law of cosines to the two triangles created by the earth center, the aircraft, and the two satellites. For this geometry

$$R1^2 = RH^2 + RS1^2 - 2*RH*RS1*(B1^T*BA) \qquad (2\text{-}28)$$

$$R2^2 = RH^2 + RS2^2 - 2*RH*RS2*(B2^T*BA) \qquad (2\text{-}29)$$

where $B1^T$ indicates the transposed column matrix B1. This matrix is defined by

$$B1^T = |B11\ B12\ B13| \qquad (2\text{-}30$$

The asterisk is used in this case for conventional multiplication. Solving equations 2-28 and 2-29 for $B1^T*BA$ and $B2^T*BA$ gives

$$B1^T*BA = \frac{RH^2 + RS1^2 - R1^2}{2*RS1*RH} = D1 \qquad (2\text{-}31)$$

$$B2^T*BA = \frac{RH^2 + RS2^2 - R2^2}{2*RS2*RH} = D2 \qquad (2\text{-}32)$$

Every quantity on the right hand side of equations 2-31 and 2-32 is known, so two of the three necessary equations can be

derived from the expansion of the dot products on the left hand side of equations 2-31 and 2-32. Expansion of these products yields:

$$B11*BA1 + B12*BA2 + B13*BA3 = D1 \qquad (2\text{-}33)$$

$$B21*BA1 + B22*BA2 + B23*BA3 = D2 \qquad (2\text{-}34)$$

The third equation necessary to solve for the aircraft direction cosine is derived from the fact that the direction cosine vector is a unit vector. This gives

$$BA1^2 + BA2^2 + BA3^2 = 1 \qquad (2\text{-}35)$$

The solution to equations 2-33, 2-34, and 2-35 is complicated by the fact that equation 2-35 is nonlinear. The equations, however, can be solved in the following manner:

Step 1. Eliminate BA2 from equations 2-33 and 2-34. Then,

$$DEL4 = BA1*DEL1 + BA3*DEL2$$

or

$$BA1 = (DEL4 - BA3*DEL2)/DEL1 \qquad (2\text{-}36)$$

where

$$DEL4 = D1*B22 - D2*B12 \qquad (2\text{-}37)$$

$$DEL2 = B22*B13 - B12*B23 \qquad (2\text{-}38)$$

$$DEL1 = B22*B11 - B12*B21 \qquad (2\text{-}39)$$

Step 2. Eliminate BA1 from equations 2-33 and 2-34. Then,

$$DEL5 = -BA2*DEL1 + BA3*DEL3$$

or

$$BA2 = (-DEL5 + BA3*DEL3)/DEL1 \qquad (2\text{-}40)$$

where

$$DEL3 = B13*B21 - B23*B11 \qquad (2\text{-}41)$$

Step 3. Substitute equations 2-36 and 2-40 into equation 2-35.

$$BA3^2 = 1 - \left[\frac{(-DEL5 + BA3*DEL3)}{DEL1}\right]^2 - \left[\frac{(DEL4 - BA3*DEL2)}{DEL1}\right]^2 \qquad (2\text{-}42)$$

which simplifies to:

$$BA3^2*SQD - 2*BA3*SUM1 + SUM2 = 0 \qquad (2\text{-}43)$$

where

$$SQD = DEL1^2 + DEL2^2 + DEL3^2 \qquad (2\text{-}44)$$

$$SUM1 = DEL2*DEL4 + DEL3*DEL5 \quad (2\text{-}45)$$

$$SUM2 = DEL1^2 + DEL4^2 + DEL5^2 \quad (2\text{-}46)$$

Step 4. Solve for BA3 by using the quadratic equation

$$BA3 = \frac{SUM1 \pm \sqrt{SUM1^2 - SQD*SUM2}}{SQD} \quad (2\text{-}47)$$

BA1 and BA2 may be determined by substitution into equations 2-36 and 2-40. Finally, aircraft latitude and longitude are determined by application of equation 2-26 and 2-27. It is worthwhile to note that when the satellites are positioned directly over the equator so that B13 = B23 = 0, the calculation of the direction cosine BA is simplified to solving two simultaneous equations in two unknowns. Equations 2-33 and 2-34 reduce to

$$B11*BA1 + B12*BA2 = D1 \quad (2\text{-}48)$$

$$B21*BA1 + B22*BA2 = D2 \quad (2\text{-}49)$$

with the solution:

$$BA1 = \frac{\begin{vmatrix} D1 & B12 \\ D2 & B22 \end{vmatrix}}{\begin{vmatrix} B11 & B12 \\ B21 & B22 \end{vmatrix}} = \frac{D1*B22 - D2*B12}{B11*B22 - B21*B12} \quad (2\text{-}50)$$

and

$$BA2 = \frac{\begin{vmatrix} B11 & D1 \\ B21 & D2 \end{vmatrix}}{\begin{vmatrix} B11 & B12 \\ B21 & B22 \end{vmatrix}} = \frac{D2*B11 - D1*B21}{B11*B22 - B21*B12} \quad (2\text{-}51)$$

Equation 2-35 is then solved for BA3, and the aircraft latitude and longitude are found as stated above.

2.3 Sector Organization for a Navigation System

Navigation using range measurements to satellite transponders in which the constant phase plane technique is used requires the use of a reference terminal at a known location. As was discussed in Section II-1.1, the constant phase plane technique relieves the navigation system of being required to continually supply updated ephemeris data to the aircraft. The function of the reference terminal is to provide the ground

control center (GCC) with the round trip range information needed to properly adjust the phase of the ranging signal to implement the constant phase plane concept.

As the objective of a satellite navigation system is to provide coverage over the widest possible area, multiple reference terminals will be required. Each reference terminal will provide the GCC with ranging phase information that will enable the GCC to generate a set of ranging phase planes that are appropriate at each reference terminal for the assumed satellite ephemeris data. This control of the ranging phase planes in relation to the various reference terminals will be performed in a time multiplexed manner. Thus, the ranging tone transmitted at any given time will only be accurate for that sector containing the reference terminal that is controlling the GCC tone transmissions. Aircraft operating in other sectors will obtain position locations which are degraded according to how far removed they are from the phase adjusted sector. By time multiplexing, however, aircraft in all sectors will have one opportunity during each cycle through all reference stations to obtain the optimum position location for their area.

The phase control information required at the GCC will be obtained from the various reference terminals by using transponding reference terminals that relay the ranging signal back to the GCC via each satellite in time division multiplexed channels common to all reference terminals. The time sharing of the GCC tone phase control among sectors will be organized such that the phase correction measured in the first time slot for sector k will be used to update the stored estimate for sector k derived from earlier measurements. Transmission of the ranging phase applicable to sector k will then be made in the second time slot. During the second time slot, the phase correction that applies to sector (k+1) is being updated.

The time slot duration allocated to each sector is regulated by a number of factors. These include:

1. The number of reference terminals to be interrogated.
2. Sector transfer time
3. Phase detector integration time
4. The acquisition time of the GCC phase-lock-loop receiver
5. The maximum allowable error introduced by configuration changes between the sector k update calculation and the subsequent transmission of that update to sector k.

The number of sectors depends on the area of earth coverage adjacent to each reference station that enables a user to fix his position with acceptable accuracy. This is discussed in detail in Section II-3.1 where it is shown that a reference terminal separation of 400 km would provide adequate position location accuracy. In the recommended navigation system, reference terminals will be interrogated sequentially by the ground control center via the digital data link. This technique insures that the appropriate terminal transponds in the correct time slot as determined by the GCC clock, and avoids the problem posed by the alternative sector transfer control method which requires updating reference terminal clocks to counteract long term drift effects. Sector control by interrogation requires that the GCC wait for a return to confirm that the message is properly received. Approximately 0.5 second will be needed to complete the interrogation of a reference terminal from the ground control center via the satellite.

Phase detector integration time relates to the available C/N_o at the GCC and is the primary constraint affecting the minimum time between successive time slots. With an available C/N_o of 24.5-Hz, the recommended integration time is one second (as shown in Section II-2.1.3).

Phase-lock-loop receiver acquisition time has a great impact on the width of the guard bands surrounding the phase detector integration time band. When one reference terminal transponder shuts off and the next one starts, the signal at the GCC may be totally absent for as long as 40 ms. Hence, the GCC will lose signal lock and will have to reacquire it again. Using a fast acquisition phase-lock-loop technique, acquisition can be easily acquired in 50 ms.

Errors introduced by configuration changes between the phase correction measurement for a given sector and the subsequent transmission of the correction during the next time slot establish the maximum time slot duration. The rate at which the navigation configuration changes can be computed by finding the slope of the curve portraying the diurnal variation of the range from the satellite to the ground control center. A graph of this function for the ATS-I satellite is shown in Figure 2-10 in Section II-3.1. Modeling the range variation as a sine wave gives

$$R_s(t) = d \sin \omega t \qquad (2\text{-}52)$$

where $\omega = 7.26 \times 10^{-5}$ radians/second

$d = 200$ km

$t =$ time in seconds.

The rate of change of range is found from the time derivative of $R_s(t)$. This results in

$$\frac{dR_s(t)}{dt} = \omega d \cos \omega t \qquad (2\text{-}53)$$

The maximum value of the derivative occurs when the cosine is unity. Hence the maximum rate of change of range is

$$\omega d = (2 \times 10^5 \text{ m}) (7.26 \times 10^{-5} \text{ sec}^{-1})$$

$$\simeq 15 \text{ m/sec}$$

Assuming a maximum error due to this factor of 75 meters, no more than five seconds may elapse between the completion of the phase correction measurement, and the completion of the phase correction transmission. Taken together, these constraints on the slot time duration indicate that the optimum slot organization is two one-second guard bands surrounding a one-second integration time band for a total of three seconds.

2.4 Range-Rate Measurement

2.4.1 Basic Technique

The measurement of range-rate between the satellite and cooperating aircraft provides data that can be used to determine aircraft velocity and range. To implement the measurement, the received carrier frequency from the satellite would be measured with respect to the stable on-board oscillator. The difference between this measured frequency and that known to exist without doppler is then a measurement of the doppler frequency which can be converted to range-rate. This technique assumes that the satellite transmitter frequency is known. This will be true if a coherent satellite transponder is used, or if the frequency is relayed to the aircraft from the ground over the data link. For simplicity in this discussion, it will be assumed that a coherent satellite transponder is used.

The method by which the frequency, as received at the aircraft, is measured with respect to the on-board oscillator is shown in Figure 2-8. The stable oscillator is used as the reference in the counter and also as the source for the multiplier in the receiver down-converter. The multiplier ratio is assumed to be M, while the actual oscillator frequency is $(f_o + \Delta f)$, and is in error by Δf from its assumed value of f_o. The frequency that is presented to the counter (f_c) is thus

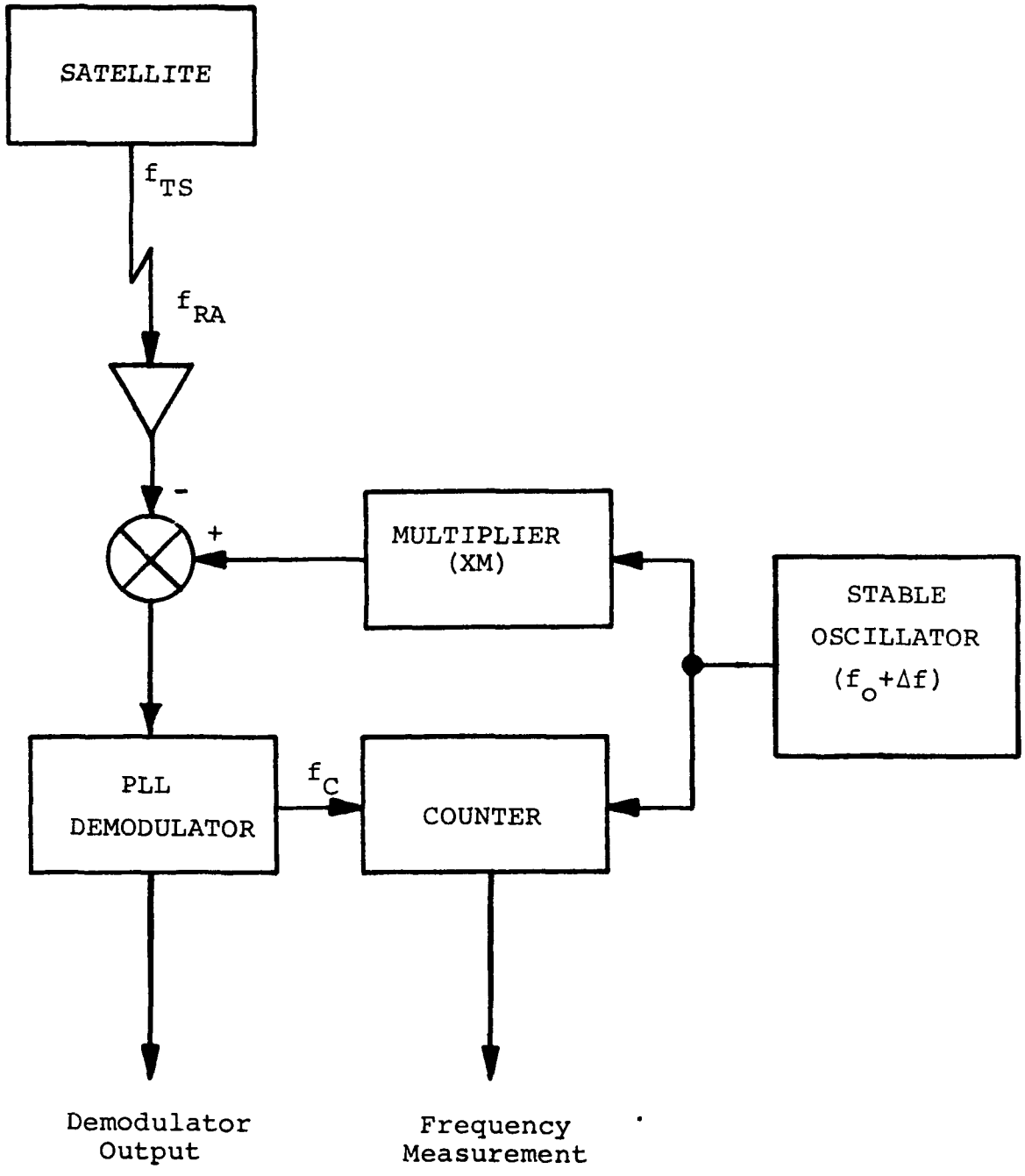

Figure 2-8. Doppler Measurement System

given by

$$f_c = M(f_o + \Delta f) - f_{RA} \qquad (2\text{-}54)$$

where f_{RA} is the frequency received by the aircraft. This frequency is given by

$$f_{RA} = f_{TS}[1 + \dot{R}_A/c] \qquad (2\text{-}55)$$

where f_{TS} = satellite transmit frequency

$\dot{R}_A$ = aircraft-to-satellite range-rate

c = velocity of light.

If the frequency measured by the counter is F, then it is related to the true frequency f_c at this point by

$$f_c = F(f_o + \Delta f)/f_o \qquad (2\text{-}56)$$

The following relationship can then be derived between the system parameters and the oscillator error.

$$1 + \dot{R}_A/c = \frac{f_o + \Delta f}{f_{TS}} [M - F/f_o] \qquad (2\text{-}57)$$

To simplify this expression it is desirable to define

$$F = F_o + \Delta F$$

where F_o = count expected with no doppler and an exact oscillator

ΔF = count increment measured due to doppler and oscillator error

Then,

$$Mf_o - F_o = f_{TS} \qquad (2\text{-}58)$$

and Equation (2-57) can be written in the form,

$$1 + \dot{R}_A/c = [1 + \Delta f/f_o][1 - \Delta F/f_{TS}] \quad (2\text{-}59)$$

This can be written approximately as

$$\dot{R}_A c \doteq \Delta f/f_o - \Delta F/f_{TS} \quad (2\text{-}60)$$

The effect of oscillator instability upon the range-rate measurement is now apparent. The error in range-rate is given by

$$\text{Range-Rate Error} = \Delta f \; c/f_o \quad (2\text{-}61)$$

An oscillator error of only one part in 10^8 will result in a velocity error of 6.7 mph. The measurement of accurate velocity thus requires a very stable oscillator.

2.4.2 Oscillator Up-Date

The oscillator stability requirement for accurate range rate measurement is sufficiently severe as to require some method whereby the oscillator drift can be corrected, and the oscillator frequency up-dated. Not only is this technique desirable for a satellite navigation system, but it is also necessary in certain cooperative collision avoidance systems (CAS) being proposed at this time.

A technique is proposed by Texas Instruments to implement on-board oscillator frequency up-date. This technique assumes that the aircraft satellite navigation equipment is also part of an aircraft satellite surveillance system. This being the case, it will be shown that the doppler frequency measurement made on-board the aircraft can be used at a ground station, together with a measurement of the received aircraft transmitter frequency as relayed by the satellite, to compute the aircraft oscillator frequency at the ground station. This data can then be relayed back to the aircraft and any desired compensation can be made.

A simplified block diagram of a single oscillator transponder is shown in Figure 2-9. This arrangement also provides approximate doppler frequency compensation of the aircraft frequency as received at the satellite. The equation relating the aircraft transponder transmit frequency (f_{TA}) and the receive frequency (f_{RA}) is

$$f_{TA} = (M + N)\, f_X - f_{RA} \quad (2\text{-}62)$$

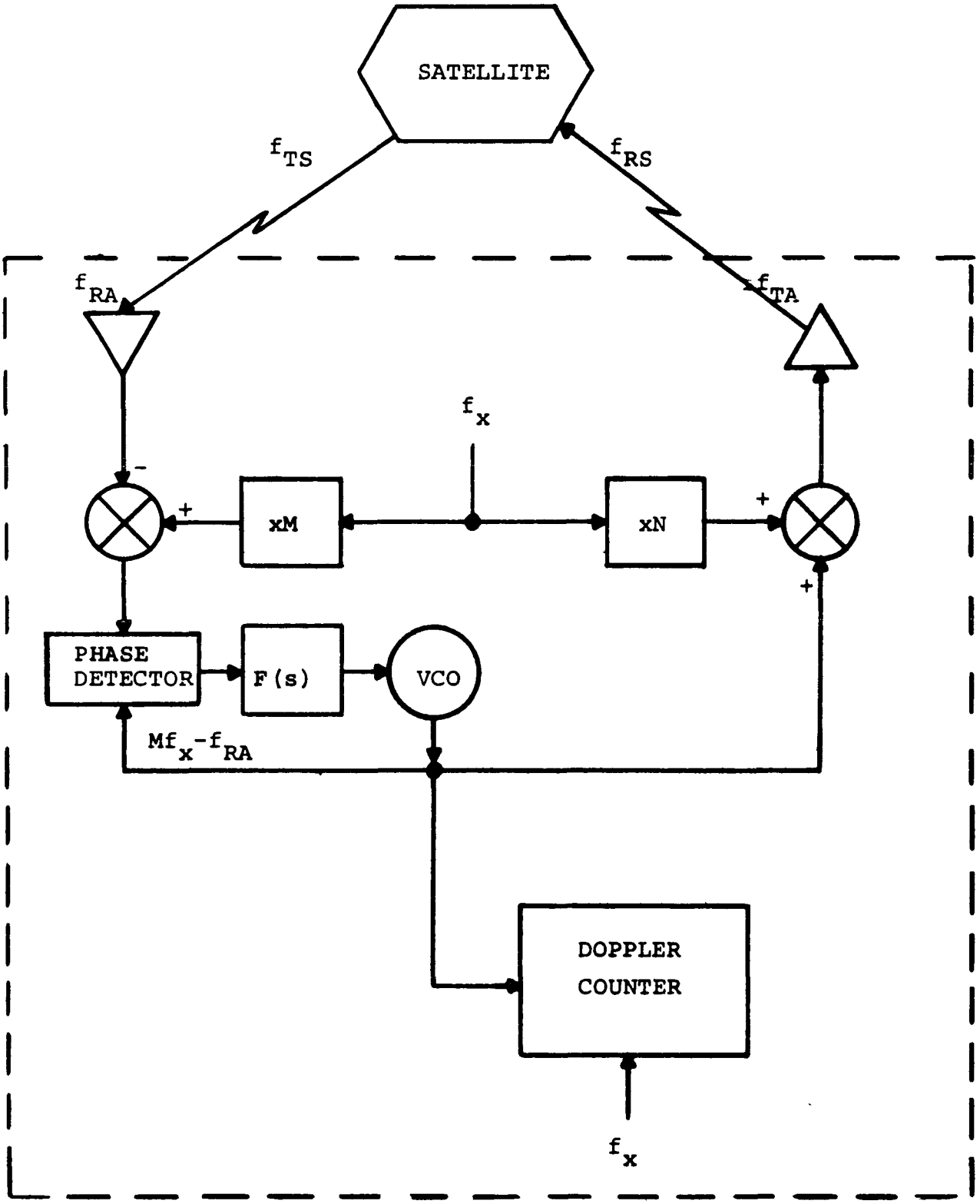

Figure 2-9. Single-Oscillator Aircraft Transponder

where f_X is the on-board oscillator frequency, and M and N are multiplier factors. The value of f_X is not known a priori and may be computed using this method. The frequency f_X is equal to the nominal oscillator frequency f_o plus the error Δf. The IF frequency in the aircraft terminal is measured as for the range-rate measurement. If the count obtained is F, then the following relationship applies,

$$Mf_X - f_{RA} = F\, f_X/f_o \tag{2-63}$$

The measurement F is relayed to the ground station.

If it is assumed further that the relay satellite is coherent and remodulating, then other frequencies in the system can be computed. These are listed below.

$$f_{RA} = f_{TS}\,[1 + \dot{R}_A/c] \tag{2-64}$$

$$f_{TS} = f_{TG}\, S_1\, [1 + \dot{R}_G/c] \tag{2-65}$$

$$f_{RS} = f_{TA}\,[1 + \dot{R}_A/c] \tag{2-66}$$

where

f_{TS} = satellite-to-aircraft transmit frequency

f_{TG} = ground station-to-satellite transmit frequency

f_{RS} = satellite-from-aircraft receive frequency

S_1 = satellite translation frequency ratio

$\dot{R}_G$ = range-rate of satellite-to-ground station

and c = velocity of light

The frequency that is measured at the ground station is the channel frequency that exists after demodulation of the received satellite carrier signal. This channel carrier frequency Δf_{RG} is derived in the coherent satellite by down-converting the received aircraft transmission with respect to the satellite

synthesizer derived frequency. In a coherent satellite transponder, all synthesizer frequencies are derived from a reference frequency transmitted by the ground. The channel frequency as measured at the ground can thus be written as

$$\Delta f_{RG} = f_{RS} - f_{TG} S_2 [1 + \dot{R}_G/c] \qquad (2\text{-}67)$$

The constant S_2 relates the satellite aircraft receiver band down-conversion frequency to the synthesizer reference frequency received in the satellite.

In the Equations (2-62) and (2-67) the unknowns are $\dot{R}_A$, $\dot{R}_G$ and f_X. The term $\dot{R}_G$ will be derived by making doppler measurements, as described above, with respect to a reference terminal located at the ground station. In this case, $\dot{R}_A$ equals $\dot{R}_G$. When $\dot{R}_G$ has been computed, the Equations (2-62) to (2-67) can be solved for $\dot{R}_A$ and f_X and hence the on-board frequency can be measured. The results of this measurement would then be relayed to the aircraft so that its oscillator frequency can be updated.

If a coherent translating satellite is used, then the aircraft oscillator frequency can still be computed. The equations involved, however, will be slightly different. If a multiple oscillator translating satellite transponder is used, then additional measurements would be necessary to eliminate the frequency uncertainty of these oscillators in the range-rate equations.

3. POSITION LOCATION ERROR ANALYSIS

3.1 Error Sources

The recommended ranging system is designed to obtain an effective ranging accuracy of 1500 meters. In actuality, the total range measurement error is caused by the combined effects of several independent error sources. The purpose of this section is to describe the effects and derive values of the errors caused by each source.

Error sources have been separated into four categories as follows:

(1) Geometric errors introduced by the diurnal position variations of the satellites

(2) Propagation errors consisting of ionospheric and tropospheric effects, multipath influence, and uncertainty in the speed of light

(3) Measurement errors caused by system noise and ground processor inaccuracies

(4) Delay errors caused by uncompensated delays of the aircraft, reference terminal, satellite transponders, and the ground processor.

Ionospheric and tropospheric propagation errors are given for a worst-case elevation angle of 10 degrees. Compensation for a large portion of the absolute range errors will be accomplished by the use of a differential measurement technique which utilizes range measurements to a reference terminal. Range error values presented for each error source are essentially worst-case values and are considered conservative, with the values seldom being exceeded. Several error values reflect improvements and innovations recommended by Texas Instruments. The exact nature and consequence of each error source are discussed in the following paragraphs.

3.1.1 Geometric Position Location Errors

The position of most synchronous satellites is not completely stationary with respect to the earth because of satellite orbital inclination of 2 to 3 degrees. During the course of one 24-hour day, the range between a point on the earth's surface (e.g., the ground station) and the satellite can vary considerably. Figure 2-10 shows the variation of the range from Dallas to ATS-I during the period between 1500 hours on April 2, 1970 and 1500 hours on April 3, 1970. From a peak range of approximately 39,480 km at 0800, the range decreases 300 km 12 hours later when it reaches the minimum value of 39,180 km. By applying the position location equations of Section II-2.2, the result of a range change unsuspected by the user can be demonstrated. Because it simplifies the position location equations, it is assumed that the satellites are directly over the equator at longitudes of 50°W and 150°W. Using these satellite positions and Equations (2-26), (2-27), (2-35), (2-48), and (2-49), as shown in Section II-2.2, the maximum range gives an aircraft position of 37.63°N, 99.14°W. The minimum range produces the aircraft position of 40.71°N, 101.27°W. (For these calculations, the second satellite is assumed to be stationary, and the value of D2 in Equation (2-49) is arbitrarily chosen as 0.50.) The distance between the minimum and maximum range locations is approximately 400 km. It is apparent that without some method to compensate for this large geometrically introduced aircraft position error, the accuracy of any satellite navigation system is severely compromised.

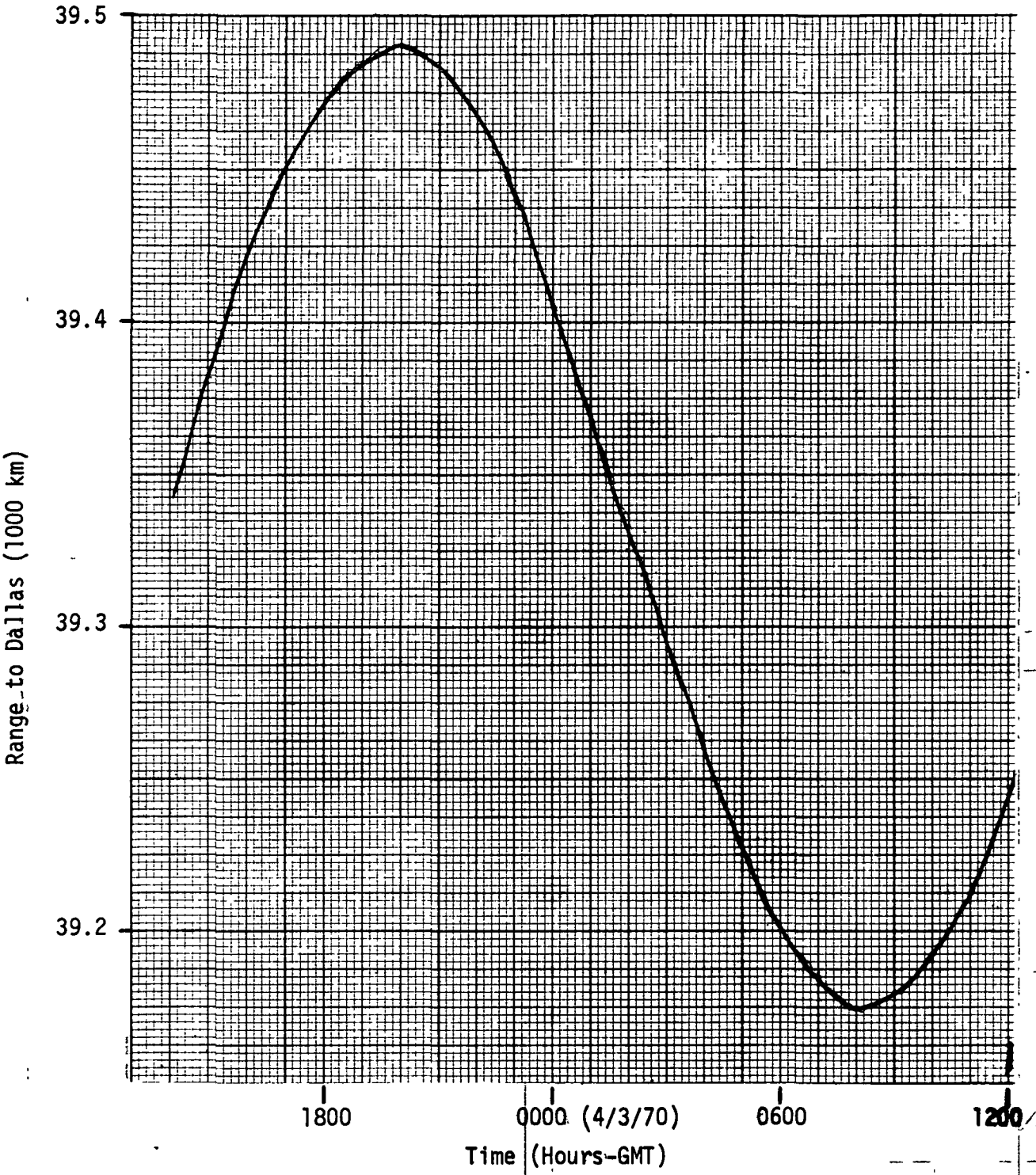

Figure 2-10. Variation of the Range of ATS-I from Dallas for One Day

Correction for these variations can take a number of forms, the most promising of which is to control the phase of the transmitted ranging tones in such a manner as to hold the signal phase constant at a reference receiver. This technique can be applied to navigation by producing a constant and stationary phase plane in the vicinity of the satellite, thus creating an effectively stationary satellite reference station. It can be implemented by using a reference terminal located at the control center, or any other judicious location on the ground, and adjusting the phase of the ranging signals generated by the satellites so as to keep a constant phase at the reference terminal on the ground.

While this technique provides increased accuracy when compared to the uncompensated system, the improved performance is degraded as the distance between the user and the reference terminal is increased. This deficiency can be corrected by providing multiple reference terminals to extend the area of coverage or, in other words, reduce the maximum distance a user can be from the reference terminal. By time multiplexing the ground control center between reference terminals, the equipment needed at each terminal can be reduced to a single transponder. The major complication introduced into the system by adding simple transponding reference terminals which are not collocated with the ground control center is that the constand phase plane transmission must be a round-trip path from the GCC to the reference station through the satellite and back so that the signal processing can be done at the GCC. This doubles the transport delay time in the phase control loop compared to the case when the reference terminal and the GCC are in the same location, and means that the phase at the reference terminal must be inferred from the average phase shift over the two-way link. The accuracy of the phase adjustment depends on the stability of the system configuration (i.e., the rate of change of ionospheric bias and the rate of change of satellite position), the phase measurement accuracy, and the delay before the computed phase adjustment is actually transmitted to the sector.

3.1.1.1 Computer Analysis of Geometric Error

Given the magnitude of aircraft position location error resulting from uncompensated satellite movement, and a constant phase plane technique to counteract this affect, the next step is to determine how completely the constant phase plane technique cancels geometrically introduced aircraft position location errors. This has been done by computer simulation of the satellite navigation system.

The computer model first precisely locates the aircraft in the zone around the ground control center situated at Dallas, Texas. Then the two satellites are perturbed from the

positions assumed for each by the aircraft, and the aircraft is located by satellite ranging using the equations developed in Section II-2.2. Next, the true aircraft position and the calculated position are compared and the maximum, minimum, and root mean square aircraft position location errors are calculated as a function of distance and direction from the ground control center. The satellite perturbations are categorized by altitude, longitude, and latitude. Figure 2-11 is a sample of the output produced by the program. The first two columns give the perturbation of each satellite in kilometers. These perturbations are made about the assumed satellite positions with the positive sign indicating movement away from the earth surface in the case of altitude, or increasing latitude and longitude in the conventional sense. The variable RGCC is the distance of the aircraft from the ground control center in kilometers. The next three columns list the maximum, minimum and root mean square aircraft position error for each radius. Inside the parentheses following EMAX and EMIN is a number indicating the direction of each error. This number shows the compass heading as referenced to the GCC, as illustrated in Figure 2-12.

The computer output reproduced in Figure 2-11 is of particular interest because the altitude and longitude cases represent the worst-case diurnal position excursions for the ATS-I satellite. The 50-km satellite latitude perturbation for both satellites, while not the maximum diurnal position excursion for either satellite, shows that the worst-case position error for satellite latitude perturbations occurs when both satellites are perturbed in the same direction. This contrasts with the altitude and longitude cases where the worst case occurs when the satellites are perturbed in opposite directions.

Another point to notice is that the errors produced by satellite perturbations are symmetrical. That is, moving ATS-I in a positive direction and ATS-III in a negative direction results in the same aircraft error as does moving ATS-I the same amount negatively and ATS-III the same amount positively. Finally, the worst-case altitude error produces a maximum aircraft error of only 190 meters at a distance of 1500 km from the ground station. This is sufficiently accurate so that ephemeris data to correct for altitude perturbations will not be required.

The error results for the most disadvantageous satellite perturbations will now be plotted on log-log axes to aid in the determination of a mathematical equation to describe the variation of aircraft position location error as a function of aircraft distance from the GCC. Choosing the worst-case satellite error perturbations insures that the aircraft position location error equations will not assess the magnitude of the geometrically introduced position errors too optimistically. Root mean square values will be used to derive the error

ATS-I ERR = 50 ATS-III ERR = 0	RGCC = 20	EMAX(7) = 1.516745D-03	EMIN(11) = 3.367243D-05	ERMS = 9.814841D-04
	RGCC = 50	EMAX(7) = 4.293735D-03	EMIN(4) = 2.396133D-04	ERMS = 2.509729D-03
	RGCC = 100	EMAX(7) = 9.920238D-03	EMIN(4) = 9.124570D-04	ERMS = 5.349183D-03
	RGCC = 200	EMAX(7) = 2.160481D-02	EMIN(14) = 8.992301D-04	ERMS = 1.198101D-02
	RGCC = 500	EMAX(10) = 4.959273D-02	EMIN(7) = 1.824127D-03	ERMS = 2.993936D-02
	RGCC = 800	EMAX(11) = 8.027441D-02	EMIN(7) = 7.988764D-03	ERMS = 4.391474D-02
	RGCC = 1000	EMAX(12) = 9.885127D-02	EMIN(11) = 2.404671D-03	ERMS = 5.536823D-02
	RGCC = 1500	EMAX(11) = 1.708104D-01	EMIN(7) = 1.430881D-02	ERMS = 9.078706D-02
ATS-I ERR = 0 ATS-III ERR = 50	RGCC = 20	EMAX(11) = 1.115355D-03	EMIN(7) = 1.130426D-04	ERMS = 7.074690D-04
	RGCC = 50	EMAX(11) = 3.204467D-03	EMIN(14) = 3.898436D-04	ERMS = 1.821818D-03
	RGCC = 100	EMAX(11) = 7.519780D-03	EMIN(14) = 3.760663D-04	ERMS = 3.952499D-03
	RGCC = 200	EMAX(11) = 1.653189D-02	EMIN(4) = 1.571088D-05	ERMS = 9.079885D-03
	RGCC = 500	EMAX(12) = 3.955096D-02	EMIN(10) = 3.128846D-04	ERMS = 2.266955D-02
	RGCC = 800	EMAX(7) = 6.077496D-02	EMIN(12) = 5.110193D-03	ERMS = 3.246962D-02
	RGCC = 1000	EMAX(6) = 8.030269D-02	EMIN(4) = 1.817230D-03	ERMS = 4.089760D-02
	RGCC = 1500	EMAX(7) = 1.301330D-01	EMIN(3) = 1.439450D-02	ERMS = 6.785598D-02
ATS-I ERR = 50 ATS-III ERR = 50	RGCC = 20	EMAX(8) = 1.653424D-03	EMIN(13) = 6.505524D-04	ERMS = 1.254077D-03
	RGCC = 50	EMAX(8) = 4.280251D-03	EMIN(4) = 1.583975D-03	ERMS = 3.162356D-03
	RGCC = 100	EMAX(8) = 8.939004D-03	EMIN(4) = 2.983635D-03	ERMS = 6.488721D-03
	RGCC = 200	EMAX(7) = 1.820516D-02	EMIN(14) = 5.944824D-03	ERMS = 1.364695D-02
	RGCC = 500	EMAX(10) = 4.981895D-02	EMIN(13) = 1.608604D-02	ERMS = 3.434251D-02
	RGCC = 800	EMAX(8) = 8.183565D-02	EMIN(13) = 2.562992D-02	ERMS = 5.340888D-02
	RGCC = 1000	EMAX(8) = 1.040256D-01	EMIN(14) = 2.766575D-02	ERMS = 6.814352D-02
	RGCC = 1500	EMAX(9) = 1.790599D-01	EMIN(13) = 4.799801D-02	ERMS = 1.108535D-01
ATS-I ERR = 50 ATS-III ERR = -50	RGCC = 20	EMAX(6) = 1.645824D-03	EMIN(2) = 6.721253D-04	ERMS = 1.164814D-03
	RGCC = 50	EMAX(7) = 4.771566D-03	EMIN(3) = 1.303541D-03	ERMS = 3.041058D-03
	RGCC = 100	EMAX(7) = 1.163359D-02	EMIN(4) = 1.846697D-03	ERMS = 6.814548D-03
	RGCC = 200	EMAX(6) = 2.832902D-02	EMIN(14) = 4.798127D-03	ERMS = 1.631457D-02
	RGCC = 500	EMAX(6) = 6.572316D-02	EMIN(2) = 1.732446D-02	ERMS = 4.054340D-02
	RGCC = 800	EMAX(11) = 8.931975D-02	EMIN(6) = 1.286777D-02	ERMS = 5.583648D-02
	RGCC = 1000	EMAX(12) = 1.275654D-01	EMIN(14) = 1.984109D-02	ERMS = 6.957194D-02
	RGCC = 1500	EMAX(11) = 1.882832D-01	EMIN(15) = 4.173095D-02	ERMS = 1.158691D-01
ATS-I ERR = -50 ATS-III ERR = 50	RGCC = 20	EMAX(6) = 1.647895D-03	EMIN(2) = 6.719752D-04	ERMS = 1.165757D-03
	RGCC = 50	EMAX(7) = 4.780050D-03	EMIN(3) = 1.302195D-03	ERMS = 3.043396D-03
	RGCC = 100	EMAX(7) = 1.165175D-02	EMIN(4) = 1.841609D-03	ERMS = 6.819169D-03
	RGCC = 200	EMAX(6) = 2.835618D-02	EMIN(14) = 4.786171D-03	ERMS = 1.632388D-02
	RGCC = 500	EMAX(6) = 6.579610D-02	EMIN(2) = 1.730588D-02	ERMS = 4.056682D-02
	RGCC = 800	EMAX(11) = 8.948512D-02	EMIN(6) = 1.283257D-02	ERMS = 5.587453D-02
	RGCC = 1000	EMAX(12) = 1.277297D-01	EMIN(14) = 1.979036D-02	ERMS = 6.962101D-02
	RGCC = 1500	EMAX(11) = 1.886544D-01	EMIN(15) = 4.166020D-02	ERMS = 1.159469D-01
ATS-I ERR = -50 ATS-III ERR = -50	RGCC = 20	EMAX(8) = 1.657072D-03	EMIN(13) = 6.519769D-04	ERMS = 1.256802D-03
	RGCC = 50	EMAX(8) = 4.289741D-03	EMIN(4) = 1.587238D-03	ERMS = 3.169232D-03
	RGCC = 100	EMAX(8) = 8.958937D-03	EMIN(4) = 2.989929D-03	ERMS = 6.502848D-03
	RGCC = 200	EMAX(7) = 1.824656D-02	EMIN(14) = 5.957213D-03	ERMS = 1.367672D-02
	RGCC = 500	EMAX(10) = 4.993226D-02	EMIN(13) = 1.612097D-02	ERMS = 3.441764D-02
	RGCC = 800	EMAX(8) = 8.202312D-02	EMIN(13) = 2.568538D-02	ERMS = 5.352587D-02
	RGCC = 1000	EMAX(8) = 1.042647D-01	EMIN(14) = 2.772283D-02	ERMS = 6.829461D-02
	RGCC = 1500	EMAX(9) = 1.794735D-01	EMIN(13) = 4.810153D-02	ERMS = 1.111035D-01

Figure 2-11(a). Position Error Simulation Program -Altitude Perturbation (km)

ATS-I ERR = 50	RGCC = 20	EMAX(10) = 2.003599D-02	EMIN(14) = 1.079932D-03	ERMS = 1.351162D-02
	RGCC = 50	EMAX(11) = 5.496609D-02	EMIN(14) = 1.757286D-03	ERMS = 3.421313D-02
	RGCC = 100	EMAX(11) = 1.230379D-01	EMIN(7) = 6.115912D-03	ERMS = 7.106616D-02
	RGCC = 200	EMAX(11) = 2.590028D-01	EMIN(3) = 2.173620D-02	ERMS = 1.535046D-01
ATS-III ERR = 0	RGCC = 500	EMAX(8) = 6.104037D-01	EMIN(11) = 1.051468D-01	ERMS = 3.847050D-01
	RGCC = 800	EMAX(3) = 9.808158D-01	EMIN(15) = 6.043571D-03	ERMS = 5.895292D-01
	RGCC = 1000	EMAX(10) = 1.141678D 00	EMIN(7) = 1.491182D-01	ERMS = 7.134883D-01
	RGCC = 1500	EMAX(4) = 1.901980D 00	EMIN(11) = 1.034134D-01	ERMS = 1.171194D 00
	RGCC = 20	EMAX(8) = 1.939967D-02	EMIN(4) = 8.004567D-04	ERMS = 1.313527D-02
	RGCC = 50	EMAX(8) = 5.122903D-02	EMIN(4) = 5.435914D-03	ERMS = 3.309279D-02
ATS-I ERR = 0	RGCC = 100	EMAX(7) = 1.097096D-01	EMIN(11) = 1.043685D-02	ERMS = 6.775912D-02
	RGCC = 200	EMAX(7) = 2.285742D-01	EMIN(11) = 8.994539D-03	ERMS = 1.426377D-01
ATS-III ERR = 50	RGCC = 500	EMAX(10) = 5.654740D-01	EMIN(14) = 1.315174D-01	ERMS = 3.580633D-01
	RGCC = 800	EMAX(15) = 8.971954D-01	EMIN(14) = 1.062599D-01	ERMS = 5.605977D-01
	RGCC = 1000	EMAX(8) = 1.074042D 00	EMIN(14) = 2.016150D-01	ERMS = 6.824775D-01
	RGCC = 1500	EMAX(14) = 1.679138D 00	EMIN(4) = 2.284850D-01	ERMS = 1.106920D 00
	RGCC = 20	EMAX(12) = 1.672310D-02	EMIN(15) = 1.250948D-02	ERMS = 1.458099D-02
	RGCC = 50	EMAX(11) = 4.862089D-02	EMIN(14) = 2.618517D-02	ERMS = 3.753162D-02
	RGCC = 100	EMAX(11) = 1.162983D-01	EMIN(14) = 3.351110D-02	ERMS = 8.139940D-02
ATS-I ERR = 50	RGCC = 200	EMAX(12) = 2.855103D-01	EMIN(4) = 7.834064D-02	ERMS = 1.880079D-01
	RGCC = 500	EMAX(14) = 6.901743D-01	EMIN(9) = 3.261453D-01	ERMS = 4.685561D-01
ATS-III ERR = 50	RGCC = 800	EMAX(3) = 9.157307D-01	EMIN(12) = 2.374173D-01	ERMS = 6.768827D-01
	RGCC = 1000	EMAX(6) = 1,188613D 00	EMIN(4) = 3.717283D-01	ERMS = 7.969157D-01
	RGCC = 1500	EMAX(4) = 2.034225D 00	EMIN(9) = 8.425808D-01	ERMS = 1.335962D 00
	RGCC = 20	EMAX(9) = 3.079782D-02	EMIN(13) = 7.065379D-03	ERMS = 2.230088D-02
	RGCC = 50	EMAX(9) = 7.728454D-02	EMIN(13) = 1.763238D-02	ERMS = 5.586661D-02
	RGCC = 100	EMAX(9) = 1.555606D-01	EMIN(13) = 3.516413D-02	ERMS = 1.124771D-01
ATS-I ERR = 50	RGCC = 200	EMAX(9) = 3.152831D-01	EMIN(13) = 6.994784D-02	ERMS = 2.290131D-01
	RGCC = 500	EMAX(9) = 8.238896D-01	EMIN(13) = 1.724729D-01	ERMS = 5.768242D-01
ATS-III ERR = -50	RGCC = 800	EMAX(9) = 1.388637D 00	EMIN(13) = 2.732639D-01	ERMS = 9.301236D-01
	RGCC = 1000	EMAX(9) = 1.806503D 00	EMIN(13) = 3.401568D-01	ERMS = 1.146358D 00
	RGCC = 1500	EMAX(9) = 3.067576D 00	EMIN(13) = 5.093059D-01	ERMS = 1.846396D 00
	RGCC = 20	EMAX(9) = 3.081971D-02	EMIN(13) = 7.052124D-03	ERMS = 2.231393D-02
	RGCC = 50	EMAX(9) = 7.733855D-02	EMIN(13) = 1.759920D-02	ERMS = 5.589857D-02
	RGCC = 100	EMAX(9) = 1.556661D-01	EMIN(13) = 3.509760D-02	ERMS = 1.125368D-01
ATS-I ERR = -50	RGCC = 200	EMAX(9) = 3.154832D-01	EMIN(13) = 6.981420D-02	ERMS = 2.291139D-01
	RGCC = 500	EMAX(9) = 8.242808D-01	EMIN(13) = 1.721350D-01	ERMS = 5.770611D-01
ATS-III ERR = 50	RGCC = 800	EMAX(9) = 1.388994D 00	EMIN(13) = 2.727184D-01	ERMS = 9.304980D-01
	RGCC = 1000	EMAX(9) = 1.806622D 00	EMIN(13) = 3.394720D-01	ERMS = 1.146781D 00
	RGCC = 1500	EMAX(9) = 3.065493D 00	EMIN(13) = 5.082732D-01	ERMS = 1.846374D 00
	RGCC = 20	EMAX(12) = 1.672578D-02	EMIN(15) = 1.250556D-02	ERMS = 1.458105D-02
	RGCC = 50	EMAX(11) = 4.863410D-02	EMIN(14) = 2.617671D-02	ERMS = 3.753166D-02
	RGCC = 100	EMAX(11) = 1.163241D-01	EMIN(14) = 3.350091D-02	ERMS = 8.139876D-02
ATS-1 ERR = -50	RGCC = 200	EMAX(12) = 2.855206D-01	EMIN(4) = 7.831485D-02	ERMS = 1.880041D-01
	RGCC = 500	EMAX(14) = 6.902813D-01	EMIN(9) = 3.261723D-01	ERMS = 4.685471D-01
ATS-III ERR = -50	RGCC = 800	EMAX(3) = 9.159412D-01	EMIN(12) = 2.373395D-01	ERMS = 6.768766D-01
	RGCC = 1000	EMAX(6) = 1.188520D 00	EMIN(4) = 3.716314D-01	ERMS = 7.969099D-01
	RGCC = 1500	EMAX(4) = 2.034759D 00	EMIN(9) = 8.426756D-01	ERMS = 1.335945D 00

Figure 2-11(b). Position Error Simulation Program - Longitude Perturbation (km)

ATS-I ERR = 50 ATS-III ERR = 0	RGCC = 20	EMAX(9) = 3.144005D-02	EMIN(13) = 1.058224D-03	ERMS = 2.212503D-02
	RGCC = 50	EMAX(9) = 7.924563D-02	EMIN(13) = 2.645340D-03	ERMS = 5.532471D-02
	RGCC = 100	EMAX(9) = 1.606919D-01	EMIN(13) = 5.289872D-03	ERMS = 1.107342D-01
	RGCC = 200	EMAX(9) = 3.305744D-01	EMIN(13) = 1.057596D-02	ERMS = 2.221016D-01
	RGCC = 500	EMAX(9) = 9.042731D-01	EMIN(13) = 2.640067D-02	ERMS = 5.650120D-01
	RGCC = 800	EMAX(9) = 1.598221D 00	EMIN(13) = 4.215262D-02	ERMS = 9.341344D-01
	RGCC = 1000	EMAX(9) = 2.148387D 00	EMIN(13) = 5.259958D-02	ERMS = 1.204030D 00
	RGCC = 1500	EMAX(9) = 3.977251D 00	EMIN(13) = 7.846828D-02	ERMS = 2.023572D 00
ATS-I ERR = 0 ATS-III ERR = 50	RGCC = 20	EMAX(9) = 2.978775D-02	EMIN(5) = 1.073371D-03	ERMS = 2.097165D-02
	RGCC = 50	EMAX(9) = 7.503956D-02	EMIN(5) = 2.682082D-03	ERMS = 5.243960D-02
	RGCC = 100	EMAX(9) = 1.520232D-01	EMIN(5) = 5.359624D-03	ERMS = 1.049531D-01
	RGCC = 200	EMAX(9) = 3.121666D-01	EMIN(5) = 1.070062D-02	ERMS = 2.104687D-01
	RGCC = 500	EMAX(9) = 8.492416D-01	EMIN(5) = 2.660277D-02	ERMS = 5.346386D-01
	RGCC = 800	EMAX(9) = 1.492869D 00	EMIN(5) = 4.230536D-02	ERMS = 8.816698D-01
	RGCC = 1000	EMAX(9) = 1.999732D 00	EMIN(5) = 5.265178D-02	ERMS = 1.133318D 00
	RGCC = 1500	EMAX(9) = 3.671517D 00	EMIN(5) = 7.804631D-02	ERMS = 1.890743D 00
ATS-I ERR = 50 ATS-III ERR = 50	RGCC = 20	EMAX(9) = 5.583197D-02	EMIN(13) = 8.791318D-04	ERMS = 3.924689D-02
	RGCC = 50	EMAX(9) = 1.408635D-01	EMIN(13) = 2.197828D-03	ERMS = 9.813724D-02
	RGCC = 100	EMAX(9) = 2.861015D-01	EMIN(13) = 4.395680D-03	ERMS = 1.964172D-01
	RGCC = 200	EMAX(9) = 5.904601D-01	EMIN(13) = 8.791654D-03	ERMS = 3.939742D-01
	RGCC = 500	EMAX(9) = 1.630439D 00	EMIN(13) = 2.198532D-02	ERMS = 1.004861D 00
	RGCC = 800	EMAX(9) = 2.907565D 00	EMIN(13) = 3.519606D-02	ERMS = 1.669271D 00
	RGCC = 1000	EMAX(9) = 3.930608D 00	EMIN(13) = 4.401802D-02	ERMS = 2.161075D 00
	RGCC = 1500	EMAX(9) = 7.369632D 00	EMIN(13) = 6.614804D-02	ERMS = 3.676660D 00
ATS-I ERR = 50 ATS-III ERR = -50	RGCC = 20	EMAX(9) = 2.518394D-02	EMIN(5) = 1.941712D-03	ERMS = 1.784032D-02
	RGCC = 50	EMAX(9) = 6.307190D-02	EMIN(5) = 4.852989D-03	ERMS = 4.461145D-02
	RGCC = 100	EMAX(9) = 1.265161D-01	EMIN(5) = 9.701515D-03	ERMS = 8.929261D-02
	RGCC = 200	EMAX(9) = 2.545115D-01	EMIN(5) = 1.938398D-02	ERMS = 1.789666D-01
	RGCC = 500	EMAX(9) = 6.472015D-01	EMIN(5) = 4.829328D-02	ERMS = 4.475448D-01
	RGCC = 800	EMAX(9) = 1.052688D 00	EMIN(5) = 7.694588D-02	ERMS = 7.160789D-01
	RGCC = 1000	EMAX(9) = 1.330070D 00	EMIN(5) = 9.587381D-02	ERMS = 8.923070D-01
	RGCC = 1500	EMAX(9) = 2.049446D 00	EMIN(5) = 1.424517D-01	ERMS = 1.344662D 00
ATS-I ERR = -50 ATS-III ERR = 50	RGCC = 20	EMAX(9) = 2.518300D-02	EMIN(5) = 1.941708D-03	ERMS = 1.783966D-02
	RGCC = 50	EMAX(9) = 6.306955D-02	EMIN(5) = 4.852974D-03	ERMS = 4.460982D-02
	RGCC = 100	EMAX(9) = 1.265113D-01	EMIN(5) = 9.701469D-03	ERMS = 8.928934D-02
	RGCC = 200	EMAX(9) = 2.545019D-01	EMIN(5) = 1.938384D-02	ERMS = 1.789601D-01
	RGCC = 500	EMAX(9) = 6.471777D-01	EMIN(5) = 4.829249D-02	ERMS = 4.475293D-01
	RGCC = 800	EMAX(9) = 1.052655D 00	EMIN(5) = 7.694396D-02	ERMS = 7.160567D-01
	RGCC = 1000	EMAX(9) = 1.330038D 00	EMIN(5) = 9.587087D-02	ERMS = 8.922828D-01
	RGCC = 1500	EMAX(9) = 2.049483D 00	EMIN(5) = 1.424454D-01	ERMS = 1.344652D 00
ATS-I ERR = -50 ATS-III ERR = -50	RGCC = 20	EMAX(9) = 5.582053D-02	EMIN(13) = 8.788378D-04	ERMS = 3.923832D-02
	RGCC = 50	EMAX(9) = 1.408376D-01	EMIN(13) = 2.197093D-03	ERMS = 9.811593D-02
	RGCC = 100	EMAX(9) = 2.860597D-01	EMIN(13) = 4.394210D-03	ERMS = 1.963755D-01
	RGCC = 200	EMAX(9) = 5.904227D-01	EMIN(13) = 8.788715D-03	ERMS = 3.938981D-01
	RGCC = 500	EMAX(9) = 1.630864D 00	EMIN(13) = 2.197797D-02	ERMS = 1.004809D 00
	RGCC = 800	EMAX(9) = 2.909729D 00	EMIN(13) = 3.518428D-02	ERMS = 1.669665D 00
	RGCC = 1000	EMAX(9) = 3.935317D 00	EMIN(13) = 4.400329D-02	ERMS = 2.162236D 00
	RGCC = 1500	EMAX(9) = 7.392806D 00	EMIN(13) = 6.612587D-02	ERMS = 3.683675D 00

Figure 2-11(c). Position Error Simulation Program - Latitude Perturbation (km)

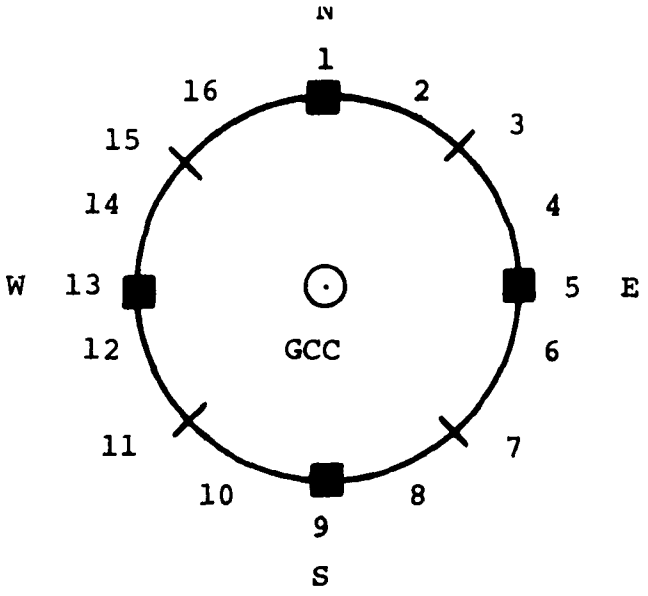

Figure 2-12. Computed Error Direction Key

equations. The rationale for choosing ERMS instead of EMAX or EMIN lies in the fact that the root mean square value is the standard deviation of the error, giving a measure of the fluctuation of the error about its mean value. Like the analogous electrical quantity, rms volts, the rms aircraft position location error is the "ac" component of the error. Figure 2-13 confirms that ERMS is a reasonable estimate of the typical aircraft position location error as it clearly matches the behavior of both EMAX and EMIN in terms of slope and linearity, but falls closer to the maximum error reflecting the prevalence of the larger error values for a given radius.

The linearity of the aircraft position error as a function of distance from the ground control center when plotted on log-log axes is shown in Figure 2-14 where four values of the parameter S_ϕ (the magnitude of the worst-case satellite latitude error perturbation) are plotted. From the figure, it is clear that multiplication of the satellite perturbation by a constant results in multiplication of the aircraft position location error by the same constant. The linearity of this relationship combined with the fact that satellite altitude, longitude, and latitude are independent makes it possible to write the following equation for aircraft position error as a function of worst-case satellite perturbation, and distance of the aircraft from the reference terminal (which is located at the GCC in this simulation).

$$E = .001\, S_A R^{1.065} + .021\, S_\lambda R^{1.023} + .034\, S_\phi R^{1.052} \quad (2\text{-}68)$$

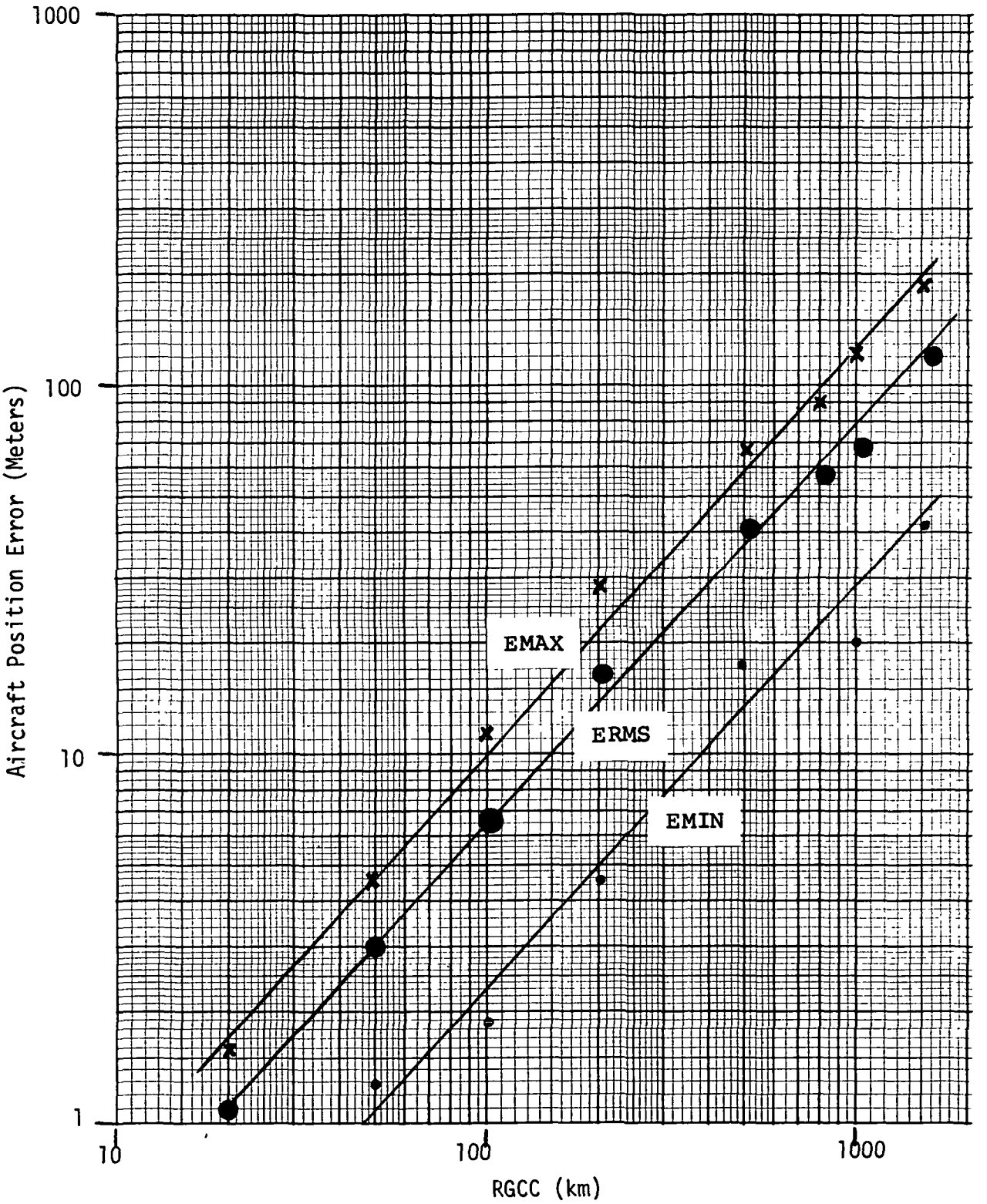

Figure 2-13. Aircraft Position Error vs Distance From GCC For Worst-Case Satellite Altitude Perturbation of 50 km

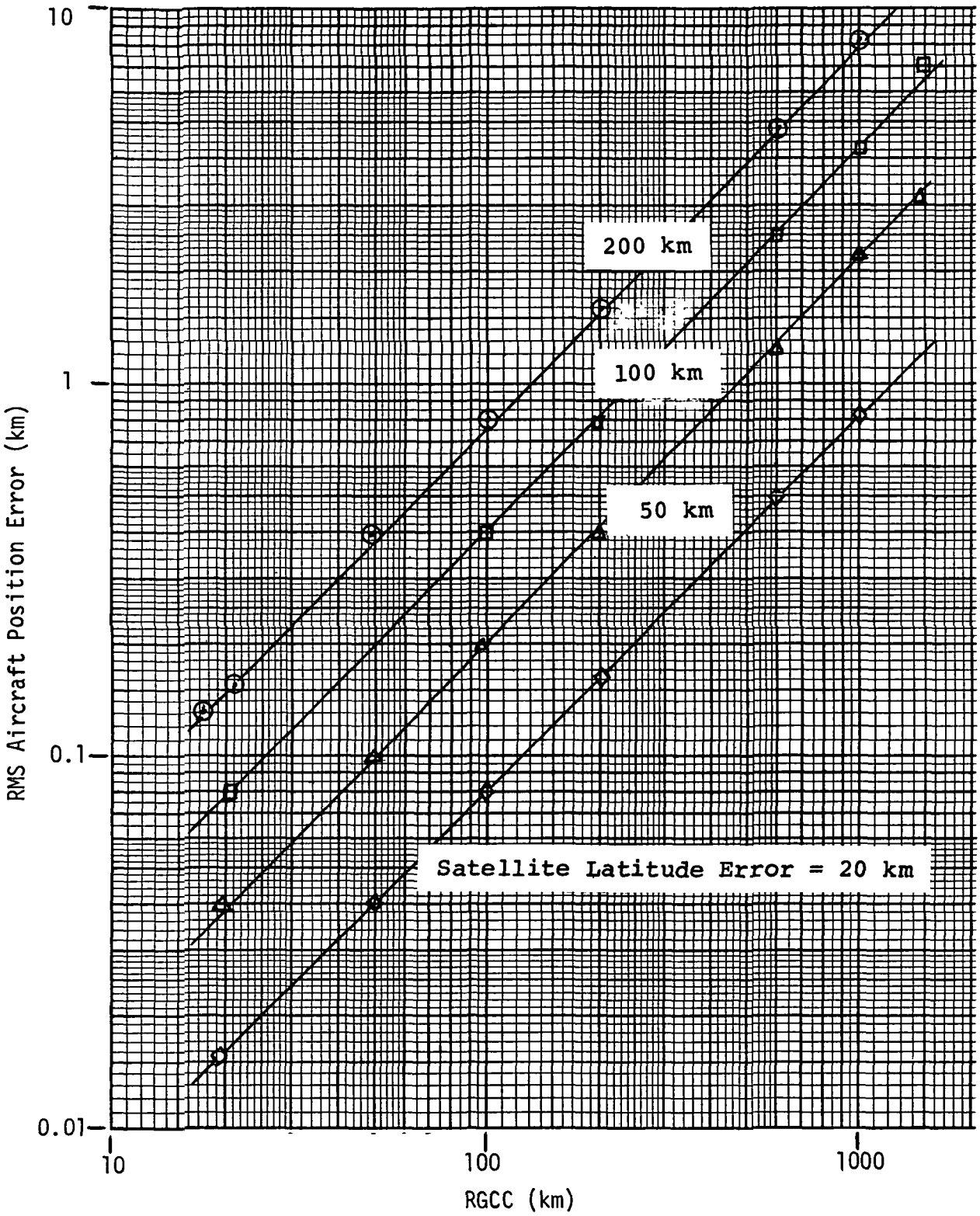

Figure 2-14. Aircraft Position Error vs Distance from GCC For Satellite Latitude Perturbations

where E = aircraft rms position error in meters

S = magnitude of satellite worst-case perturbation in km with subscripts: (A) indicating altitude perturbation, (λ) indicating longitude perturbation, and (ϕ) indicating latitude perturbation.

R = distance of aircraft from ground control center in km.

The exponents of R account for the slope of the straight line approximating the distribution of data points plotted on the log-log axes. This equation depends on the position of the satellites. In this case, both satellites were placed over the equator with one at 50°W and the other at 150°W. To modify the equation for a different satellite placement requires that the new coordinates be inserted in the computer simulation and a new set of error curves generated. It is important to note that the error predicted by this equation results from the most detrimetal combination of satellite perturbations and may be as much as a factor of three more pessimistic than the typical rms error resulting from a more optimum conjunction of satellite position errors.

The equation for aircraft error magnitude as a function of satellite position error and distance from the GCC was used to plot error contours showing aircraft error as a geographic function of position in order to determine the location of secondary reference stations. The data for the maps shown in Figures 2-15 and 2-16 was obtained by re-formatting and sorting the output of the aircraft navigation simulation program. The striking feature about these maps is the way that the error falls in bands of latitude. This means that reference stations need to be placed only on one line of constant longitudes, north and south of the ground control center to adequately compensate the phase of the ranging tones over a longitudinal distance of 1500 to 2000 km. The other conclusion which can be drawn from the maps is that the bands of constant aircraft error are more densely packed south of the ground control center than north of it, particularly in the case of satellite-latitude generated errors. This suggests that the ground station which generates the ranging tones is best located at the extreme southern end of the area of navigation coverage. The maps are drawn for the worst-case satellite error perturbations and for satellite excursions of only 50 km. In the case of satellite-latitude perturbation induced aircraft errors, 50 km is only a fraction of the expected satellite excursion. Since ephemeris data will be used (as described in the following section) to keep each user more up to date on satellite movement, basing the reference station placement on error contours generated with

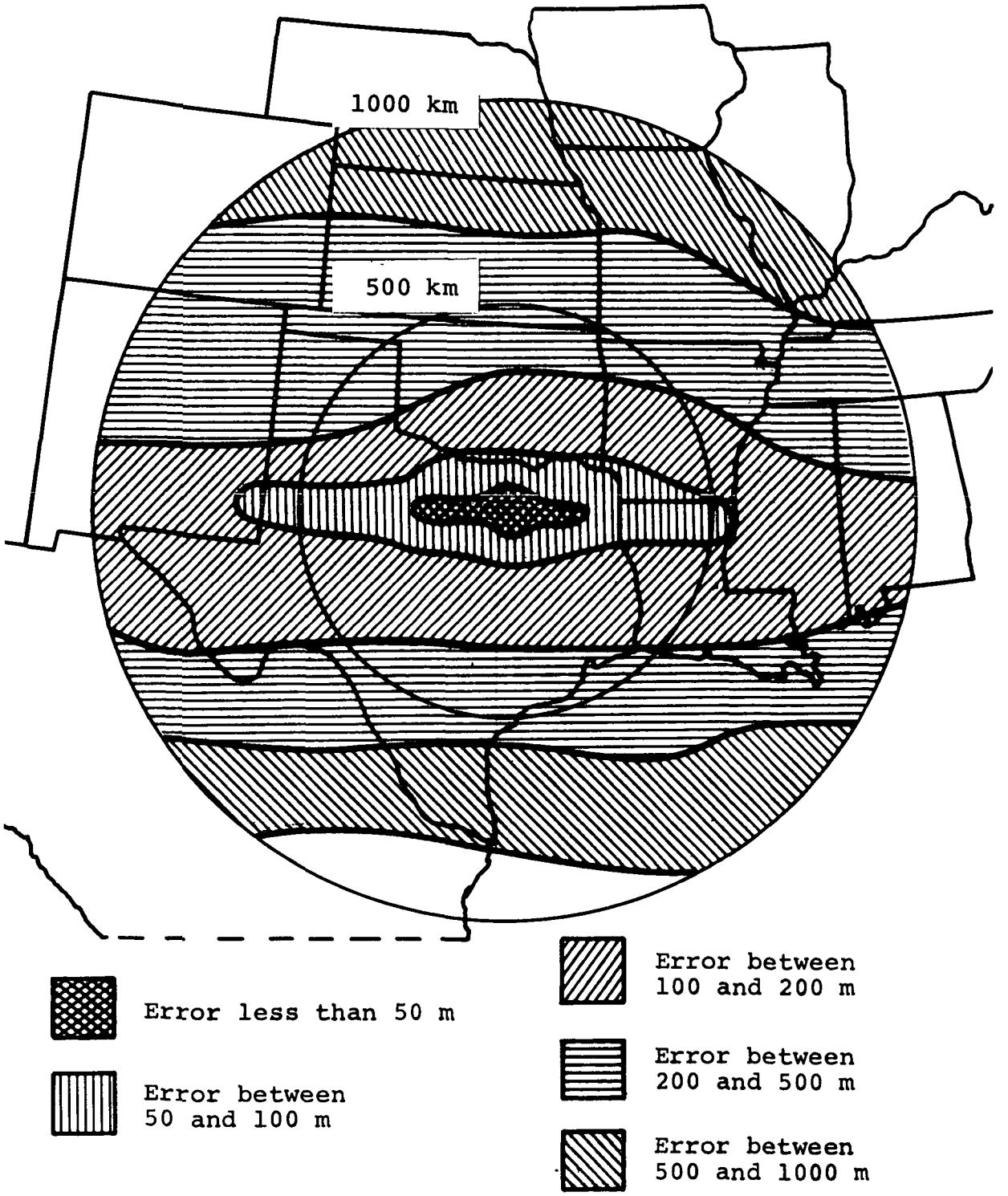

Figure 2-15. Aircraft Position Error Contours For Satellite Longitude Errors of 50 km

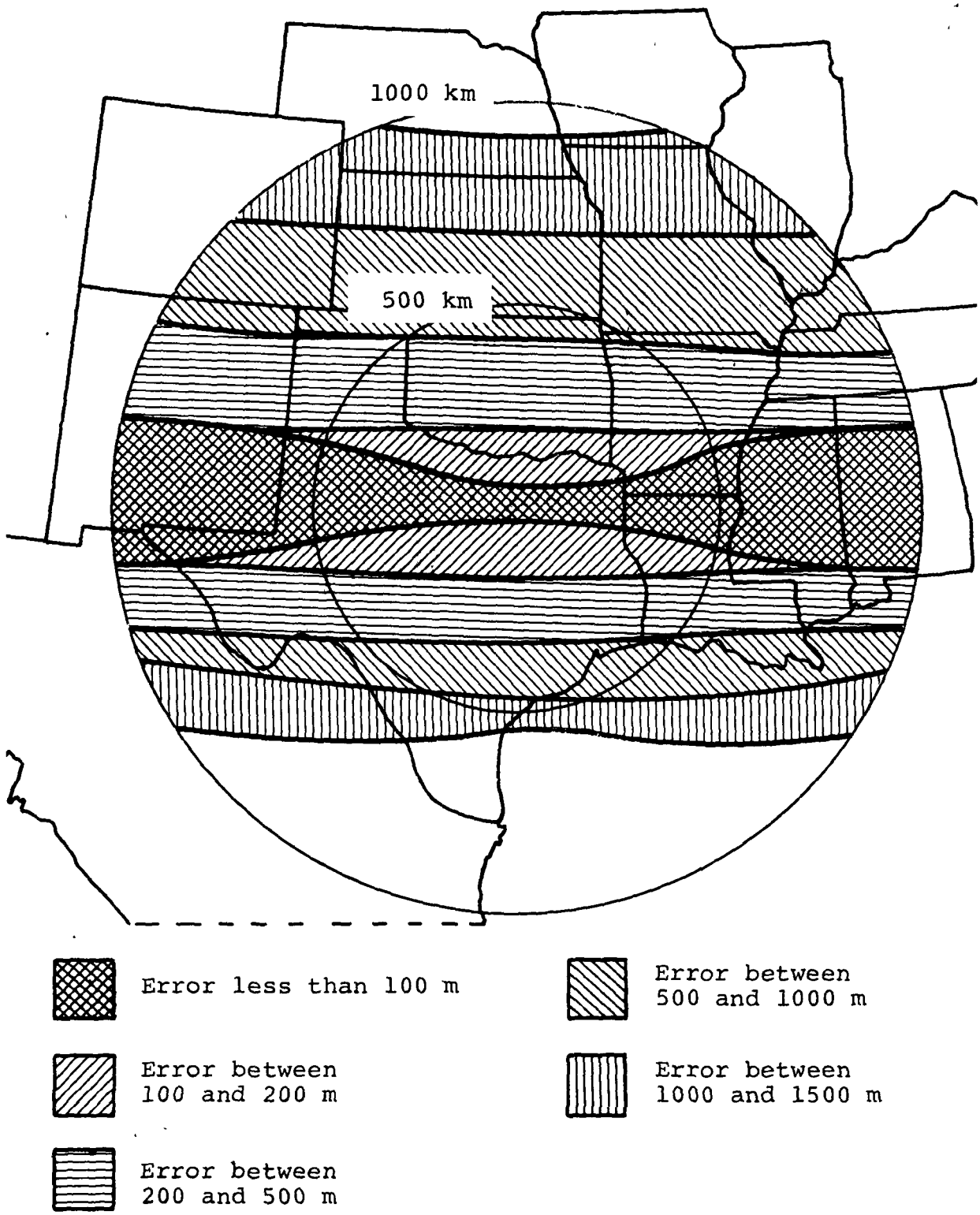

Figure 2-16. Aircraft Position Error Contours for Satellite Latitude Errors of 50 km

50 km satellite errors is valid. If the ephemeris data provides the user with satellite positions with a 50-km accuracy, reference stations must be placed no further than 350 km apart, south of Dallas, or 400 km apart north of Dallas (if the ground control station is located at Dallas) in order to hold the aircraft error resulting from satellite geometry to less than 500 meters. As a result of this error constraint, only 10 simple transponding reference stations would be required to provide coverage over the whole region of the United States if both satellites were placed over the equator at 50°W and 150°W longitude.

3.1.1.2 Ephemeris Data

Geometrically introduced aircraft position errors can also be lessened by providing users with ephemeris data describing the position of each satellite. Two alternative approaches exist. The ephemeris data can be in the form of a table, giving the satellite latitude and longitude for a list of times, or it can be a pair of equations approximating the latitude and longitude of each satellite.[1] The table approach is potentially more accurate because the increment between each time that satellite coordinates are provided may be reduced without limit. The disadvantage of use of tables is that, a table of ephemeris data accurate enough to pinpoint a satellite within 10 km of its true position quickly approaches an impractical size if constrained by small storage capacity of the on-board data processor. Hence, two equations for each satellite will be derived to provide ephemeris data.

The constants governing the exact form of the equation will vary depending on the particular behavior of the satellite involved. The process of setting up the equations is quite straight forward, however. The diurnal position variation of a satellite is well approximated by a two dimensional lissajous figure. The frequencies and phases of the two orthogonal sine waves which are components of such a lissajous figure describe the diurnal behavior of the latitude and longitude coordinates. Figure 2-17 is a picture of the path of the subsatellite point of ATS-III for one day in July, 1970. ATS-III was still drifting eastward then, at the rate of 0.06° per day. The drift is easily accounted for in the ephemeris equation for longitude, although it is not expected that the satellites will be drifting when the experiment is carried out. The two sine wave approximations are

1. Ephemeris data will not be provided for satellite altitude because altitude variations have an insignificant affect on aircraft position error (see Section II-3.1.1)

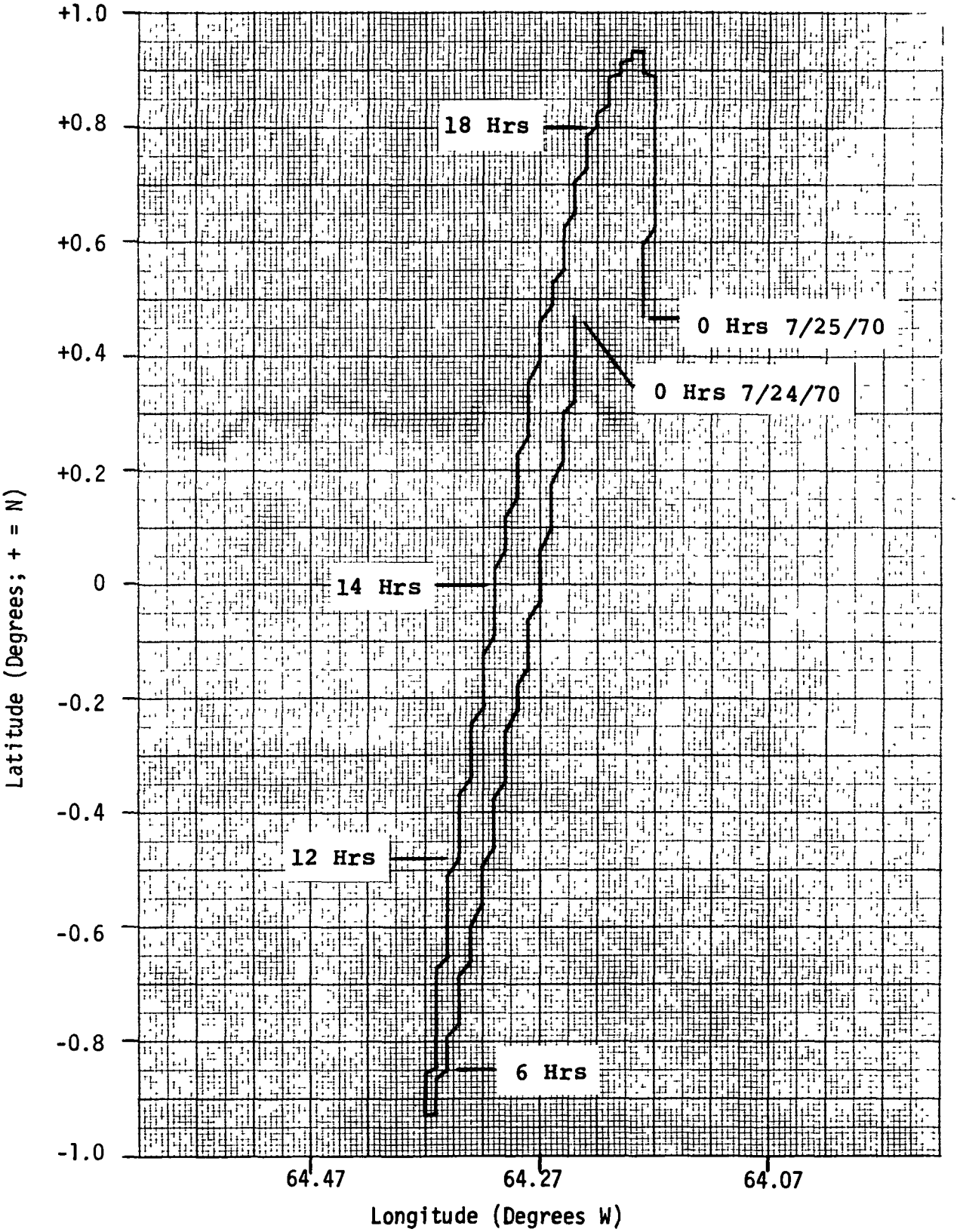

Figure 2-17. Trajectory of ATS-III From Computer Projection

$$\phi = \text{LAT} = 0.94 \cos 2\pi(t/144 + 1/6) \quad (2\text{-}69)$$

$$\lambda = \text{LON} = 0.04 \sin 2\pi(t/144 + 1/6) - \frac{0.06}{144} t + 64.24 \quad (2\text{-}70)$$

where t is marked off in units of ten minutes. For the more typical figure-eight satellite path the latitude sine wave component would contain a sine wave oscillating at twice the rate of the longitude frequency oscillation in order to account for two maximums and two minimums that occur every cycle. The accuracy of this approach is calculated to be $\pm 0.05°$ of latitude or longitude which is approximately ± 35 km at the satellite. Implementation of two sets of these equations on the aircraft data processor, requiring only five constants each, is easily within the capabilities of the machine memory. As the satellite ephemeris varies from the behavior predicted by these equations over the span of a week, provision will also be made to update the equations by inserting new constants.

3.1.2 Propagation Errors

The propagation effects fall into two classes: those that occur along the satellite-to-aircraft path due to the variation of refractive indexes of the troposphere and ionosphere, and those that are due to reflection of the electromagnetic wave by the earth's surface. Since the indexes of refraction of both the troposphere and ionosphere vary with height above the earth's surface, the direction of the wavefront is changed as it passes through the medium, and a range error is introduced because the actual transmission path is longer than the line-of-sight path. In order to gain adequate coverage, a fairly large sector of the earth's surface is illuminated by the satellite antenna, and some of the energy incident upon the earth will be reflected toward the aircraft and interfere with the direct-path signal. These two classes of propagation effects are discussed in detail in this section.

3.1.2.1 Multipath Effects

As described in Appendix C, multipath interference introduces both amplitude and frequency modulation to the direct path signal. The net result is amplitude fading and a time-varying phase shift that introduces a ranging error.

Bergemann and Kucera [7,8], have obtained amplitude fading distributions from 135.6-MHz transmissions between ATS-I and ATS-III and aircraft equipped with a Dorne and Margolin SATCOM antenna, and Kucera [9] has obtained fading spectra for these transmissions. Since their results are directly applicable to this program, they were used in analyzing the multipath effects in Appendix C.

The aircraft signal fading parameters are summarized in Table 2-1. For satellite elevations between 0 and 30 degrees the fading is parimarily specular, and the fading frequency is generally less than 0.3 Hz. For higher satellite elevations, the fading is parimarily diffuse although some specular fading may be present. The bandwidth of the diffuse fading spectra is only a few Hertz.

Table 2-1. Multipath Fade Parameters

Satellite Elevation	Type of Fading	RMS*	Worst-Case†	Fading Bandwidth
0° - 30°	Specular	-2 dB	-7 dB	<0.3 Hz
30° - 50°	Diffuse	-1.6 dB	-3.8 dB	<5 Hz
50° - 70°	Diffuse	-1.1 dB	-2.3 dB	<5 Hz

* The diffuse fade margins are 90 percentile values

† These are 99 percentile values

The differential tone demodulation process described in Appendix C minimizes the specular multipath phase error because the magnitudes of the acquisition/reference(A/R) tone and ranging tone phase errors will be approximately equal. The diffuse phase error, however, will increase somewhat because the A/R tone and ranging tone phase noise will be additive. The multipath ranging errors for ranging tone frequencies of 600 Hz, 2.4 kHz and 10.2 kHz are given in Table 2-2.

Table 2-2. Multipath Ranging Errors

Satellite Elevation	Type of Fading	Nominal Ranging Error			Worst-Case Ranging Error		
		600Hz	2.4kHz	10.2kHz	600Hz	2.4kHz	10.2kHz
0 - 30°	Specular	0.76km	0.62km	0.38km	2.25km	3.4km	1.7km
30° - 50°	Diffuse	9.7 km	2.4 km	0.56km	-	-	-
50° - 70°	Diffuse	6.8 km	1.7 km	0.39km	-	-	-

3.1.2.2 Ionospheric Effects

As described in Appendix B, the ionosphere reduces the group velocity of an electromagnetic wave, and thereby increases the path length relative to free space. This path length - or ranging - error is a function of the integrated electron density and satellite elevation, and occurs on both the GCC-to-satellite and satellite-to-aircraft links. Mean ionospheric range errors for several conditions of satellite elevation and integrated electron density are given in Table 2-3, where $I = 2 \times 10^{16}$ electrons/m^2 corresponds to a night-time minimum electron density, $I = 3 \times 10^{17}$ electrons/m^2 corresponds to a typical day-time maximum value, and $I = 8.6 \times 10^{17}$ electrons/m^2 is a worst-case value. It is evident from the figures in this table that ionospheric corrections must be introduced in order to avoid substantial ranging errors.

Table 2-3. Mean Ionospheric Range Error*

Satellite Elevation Angle(ε)	$I = 2\times10^{16}$ $\frac{elec}{m^2}$		$I = 3\times10^{17}$ $\frac{elec}{m^2}$		$I = 8.6\times10^{17}$ $\frac{elec}{m^2}$	
	One-way Path Error	Two-way Path Error	One-way Path Error	Two-way Path Error	One-way Path Error	Two-way Path Error
$\varepsilon = 20°$	-0.16km	-0.32km	-2.6km	-5.1km	-6.5km	-13km
$\varepsilon = 45°$	-0.12km	-0.25km	-2km	-4km	-5.3km	-10.7km
$\varepsilon = 60°$	-0.11km	-0.23km	-1.8km	-3.8km	-4.9km	-10km

* Satellite Elevation at GCC = 25°

Irregularities in the structure of the ionosphere also introduce signal amplitude fluctuations or scintillations. The scintillations are produced by regions with irregular boundaries, and both the magnitude of the scintillation and time of occurrence are quite variable. In general, mid-latitude scintillations are neither as large nor occur as frequently as do scintillations at equatorial and high latitudes [10].

Mid-latitude VHF scintillations were measured by Aarons and Whitney [11]. Their data gave a 90 percentile scintillation fade margin of 1.3 dB and a 99 percentile scintillation fade margin of 9.4 dB. The distribution of the

periods of the scintillation fades is given in Table 2-4 where it can be seen that the scintillation fading period will generally exceed one second. Since the fading period is so large, compensation for the accompanying ranging error can be readily achieved.

Table 2-4. Mid-Latitude Scintillation Fading Periods [11]

Fading Period	Percentage of Occurrences
$T_s \leq 5$ sec	43
6 sec $\leq T_s \leq$ 14 sec	29
15 sec $\leq T_s \leq$ 59 sec	28

3.1.2.3 Tropospheric Effects

Since the index of refraction of air (n) is nearly unity, varying from an average of about 1.00032 at the surface to 1.000005 at 100,000 feet, the N unit, where

$$N = (n-1) \times 10^6$$

is commonly used for refractivity studies. The variation of N with altitude is given by[12]

$$N(h) = N_s + (h-h_s)\ \Delta N, \qquad h_s<h<h_s+1\text{km}$$

$$N(h) = N_1 \exp[\ln\{(N_1/105)(h-h_s-1)\}/(h_s-8)], \qquad h_s+1\text{km}<h<9\text{km}$$

$$N(h) = 105 \exp[0.1424\ (9-h)], \qquad h>9\text{km}$$

$$\Delta N = -7.32 \exp[5.577\times10^{-3}\ N_s]$$

where h = height in kilometers

h_s = height of the surface above MSL in kilometers

N_s = surface value of refractivity

and $N_1 = N_s + \Delta N$

For elevation angles (ψ) greater than 10 degrees, the tropospheric refraction error is given to within three percent [12] by

$$\Delta R_{tropo} = \int (10^{-6}/\sin\psi)\ N(h)\ dh.$$

The range error determined from the above equation is plotted in Figure 2-18 as a function of satellite elevation with respect to the aircraft altitude for $N_s = 400$. For an aircraft flying at 20,000 feet or higher, the maximum tropospheric range error will be less than 6.5 meters. Since this error is much smaller than the multipath and ionospheric ranging errors, it may be neglected.

3.1.2.4 Velocity of Light Effect

Since the basic sidetone range measurement process of this satellite navigation system is dependent upon conversion of round-trip time delay in the range signals to an equivalent aircraft range, a range error component proportional to the error in the velocity of signal propagation is introduced. The best accepted value of uncertainty in the speed of light (signal propagation constant) is ±300 meters/second [13]. The uncompensated portion of the range measurement path for this error source can be as large as twice the Earth's radius with an uncompensated path length of 12,740 km corresponding to a nominal propagation time of 0.04 second. Therefore, the resulting range uncertainty due to speed of light error is ±13 meters, which is considered to be a random error because of the proposed differential range measurement technique.

3.1.3 System Noise and Measurement Errors

3.1.3.1 System Noise Effect

System noise effect is that range error contribution attributed to the combination of received and self-generated input noise imposed with the ranging tones at the output of the aircraft receiver. There is no direct range error caused by input noise to the satellite transponder because phase comparisons or measurements of the ranging tones are not made in this equipment. It is necessary, however, to consider the indirect error effect related to the retransmission of noise superimposed on the tone signals. The net result of total system noise received by the various communication links is to present a 30.5 dB-Hz signal-to-noise power density tone package to the aircraft receiver. Therefore, the worst-case signal-to-noise power density per tone becomes 24.5 dB-Hz; this value was used for the worst-case system noise error effect calculations developed in Section II-2.1.3 for a one-second signal integration

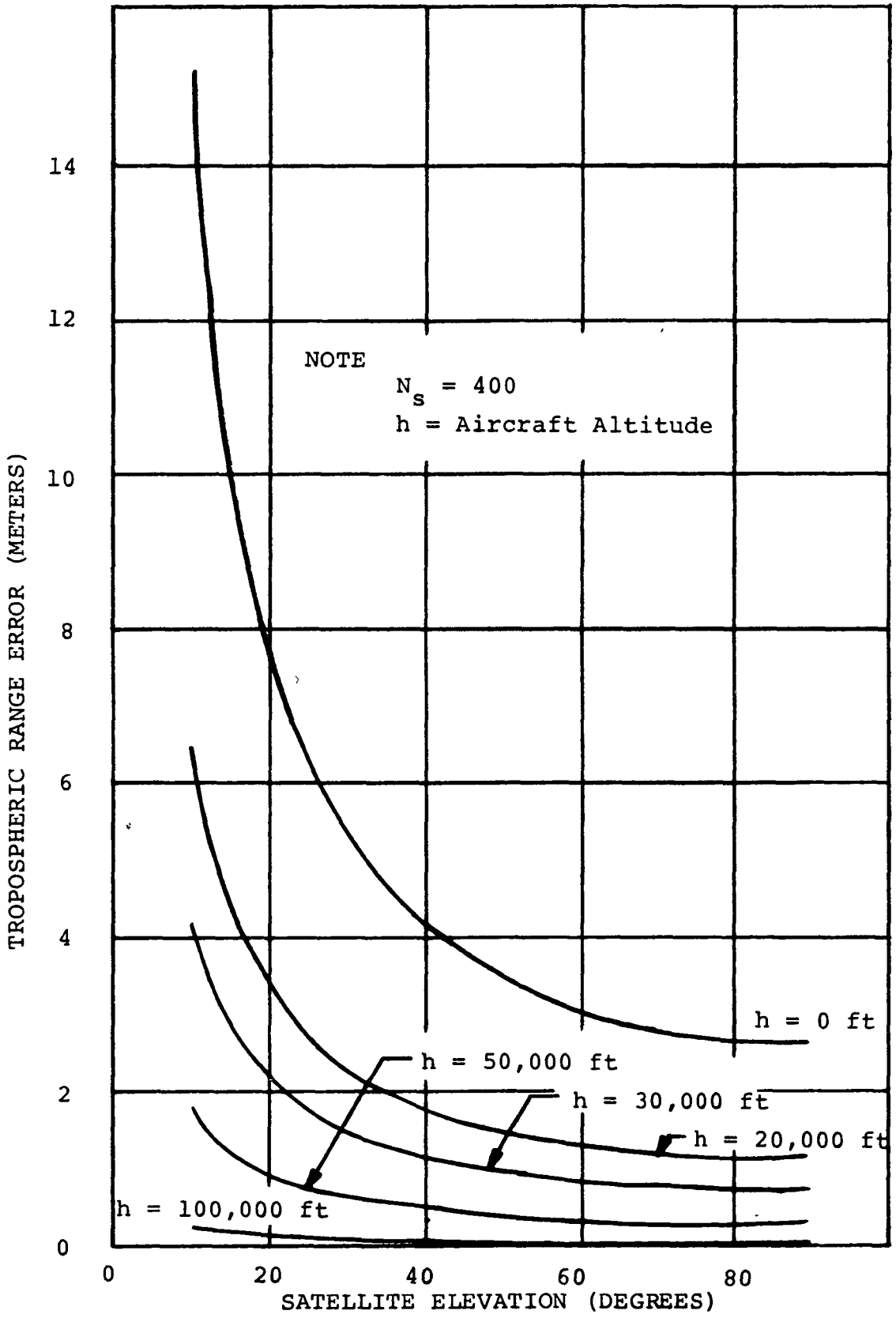

Figure 2-18. Tropospheric Range Error vs. Satellite Elevation Angle

period. For this worst-case signal-to-noise power density condition, the rms value of the noise-related ranging error for the 10.2 kHz tone is 200 meters.

3.1.3.2 Ranging Tone Processor Effect

The fine grain ranging signal will be processed and measured digitally. The accuracy of digital processing can be an order of magnitude better than the corresponding analog implementation. The detail design of the processor is discussed in Section II-2.1; however, accuracy and processor requirements are presented in the following paragraphs.

The general processor block diagram is shown in Figure 2-19. The input signal f(t) (consisting of signal and noise effects) is filtered and sampled using pairs of quadrature samples. Each sample value is converted to a digital word. The digital words are accumulated for the one-second ranging signals that are present and usable.

To determine the accuracy of the processor it is necessary to consider the quantization effects of both the analog-to-digital converter and the accumulators. Analog-to-digital converter accuracy is typically stated in terms of the number of bits of the converter. An n-bit analog-to-digital converter is assumed to be accurate to within one-half the quantization level. (That is, the accuracy $1/2^{n+1}$).

The accumulator word size requirement is determined first. Range measurement errors for the range phase should not exceed 0.1 degree to assure a negligible error contribution due to the instrumentation inaccuracy. Noise effects are related to phase errors by the expression

$$\sigma_n = \frac{1}{(2E/N_o)^{1/2}} \text{ radians} \qquad (2\text{-}71)$$

Therefore, for $\sigma_n = 0.1°$ or 1.75×10^{-3} radians, the energy-to-instrumentation noise ratio will be 55 dB.

It may be shown that the required quantization interval (Δ_s) in the accumulator is given by the expression

$$\Delta_s = \frac{S_o(t_o)}{(2E/N_o)^{1/2}} \qquad (2\text{-}72)$$

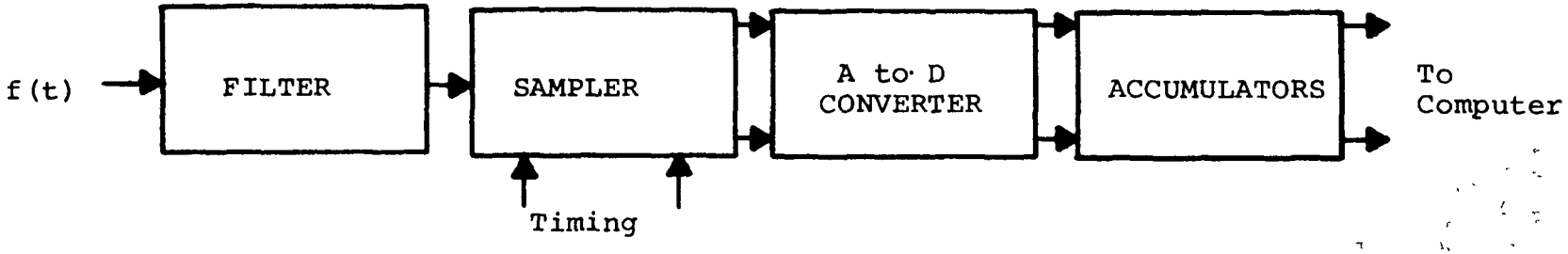

Figure 2-19. General Processor Block Diagram

where $S_o(t_o)$ = peak signal amplitude that may be sampled

$2E/N_o$ = energy-to-noise power density ratio (In this case, signal energy-to-instrumentation noise power density ratio)

Then, it can be shown that $\Delta_s = 1/573$. Therefore, the number of bits (n) in each accumulator is

$$1/2^n = \Delta_s \tag{2-73}$$

or $n = 10$

Since the signal energy-to-noise power density ratios are smaller than the above (55 dB) instrumentation noise effect, the quantization level allowable for signal measurement is larger than that for the accumulator.

The analog-to-digital converter (A to D) size can be determined by investigating the effect of the quantizer on the mean and variance of sampled signal. It is desired to choose an A to D converter size that will cause a minimum degradation of these parameters. Assuming a noise effect that is distributed in a Gaussian manner, it can be shown that the A to D converter effect will be negligible (less than .001 percent) for,

$$\Delta \leq \sigma \tag{2-74}$$

where

Δ is the A to D converter quantization interval

σ is the standard deviation of the noise.

The minimum required energy-to-noise ratio of the fine-grain ranging tone is approximately 24.5 dB-Hz. The maximum energy-to-noise ratio may exceed this value by 10 dB which gives the smallest value of σ to be expected; this is the worst case and yields

$$\sigma_m = \frac{1}{(2E/N_o)^{1/2}} = \frac{1}{75} \tag{2-75}$$

The value of σ_m^2 is the final measurement variance after samples have been accumulated. The relationship between the variance of the independent samples (σ_n^2) and the final measurement

variance is given as

$$\sigma_m^2 = \sigma_n^2/L \qquad (2\text{-}76)$$

where L is the number of accumulated samples.

To complete these considerations it is necessary to determine the number of independent samples (L) that can be accumulated during the one-second period. Since the minimum filter noise bandwidth will be 500 Hz the Nyquist sampling rate will exceed 1000 samples per second, or a minimum of 1000 samples for the one-second accumulation period. Therefore,

$$\sigma_m^2 = \sigma_n^2 \cdot \frac{1}{1000} \qquad (2\text{-}77)$$

which is a processor signal-to-noise ratio improvement of 30 dB.

A maximum energy-to-noise ratio of 4.5 dB-Hz is expected at the A to D converter input. The corresponding value of σ_n in radians is

$$\sigma_n = \frac{1}{(2E/N_o)^{1/2}} = \frac{1}{2.38} \text{ radians} \qquad (2\text{-}78)$$

Since

$$\Delta = \frac{1}{2^n} \leq \sigma_n \qquad (2\text{-}79)$$

then

$$2_n \geq 2.38 \qquad (2\text{-}80)$$

which requires a value of n = 2.

Therefore, for the signal-to-noise ratios, bandwidths, and total processor accuracy required a two-bit A to D converter used in conjunction with a 10-bit accumulator word is adequate to digitally process the fine grain ranging signal with a negligible error. In practice, the A to D converter will be larger and the accumulator word will be longer. This provides increases performance margins and improved operational reliability.

3.1.3.3 Clock Timing Error

Each of the three reference tones used at the aircraft

in measuring the phase of the received ranging tones is derived by dividing down the aircraft clock frequency. The ranging error caused by an unsynchronized clock is directly proportional to the accumulated phase difference between the aircraft and the ground station clocks. Clock errors result from long term oscillator drift, temperature instability, and initial frequency and phase offsets remaining uncorrected at the time of synchronization. For a crystal clock, the instantaneous frequency error ($\Delta\omega_c$) at any time (t) following clock synchronization is given by

$$\Delta\omega_c = \omega_c \, \varepsilon_{LTS} \, t + \omega_c \, \varepsilon_{CAL} \qquad (2\text{-}81)$$

where

ω_c = nominal clock frequency

ε_{LTS} = long term stability

= $\Delta\omega_c/\omega_c$/24 hour period

ε_{CAL} = measure of the frequency offset after synchronization

= $\Delta\omega/\omega_c$ at t = 0

It is seen that the long term drift produces a clock frequency change which is a linear function of time.

Equation (2-81) can be integrated with respect to (t) to determine the accumulated clock phase error.

$$\Delta\theta_c = 1/2 \, \varepsilon_{LTS} \, t^2 + \varepsilon_{CAL} \, t + \frac{\Delta\theta_{0c}}{\omega_c} \qquad (2\text{-}82)$$

where

$\Delta\theta_c$ = the instantaneous clock phase error

$\Delta\theta_{0c}$ = the initial clock phase error

The ranging error is given by

$$\Delta R = c(1/2 \, \varepsilon_{LTS} t^2 + \varepsilon_{CAL} t + \frac{\Delta\theta_{0r}}{\omega_r}) \qquad (2\text{-}83)$$

where

ΔR = the ranging error

c = speed of light

ω_r = the nominal ranging tone frequency

$\Delta\theta_{0r}$ = the initial phase error in the reference tone

$= \Delta\theta_{0c} \cdot \omega_r/\omega_c$

To minimize the effect of clock errors on the total system ranging accuracy, the allowable clock-related ranging error was set at 100 meters.

It would be convenient if the update interval (the time between successive synchronizations of the aircraft clock with the ground clock) required to maintain the accuracy be longer than any flight duration that might take place in the area of coverage. This implies an update interval on the order of one day.

Using a precision, temperature compensated, crystal oscillator with $\varepsilon_{LTS} = 5\text{x}10^{-10}$ and $\varepsilon_{CAL} = 1\text{x}10^{-10}$ and which can be set to within ± 0.1 degrees, the 100-meter limit would be exceeded in slightly less than 50 minutes. For this time period the greatest source of phase error is the initial frequency offset. It is therefore apparent that some method must be used to compensate for clock errors since it is difficult to achieve much better drift rates and offsets.

Compensation for frequency drift can be effected once this parameter has been accurately measured. In one technique [14] a positive frequency drift is partially compensated in the synchronization process by inserting a positive phase shift equal to the largest allowable error, and adjusting the clock frequency to obtain a negative frequency offset. By the time the positive frequency drift has exactly cancelled the negative frequency offset the aircraft clock lags the ground clock by the maximum allowable phase error. At this point, the positive frequency drift predominates and begins to advance the phase until it again leads the ground station clock by the maximum allowable phase error. When this occurs the clock must be re-synchronized. The time interval, during which the clock remains within the maximum phase error limit, is determined by the maximum allowable phase error and the long term stability.

By applying the technique to a clock with the same parameters listed in the previous paragraph, the allowable range error would be exceeded after eight hours. Even though this technique provides considerable improvement over an uncompensated system it still does not meet the 24-hour criterion.

An alternate technique is available, and does provide superior compensation for clock errors. Since an on-board computer is available, the accumulated phase error given by Equation (2-82) can be calculated and used to modify the measured phases of the received ranging tones. The only inputs required by the computer are the measured values of the initial frequency and phase offsets, the long term stability, and the elapsed time from synchronization. Since the accumulated phase error is removed before ranging calculations are made, the requirements for an extremely high long term stability and low frequency and phase offset are not nearly as critical as for the other techniques. The following clock specifications are considered adequate and can be met by most general purpose precision crystal oscillators,

$$\text{long term stability} \leq 3.0 \text{ parts in } 10^7/\text{day}$$

$$\text{frequency offset} \leq 1.0 \text{ part in } 10^8$$

$$\text{inital phase offset} \leq 0.1^{\circ}$$

In practice, the frequency standard would serve as the clock for the elapsed-time counter. The output of this counter would be available as an input to the on-board computer. The phase of the aircraft reference oscillator would be set by using phase measuring techniques similar to those used in the ranging tone processor, and adjusting the oscillator frequency up or down until zero phase is measured. The accuracy of the phase synchronization is the accuracy of the phase comparator in the ranging tone processor, which is designed to be ± 0.1 degrees.

The initial frequency offset would be measured after each synchronization for entry into the on-board computer. The frequency drift remains relatively constant and does not need to be measured each time the clock is synchronized. The implementation of this technique is therefore straightforward and will maintain the clock-related ranging error over a 24-hour period within the 100-meter limit without resorting to extremely high stability clocks.

3.1.4 System Delay Errors

3.1.4.1 Aircraft Terminal Uncompensated Delay Effect

The effect of uncompensated time delay and phase shift

variations expected to occur in the aircraft terminal is an equivalent range error of 60 meters in the ranging path from the ground station-to-aircraft. The resulting error is assumed to be random because the nominal values of time delays and phase shifts are to be removed by calibration. The balance of the range error effects caused by signal amplitude and frequency changes, temperature variations, input voltage variations, etc., contribute "random" errors.

3.1.4.2 Satellite Transponder Uncompensated Delay Effect

The nominal value of the satellite transponder group delay will be removed through simultaneous aircraft and reference terminal range measurements. The residual or uncompensated time delay which is caused by variations in the signal amplitude and frequency is conservatively estimated to be 0.1 μseconds corresponding to a range error of 30 meters.

3.1.4.3 Sector Interrogation

The constant phase plane adjustment which is transmitted by the ground control center during a given time slot applies to only one sector. While the GCC is transmitting the constant phase plane correction for sector k, it is measuring the return from sector k+1 to determine the required correction to be transmitted in the next time slot. Because the GCC updates the constant phase plane of a sector with no feedback signal from that sector as the phase is being transmitted, an error is introduced as a result of satellite movement during the transmission. Section II-2.3 shows that this error can have a maximum value of 15m/second (calculated for ATS-III). The duration of the ranging tone transmission for each sector is three seconds, implying a maximum error of 45 meters. This translates to an aircraft position error of approximately 60 meters at 35° North Latitude.

3.2 Error Sensitivity Analysis

3.2.1 Differential Error Sensitivity Factors Affecting Position Location

Error sensitivity factors are calculated for the dual satellite navigation configuration by taking the partial derivative of each of the aircraft-to-satellite range equations and taking the rms sum of the appropriate errors. The following equations express the measured range from the aircraft to the satellite in terms of all the delays appearing in each segment of the ranging tone navigation link. The parameters are as shown in Figure 2-20.

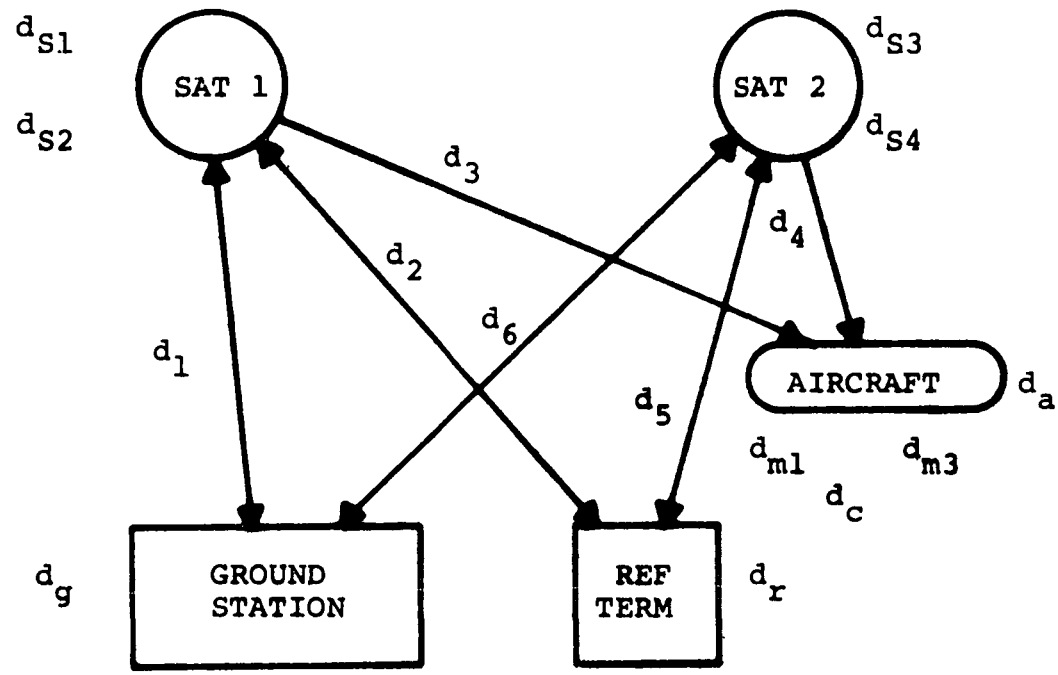

Figure 2-20. Differential Master/Master Navigation Configuration

The following equations describe the path delays used in this analysis.

$$R_{a1} = 2(d_1 + d_3 + d_{s1} + d_a + d_{m1} + d_c) \quad (2\text{-}84)$$

$$R_{r1} = 2d_1 + 2d_2 + d_{s1} + d_{s2} + d_r + d_g \quad (2\text{-}85)$$

$$R_{a2} = 2(d_6 + d_{s3} + d_4 + d_a + d_{m3} + d_c) \quad (2\text{-}86)$$

$$R_{r2} = 2d_6 + 2d_5 + d_{s3} + d_{s4} + d_r + d_g \quad (2\text{-}87)$$

$$d_3 = \frac{1}{2}[R_{a1} - R_{r1} + 2d_2 + d_{s2} + d_r + d_g - 2d_a - 2d_{m1} - d_{s1} - 2d_c] \quad (2\text{-}88)$$

$$d_4 = \frac{1}{2}[R_{a2} - R_{r2} + 2d_5 + d_{s4} + d_r + d_g - 2d_a - 2d_{m3} - d_{s3} - 2d_c] \quad (2\text{-}89)$$

where

d_1 = range from ground station to satellite 1

d_2 = range from satellite 1 to reference terminal

d_3 = derived range from satellite 1 to aircraft

d_4 = derived range from satellite 2 to aircraft

d_5 = range from satellite 2 to reference terminal

d_6 = range from satellite 2 to ground station

R_{a1} = twice the one-way range measurement from GCC to aircraft via satellite 1

R_{r1} = two-way range measurement from GCC to reference terminal via satellite 1

R_{a2} = twice the one-way range measurement from GCC to aircraft via satellite 2

R_{r2} = two-way range measurement from GCC to reference terminal via satellite 2

d_a = range delay effect of aircraft terminal

d_r = range delay effect of reference terminal

d_c = range delay effect caused by on-board clock error

d_{s1} = forward signal range delay effect of satellite 1 transponder for R_a measurement

d_{s1}' = forward signal range delay effect of satellite 1 transponder for R_r measurement

d_{s2} = return signal range delay effect of satellite 1 transponder for R_a measurement

d_{s2}' = return signal range delay effect of satellite 1 transponder for R_r measurement

d_{s3} = return signal range delay effect of satellite 2 transponder for R_a measurement

d_{s3}' = return signal range delay effect of satellite 2 transponder for R_r measurement

d_{s4} = forward signal range delay effect of satellite 2 transponder for R_a measurement

d_{s4}' = forward signal range delay effect of satellite 2 transponder for R_r measurment

d_g = range delay effect of ground processor for R_a measurements

d_g' = range delay effect of ground processor for R_r measurements

d_{m1} = range error effect due to multipath in satellite 1 to aircraft link

d_{m3} = range error effect due to multipath in satellite 2 to aircraft link

From the above equations the sensitivity factors relating satellite-to-aircraft range error to the various parameters of uncertainty are calculated. The results are tabulated in Table 2-5. The calculations used to determine the sensitivity factors are made according to the following analysis:

Table 2-5. Derived Satellite-to-Aircraft Range Error Sensitivity Factors

Error Source	Sensitivity Factor
System Noise	0.707
On-board Clock Error	1.0
Terminal Delay	0.707
Ground Processor Delay	0.707
Satellite Transponder Delay	1.0
Along Range Satellite Position	0.008
Cross Range Satellite Position	0.13
Atmospheric Effects	1.41
Satellite-to-Aircraft Multipath Effect	0.5

NOTE: Delay uncertainty for differential configurations include only short-term variation of delay that occurs during time intervals of 1 minute.

From Equation (2-88), sources of measurement error are R_{a1} and R_{r1}. These two sources are assumed to cause equal and independent errors. Therefore, the total error sensitivity

factor is the rms sum of the factors for the two sources. The error sensitivity of d_3 to R_{a1} is

$$\frac{\partial d_3}{\partial R_{a1}} = 1/2 \tag{2-90}$$

and for R_{r1} the sensitivity is

$$\frac{\partial d_3}{\partial R_{r1}} = 1/2 \tag{2-91}$$

Assuming independent range measurement errors, the error sensitivity to range measurement is given by

$$\left[\left(\frac{\partial d_3}{\partial R_{a1}}\right)^2 + \left(\frac{\partial d_3}{\partial R_{r1}}\right)^2\right]^{1/2} = 0.707 \tag{2-92}$$

Therefore, the error sensitivity to range measurement is 0.707 which is the first entry to the Table 2-5.

In a similar manner the error sensitivity factor due to terminal delay uncertainty is calculated to be 0.707. This value is based on the assumption that the uncertainties in both aircraft and reference terminal delay (d_a and d_r) generate errors which are independent and of Gaussian distribution.

The range error sensitivity to variations of the ground processor delay occurring between the aircraft and the reference terminal measurements is given by

$$\left[\left(\frac{\partial d_3}{\partial d_g}\right)^2 + \left(\frac{\partial d_3}{\partial d_g'}\right)^2\right]^{1/2} = 0.707 \tag{2-93}$$

The sensitivity to satellite delay involves the sum of four independent delay factors corresponding to four one-way passes through the satellite transponder. Hence, for equal value of uncertainty for all four passes the range sensitivity factor to satellite delay becomes

$$\left[\left(\frac{\partial d_3}{\partial d_{s1}}\right)^2 + \left(\frac{\partial d_3}{\partial d_{s1}'}\right)^2 + \left(\frac{\partial d_3}{\partial d_{s2}}\right)^2 + \left(\frac{\partial d_3}{\partial d_{s2}'}\right)^2\right]^{1/2} = 1 \tag{2-94}$$

The calculation of range error sensitivity to satellite position error for the differential navigation configuration is complicated by the fact that this error sensitivity is not constant over the area of coverage, but rather is a function of the geometry between the aircraft, reference terminal, and satellite. In particular, this error sensitivity is shown in the following paragraphs to be proportional to the angle formed by lines joining the satellite to the positions of both the aircraft and the reference terminal.

Satellite position uncertainty is defined to be the difference between the assumed position and the actual position of each satellite. This position uncertainty is then broken into two components, the first one being the projection of satellite position error along the satellite-to-aircraft range line, and the second one being the projection of satellite position error across the satellite-to-aircraft range line. Assuming differential range measurements, the geometric relationship showing the residual or uncompensated satellite-to-aircraft derived range error for the along-range projection of satellite position is shown in Figure 2-21. The resulting derived range sensitivity factor to the along-range projection is expressed by the following equation

$$F_{sa} = [2 \sin^2 (\alpha/2)] \qquad (2\text{-}95)$$

$$= 0.008$$

for $\alpha = 7.5°$

and where F_{sa} is the sensitivity factor between derived range and satellite position uncertainty in the along-range projection, and α is the worst-case differential angle at the satellite between the reference and aircraft terminals.

The geometry relating the effect of satellite position uncertainty in the cross-range direction to satellite-to-aircraft range error is shown in Figure 2-22. The effect of satellite position uncertainty in this direction is not cancelled by the differential navigation configuration and the sensitivity factor is expressed by the following equation.

$$F_{sc} = \sin \alpha$$

$$= 0.13 \text{ for } \alpha = 7.5° \qquad (2\text{-}96)$$

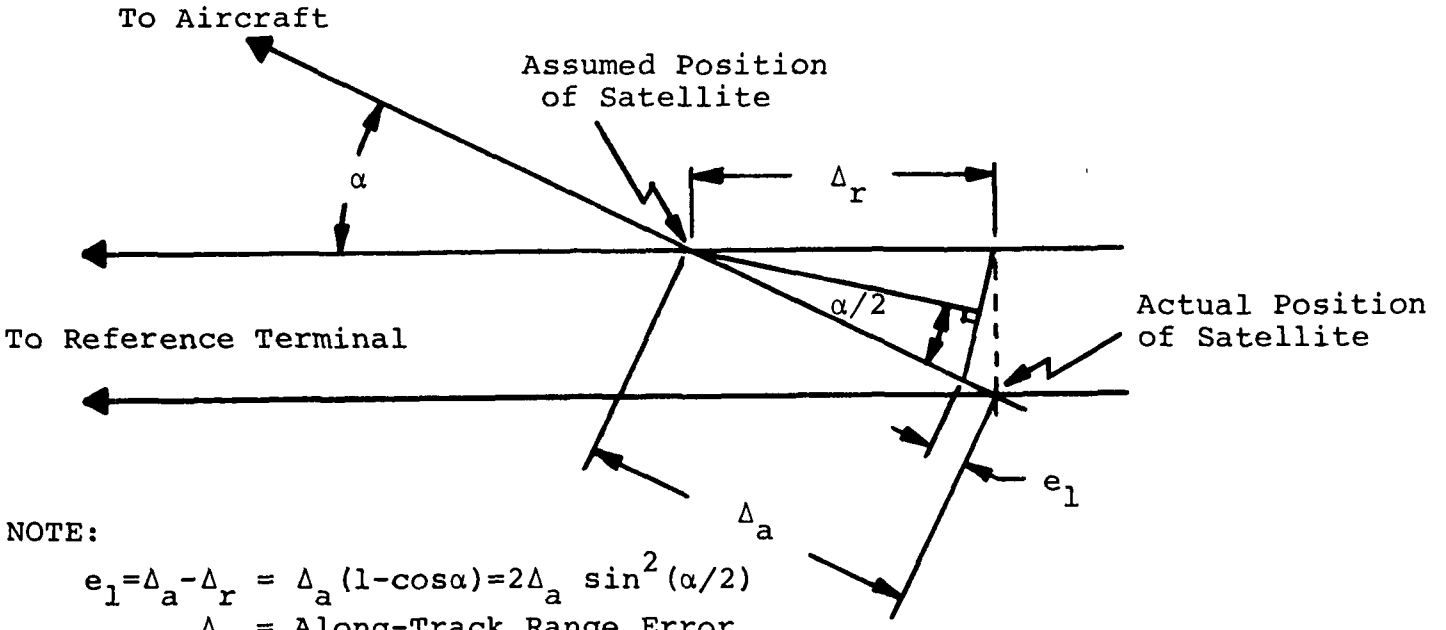

NOTE:

$e_l = \Delta_a - \Delta_r = \Delta_a(1-\cos\alpha) = 2\Delta_a \sin^2(\alpha/2)$

Δ_a = Along-Track Range Error

Δ_r = Compensated Range Error

e_l = Uncompensated Range Error

Figure 2-21. Differential Range Error Geometry for Along-Range Position Uncertainty

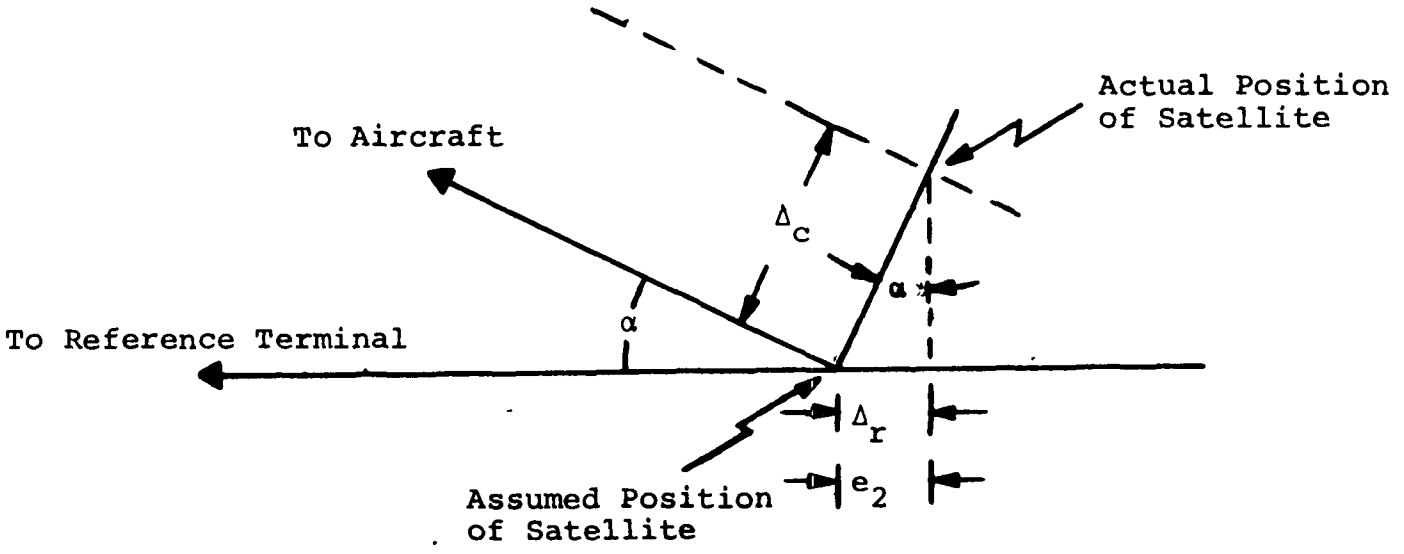

NOTE:

$e_2 = \Delta_r = \Delta_c \sin \alpha$

Δ_c = Cross-Track Range Error

Δ_r = Compensated Range Error

e_2 = Uncompensated Range Error

Figure 2-22. Differential Range Error Geometry for Cross-Range Position Uncertainty

where F_{sc} is the sensitivity factor relating aircraft-to-satellite range error to satellite cross-range position error, and α is the differential angle from the satellite between the aircraft and reference terminals.

The sensitivity factor for the atmospheric effect is defined to include the range error due to propagation uncertainty through both the ionosphere and the troposphere. The listed sensitivity factor of 1.41 is based upon the assumption that independent errors due to atmospheric effects occur in both the satellite-to-aircraft and satellite-to-reference terminal range paths (d_3 and d_2 for satellite 1). The listed value for this sensitivity factor does not take into account common mode rejection of the atmospheric bias error which is achieved in the differential navigation configuration. This rejection is expected to significantly reduce the sensitivity factor when the separation distance between the reference and aircraft terminal is less than 400 kilometers.

3.2.2 Position Location Accuracy

The technique used to derive the aircraft position location accuracy is summarized by the following equations expressing standard deviations. The rms range error (σ_{R1}) in the aircraft-to-satellite 1 link is related to range error sensitivity factors (F_{1i}) and the individual rms parameter errors (σ_i) by the expression

$$\sigma_{R1} = \left\{ \sum_{i=1}^{n} \left[(F_{1i})^2 \, (\sigma_i)^2 \right] \right\}^{1/2} \qquad (2\text{-}97)$$

The expression for the range error (σ_{R2}) in the aircraft-to-satellite 2 link is

$$\sigma_{R2} = \left\{ \sum_{i=1}^{n} \left[(F_{2i})^2 \, (\sigma_i)^2 \right] \right\}^{1/2} \qquad (2\text{-}98)$$

The aircraft latitude position error (σ_{LAT}) is related to the latitude geometric dilution of precision factors for both satellites (G_{1LAT} and G_{2LAT}) by

$$\sigma_{LAT} = \left[(\sigma_{R1})^2 (G_{1LAT})^2 + (\sigma_{R2})^2 (G_{2LAT})^2\right]^{1/2} \quad (2\text{-}99)$$

The aircraft longitude position error (σ_{LON}) is given by a similar expression which is

$$\sigma_{LON} = \left[(\sigma_{R1})^2 (G_{1LON})^2 + (\sigma_{R2})^2 (G_{2LON})^2\right]^{1/2} \quad (2\text{-}100)$$

Finally, the aircraft's total position error (σ_{POS}) is the rms sum of the errors in latitude and longitude. This expression is

$$\sigma_{POS} = \left[(\sigma_{LAT})^2 + (\sigma_{LON})^2\right]^{1/2} \quad (2\text{-}101)$$

The next required step in the determination of the relative position accuracies is to establish an error allocation for the various parameters that are involved in the fine-range measurement. Table 2-6 summarizes the error allocation for the 10.2-kHz ranging tone. The allocated projections of satellite position error with a constant phase plane adjustment and approximate ephemeris data can be calculated from the following typical values of satellite position parameters.

Satellite position error in latitude = 2 km

Satellite position error in longitude = 1 km

Satellite position error in altitude = 0.3 km

Satellite differential angle between earth's center and aircraft (maximum for a 10-degree satellite elevation angle) = 8.5 degrees

The rms value of errors in the derived satellite-to-aircraft range were calculated by multiplying the individual sensitivity factors by the respective allocated errors. The results are tabulated in Table 2-7.

Table 2-6. Error Allocation for Basic Range Measurements (10.2-kHz tone)

Error Source	RMS Error (meters)
Range Measurement Error caused by Noise (Tone E/N_o = 24.5 dB-Hz)	200
On-board Clock (Phase error = 1.2°@10.2 kHz)	100
Terminal Delay Uncertainty (Delay Error = 0.4 μsec)	60
Ground Processor Delay Uncertainty (Delay Error = 0.1 μsec)	30
Satellite Transponder Delay Uncertainty Delay Error = 0.1 μsec)	30
Satellite Position Uncertainty	
Along-Range Projection	445
Cross-Range Projection	2200
Ionospheric Effects (Satellite elevation angle = 10°)	60
Satellite-to-aircraft Link Multipath Effect (Phase Error = 1°)	90

Table 2-7. RMS Errors in the Derived Satellite-to-Aircraft Range

Error Source	RMS Error (meters)
System Noise	141
On-board Clock	100
Terminal Delay	43
Ground Processor Delay	22
Satellite Transponder Delay	30
Along-Range Satellite Position	4
Cross-Range Satellite Position	290
Ionospheric Effects	85
Satellite to A/C Multipath Effect	45
Total rms Error	354

SECTION III

EXPERIMENTAL SYSTEM DESIGN

1. INTRODUCTION

The preceding design study has shown that a system can be realized which will determine position location at a remote point on earth's surface to within 1500 meters by measuring a set of ground originating signals emanating from two synchronous satellites. The system can be used aboard an aircraft if altitude inforamtion is provided . The baseline system proposed herein will demonstrate the capabilities of an experimental system utilizing existing equipment to a maximum, and will illustrate extendability to a more sophisticated system for operational status.

The system will be designed around the ATS-I and ATS-III VHF synchronous satellites using the ground control center (GCC) incorporated in the VHF Satellite Navigation Experiment. Because of these two considerations, some system parameters are pre-determined which result in constraints on the design. These constraints must be used as the basis for operational analysis and for performance prediction.

Of primary consideration is the satellite system made up of ATS-I, ATS-III, and the Earth, which has the following major characteristics:

(1) The satellites are synchronous but due to orbital inclination, their positions vary with time.

(2) Satellite operation frequencies are:

Transmit - 135.6 MHz

Receive - 149.22 MHz

Bandwidth - 100 kHz

(3) Satellite transmit power is fixed, which limits the signal-to-noise ratio at the Earth's surface.

Implications of these characteristics are quite broad and will be covered as they fit in context.

The addition of the GCC to the system further reduces the number of design choices and limits system performance because:

(1) The GCC-generated ranging tones are 426 Hz, 707 Hz, and 941 Hz.

(2) The GCC is limited in phase measurement accuracy.

(3) The VHF link parameters limit the signal-to-noise performance of the system, as discussed in detail in Appendix A.

The preceding factors illustrate that the optimum navigation system discussed in Section II cannot be realized with the ATS-I, ATS-III, and GCC as now configured. Nevertheless, these components are sufficient to demonstrate the principle and feasibility of on-board navigation by ranging to two satellites, and the following base-line system is proposed to effect this demonstration.

2. BASELINE SYSTEM

Certain operational aspects of the navigation system must be selected prior to describing the general electronic design. These aspects are discussed in the following paragraphs.

The study has shown that a simple phase plane correction cannot completely compensate for the satellite position uncertainty; however, a combination of two techniques can complement the phase plane correction to attain adequate accuracy. First, satellite motion can be partially compensated for by a very simple approximate equation. Second, the geometric errors can be reduced by placing reference terminals at the center of geographic sectors to time share the GCC. The first technique requires a software function to be implemented in the GCC computer and in the remote aircraft terminal computer. (Throughout this discussion the computer and other equipment at the navigation site will be termed aircraft (A/C) terminal). The second technique requires a selection of an appropriate number of sectors based upon the end requirement of demonstrating adequate navigational capability and extension to operational status. In an operational system, the number of sectors would be determined by a different criteria such as satellite coverage, maximum allowable time between position fixes, minimum time to obtain an accurate fix, and others. For this experiment, it is expected that three sectors would be adequate to perform the various tests.

Figure 3-1 is a diagram of the resulting system components. The multiplicity of RF links is apparent, and for simplicity throughout the discussion the following representation will be used to designate a link:

ATS-I to A/C

or (Transmitter) to (Receiver)

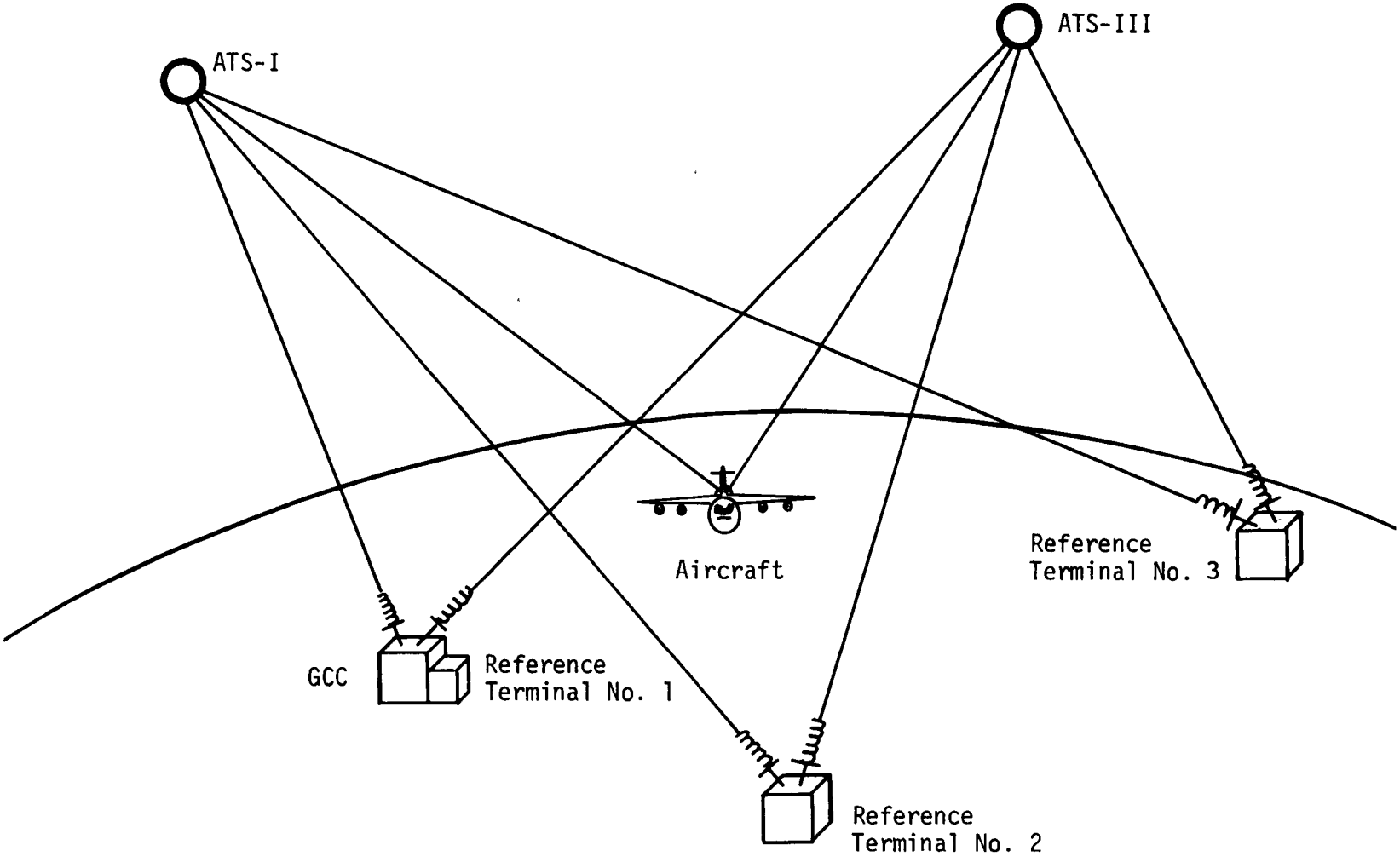

Figure 3-1. Major Elements Of A Dual Satellite Navigation System

That is, the transmitter will be the first element mentioned. Channelization is an additional aid in the description of the various link frequency spectra. The satellites are entered (receive) at 149.22 MHz and transmit at 135.6 MHz band center frequencies. For convenience their 100-kHz bandwidths are divided into 40 equal 2.5-kHz intervals or channels, numbered from 1 to 40 beginning with 1 as the lowest frequency 2.5-kHz channel. This is illustrated in Figure 3-2. Figure 3-3 then shows the channels used and/or occupied in each of the links.

Six major implications are embodied in Figure 3-3.

(1) The channels selected are grouped within a 50-kHz bandwidth so that the GCC may be operated with its narrow (50 kHz) bandwidth receiver IF filters.

(2) The GCC antenna gains are approximately 20 db down in the direction of the opposite satellite such that any radiation in, or reception from, that direction is negligible. This is represented by the figure in that no GCC-to-ATS-I channel 14 appears at ATS-III, etc.

(3) The antennas at the reference terminals are assumed narrow beam even though the frequency multiplexing would conceptually allow illumination of both satellites. The directivity is specified to improve the equivalent radiated power of the link and to prevent unnecessary power sharing at the satellites.

(4) The selected channels are arbitrary and are chosen as shown only to give a reference point for discussion. They may be relocated any time up to final design of the hardware, within the constraint of the 50-kHz GCC receiver IF bandwidth.

(5) A pilot tone will be used with ATS-III to allow tracking out the jitter known to be present in the transponder.

(6) The tone package is transmitted from the GCC to the satellites(s), then to the A/C and reference terminal, from the reference terminal back to the satellite(s) and finally back to the GCC.

Reviewing briefly, the baseline system is to consist of a GCC which controls the system operation by applying phase correction to the ranging tones such that the phase received at the A/C can be used to determine position with minimal error.

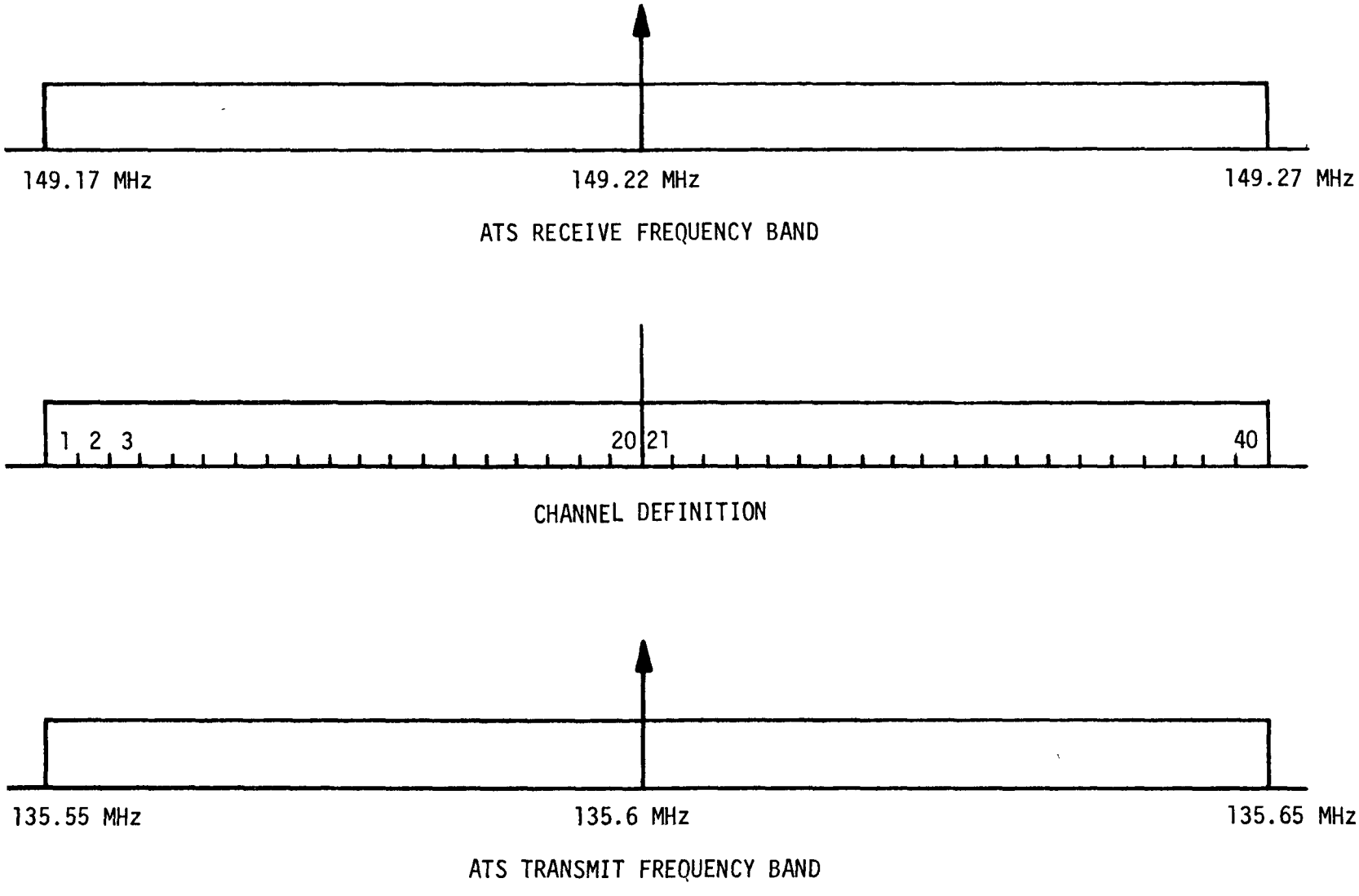

Figure 3-2. ATS-I And ATS-III Frequency Spectra

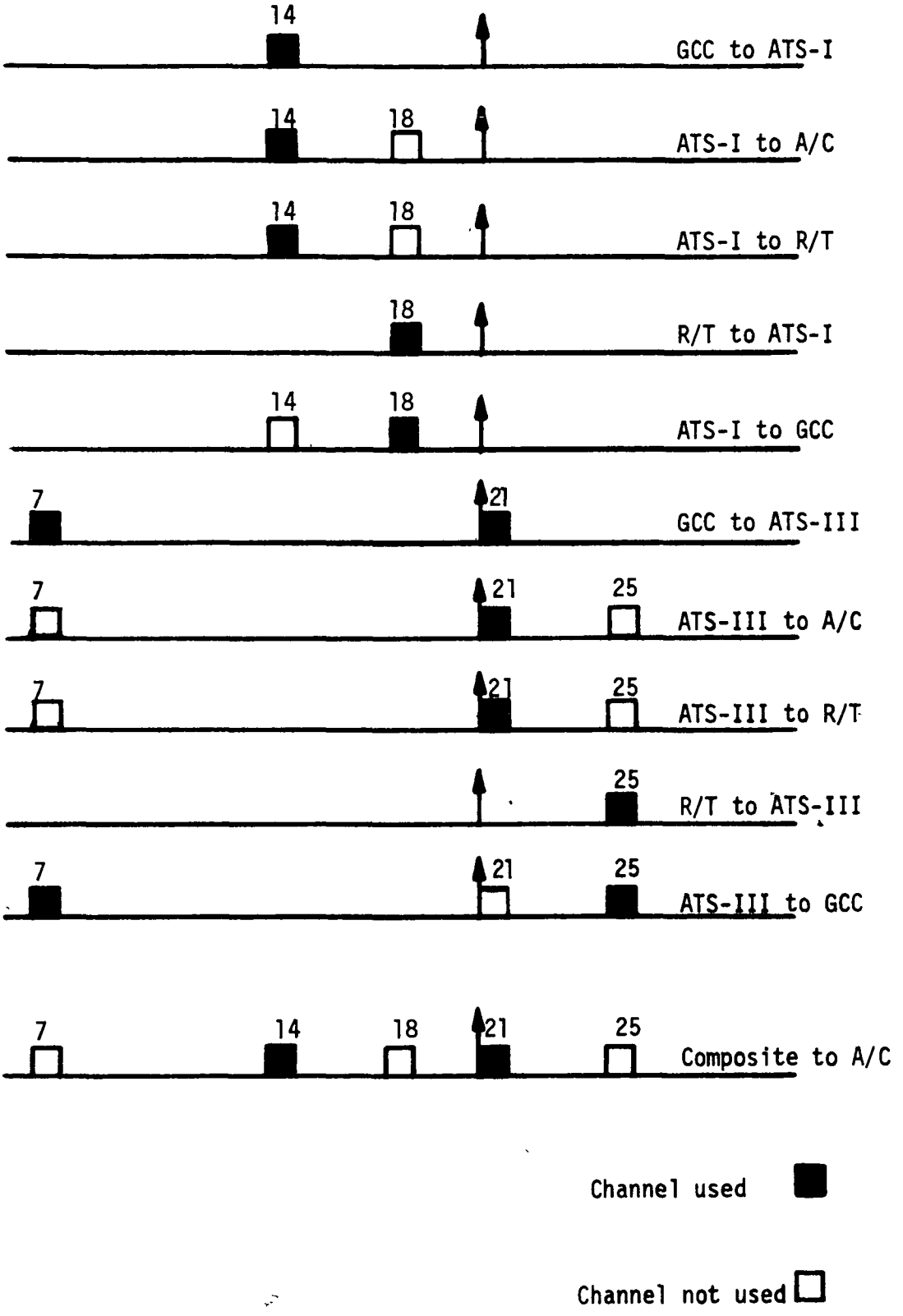

Figure 3-3. Link Spectra

In addition, three reference terminals to return the signals to the GCC for measurement and subsequent phase correction calibration, and an A/C terminal to effect the phase measurements and position determination while airborne constitute the total system component complement.

3. SYSTEM OPERATION AND CONTROL

3.1 Cycle Description

3.1.1 General

The experimental system consisting of the components stated in the preceding section operates in a cyclic fashion. This arrangement was shown diagrammatically in Figure 3-1 and can be referred to here for clarity. The primary function of the GCC is to measure phase perturbations caused by satellite movement and/or atmospheric diurnal variations. From this measurement the GCC then calculates a transmit phase such that the perturbation effects are minimized at the center of the sector; i.e., at the reference terminal. The overall result is that phase compensation at the GCC corrects for the phase errors caused by these perturbations that otherwise would occur in the navigational sector.

A simplified block diagram of the GCC system for one tone is illustrated in Figure 3-4. As shown, the transmitted phase is directly controlled by the computer. The signal returned from the reference terminal is coherently compared to the original master clock and digitized so that the phase shift over the link can be calculated by the computer. It is corrected (or biased) for ephemeris, added as a sector offset constant, and stored for later transmission.

3.1.2 Sequence and Control

System sequence and control will be synchronized by stable clocks which control the time division multiplexing among the sectors. During the time a phase corrected navigation tone package is being transmitted to a sector, the reference terminal in the next sector in sequence will transpond the signal. This is done so that the GCC can compute the applicable phase shift as near as possible to the time it will be applied. Figure 3-5 shows the operating time relationships for the three reference terminals. As the GCC transmits the corrected phase signals for sector 3 the signal is transponded from the sector 1 reference terminal. In the next time slot the corrected phase as just measured for sector 1 is transmitted and transponded from sector 2. Next, sector 2 corrected phase is transmitted and sector 3 transponds, with the following step completing the cycle.

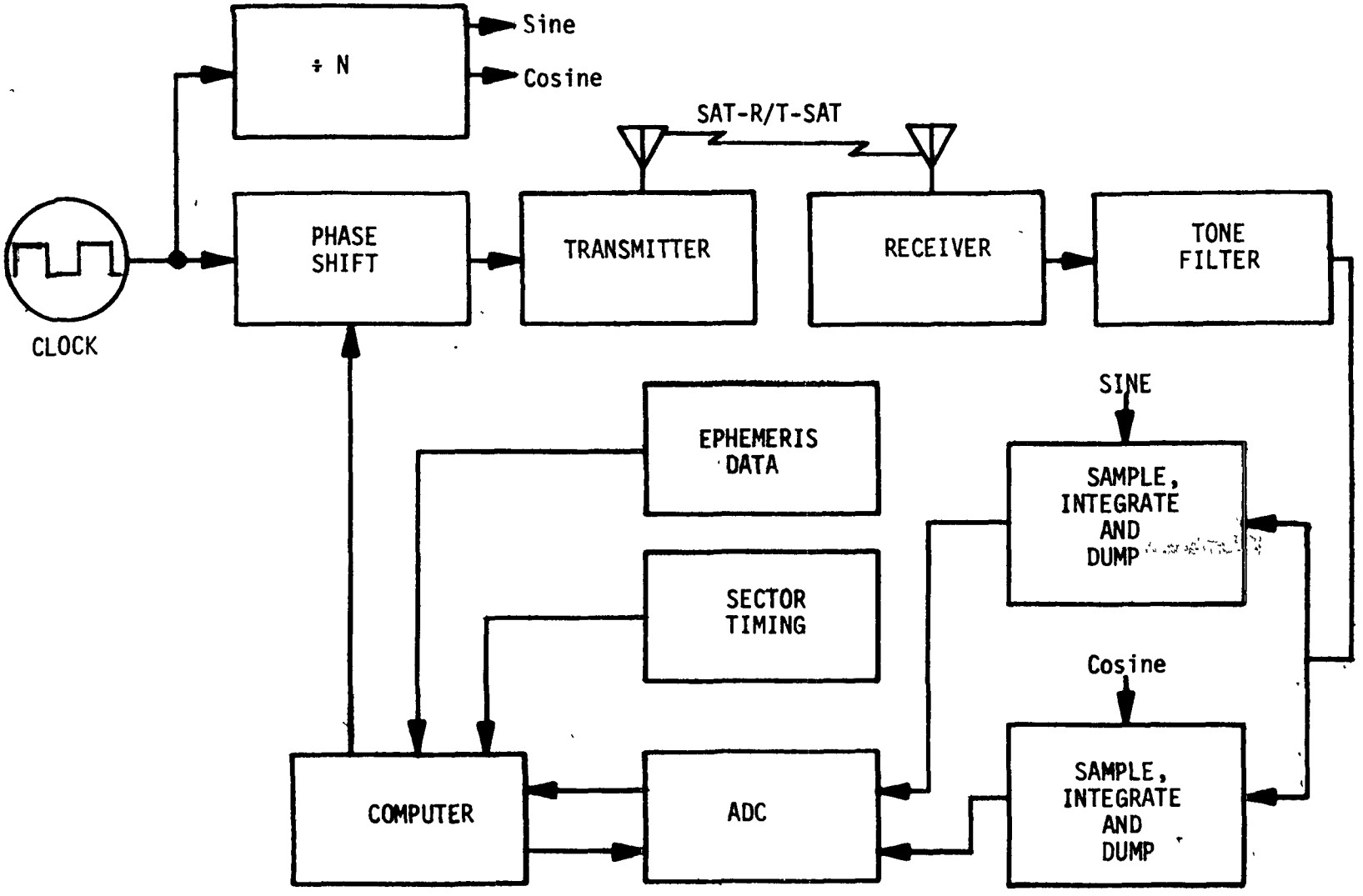

Figure 3-4. GCC Functional Diagram

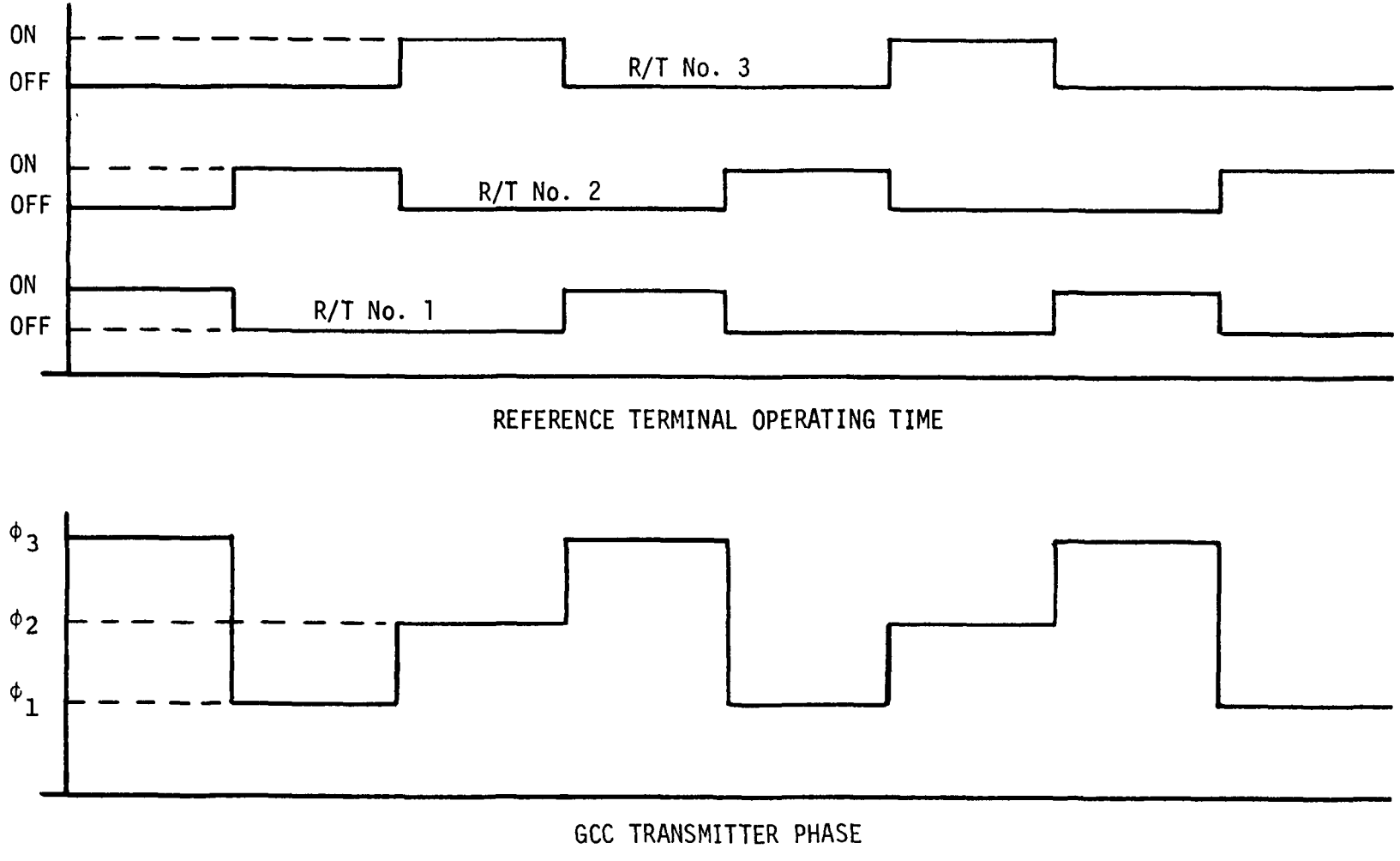

Figure 3-5. Sector Multiplexing Sequence

3.1.3 Sector Period

The duration of transmission to each sector has an upper limit dependent upon a number of factors:

(1) Number of sectors

(2) Time between position fixes

(3) Phase measurement time required

(4) Circuitry settling time

(5) Transmission time guard band

The number of sectors limits the duration only if the number is so large that acceptable time between position fixes would be exceeded. Assuming that the maximum allowable time is three minutes between required position updates [15], then 10 sectors would allow 18 seconds of tone transmission per sector, or 50 sectors would allow 3.6 seconds per sector. Obviously for the experiment with only 3 sectors no time limitation problem will exist. For an operating navigation system the number of sectors will depend upon allowable phase error at the sector edge and the total area of coverage. Here it is seen that the experiment results will define the sectorization parameters, and therefore will provide a solid base for trade-off decisions.

The amount of time required to integrate for noise error reduction is plotted in Figure 3-6. The point (X) shows that for a carrier-to-noise power density of 30 db-Hz, with a two-second integration period after the detector, the rms phase error would be 0.9 degree. The experimental system is expected to have closer to 40dB-Hz C/N_o for which two seconds of integration reduces the rms phase error to 0.3 degree. The integration period will be selected so that noise error does not dominate, thereby assuring other less controllable factors are the system limitations.

The circuit response times fall into three categories: (1) time of transmission, (2) settling time, and (3) acquisition time. Differences in transmission time from sector to sector and settling times for the 40-Hz bandwidth filters are on the order of tens of milli-seconds, whereas the phase-locked loop acquisition cycle is four seconds. For the three - sector system this could be tolerated. It is planned, however, to subsitute new fast acquisition phase-lock-loop receivers developed by Texas Instruments to verify system operation timing.

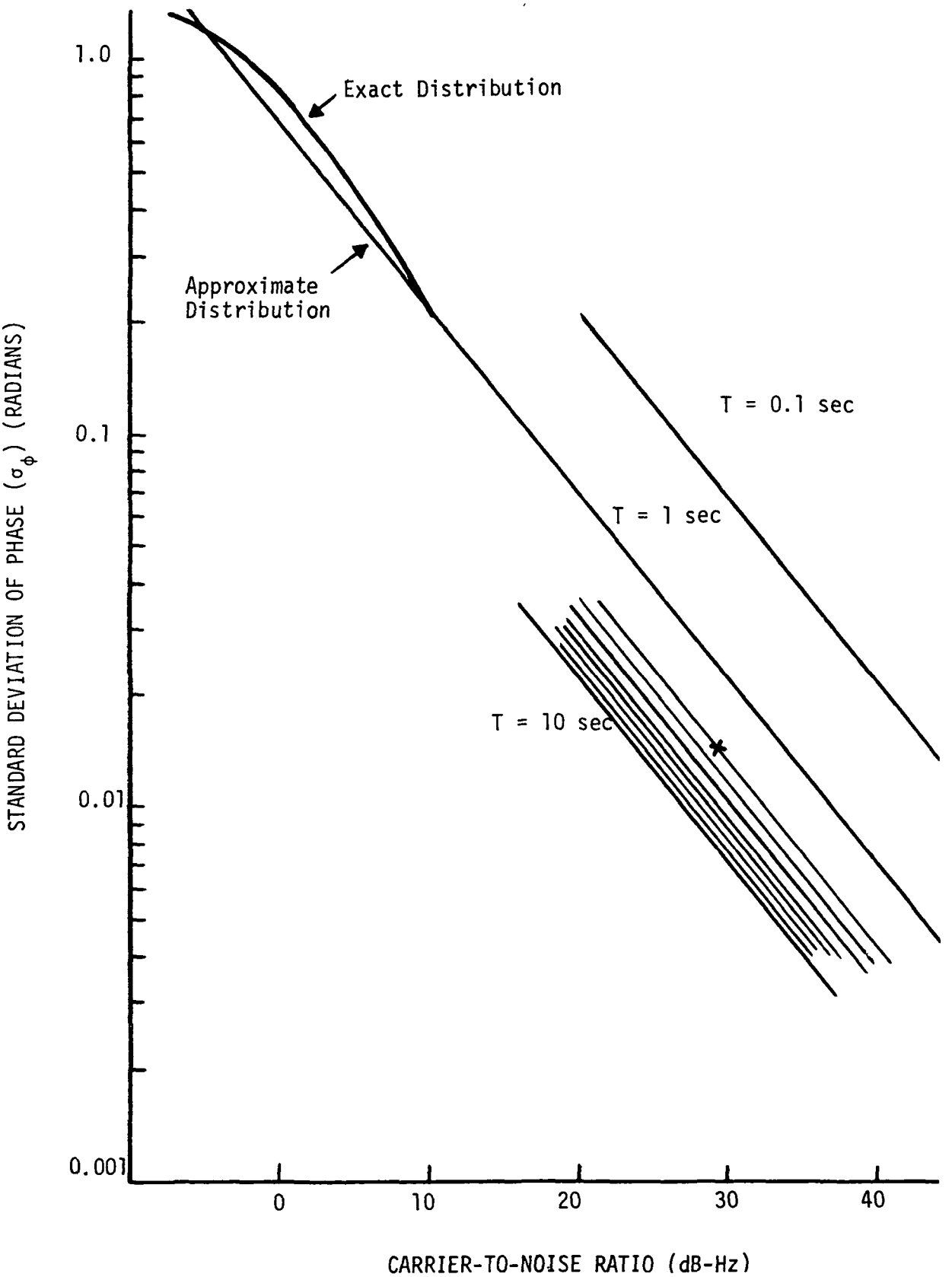

Figure 3-6. Phase Distribution vs Carrier-To-Noise Ratio

Finally, the guard band time is selected to accommodate the differences in satellite-to-sector distances, the maximum change in satellite apparent range, and the sector timing inaccuracy. From the above considerations, a sector period of five seconds has been selected for the experimental system.

3.1.4 Navigation Signal

From the preceding section, it is seen that for one third of the system cycle a phase-corrected tone package will be available at each sector for determination of position. During the other two-thirds of the cycle a tone package corrected for a distant sector will be available for range computation. The range calculated during this portion of the cycle will be in greater error than would be attained with the proper sector signal.

The frequency spectrum of the tone package prior to the GCC transmission is as shown in Figure 3-7. This spectrum is identical to the OCC self-check subsystem set of tones.

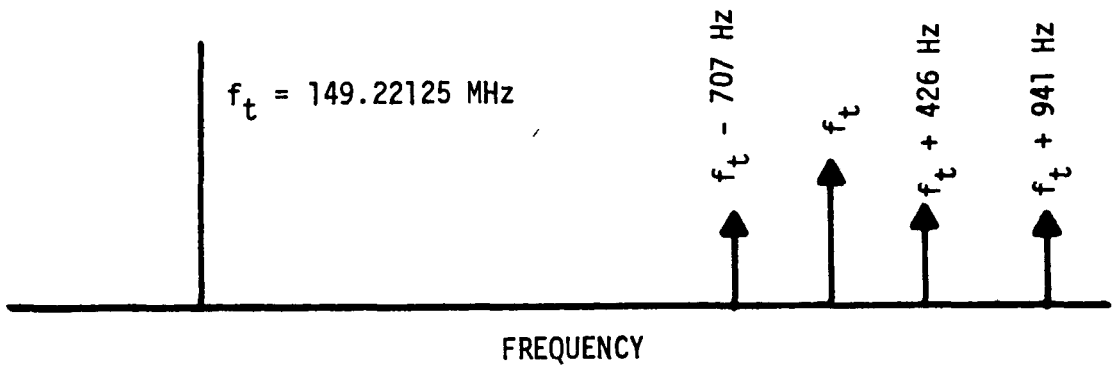

Figure 3-7 GCC To ATS-III Ranging Tone Spectrum

Conversion to computer controlled phase is, therefore, simply a replacement of the OCC Self-Check Amplitude and Interval Selector circuit with a Controlled Phase Oscillator circuit. A block diagram of the Self-Check Subsystem is shown in Figure 2-19 of the OPLE Maintenance Manual [16], in which the Amplitude and Interval Selector is shown as one printed wiring board. The conversion to computer controlled phase would simply require removal of this card and connection of the three-tone Controlled Phase Oscillator, as shown in Figure 3-8, in its place. The resulting circuitry will be sufficient to generate the tones for one satellite. To generate the tones needed for the second satellite the circuits described will be duplicated, except where signal or function sharing is possible.

3.1.5 On-Board Measurement

The signals as received at the A/C during the assigned time interval for the sector in which it is situated will be corrected such that the on-board assumed satellite position will provide the best range calculations. To assure reception of both satellites the A/C antenna will be broadbeam with the following electronics split into two channels. One channel will accept the ATS-I signals and the other the ATS-III signals. The twelve sine and cosine function measurements (3 tones, 2 satellites) which will be the system outputs will then be digitized and used by the computer along with altitude obtained from other on-board instrumentation to compute position. The resulting position will then be displayed.

3.2 Ground Control Center (GCC) Functional Description

Fundamental design of the GCC is the OPLE Control Center (OCC) as modified for the VHF Satellite Navigation Experiment, and as shown in simplified block diagram form in Figure 3-9. Figure 3-10 is the same block diagram with the additions for the Dual Satellite Navigation Experiment super-imposed. These diagrams can be compared to most easily view the system additions. The predominant changes are the additional transmit channel and the controlled phase oscillators with the computer control.

The modifications result in a system consisting of two sets of VHF transmit-receive equipment controlled by a single computer with one side assigned to the ATS-I satellite and the other to ATS-III. The primary function of the GCC is phase control of the ranging tones. Since both sets operate in identical fashion, discussion of one side is sufficient to describe both. The ultimate output is a time multiplexed phase-adjusted tone package, which is transmitted to the satellite so that it can be relayed to and for use in the sector to which the time slot is allotted. The total sequence from the

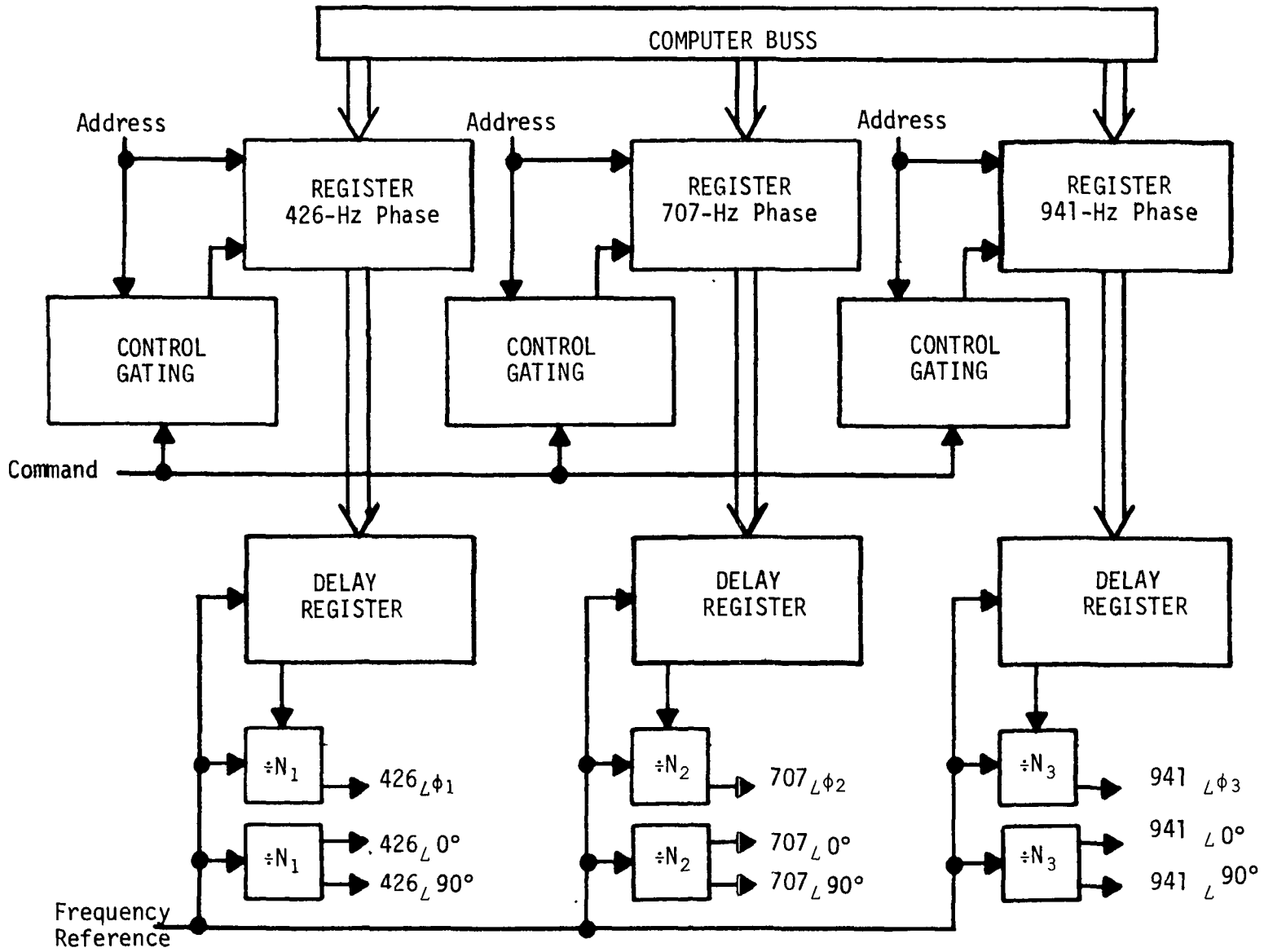

Figure 3-8. Three-Tone Controlled Phase Oscillator

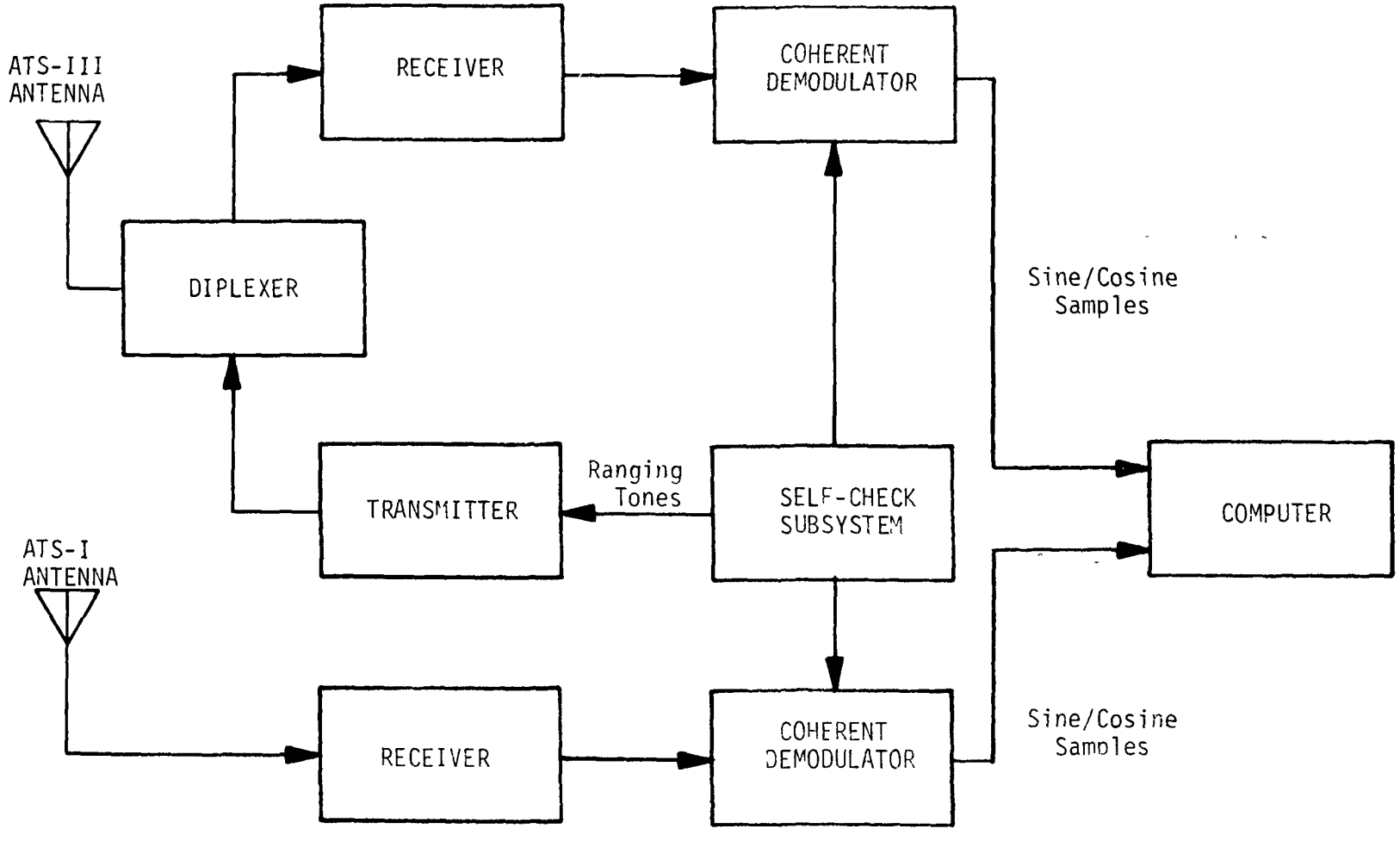

Figure 3-9. VHF Satellite Navigation Experiment GCC Simplified Block Diagram

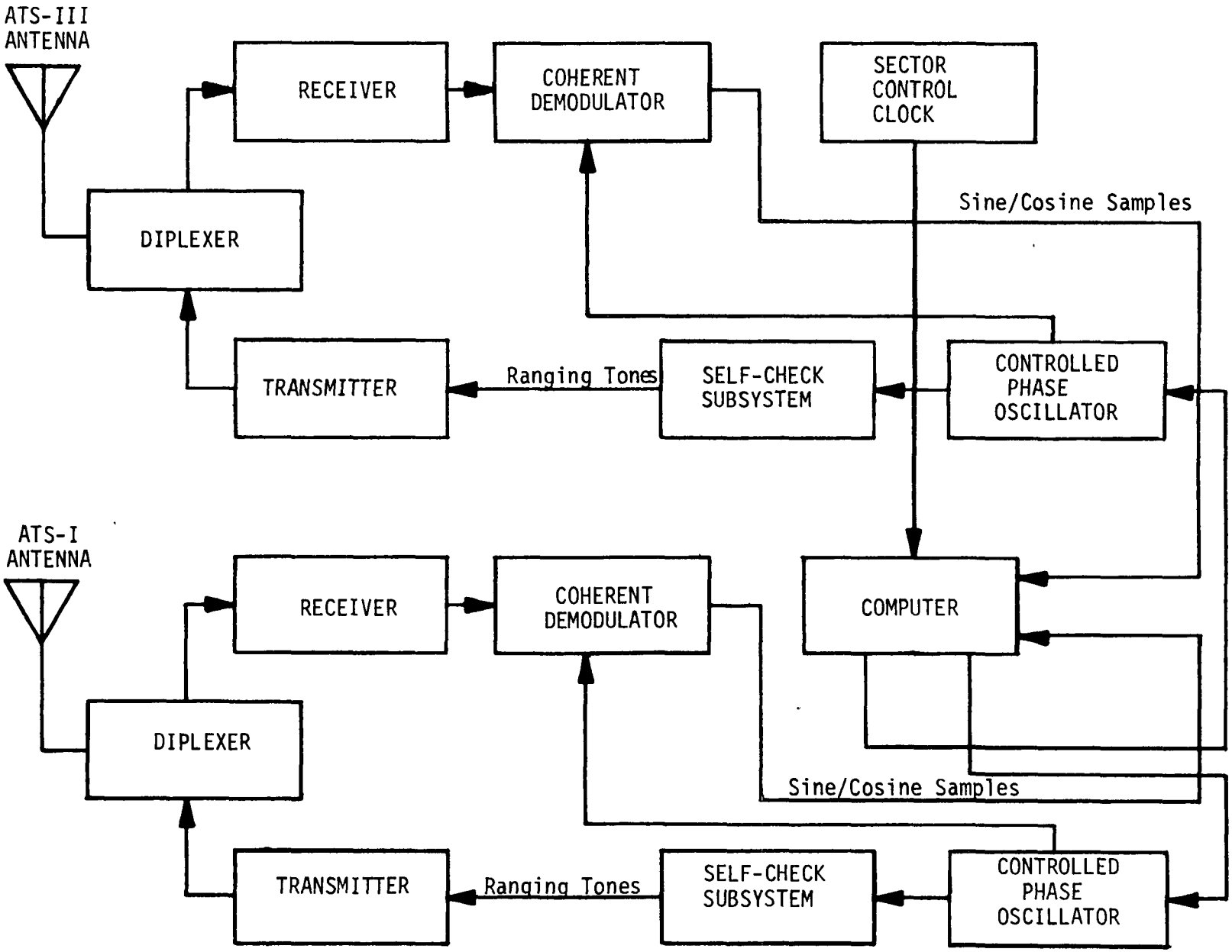

Figure 3-10. Dual Satellite Navigation GCC Simplified Block Diagram

beginning proceeds in the following manner: The computer senses the sector clock output and selects from memory the tone phase information stored there. After turning the system on, the phase in memory for the first sector would be zero, resulting in an uncorrected navigational signal. The phase from memory is transferred to the controlled phase oscillators which generate squarewaves at the tone frequencies and with proper phase shift. The squarewaves are inputs to the self-check subsystem which reject the higher order harmonics, leaving sine wave tones. In the -check subsystem the tones are also translated up, summed with the A/R tone, and translated to the 500-kHz intermediate frequency. The next signals are fed into the VHF transmitter where the tone package is translated to the 149.2-MHz transmit frequency and placed at the center of the assigned channel. This signal is routed through the diplexer to the antenna for transmission to the satellite. The satellite then retransmits the signal, at 135.6 MHz into the entire area of coverage. The satellite-relayed signals are utilized in two different processes. In one, users in the sector to which the transmission is intended make their phase measurements and calculate position. In the other, the reference terminal in the next sector in the sequence transponds the signal, shifting it to a different channel, and transmits back to the satellite at 149.2 MHz. The satellite transponded signal then arrives back at the GCC at 135.6 MHz in a different channel than originally transmitted. The receive portion of the GCC down-translates the tones and samples them with quadrature signals in exactly the same way that the OCC receivers now operate. The computer then calculates the received phases, compares them to the transmitted phases, and calculates the new phases to be transmitted to the next sector. The phase data is stored in memory to be applied at the next signal from the sector clock. Succeeding sectors are handled in the same manner.

3.3 Reference Terminal Functional Description

In order to correct the signal phase a reference terminal transponder is placed mid-sector to return the tone package to the GCC. Since the geographic position of the reference terminal is known the phases received at the GCC describe the range perturbations due to satellite movement and atmospheric change. These may then be compensated by altering the transmitted phase. The reference terminal requirements for this function are simply to transpond the ranging tones during the sector time allotted with minimal phase shift of the tones.

The block diagram of the reference terminal shown in Figure 3-11 is precisely the VHF Satellite Navigation Experiment reference terminal with the addition of the clock to control time of transmission. Note that the phase-lock-loop receives the A/R tone (and ranging tones) at all times, and the

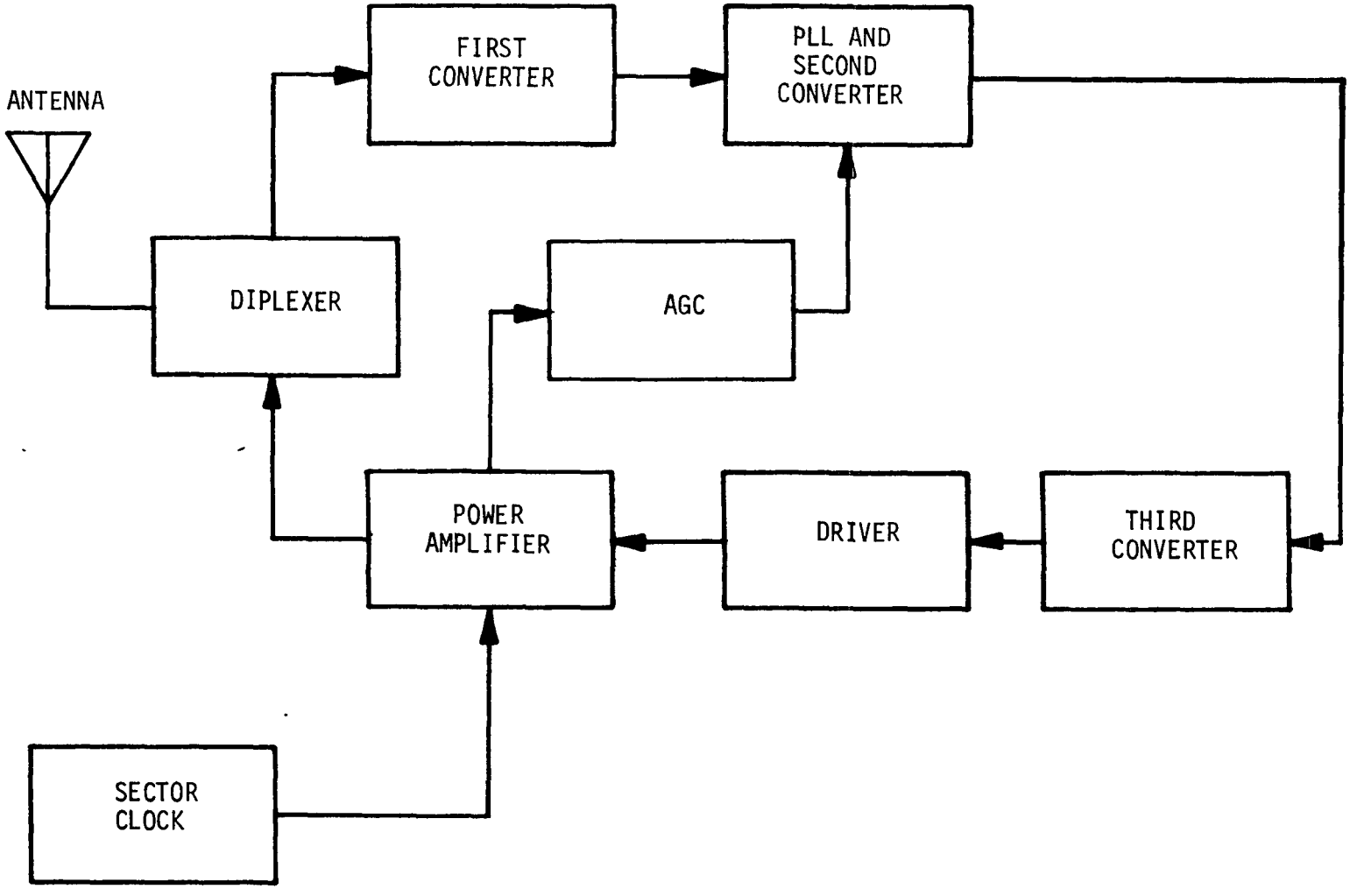

Figure 3-11. Reference Terminal Simplified Block Diagram

multiplexing is carried out on the transmit side. This effectively eliminates consideration of acquisition time.

3.4 Aircraft Terminal Functional Description

In the system being described, the term Aircraft Terminal means much more than a translational transponder, as used in the VHF Satellite Navigation Experiment. The A/C terminal becomes the phase measurement, the range calculation, and the position computation equipment, implying of course, that the A/C need not retransmit the signal for ground measurement and calculation. Figure 3-12 is a simplified block diagram of the A/C terminal. There are two receiver sides, one to accept ATS-I signals and the other for ATS-III signals. The VHF broadbeam antenna receives both satellite signals which are pre-amplified and power-split to drive the two sides. Considering one side, the signal is down-converted to IF in the receiver and phase-lock converted further in the following stage. The resultant baseband tones are sampled by in-phase and quadrature signals with the sampled components feeding an integrator. The integrated samples are then digitized and input to the computer for phase and range calculation. The altitude information for the third sphere of position is multiplexed into the computer along with the phase detector outputs. Calculated position is then displayed as latitude and longitude.

Compensation for accumulated on-board clock phase errors will be accomplished by implementing the technique described in Section II-3.1. During the experiment the clock will be synchronized on the ground every 24 hours. The frequency offset will be measured and stored in the computer along with the frequency drift rate. The elapsed time indicator, which will be an integral part of the clock, will be reset each time the clock is synchronized.

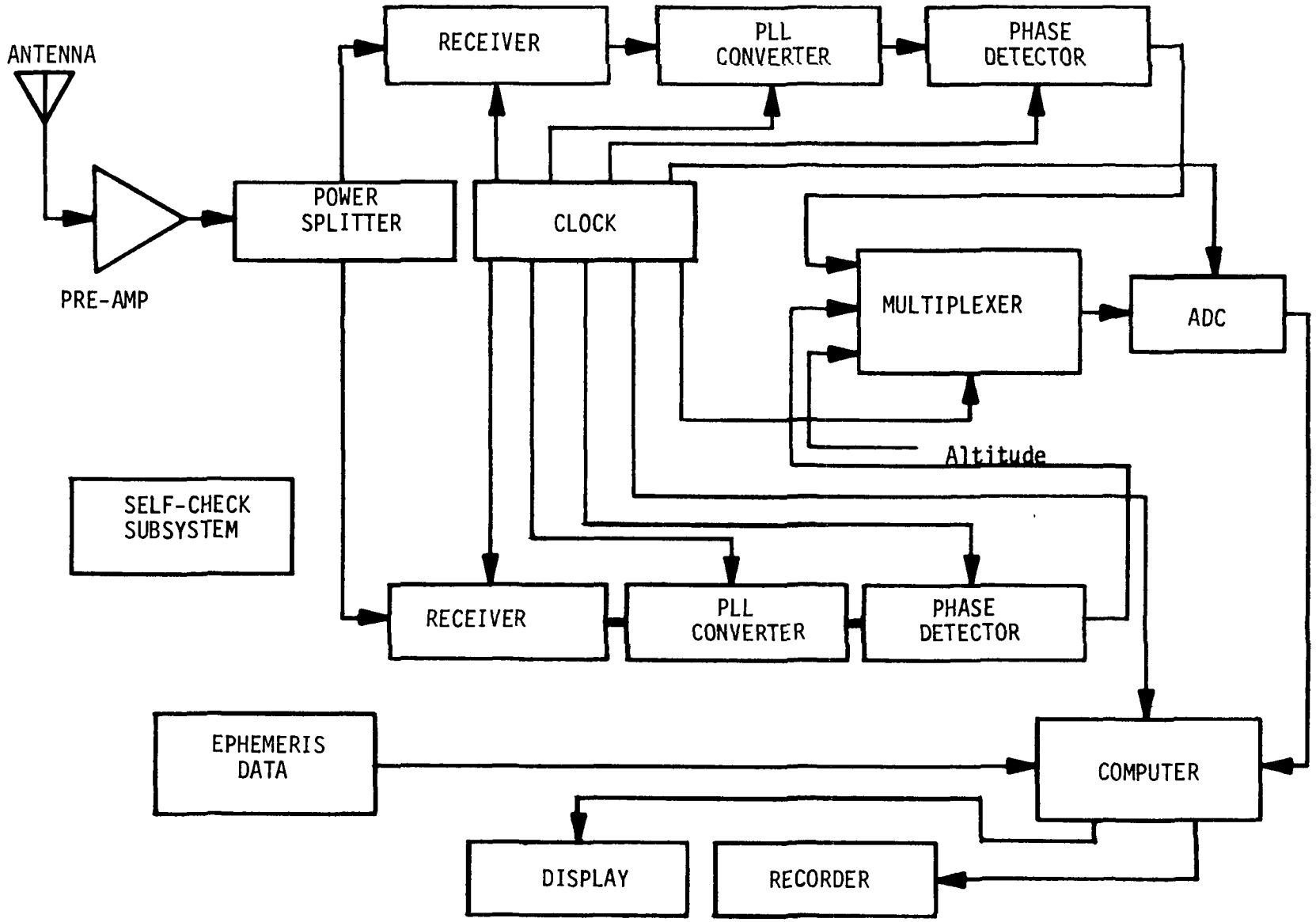

Figure 3-12. Aircraft Terminal Simplified Block Diagram

SECTION IV

EQUIPMENT RECOMMENDATIONS

1. INTRODUCTION

The equipment recommendations in the following paragraphs reflect an effort to use as much as possible the existing hardware and design that was developed for the OPLE Experiment and the VHF Satellite Navigation Experiment. Primary emphasis in the discussion, however, is given to the new key designs unique to the Dual Satellite Navigation system requirements. The three equipment groups - GCC, Reference Terminal, and A/C Terminal - are discussed in separate paragraphs followed by a concluding paragraph in which the expected system performance is summarized.

2. GCC EQUIPMENT

2.1 Unmodified Equipment

Much of the GCC as it now exists, unmodified, will be used. The computer and peripheral devices; i.e., ADC, magnetic tape recorder, and teletype, have the capacity and capability to perform the functions required for the system. New programming is the only requisite to bring the computer system up to operating status. One statement of reservation is in order at this point: The computer system has had problems with reliable operation in the past. As a result the experiment must allow schedule and cost for the purpose of computer maintenance and to cover reruns if a problem occurs mid-experiment.

The entire RF sections now in use will be employed as is. These include all parts starting at the two VHF antennas and positioners, through to the phase-locked converters. There are needed components missing, however, these will be discussed later.

The digital control electronics also will be used without modification, but a large portion of it will be idle as is the case in the VHF Satellite Navigation Experiment. The operation of this subsystem can be set up by the control signals and needs little special effort.

Various portions of the low frequency analog electronics are also to be used. In particular, the self-check subsystem tone filters and associated converters will be implemented to condition the ranging tone package prior to transmission. The other analog circuits to be used are simple buffer amplifiers,

filters, shaping circuits, etc., which interface the parts of the system.

Finally, the computer-addressed buffer registers which constitute the data flow electronics will be reconnected where needed to permit their usage in transferring the phase information to the proper oscillator.

2.2 Modified Equipment

Two areas of the GCC require modification to permit use in this system, the most important of which is the phase measurement subsystem. Recent measurements in the VHF Satellite Navigation Experiment have indicated that the rms error of the present circuitry is approximately 1.5 degrees, which at a maximum tone frequency of 941 Hz corresponds to 1.3 km rms range error. This error magnitude is considered excessive. The linear integrated circuit-operational amplifier technology available today makes possible improvement in the circuit functions. Figure 4-1 is a schematic of the present phase measurement circuit for one tone. The four major circuit functions represented include:

(1) Passive Bandpass Filter

(2) Symmetric Limiter

(3) Active Bandpass Filter

(4) Quadrature Sample, Integrate, and Dump

The latter three of these can definitely be improved. The symmetric limiter is easily replaced with a high-gain comparator operational amplifier followed by low-offset clamp switches to accurate plus and minus voltage references. Such a limiter ensures clipped signals at minimum signal-to-noise ratio and suppresses second harmonic components. This simplifies the active bandpass filter and prevents wide amplitude deviations from appearing at the sampler input.

The active bandpass filter can be synthesized using operational amplifiers with high feedback ratios to insure gain stability. This results in an improved transfer function stability, controlability, and accuracy.

Last, the quadrature (sine - cosine) sampling and the integrate and dump functions can be improved. The dynamic range and impedance requirements for the series modulating FET switch (see Figure 4-1, Q_6 and Q_9) limit the sampling accuracy possible with this method.[6] An improved circuit results if the FET is enclosed in the feedback loop of a zero-order hold circuit. The sample and hold function, which this creates, will give less switching error, and after integration is the

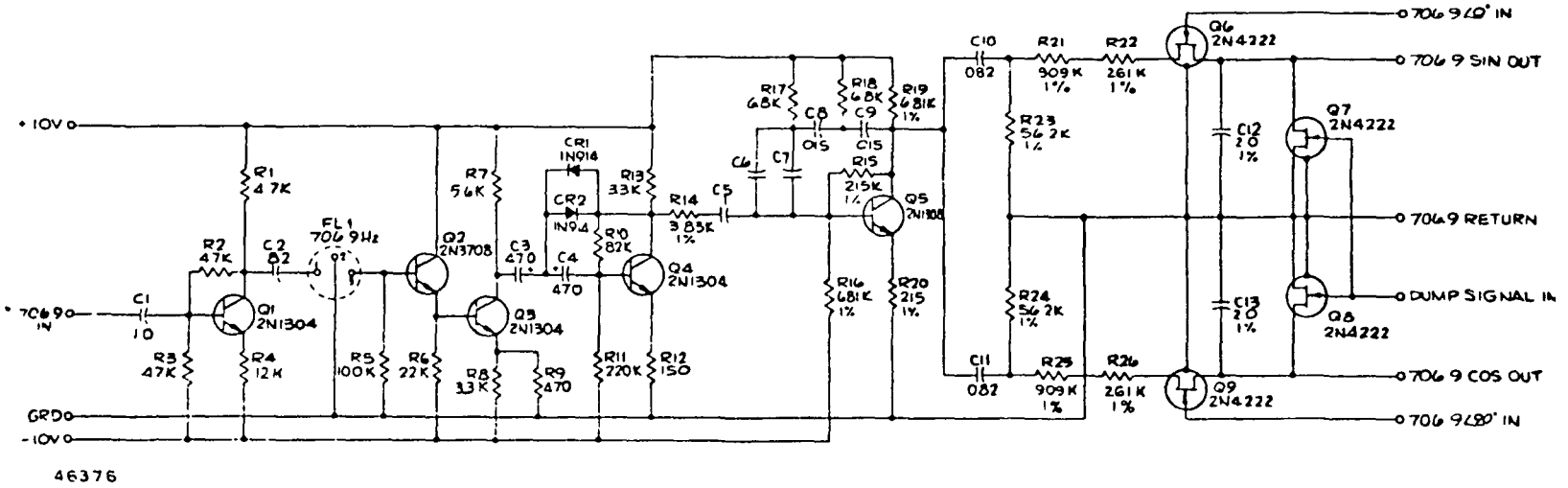

Figure 4-1. OPLE Receiver (707 Hz)

same as the gate and integrate for one-half period intervals which describes the present circuit. In addition, the passive RC integration can be improved by replacing it with a capacitor feedback operational amplifier Miller integrator. Thus, the RC time constant can be decreased so that the 1-megohm resistor can be reduced to a more reasonable value.

2.3 Duplicated Equipment

The GCC as it is in operation in the VHF Satellite Navigation Experiment does not have the capability of transmitting to two satellites simultaneously. Conversely, the receiving elements are all in existence including two VHF antennas. In order to supply the second transmit capacity the diplexer, transmitter subsystem, and self-check subsystem will be duplicated.

The diplexer, frequency synthesizer, and VHF power amplifiers in the GCC are purchased items and will be duplicated by buying equivalent units. The rest of the transmitter subsystem is circuitry which can be component for component reproduced from drawings that are on file. These circuits will be tested and adjusted to procedures that are proven, and interconnected with confidence in wire list accuracy. There will be some design effort required to determine what circuits can be deleted and to compensate in loading, etc., for their absence; however, the overall duplication effort is minimal.

The necessary effort to reproduce the required portions of the self-check subsystem is similar to the effort required for the transmitter subsystem as described above. An exception is that no major element need be purchased.

2.4 Additional Equipment

The preceding paragraphs of this section have dealt with use of the GCC essentially as it is. There are, however, two new additional requirements. These are the computer controlled variable phase circuits (Phase Shift Subsystem) which control the transmitted tone phase, and a totally new set of computer programs.

2.4.1 Phase Shift Subsystem

The Phase Shift Subsystem will interface with the GCC at the control electronics data output register as shown in Figure 4-2, which for simplification shows the block diagram for one tone only. Total complexity would include two more circuits which differ only in the divider ratios and the connection to different data output registers. As shown in the block diagram, the data from the computer is transferred (under software control) into the data output register. After a short delay a transfer pulse is generated in the gate circuit to transfer the

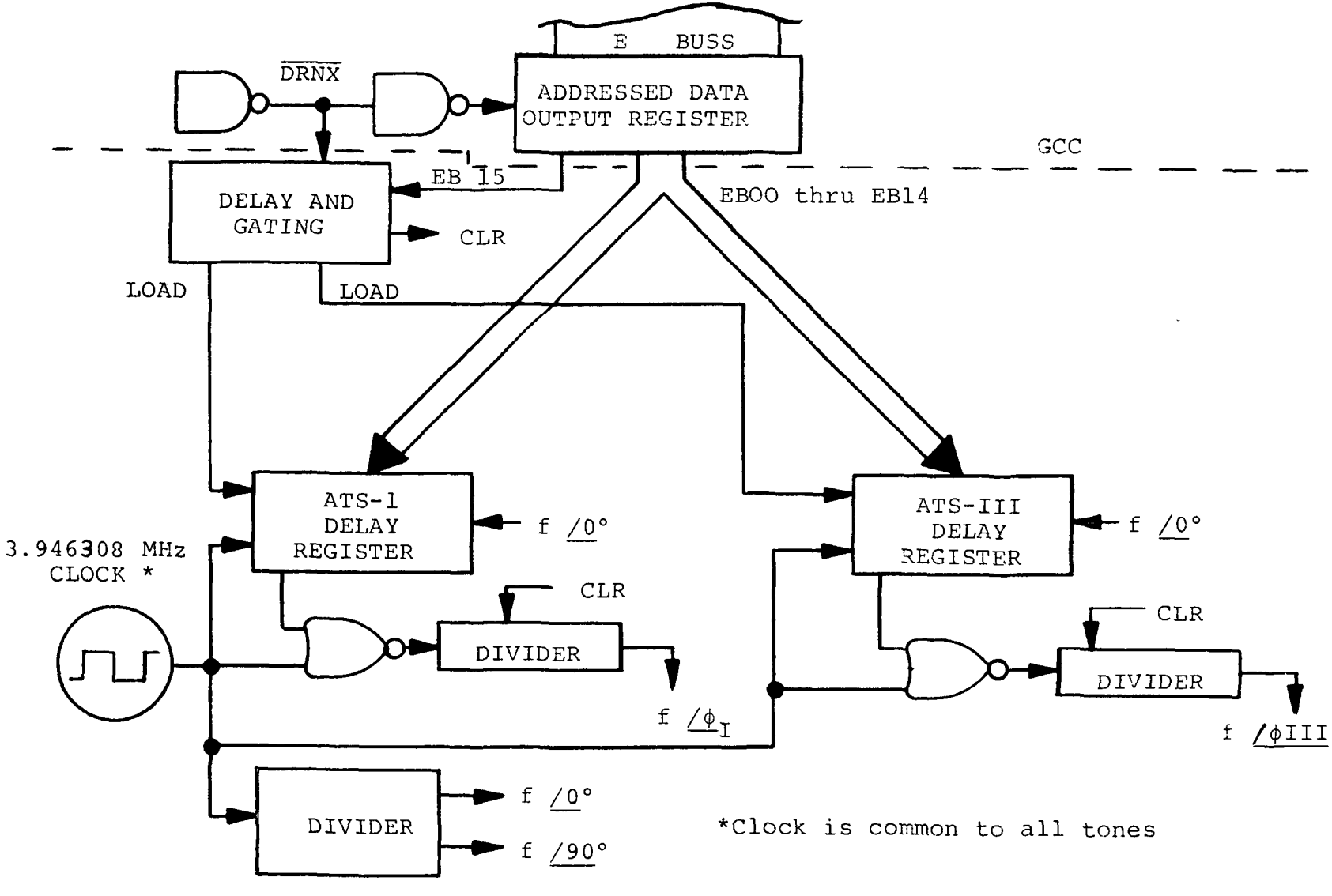

Figure 4-2. Block Diagram of Phase Adjust Subsystem for One Tone

data to either the delay register for ATS I or ATS-III delay as determined by the state of bit EB15, which is also computer controlled. This transfer also gates the clock off at the divider for the Phase Shifted signal (f $\angle\phi$) and sets the divider to state zero. On the next positive transition of the reference frequency, at zero phase, the delay register begins to count down. When it reaches zero the divider clock is enabled and the phase shifted signal commences. Thus, in less than 2 cycles of the tone its phase has been shifted by an integral number of periods of the master clock. The clock frequency of 3.946308 MHz has been selected to give the frequencies and minimum phase shift increments as shown in Figure 4-3.

Figure 4-4 and 4-5 are logic diagrams of the period generators [17] for the 941-Hz and 707-Hz signals. The 426-Hz divider is similar, but requires three more circuit packages. Each divider is used twice, first to generate the tone references in quadrature to drive the sample gates, and second, to be preset and gated to generate the shifted tones which are filtered and shifted for transmission by the self-check subsystem. Figures 4-6 and 4-7 represent the logic diagrams of the Delay Registers and the Delay and Gate circuit. Operation of the period generator dividers is described in the referenced report [17]. The delay registers are 15-stage shift registers made up of three 5-bit binary counters, with decoding of the zero state used to disable the clock and to enable the divider. Finally, the Delay and Gate senses the EB15 and the DRNX gated with the address signals from the GCC to produce the pulses that transfer the data to the proper register, ATS-I or ATS-III, and clears the divider to the beginning state.

2.4.2 Software

In Section II.3.2 it was shown that the system sequence is under computer control, and since this operation is different than either OPLE or the VHF Satellite Navigation Experiment, new computer software is required for this system. The GCC general software organization has been covered in the "Design Study Report for Omega Position Location Equipment Control Center" [18] and is directly applicable to this system.

Computer control is under an "executive" program that waits for an interrupt signal to initiate a subroutine. The executive program is described in the aforementioned document; therefore, only the needed new subroutines will be discussed here.

Sequence of operation is triggered by a clock signal on one of the interrupt lines which indicates either time to output new phase data or time to read and process measured phase. The two subroutines needed then are the Signal Phase Measurement and the Phase Data Output subroutines which will be described below.

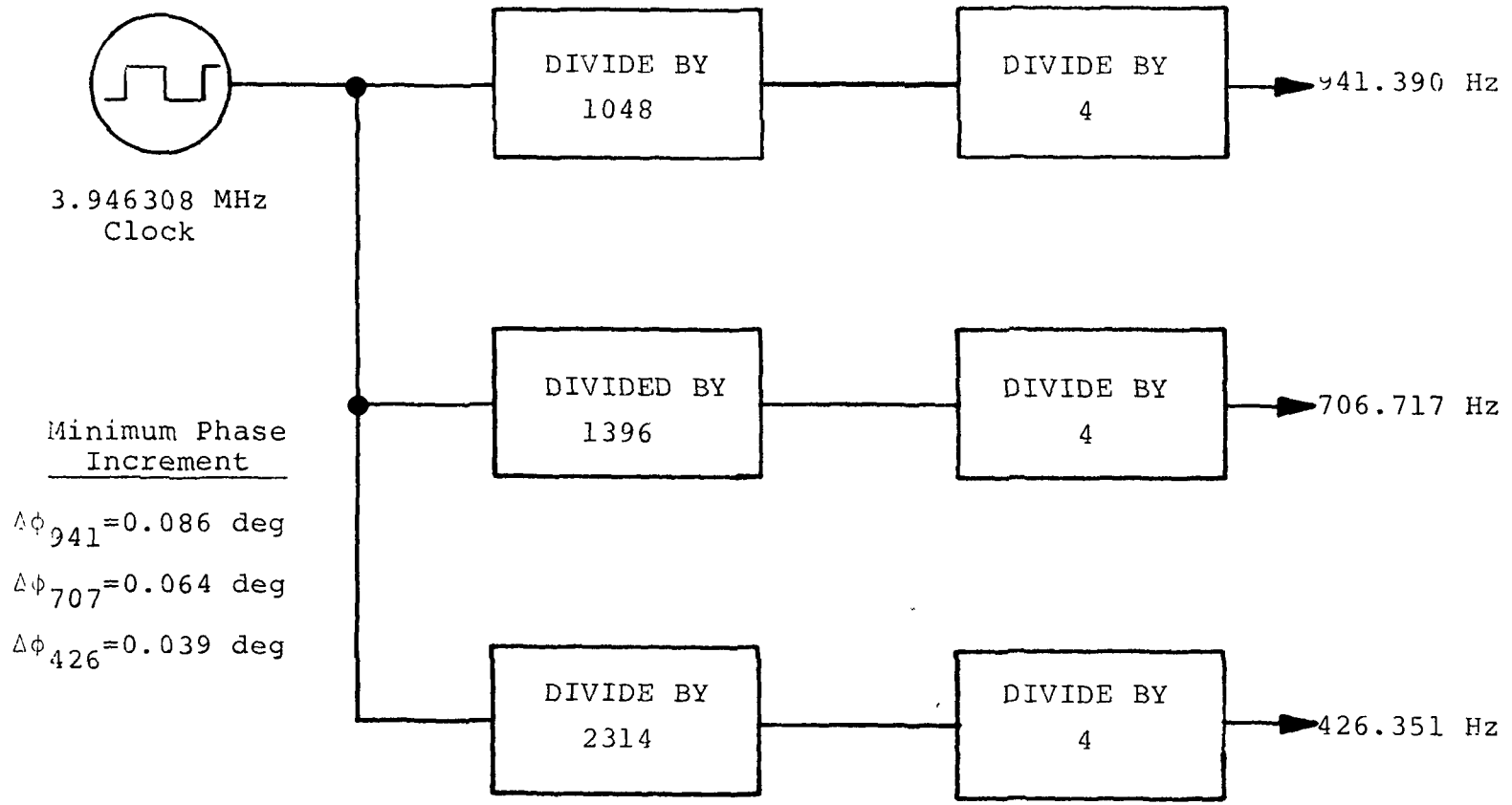

Figure 4-3. Ranging Tones Dividers

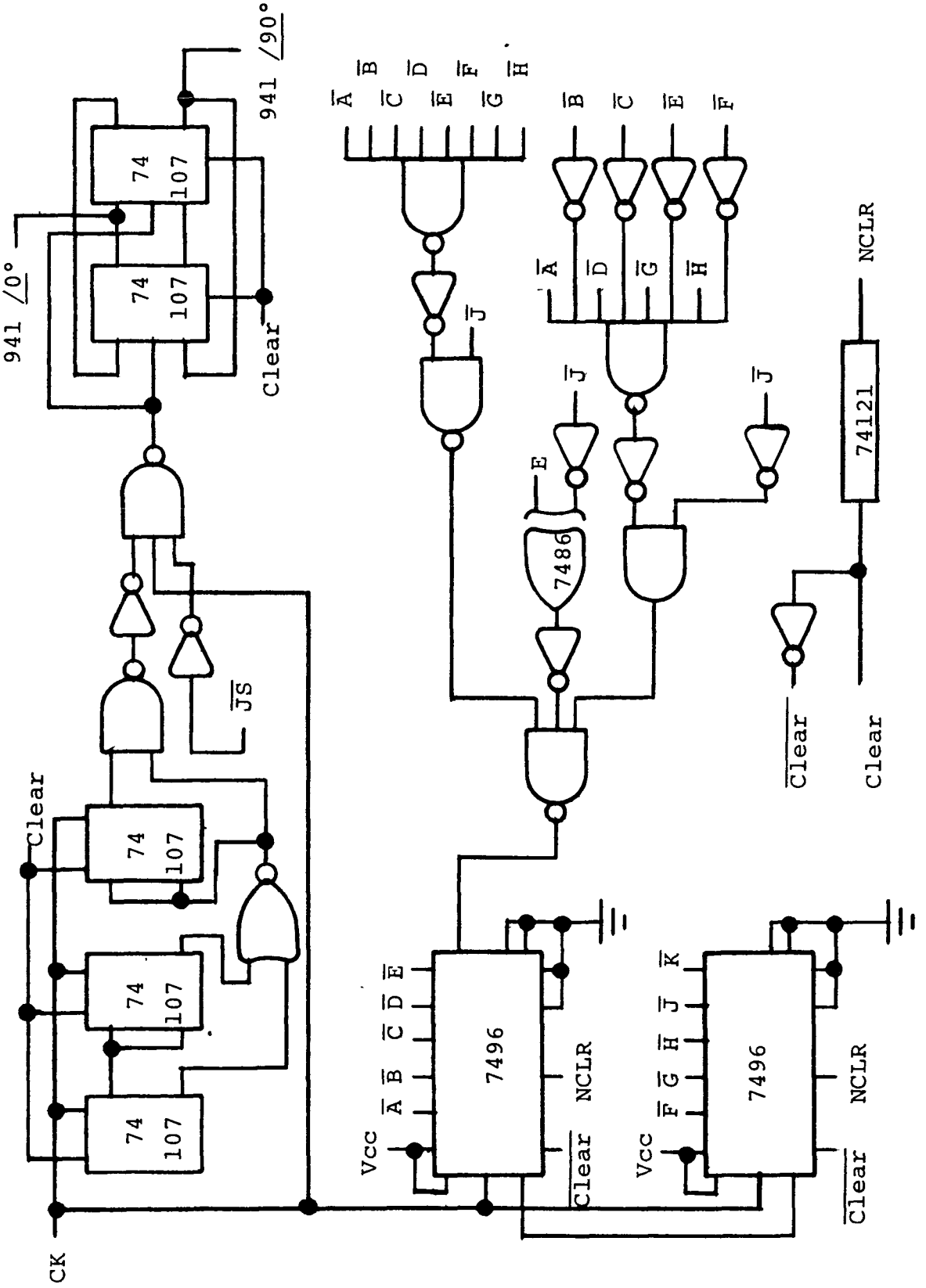

Figure 4-4. 941-Hz Divider

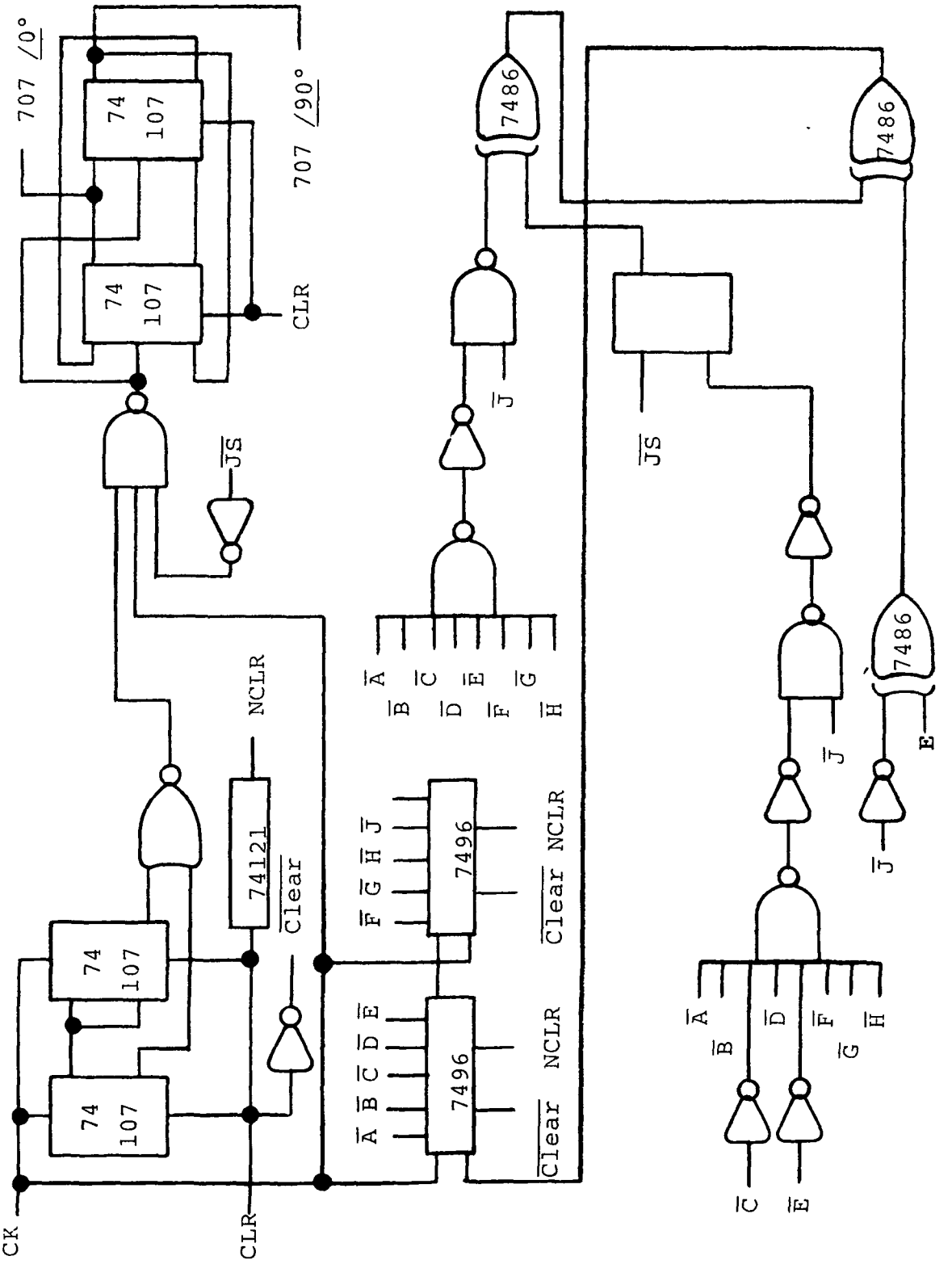

Figure 4-5. 707-Hz Divider

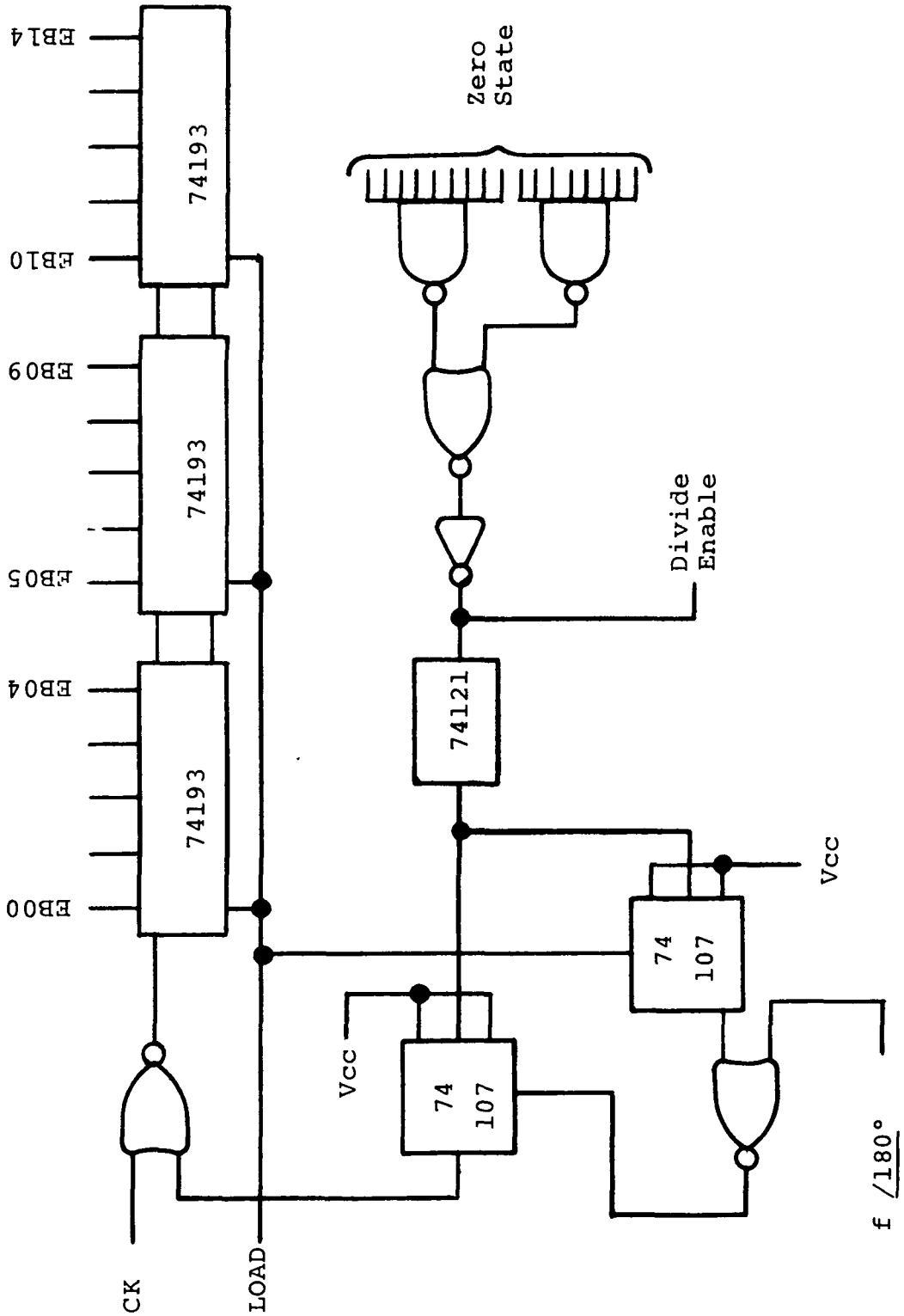

Figure 4-6. Delay Register

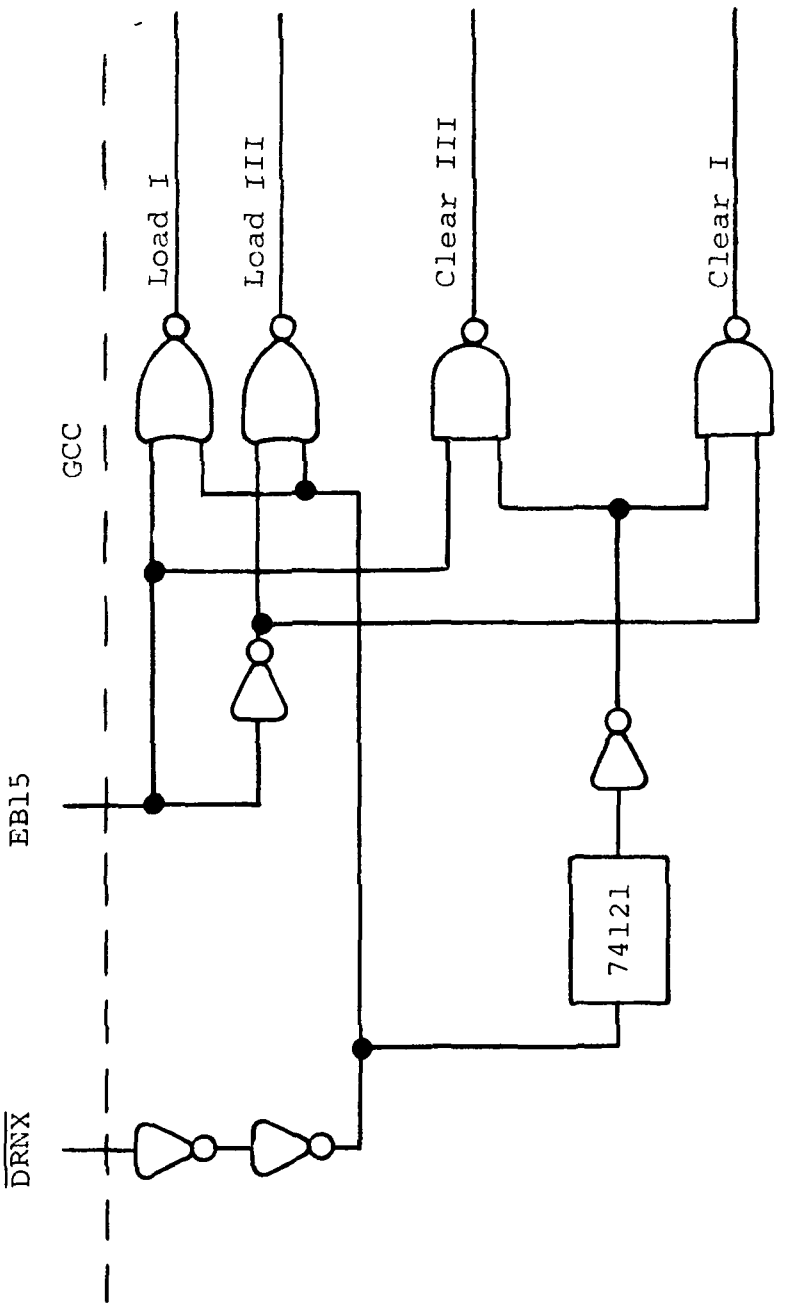

Figure 4-7. Delay and Gate Circuit

Signal Phase Measurement (SPM)

At the end of the phase measurement integration period the digitized signals are transferred into a buffer register and the interrupt line associated with the sector being received is pulsed. The phase data (sine and consine) are reduced to a phase angle, which is used with the transmitted phase to compute the phase at the reference terminal. From this information, and a calculation of the assumed satellite position and range, a new transmit phase for each tone is produced. This data is converted to number of cycles of the master clock, keyed in the 16th bit as to application for ATS-I or ATS-III, and stored in the appropriate memory location.

Phase Data Output (PDO)

The beginning of each sector transmission will be initiated by one of three interrupts to the computer. This essentially asks for the phase information for the appropriate sector to be output to the controlled phase oscillator. The subroutine will control the data flow so that the proper memory locations are output in sequence until all of the tone phases have been adjusted. Control is then returned to the Executive Program to await the next SPM interrupt.

In total, then, six interrupts will be required to perform the control required.

3. REFERENCE TERMINAL EQUIPMENT

Each Reference Terminal (R/T) is simply a transponder which returns the signals to the GCC, via the satellites, to provide a known range reference against which the system perturbations caused by satellite position uncertainty and ionosperic range bias can be compensated.

A block diagram of the R/T is shown in Figure 4-8 which is the basis for the following discussion of the circuits and hardware involved.

The link parameters derived in Appendix A assume 0-dB gain antennas at the A/C and R/T. This is not a constraint at the stationary R/T, however, and it is proposed that two relatively inexpensive 8 to 10-dB VHF helical antannas be used. This is done to improve the C/N_o at the GCC in that the gain of the antennas improves both the ATS-to-R/T and the R/T-to-ATS links, while also minimizing satellite power sharing with unnecessary signals intended for the other satellite.

The associated diplexers will be the same as those now used in the VHF Satellite Navigation Experiment.

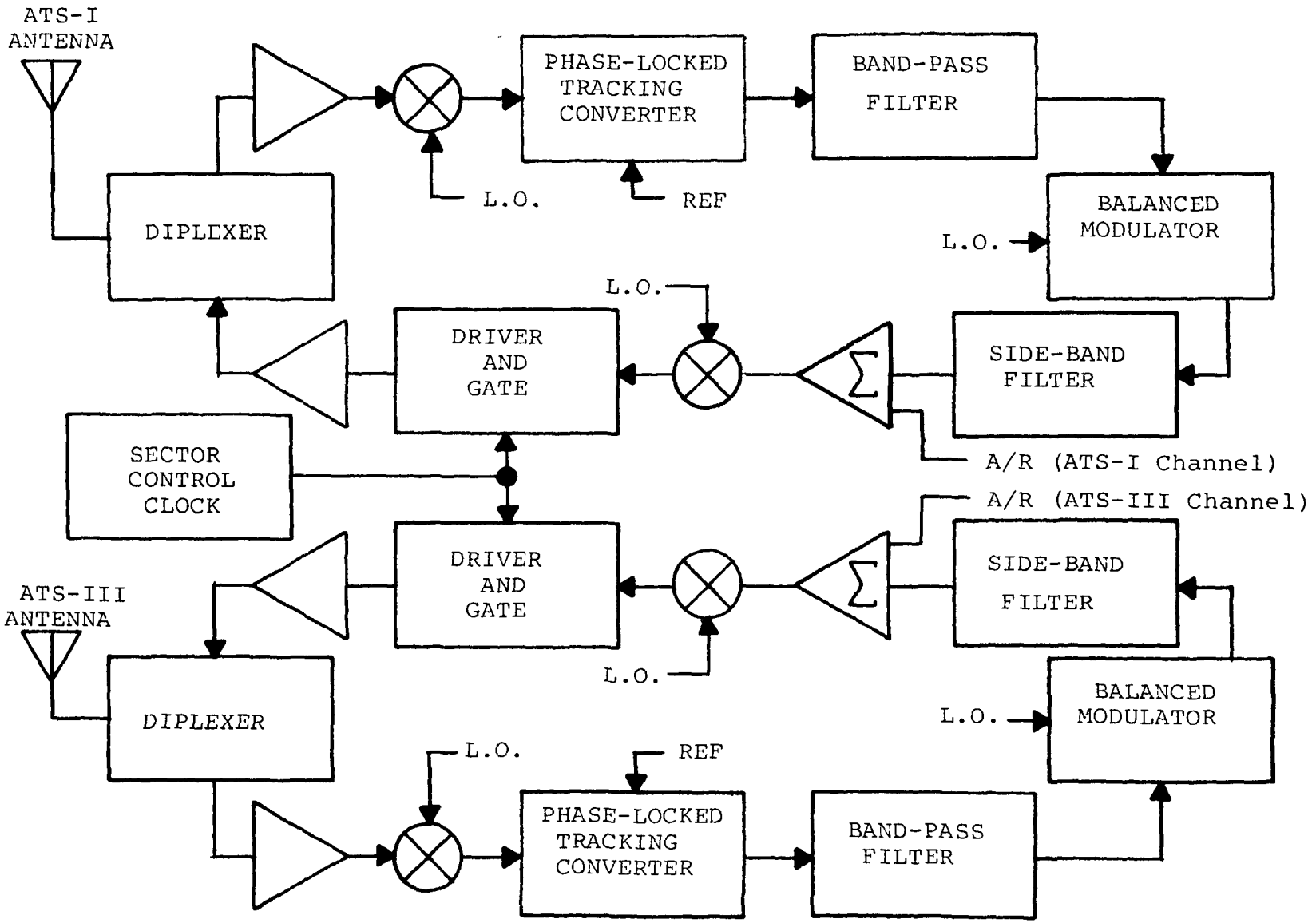

Figure 4-8. Reference Terminal Block Diagram

On the receive side the pre-amplifiers, first converters, and the phase-lock tracking converters will also be the same as existing equipment with slight modifications. In the transmit electronics the bandpass filters, balanced modulators, sideband filters, summers, and up-converters will be very similar to those in the OCC self-check subsystem.

The control clock and gated pre-amplifiers perform the time multiplexing function as required for sector switching. The clock will be sufficiently stable so that synchronization may be accomplished by methods such as the following: (1) a telephone line from the GCC, (2) a WWV receiver at the R/T site, or (3) a synchronizing signal transmitted from the GCC. It is assumed that a WWV receiver will be available at each R/T site, so the second method is planned here.

In review, the reference terminal with the exception of the antennas, clock, and the gated preamplifiers on the transmit side is made up of existing proven circuitry, and is therefore, a straight-forward design.

4. AIRCRAFT TERMINAL EQUIPMENT

4.1 Introduction

In Section III-3.4 a brief description of the functions to be performed by the aircraft equipment was presented. In this section a more detailed description will be presented, and will include specific equipment recommendations.

In specifying the aircraft equipment the primary criterion is to use as much equipment as possible that has been designed and is operationally proven. In addition, a particular airborne qualified computer which may be made available by Texas Instruments on a loan basis during the experiment will be recommended. This approach will allow maximum concentration of effort on experimental goals rather than hardware design considerations. In the VHF Satellite Navigation Experiment (NAS 5-21079) and the Omega Position Location Experiment (NAS 5-10248) considerable equipment has been designed, built, and tested for some functions which are identical to those required in this experiment. This equipment will be recommended with little or no modification.

The aircraft equipment can be divided into four main subsystems: (1) receiver demodulator, (2) phase measurement, (3) data processor, and (4) timing and control. The signal is received by the receiver demodulator subsystem where it is demodulated by phase locking to the A/R tone in the ranging tone package. Since the phases of the incoming signal tones contain the desired information, one of the primary constraints on the receiver demodulator subsystem is that it preserve this phase information for presentation to the phase measurement subsystem

for subsequent measurement by comparison with the on-board reference tones. Since the phase measurement subsystem must accommodate two sets of three non-harmonically related tones, a sampled data system implementation was selected. The data processor subsystem will be used to accumulate the phase data and calculate the latitude and longitude, while control of the aircraft system will be performed by the timing and control subsystem. Although a high stability crystal oscillator will be used, compensation must be made for any accumulated clock phase error resulting from a frequency offset or drift. By removing the accumulated phase error from the measured phase angle, (see Section II-3.1), the system will perform as if the on-board clock were closely synchronized with the ground clock.

4.2 Receiver Demodulator Subsystem

4.2.1 General Description

The aircraft will simultaneously receive signals from both the ATS-I and ATS-III satellites. As discussed in Section II-2.3, the error caused by satellite movement restricts the maximum time the correct signals will be available for measurement (sector time interval). With this limit, both phase measurements must utilize as much of the interval as possible for signal integration and processing. Some of the time will be required for instrument settling; however, the A/R tone will be present continuously, which excludes PLL acquisition time from consideration.

The block diagram in Figure 4-9 shows the receiver demodulator subsystem. This subsystem receives the signals from ATS-I and ATS-III.down-converts them to baseband, and filters out the six ranging tones. The ranging tones are then sampled by the phase measurement subsystem to be discussed in the next section.

Since the two sections of the subsystems are identical for ATS-I and ATS-III except for the different channel frequencies of the tone package, it will be sufficient to discuss the receiver demodulator for one satellite. As shown in Figure 4-9, the incoming signal is first down-converted to a 70-MHz IF, then further down-converted to 10.7 MHz using a phase-lock loop converter. The baseband output of the phase detector is then filtered using three 50-Hz bandwidth filters to separate the three tones. The tones are processed next by the phase measurement subsystem.

4.2.2 Equipment Considerations

All of the circuits enclosed by dotted lines have been designed and packaged for airborne equipment in the VHF satellite Navigation Experiment now being performed by Texas Instruments.

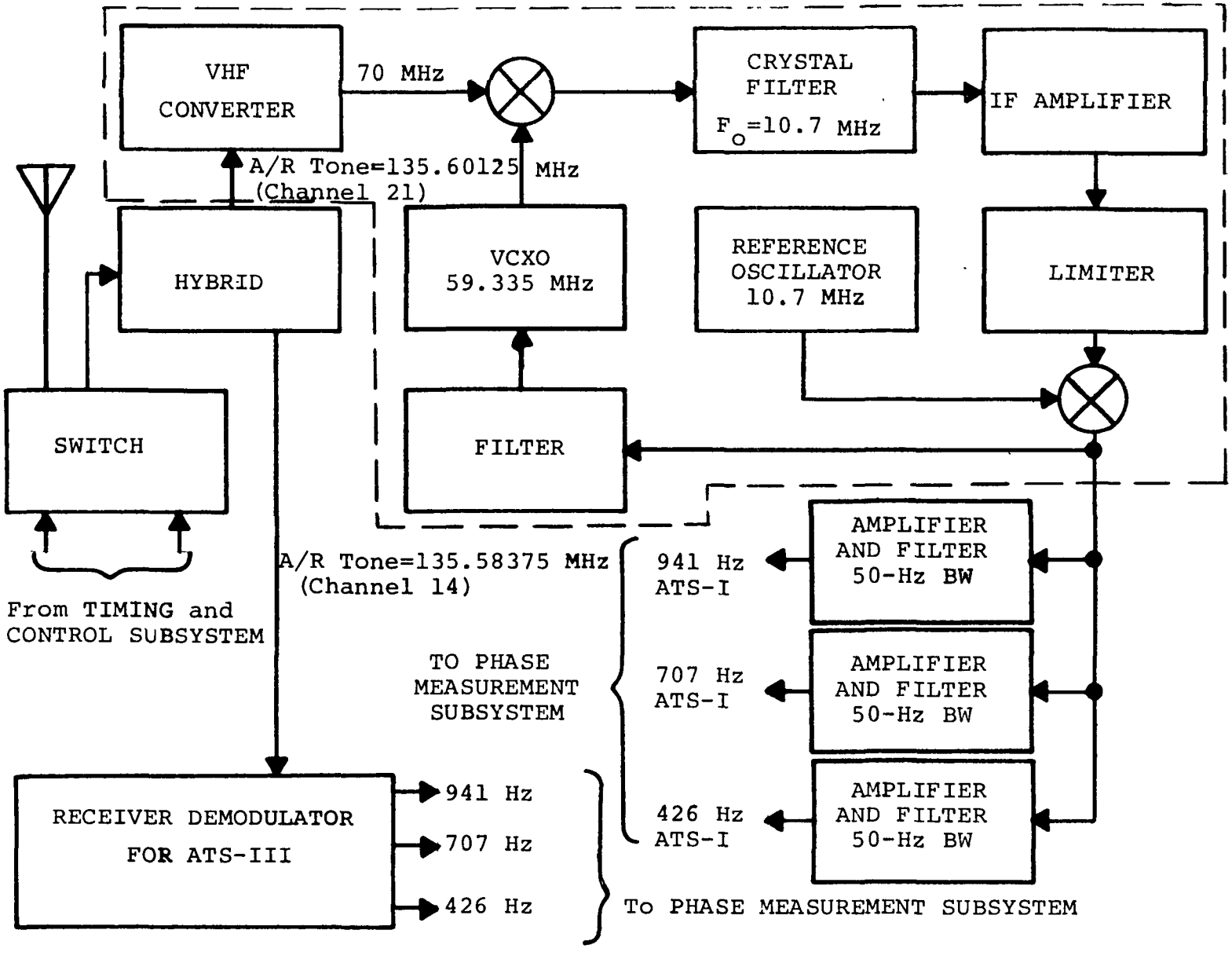

Figure 4-9. Receiver Demodulator Subsystem

The remaining circuits are currently being used in the ground control center of the above mentioned experiment and will be repackaged for airborne use with only slight modification.

4.2.3 Self-Check Section

It is essential for the aircraft equipment to have the capability of completely checking the operation of the on-board system without requiring signals from the GCC. To perform this function, a self-check section of the Receiver Demodulator subsystem is included. The block diagram in Figure 4-10 shows the elements of the self-check section. In operation, the reference tones simulate ranging tones by modulating a self-generated A/R tone. These tones are then up-converted to the receive frequency channels of approximately 135.6 MHz. When the self-check switch is "on" this signal is switched into the two receivers. The resulting output on the display will be a fixed quantity which can be used not only to indicate system operation, but to provide some quantitative measure of its performance.

4.3 Phase Measurement Subsystem

4.3.1 General Description

The primary function of the on-board equipment is to measure the phases of the ranging tones, as received from both satellites, with respect to an on-board generated reference. The receiver demodulator subsystem discussed in the previous section separates the six tones and presents them to the phase measurement subsystem for phase comparison with the reference tones. The equipment used to make the phase measurement is discussed in this section.

The tone phase will be measured by a sampled data digital system. Each tone frequency (426 Hz, 707 Hz and 941 Hz) will be sampled at a different rate. The sampling rate is derived from the stable master clock. It can be shown that by sampling the received tone with one sampling signal that is in phase with the reference tone and another which is 90° out of phase with the reference tone, the phase of the received signal with respect to the reference can be found. In addition, the Nyquist sampling theorem states that a signal of bandwidth B need only be sampled at the rate of 2B. In this case, in which the tones are separated by a 50-Hz bandwidth filter prior to sampling, a sampling rate of only 100 Hz is required; however, the 50-Hz filters are not perfect and a sampling rate of 200 Hz was chosen to prevent aliasing.

4.3.2 Sampler Timing

Since the three tone frequencies are non-harmonic a

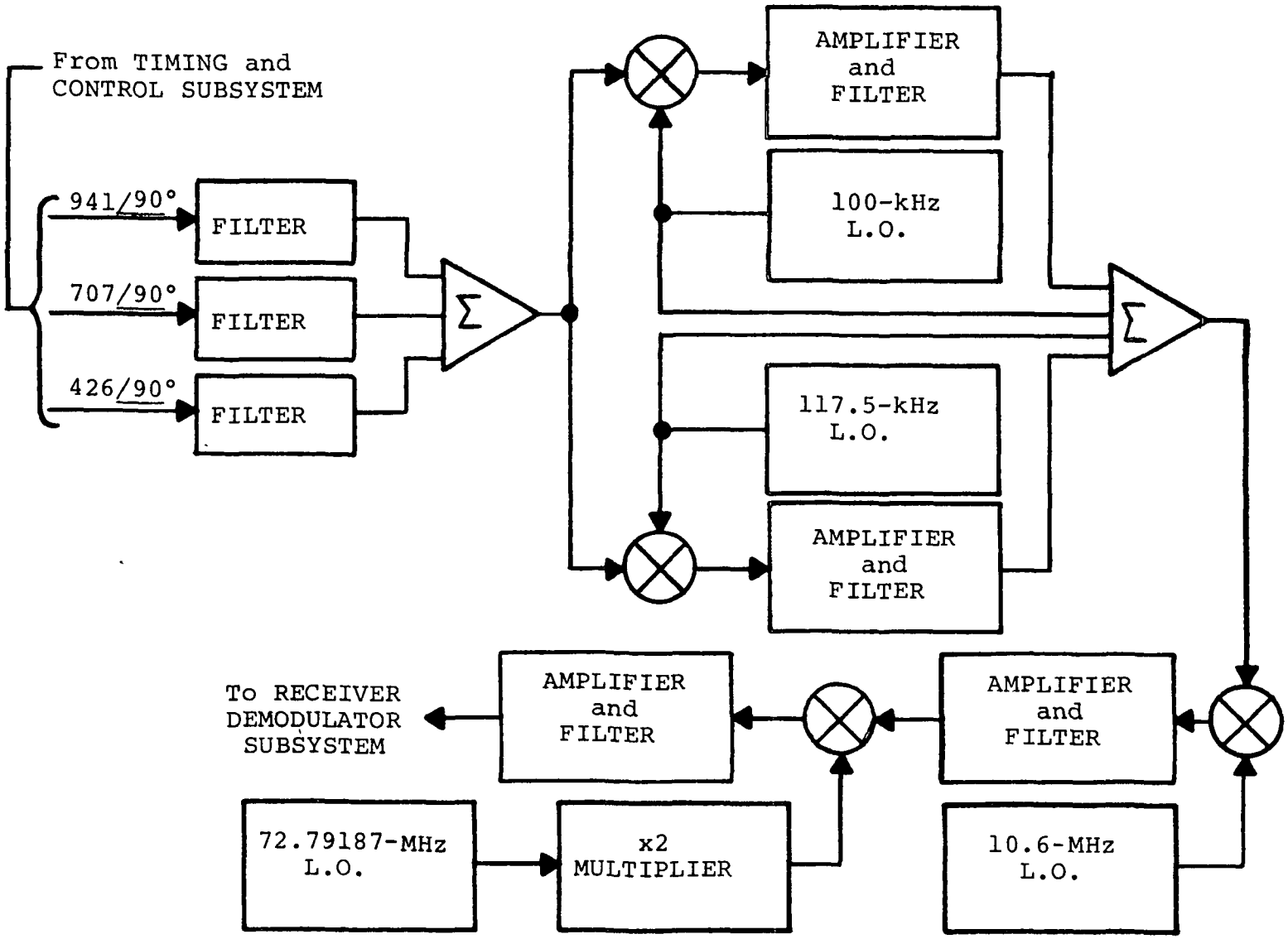

Figure 4-10. Self-Check Subsystem

common sampling rate could not be chosen. This situation necessitated the selection of a separate sampling system for each tone. The same frequency tone from both satellites may be sampled by the same sampler; however, since the tones do not have to be sampled on each cycle the sampler can be switched between them. A timing diagram of the sampling of the two 941-Hz tones is shown in Figure 4-11. The sampling rate is derived from a clock which is four times 941 Hz so that both the in-phase and the quadrature phase samples can be decoded. Note also that the quadrature samples are taken 270° out of phase rather than 90°. This is to allow more settling time for the sample and hold and analog-to-digital converter. The quadrature sample will be inverted to obtain the 90° sample from the 270° sample, and its sign changed either in the computer or in the ADC.

4.3.3 Subsystem Detailed Description

A block diagram of the phase measurement subsystem for the 941-Hz tone is shown in Figure 4-12. The equipment for the other two tones is identical except for sampling rates. The counters used to generate the multiplexing and sampling signals are shown in this diagram for clarity; however, they will be located with the master clock so that they can be preset to the GCC timing. This will be discussed in Section IV-4.6. The sampling and digitizing are performed in the phase measurement subsystem while the integrating is performed in the data processor.

The number of bits required by the accumulator and digitizer is discussed in paragraph II-3.1. The number of bits in the accumulator remains the same for this system (10 bits); however, since the system proposed for this experiment will be using the same ranging tones as currently instrumented in the GCC, there will be a different number of bits required by the ADC. The number of bits in the ADC is dependent upon the signal-to-noise power density ratio expected at the input to the aircraft receiver. From the link calculations in Appendix A the worst-case E/N_o = 24.5 dB-Hz. In specifying the ADC requirements the best E/N_o should be chosen, and the best E/N_o that can be expected is less than 40 dB-Hz.

Since the tones will pass through a 50-Hz bandwidth filter, the signal-to-noise ratio at the ADC is 23 dB. This corresponds to a σ_n = 1/20.1 radians. Since the ADC half scale must equal $\pm$ $\pi/4$ radians, $\Delta = \pi/2^n$. From Section II-3.1 it is seen that

$$\Delta = \pi/2^n \leq 1/20.1$$

or $$2^n \geq 63.2$$

or $$n = 6$$

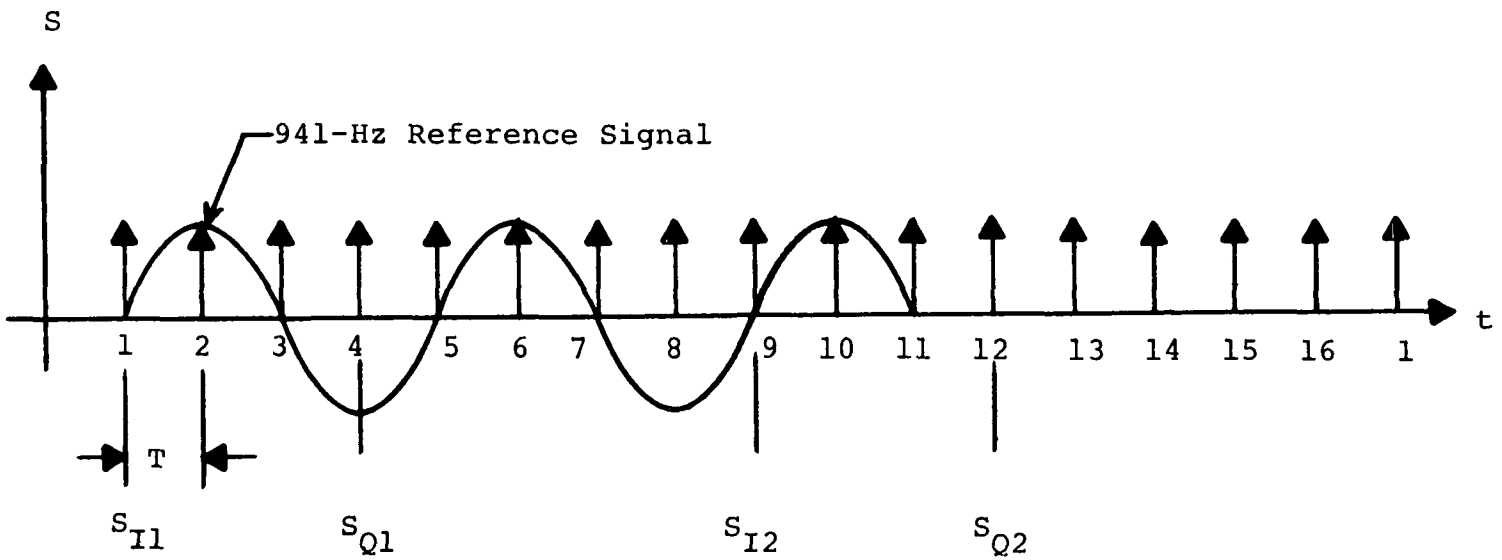

S_I=In-Phase Samples

S_Q=Quadrature Samples

T =1/(4)(941)=1/3764

Figure 4-11. Sampling Signals for the 941-Hz Tones

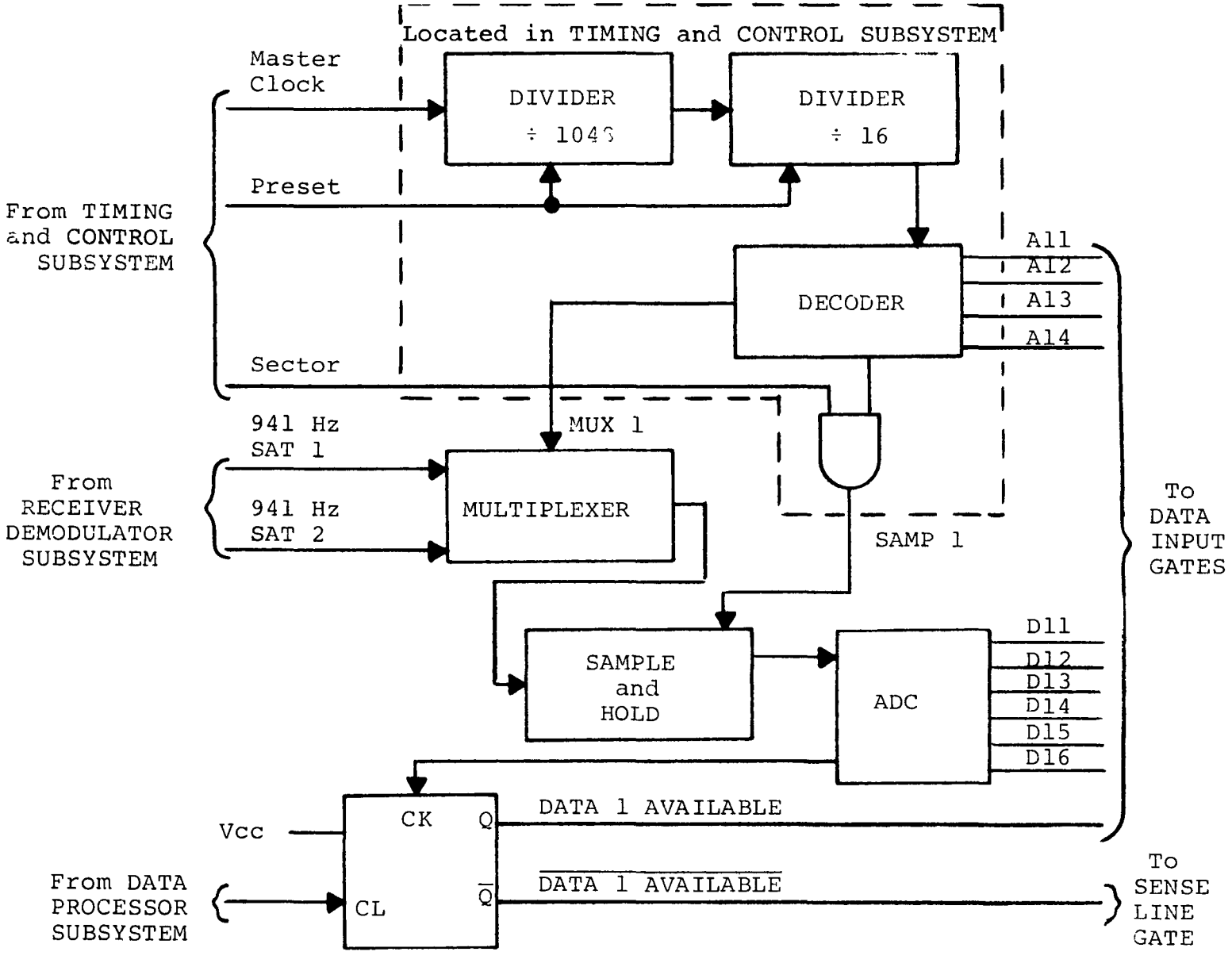

Figure 4-12. Phase Measurement Subsystem for the 941-Hz Tones

After the sample has been digitized a signal must be sent to the computer to indicate that digitization is complete. This is the $\overline{\text{DATA 1 AVAILABLE}}$ signal shown in Figure 4-12. Also, an identity code generated in the sampling decoder is read in with the data to identify the data word; i.e., satellite 1, 941 Hz, in-phase, etc.

4.3.4 Data Handling

One problem that occurs because the three tone frequencies are asynchronous is that more than one ADC can have completed its cycle and be waiting to be read by the data processor at the same time. To solve this problem the first word that the processor reads in will tell the processor which ADC to read. As can be seen in Figure 4-13, bits B0, B1, and B2 indicate which ADC is complete. The processor then reads each completed ADC by sending out a read command with the address of the ADC to be read. The address decoder receives the read command, gates in the proper A/C data and resets that DATA AVAILABLE flip flop. After the data is received by the processor it checks bits B0 to B2 to see if another ADC is to be read. If true, the aboye process is repeated. If not true, a clear data command is sent and the processor waits for the next signal on the sense line.

4.4 Data Processor Subsystem

4.4.1 Required Tasks

The Data Processor subsystem is required to perform several tasks which are summarized under general headings below.

(1) Read and accumulate phase data

(2) Read altimeter data and time of day

(3) Calculate satellite constants from ephemeris function

(4) Calculate latitude and longitude

(5) Output data to the display

(6) Determine if system is in self-check mode

This section will describe what equipment is necessary to perform the tasks listed above and then describe and justify the choice proposed for this experiment.

4.4.2 Hardware Requirements

Some of the considerations in selecting a data processor are word length, speed of operation, input/output, and data/

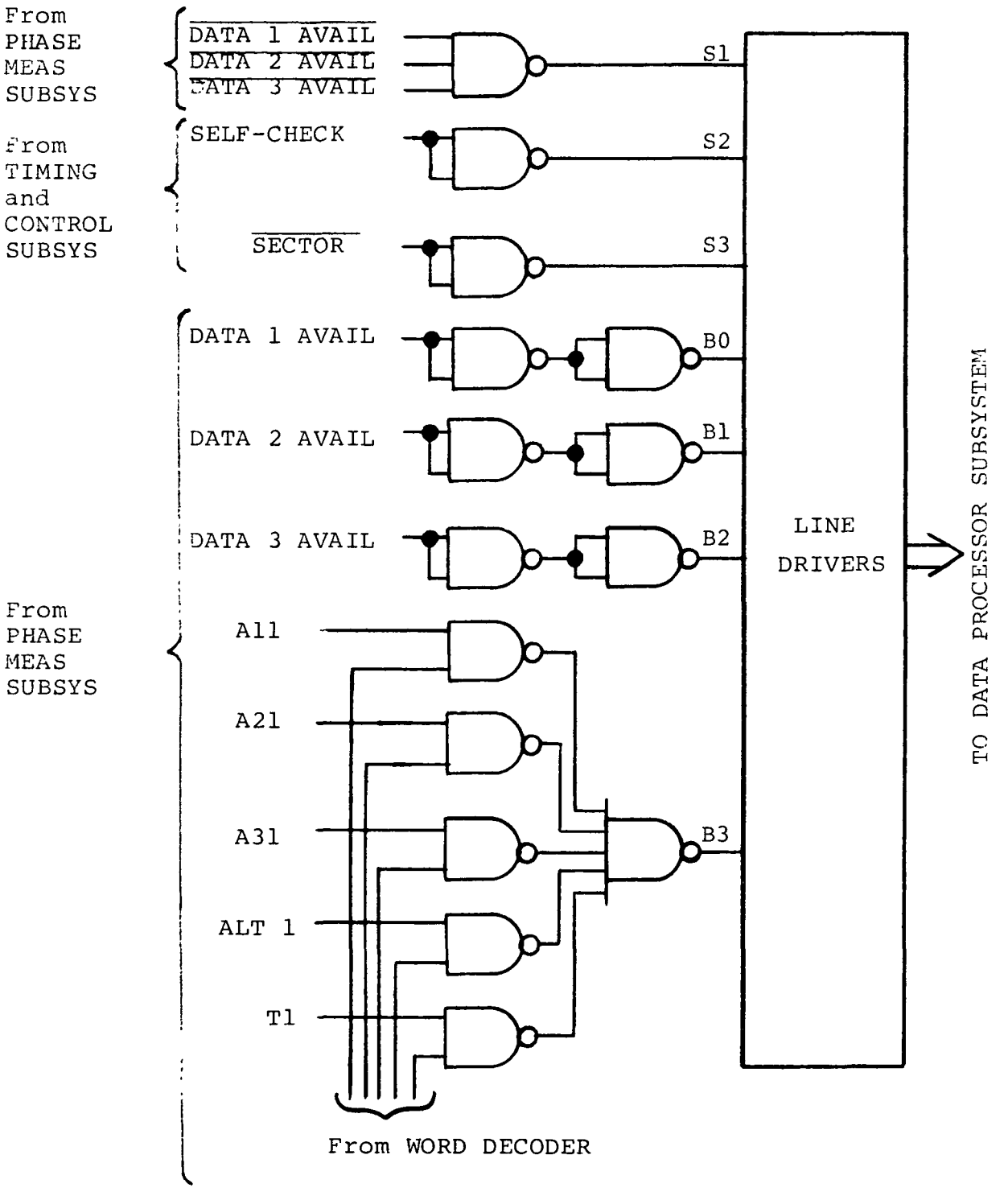

Figure 4-13(a). Data Input Gates and Word Decoder

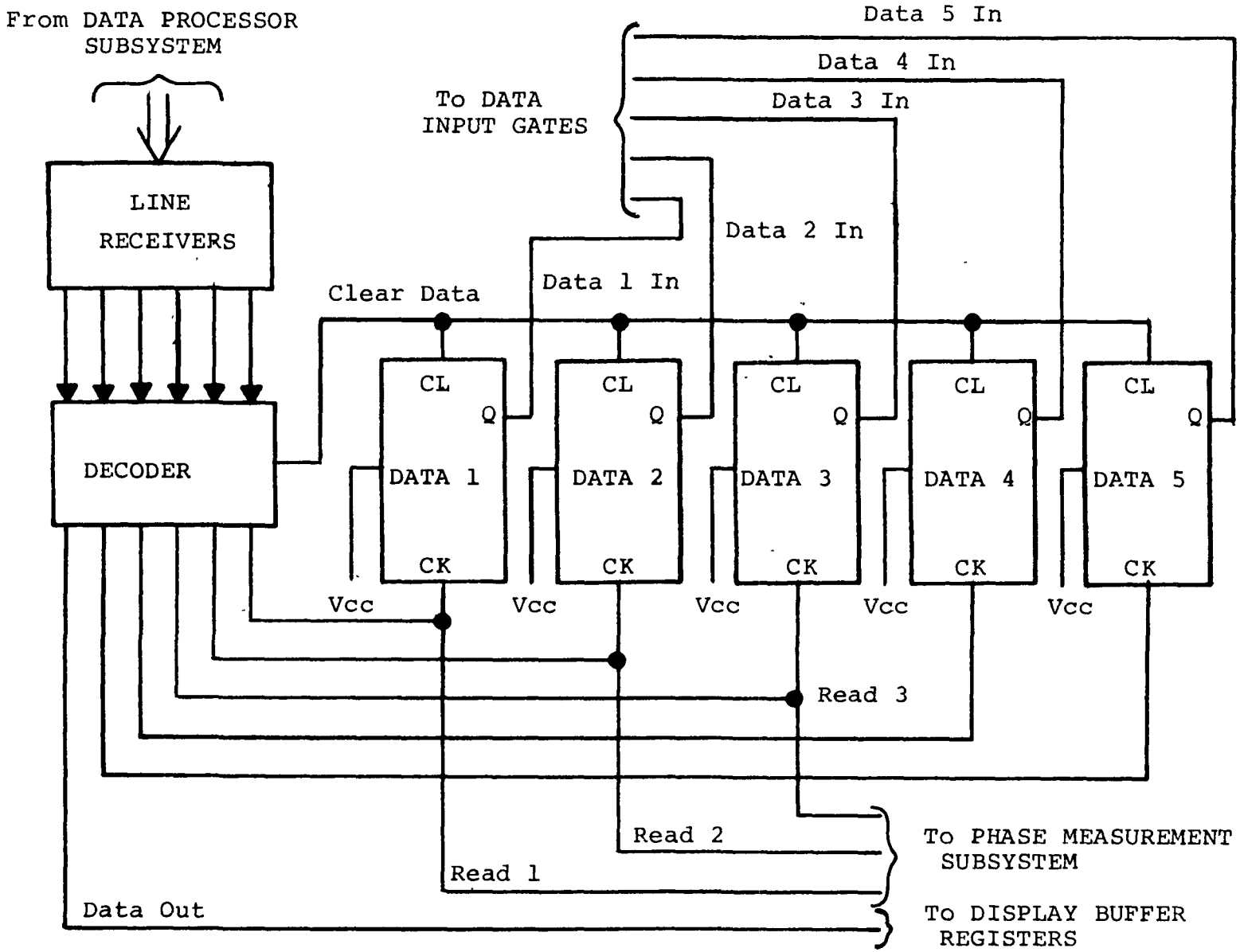

Figure 4-13(b). Data Input Gates and Word Decoder

program storage. Examining these one at a time will serve to determine the equipment requirements. The choice of word length can be based upon processor considerations such as number of operation codes and directly addressable words in memory, or on data word size. Since the processor does not need to have exceptional programming flexibility the word size will be chosen based on the data. Each word to be transferred in is 13 bits long (6 bits data, 4 bits identity code, 3 bits ADC identity). This would indicate that a 16-bit processor would be appropriate allowing some margin for increased data resolution if necessary. A 16-bit word also allows a floating point number to be represented with 22-bit accuracy with two words. This accuracy has been proven sufficient for making latitude and longitude calculations with programs now in operation at Texas Instruments.

One method to estimate the amount of time required to perform a particular program is to count the number of mathematical operations and then multiply by the number of computer operations required for each. This will give a rough total number of computer operations. The computer cycle time may be deduced knowing the amount of time available for the calculation. In this case, assuming all calculations will be performed in floating point arithmetic, there will be approximately 350,000 operations. The calculation will be performed when the ground station is transmitting phase data for the sectors other than the one in which the aircraft is located. This means that the time available for calculation is on the order of seconds. If one second is chosen for calculation time, a two-microsecond cycle time processor will be sufficient. The calculation will be complete in 700 milliseconds allowing 300 milliseconds to output the data.

The input/output requirements for this data processor are not very demanding. In the discussion of the phase measurement subsystem it was mentioned that the sampling rate will be 200 Hz. The 941-Hz tones will be sampled in-phase and 270° out of phase in the same cycle; therefore, there will be a minimum time of 785 microseconds between 941-Hz samples. Also, it is possible to have data samples ready from the two other samplers during this time. The input rate must, therefore, be greater than one 16-bit word per 261 microseconds; however, since the computer must perform several operations between data inputs, the time for inputting will be reduced. For 30 computer operations between data word inputs the time allowed to transfer one word into the computer is 200 microseconds. For data output there are three items: latitude, longitude, and time of day. If latitude and longitude are outputted in degrees, minutes, and seconds, and time of day in hours, minutes and seconds, the required output is 6 words after each calculation.

Another consideration is the interrupt and sense line requirement. Since there is more than ample time to make the position calculation the data processor may be completely dedicated to data input and then completely dedicated to calculation of position. In other words, an interrupt capability is not required. A number of sense lines are required, however, so that the data processor will know when to read data and when to start calculating.

It is obvious that such features as direct memory access and channel controllers are not necessary. In fact, while airborne all that is required for input and output is a 16-bit data bus and buffer registers. For programming the data processor on the ground it is suggested that some type of I/O device such as a teletype be used. This will be especially useful for an experimental system in which changes in the programming will be required more frequently than in an operational system.

The final point to be discussed is the data and program storage requirements. The data storage for this system is 20 words for each calculation. If it is desired to store the intermediate values of certain variables used during the calculation there are 120 words per calculation. For an experimental system it is desirable to be able to store the intermediate values for many calculations for playback and analysis on the ground after each flight. Obviously some compromise must be made concerning what will be stored. The suggested approach in the experimental system is to use as much storage area as is available for storing data which may be used in post real-time analysis. To accurately estimate the amount of storage for the program would require the program to be written. Although the exact program for this system has not been written a similar program was written to make the same position calculation at the ground control center in the VHF Satellite Navigation Experiment. This program took less than 4K of memory. In conclusion, it is recommended that an 8K memory for this experiment be available for program changes and storage of data for ground-based analysis.

To summarize the data processor requirements Table 4-1 is included below.

Table 4-1. Data Processor Requirements

Word Size	Cycle Time	Input/Output	Interrupts	Sense Lines	Storage
16 bits	2μ sec	16-bit data bus + buffer registers (airborne) teletype (ground)	None	4	8K

4.4.3 Equipment Considerations

There are several alternatives in choosing a data processor to meet the requirements presented in the previous section. First, a data processor could be designed specifically for this experiement. Second, a non-airborne qualified computer can be modified to enable it to withstand the environment expected in this experiment. Third, a qualified airborne computer can be chosen. The third choice has many advantages in that its performance is guaranteed for an airborne environment and design of a new data processor will not be required. A major problem with airborne computers is cost. Rigid vibration, thermal, RFI, and altitude specifications necessitate high cost and make the purchase of an airborne computer unreasonable for this experiment. However, there is a possibility that for the duration of this experiment Texas Instruments will be able to furnish the CP-967 (V)/UYK computer on a loan basis.

4.4.4 CP-967 (V)/UYK Computer

This computer is in operation for the Naval Ship Systems Command and its performance has been demonstrated. Although it is not packaged for airborne use it is small enough to fit on board many aircraft. In addition, software has been developed for this computer, such as assembler, teletype I/O routines, and fixed and floating point arithmetic. Some of the characteristics of this computer are summarized in the table below.

Table 4-2. CP-967(V)/UYK Digital Data Computer

Volume	9.6 cubic feet
Weight	215 pounds
Power Requirement	115 $\pm$20 VAC, 400 Hz $\pm$5%, single phase
Input Power	400 watts average
Size	32.81"H x 21.25"W x 24.00"D
Environment	MIL-E-16400F Amendment 2
Shock	MIL-S-901 Grade A
Vibration	MIL-STD-167, Type 1
Interference	MIL-I-16910
Word Size	16 bits
Cycle Time	2.0 microseconds
Storage	8K to 64K
Input/Output	ASR 32

4.4.5 Flow Charts

The functions of the data processor can best be expressed by a flow chart. For clarity a very general flow chart will be shown and then each block will be broken down into a more detailed flow chart. The flow charts are shown in Figures 4-14 through 4-18.

4.4.6 Display

As previously mentioned, the outputs to be displayed are latitude and longitude in degrees, minutes, and seconds, and time of day in hours, minutes, and seconds. This will require a storage of six 16-bit words. The display can be implemented with six 16-bit shift registers and 20 BCD decoder lamp drivers or with the serial type display now being tested at GSFC in conjunction with the VHF Satellite Navigation Experiment.

4.5 Aircraft Antenna

The aircraft antenna recommended for use in this experiment is the Dorne and Margolin DMC33-2 VHF Airborne Satellite Communication Antenna. Extensive tests have been performed with this antenna in conjunction with investigative work now being performed by Texas Instruments on VHF sidetone ranging using the ATS-I and ATS-III satellites. The experience gained from using this antenna will be very useful in this experiment. Some of the characteristics are tabulated in Table 4-3.

Table 4-3. DMC33-2 Satellite Communications Antenna Specifications

Frequency Range	135 to 150 MHz
Operating Frequencies	135.6 and 149.2 MHz
Bandwidth at each Frequency	1 MHz
VSWR	< 2:1, typically 1.5:1
Radiation Patterns	
Azimuth	Omnidirectional
Polarization	LH circular or RH circular
Power Handling (CW)	500 W
Gain (Referred to a CP Source)	
Low Angle Average	+1 dB
Minimum	Isotropic
High Angle Average	+3 dB
Minimum	Isotropic

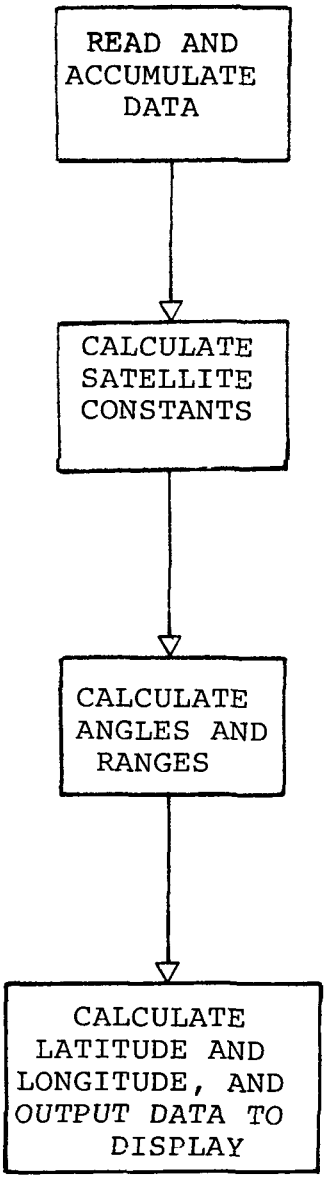

Figure 4-14. General Flow Chart

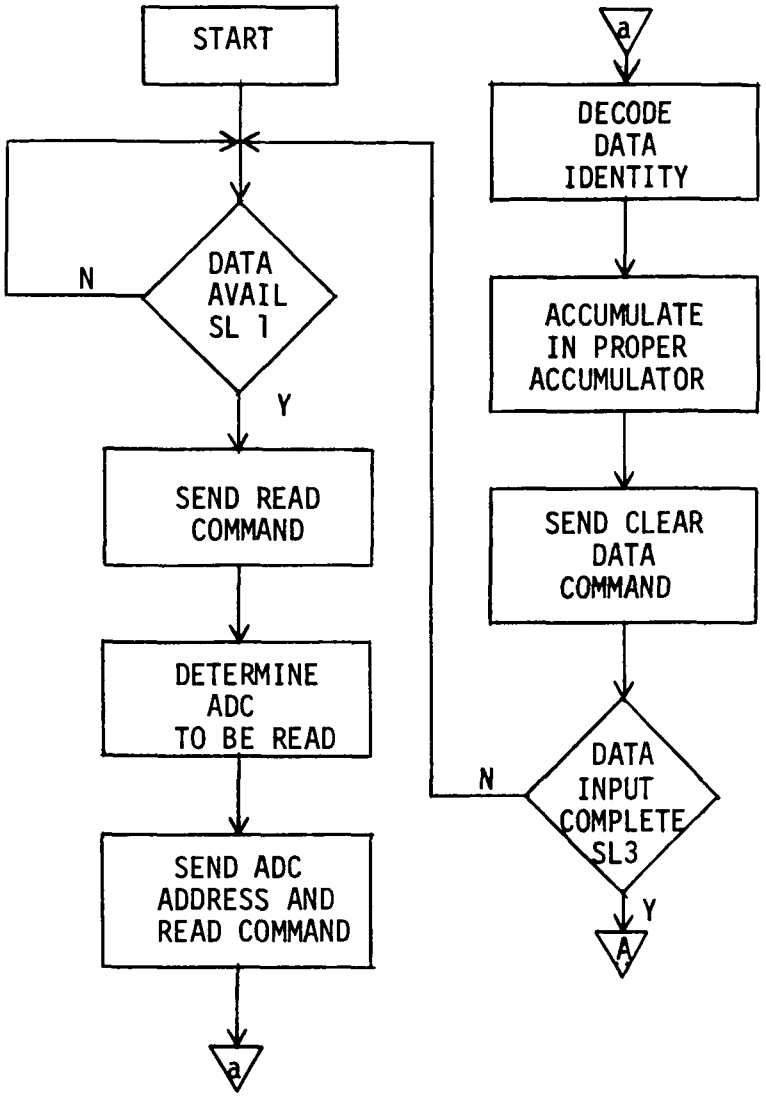

Figure 4-15. Read and Accumulate Data Flow Chart

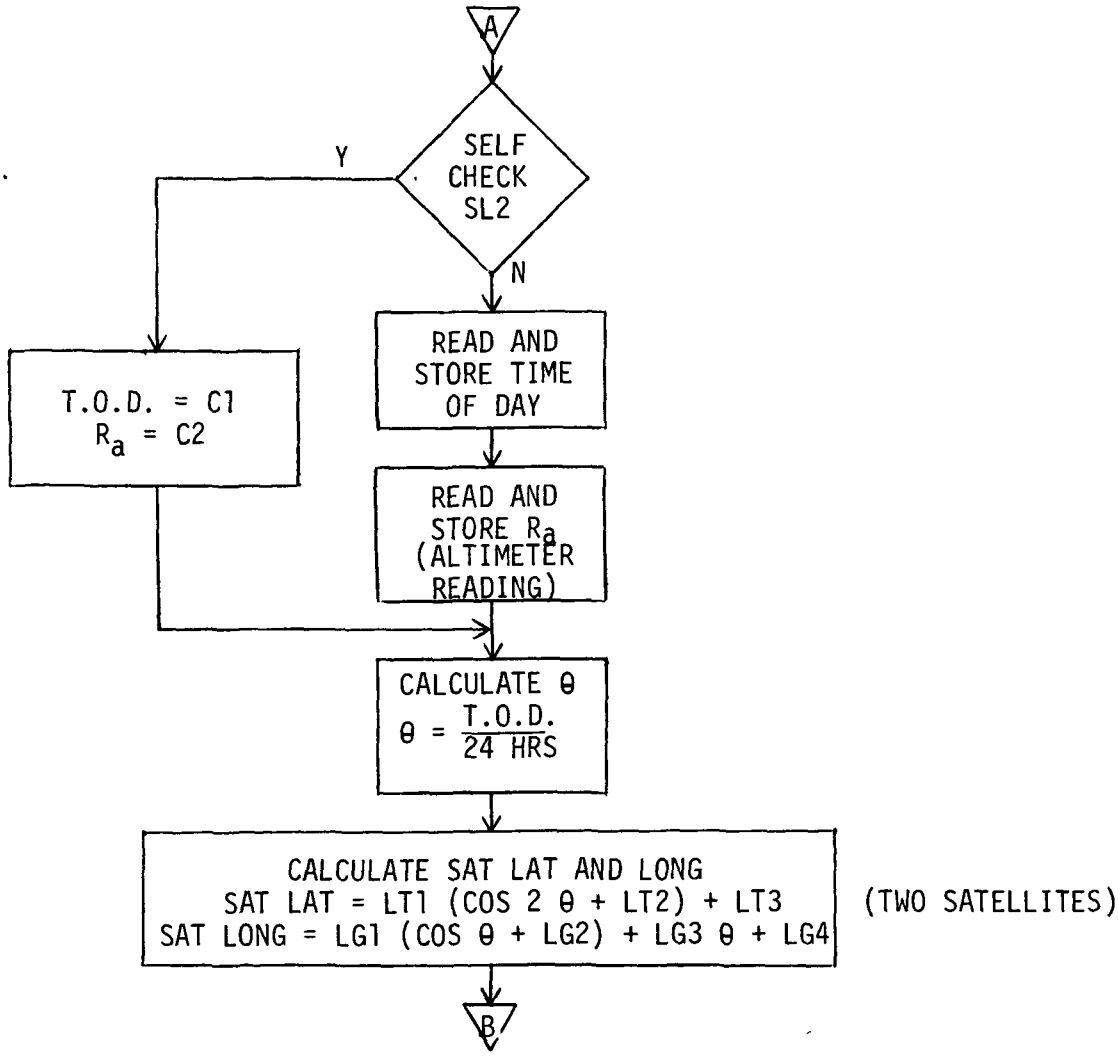

Figure 4-16. Calculate Satellite Constants Flow Chart

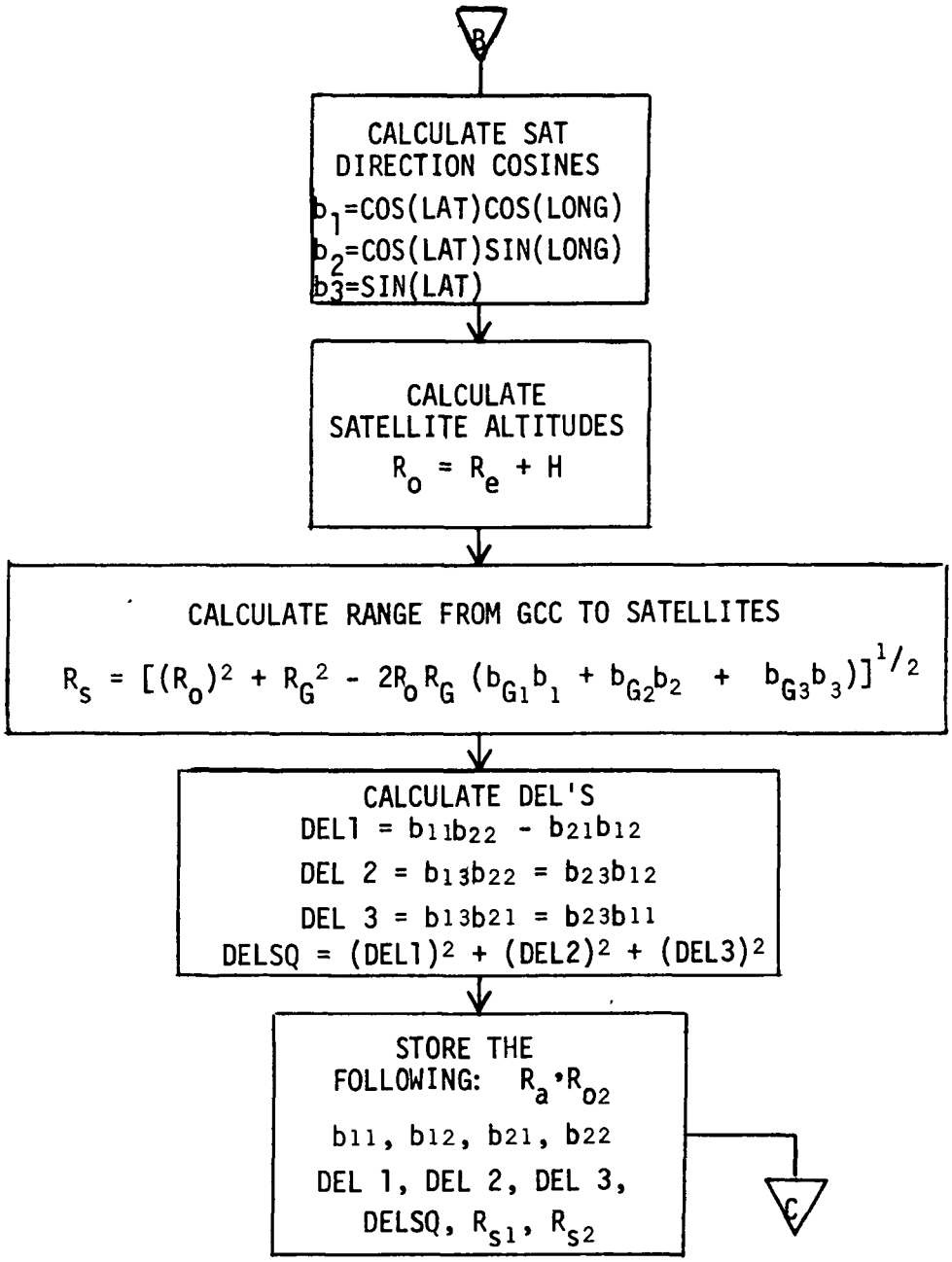

Figure 4-16 (cont.). Calculate Satellite Constants Flow Chart

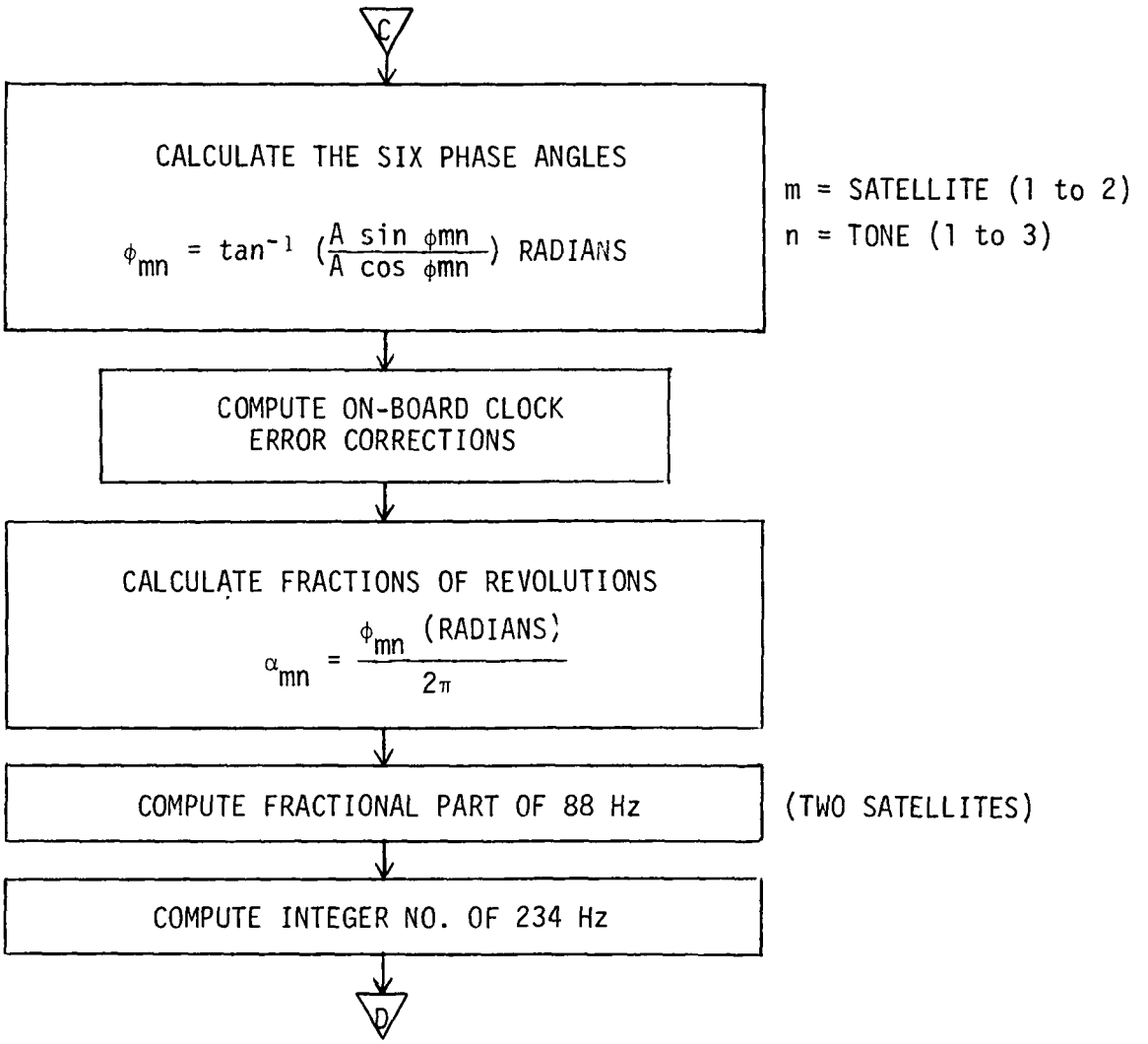

Figure 4-17. Calculate Range Flow Chart

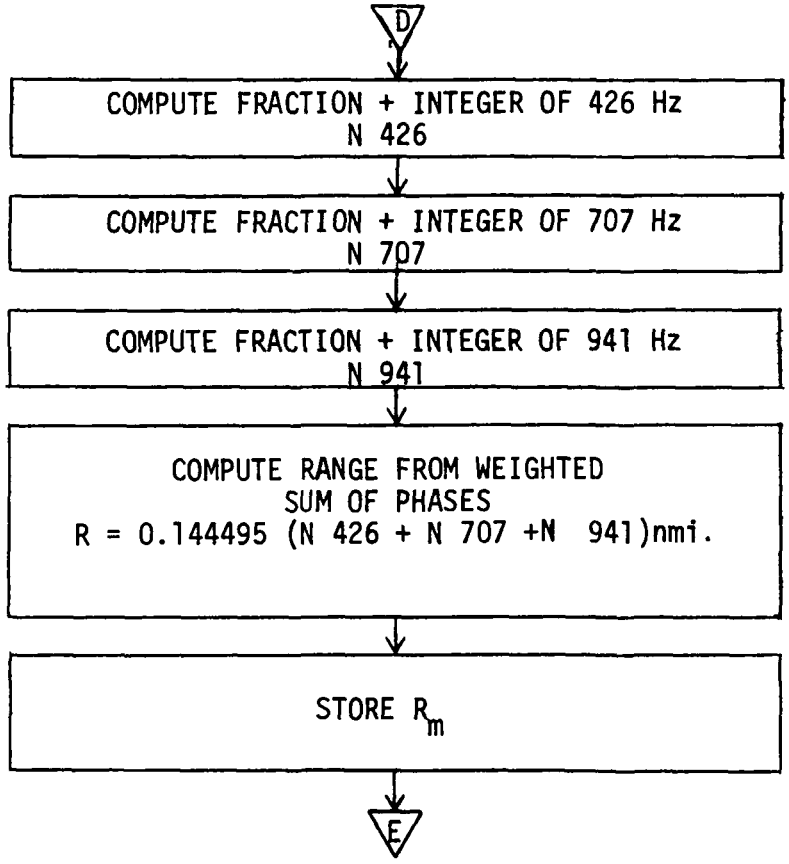

Figure 4-17 (cont'd.) Calculate Range Flow Chart

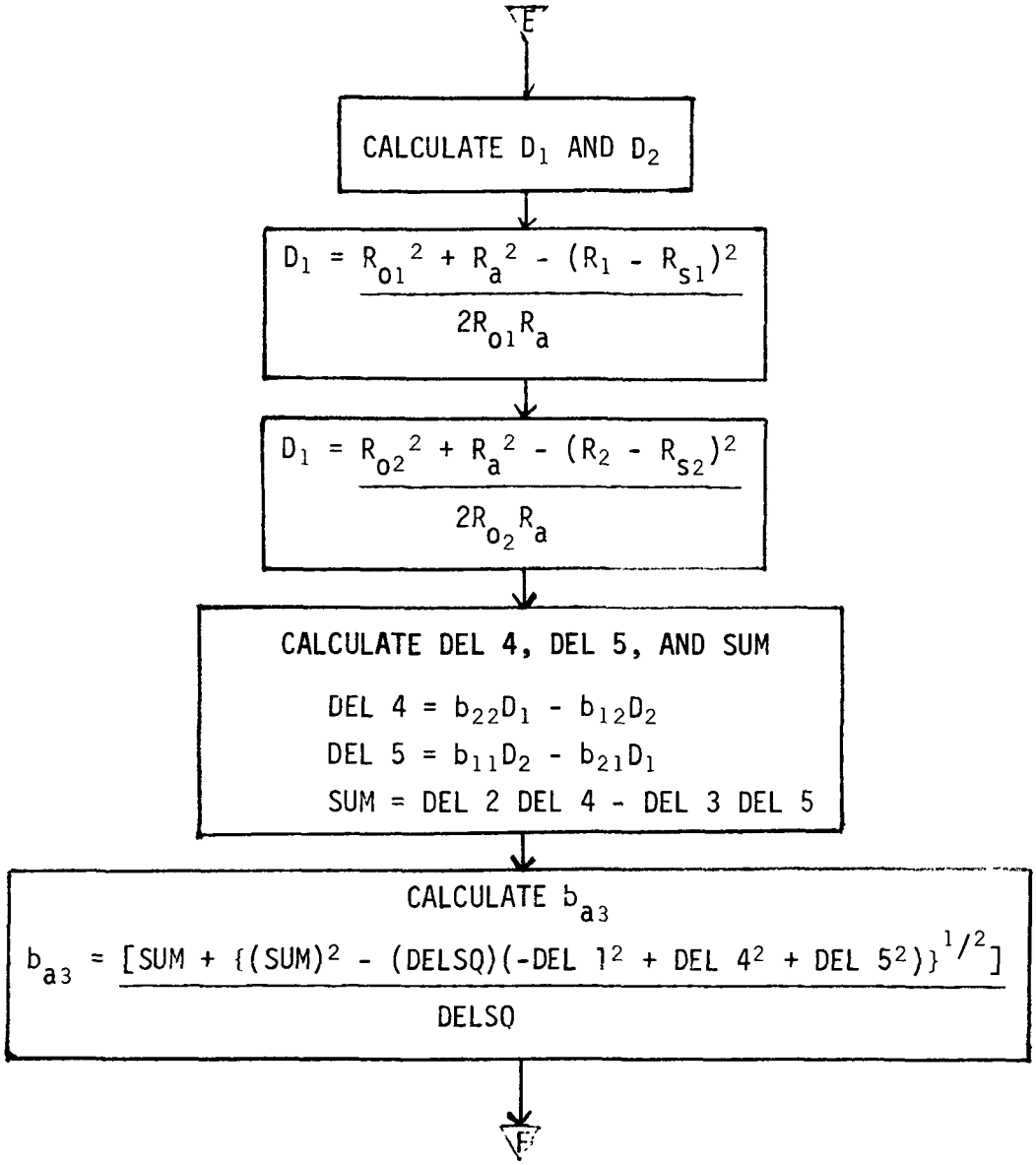

Figure 4-18. Calculate Aircraft Latitude and Longitude Flow Chart

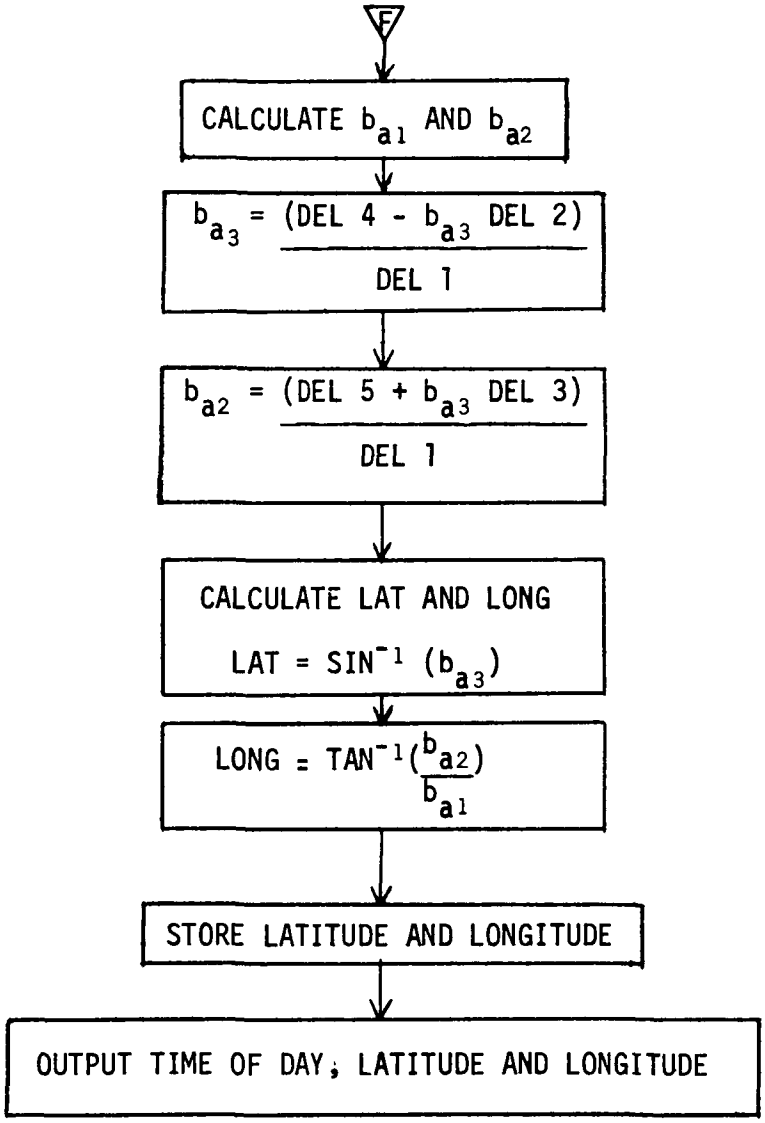

Figure 4-18 (cont'd.) Calculate Aircraft Latitude and Longitude Flow Chart

Table 4-3. DMC33-2 Satellite Communication Antenna Specifications (Continued)

Impedance	50 ohms
Weight	50 lbs

4.6 Timing and Control Subsystem

4.6.1 General Description

The Timing and Control Subsystem coordinates the actions of the Phase Measurement Subsystem and the Data Processor Subsystem. The heart of this subsystem is the master clock which was selected based on the requirements discussed in Section II-3.1. The master clock controls the sector decoder, all of the sampler decoders in the phase measurement subsystem, and the elapsed time from synchronization counter. In addition, the time of day clock, sector select switch, and self-check switch are located in this subsystem. A block diagram is shown in Figure 4-19.

4.6.2 Clock Updating

In this experiment the master clock will not be updated while in flight. All updating will be performed on the ground at the GCC since the phase error prediction technique will provide the required ranging accuracy over a 24-hour period. In addition to the updating of the master clock, the counters which control the samplers in the phase measurement subsystem must be updated on the ground at the GCC. This is required because those counters which count down the ranging tone reference frequencies from the master clock must be synchronized with the corresponding counters at the GCC. If this were not so, there would be a fixed delay between the on-board reference and the reference at the GCC. Since the entire system is based on these two being identical the delay would cause an incorrect phase measurement. In addition, the sector decoder must also be updated at the GCC to insure that the aircraft will be able to recognize the proper sector for making phase measurements.

The fact that the master clock and the two decoders must be synchronized at the GCC poses some operational difficulties. First of all, the clock and counters must be portable so that they may be carried from GCC to aircraft while in operation. Secondly, every precaution must be taken so that the synchronization is not disturbed while in flight. In order to accomplish this a battery and power supply must be part of the timing and control subsystem. Further, RFI shielding must be provided to protect and clock and counter synchronization.

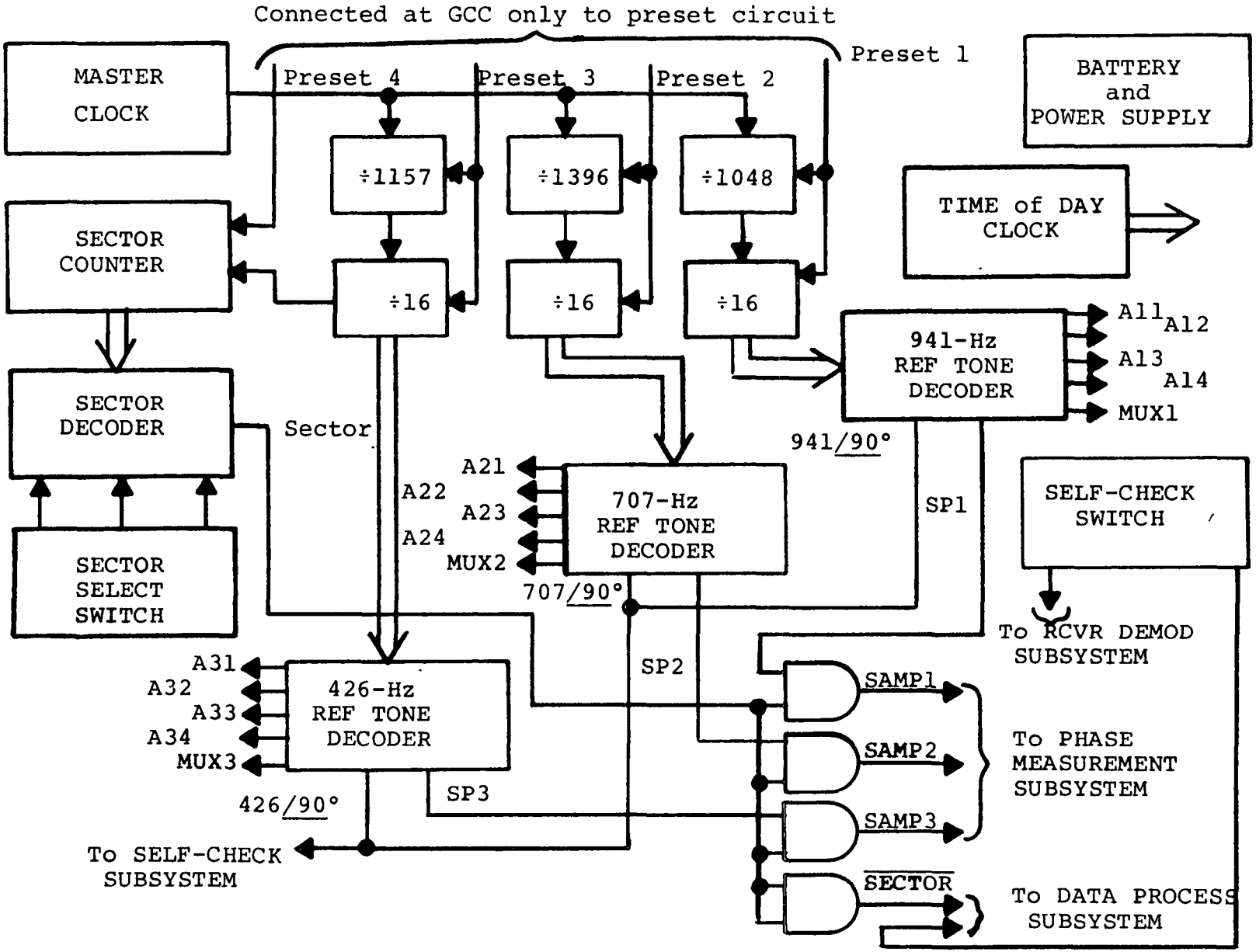

Figure 4-19. Timing and Control Subsystem

4.6.3 Sector Selection

As discussed in previous sections, there will be three different sectors in this experiment. Each time the aircraft moves into a different sector it must perform the phase measurements in a different time slot. This will be under the control of the sector decoder and the sector select switch. As shown in Figure 4-20, the output of the sector decoder is three signals: S1, S2 and S3. S1 is high when the GCC is transmitting signals for sector one, S2 is high when the GCC is transmitting signals for sector two, etc. When in sector one, the aircraft switch must be in position one (sel 1) in order to allow the samplers to sample when the GCC is transmitting sector one signals. Note that there is some dead time between the sector signals. This is to prevent the on-board system from sampling during the step change in phase from the GCC when changing sectors.

4.6.4 Time of Day Clock

A clock which reads the time of day must be available on board because the calculation of satellite constants from the ephemeris data requires the time of day to determine satellite position. The clock will have a BCD output of hours, minutes, and seconds which is fed to the data input gates of the Data Processing Subsystem.

4.6.5 Master Clock

The master clock chosen is the Motorola S1081A Oscillator. This clock has the required long term stability of 1×10^{-9} per day and 5×10^{-9} over its temperature range. In addition, it may be adjusted to within $\pm 1 \times 10^{-9}$, and stabilizes to within 1×10^{-9} in only 30 minutes.

5. EXPECTED SYSTEM PERFORMANCE

As stated earlier the experimental system is not the optimum configuration. It is generally true that a specifically tailored design will perform better than a rebuilt adapted old system. It is also true, however, that operation and concepts can be verified without attaining the ultimate in performance. Consequently the evaluation of the expected system performance, in the areas in which it may fall short in technological capability, may require more data points for statistical interpolation or carefully designed experimental procedures to circumvent the problem.

Table 4-4 is a tabulation of errors caused by various portions of the hardware, as obtained from the study of equipment

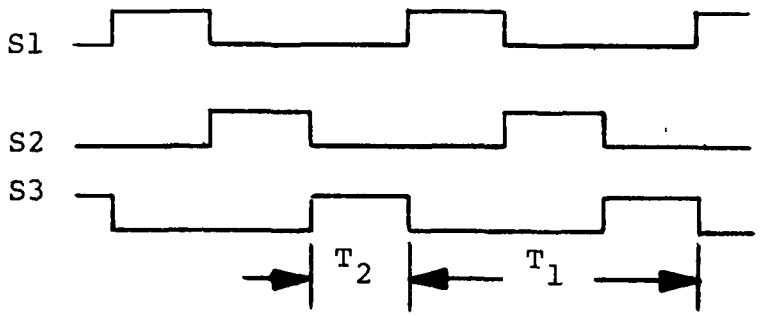

T_1 = Time interval for all three sectors

$T_2 = T_1/3-\tau$

= Time for one sector

τ = Delay between sectors

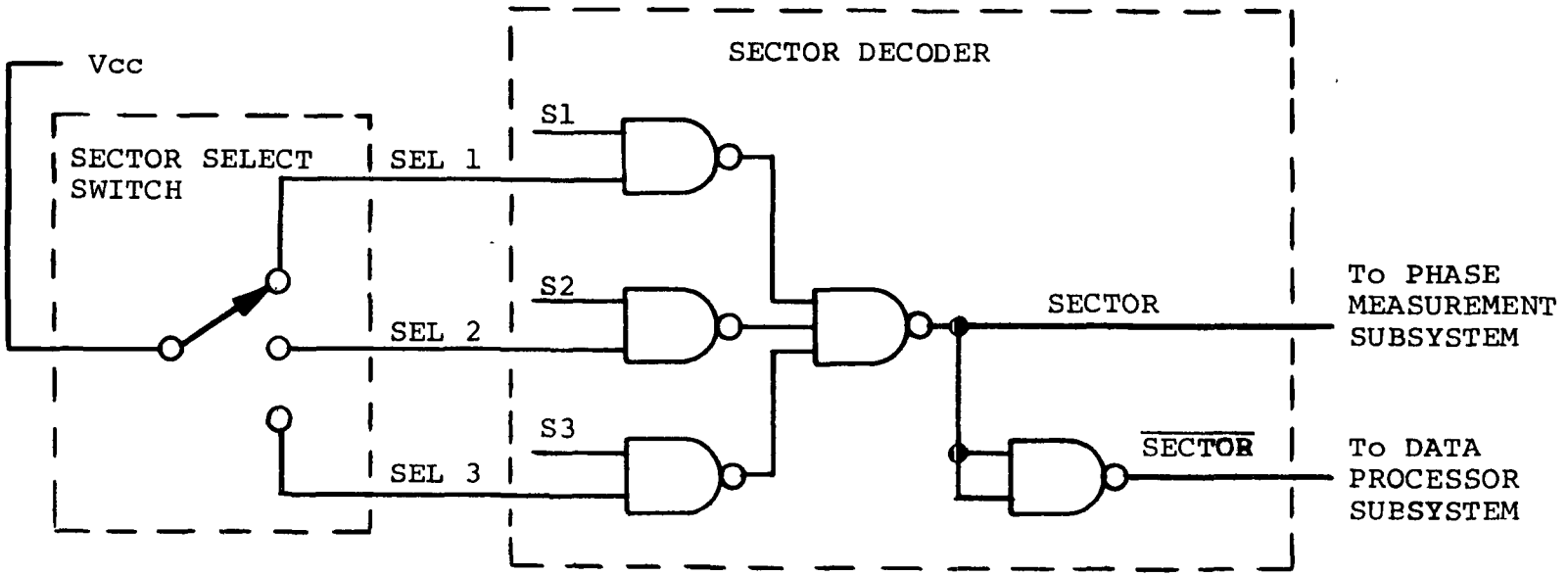

Figure 4-20. Sector Selection Timing and Gating

capability and expected design performance. It is emphasized that these numbers are estimates. These values are based upon the study results, similar design experience, and in some cases computer simulation.

Table 4-4. Range Errors Attributable to Hardware

Error Source	RMS Range Error (meters)
GCC Processing and Control Errors	
Phase Measurement, 0.8° rms (2-seconds of integration time at 40 dB-Hz)	710
Quantization	178
Time Delay Between Sectors	75
A/C Processing Errors	
Phase Measurement, 0.4° rms (2-seconds of integration at 40 dB-Hz)	355
Quantization	30
Altitude Uncertainty (Equivalent for 200-meter altitude error)	100
Reference Terminal Delay Uncertainty	120
Uncompensated Satellite Transponder delay	30

In addition to the errors attributable to hardware performance, other ranging errors are encountered as a result of the general system component configuration. These errors are listed in Tables 4-5 and 4-6.

Table 4-5. Multipath Ranging Errors

Satellite Elevation	Type of Fading	Nominal Ranging Error (km)			Worst Case Ranging Error		
		426Hz	707Hz	941Hz	426Hz	707Hz	941Hz
0°-30°	Specular	0.76	0.73	0.72	3.8	3.6	3.7
30°-50°	Diffuse	13.8	8.1	6.2	-	-	-
50°-70°	Diffuse	9.5	5.7	5.3	-	-	-

Table 4-6. Ranging Errors Attributable to System Configuration

Error Source	RMS Range Error (meters)
Ionospheric & Tropospheric Perturbations	120
Uncompensated Satellite Position Uncertainty (Worst case: Sector Boundary)	500
Satellite-to-A/C Multipath	
(0°-30° nominal)	720
(30°-50° nominal)	6200

The multipath errors for the 0° to 30° satellite elevation angles apply to the experimental system. In order to provide a larger area of coverage in an operational system satellite elevation angles greater than 30° will be encountered. The use of a higher frequency ranging tone (10.2 kHz) will tend to cancel the increased multipath effects.

This combination of all errors listed in the above tables gives the total root mean square error in range that may be expected for the experiment. Positioning the ATS-I and ATS-III satellites at 50°W and 150°W longitude provides a sector of satellite coverage centered at the mid point of the continental United States. The minimum satellite elevation angle in this sector is 10° and the maximum is approximately 30°. Therefore, the lower value of multipath error listed in Table 4-6 is applicable to the experimental system. The sum of all root mean square errors is formed by taking the square root of the sum of the squares and is equal to 1210 meters of range error. At the latitudes of interest (approximately 35°N) this range error translates to 1600 meters of radial position location error.

SECTION V

EXPERIMENT OUTLINE

This study has shown that in principle it is feasible to perform on-board navigation using the ATS-I and ATS-III as relays for the sidetone ranging signal generated at the modified OPLE Control Center. The primary objective of an experiment following the study would be to demonstrate this feasibility; i.e., to demonstrate that the navigation function can be reliably performed in a predictable manner.

In Section III of this report a system design was developed around three major unique features:

(1) Real-time differential sidetone ranging in a Range/Range mode

(2) Real-time compensation for satellite position uncertainty and ionospheric range bias

(3) Sector time-slot organization for system control

Presented in the following paragraphs is a general outline of an experiment which will illustrate the feasibility and practicability of a system with these features, thereby serving as a testbed for more advanced satellite ranging navigation systems not constrained by the specific characteristics of the OPLE Control Center, ATS-I and ATS-III.

1. SYSTEM ENGINEERING TESTS

As a first step certain static system parameters must be verified. Principal among these is the verification of the expected C/N_o for all communication links. In the course of the VHF Satellite Navigation Experiment it was found that the ATS transponder noise characteristics differed from the predicted, which required modification of the design signal power sharing within the satellite transponders. For the Dual Satellite Navigation Experiment the option of modifying the ground control center (GCC) and the reference terminal (R/T) transmitted power levels must be maintained to optimize the satellite transponder power sharing and maximize the probability of usable signal acquisition.

Because the ranging system is basically a timing system, the calibration of time delays through the system components must also be verified at the beginning of the experiment. These include the delay through the R/T transponder and the delay through the receiving system at the GCC for use in subsequent R/T range calibration, the aircraft receiving system delay to

calculate the fixed range bias for use in the on-board computer subsystem, and the GCC transmitter subsystem delay for use in predicting the phase of the compensated transmitted tone.

The principal feature of the aircraft equipment performance to be verified in the engineering tests is the stability of the on-board clock. When the drift characteristics of the clock are predictable, the phase and frequency may be "over compensated" when initialized to drift through the usable region during the period of testing. It is anticipated, however, that the on-board computer will be programmed to compensate for a well-behaved clock error even though this technique requires very high precision in the measurement of initial frequency offset. In either case, to preclude the requirement for a costly clock the stability characteristics of the clock must be verified at the beginning and periodically throughout the experiment.

2. REFERENCE TERMINAL RANGE CALIBRATION

In the second group of tests the capability to perform real-time compensation for satellite position uncertainty and ionospheric range bias is verified. In addition to ascertaining proper sequencing among the R/T sectors and GCC signal acquisition from each R/T, it is in these tests that the GCC algorithm for range computation and compensation with the satellite ephemeris update program will be validated. Since the geographical positions of the R/T's will be known, the applicable equipment time delays will have been measured, the satellites' true positions will be available from published ephemeris data, and an estimate of the ionospheric range bias may be made, the expected GCC-to-R/T range can be calculated and compared with the measured results. These measurements and corresponding transmitted phase adjustments may then be monitored through the diurnal ionospheric changes and, with cognizance of the true satellite ephemeris, the proper operation of the real-time constant phase compensation may be verified.

3. STATIC AIRCRAFT LOCATION TESTS

These tests represent the first evaluation of the navigation capabilities of the system and immediately precede the navigation demonstration. It is here that the position location algorithm in the aircraft terminal is verified with the terminal placed at a known location. A two-step plan will be followed:

(1) Measurement and computation of range from each satellite, verifying the operation of the range measurement subsystem and validating the constant range compensation performed by the GCC

(2) Combination of both satellite ranges and altitude to verify the position location computation

During these tests the predictability of the effects of various error sources will also be determined. These sources include:

(1) Aircraft altitude uncertainty determined by simulating changes in altitude

(2) On-board clock timing error, determined by offsetting clock phase

(3) Received S/N influence, determined by varying the GCC-transmitted signal power and/or the aircraft antenna/receiver gain

(4) Satellite position uncertainty, determined by modifying the precision of the satellite ephemeris predict in the aircraft and GCC algorithms

(5) Time delay between sectors, determined by modifying the sector timing intervals

(6) Data processor error, determined by reprogramming the on-board computer for various digitizing levels or data word lengths

4. NAVIGATION DEMONSTRATION

In the last series of tests the aircraft terminal will be mounted on-board the aircraft for flight demonstration of the system to culminate the essential tests. Position determination accuracy will be established by comparison of the satellite navigation measurement with a prearranged external navigation reference.

In addition to the capabilities demonstration, two additional sources of position error will be investigated during in-flight tests:

(1) Multipath

The gross effect will be measured by performing tests in the same hour with the aircraft grounded and with the aircraft airborne.

(2) Geometric Dilution of Precision (GDOP)

The effect of reference terminal-to-aircraft separation distance will be examined, as well as the effect of aircraft transition into an adjacent sector. In

addition, both the aircraft and a mobile reference terminal will be moved a considerable distance to verify the expected gross GDOP effect.

5. EXTENDED EXPERIMENTATION

With a successful experiment incorporating the essential tests outlined above, the Dual Satellite Navigation System as developed in this study can form the framework for considerable additional investigations. A list of potential extensions would include:

(1) For further testing the GCC may be again modified to incorporate the optimum higher frequency (10.2 kHz) fine ranging tone discussed in Section II of this report.

(2) With the higher measurement precision permitted by the 10.2-kHz ranging tone more extensive multipath investigations may be conducted, including examination of the effect of multipath spreading at various climb and descent rates, and the influence of terrain (land/water) at various aircraft velocities.

(3) The system may be combined with the VHF Satellite Navigation System in an integrated VHF navigation/surveillance system. In essence, this may be accomplished merely with the installation of a VHF transmitter in each aircraft.

(4) Additional navigation modes may be investigated; e.g., Range Rate, Range Difference.

(5) In-flight on-board clock up-dating techniques may be instrumented for feasibility demonstration and examination.

Although the above represents only a partial listing of candidate programs, the list is nevertheless formidable. With the hardware in this system as a nucleus, near-term experimentation in the field of VHF satellite navigation, surveillance, and data relay may be cost-effectively conducted.

SECTION VI

PROGRAM COST ESTIMATION

To maintain the Dual Satellite Navigation System and Experiment costs as low as possible four major assumptions have been made:

(1) Every effort has been made to minimize the required modification of the GCC.

(2) A majority of the circuits and the construction techniques used in the development of the VHF Satellite Navigation Experiment remote terminals are applicable to the R/T and A/C terminal requirements.

(3) A suitable computer for airborne use will be made available.

(4) A suitable navigation data display for airborne use will be made available as required on a loan basis from Goddard Space Flight Center.

With these considerations it is estimated that the development, production, testing, and integration of the system recommended in this study will require between 12 and 18 months to complete, and the essential tests in the experiment outline will not require more than four months to complete. It is further estimated that the total program can be completed in three phases as follows:

Phase I

Ground Control Center

Engineering Labor	21 man-months
Redesign of OPLE receivers Modification of SELF-CHECK Subsystem Design of PHASE SHIFT Subsystem Modification of SELF-TEST Subsystem Modification of Software	
Material	
Transmitter power amplifier	$1,000
Frequency synthesizer	7,000
Antenna diplexer	5,000
Components and hardware	7,000

Reference Terminals

Engineering Labor	3 man-months
Dual channel design Timing and control logic design	
Material	
Antennas (4)	$4,000
Components and hardware (3)	11,000
TOTAL COST FOR PHASE I - Approximately	$110K

Phase II

Aircraft Terminal

Engineering Labor	30 man-months
Receiver and demodulator design PHASE MEASUREMENT Subsystem design Timing and Control logic design SELF-TEST Subsystem design Software design Portable clock integration design	
Material	
Antenna	$3,000
Master clock	3,000
Components and hardware	20,000
TOTAL COST FOR PHASE II - Approximately	$120K

Phase III

System Integration and Check-Out

Engineering Labor	16 man-months

Minimal Experiment

Engineering Labor	14 man-months
TOTAL COST FOR PHASE III - Approximately	$90K

Total Program Effort

Engineering Labor	84 man-months
Material	$61,000
TOTAL PROGRAM COST - LESS THAN	$350,000

The figures itemized above are presented with a confidence originating from a complete and thorough understanding of the GCC, which is based upon Texas Instruments original effort in the design, development, and manufacture of the GCC, the operation and maintenance of the GCC throughout the OPLE Experiment, and its modification for use in the VHF Satellite Navigation Experiment. In addition, the effort involved in these two programs has provided us with an appreciation of the capabilities and the limitations of the ATS-I and ATS-III with respect to the use of the VHF transponders. We are confident, therefore, that the program outlined in this report, incorporating the concepts developed in the study, will prove the feasibility of on-board VHF sidetone ranging navigation.

SECTION VII

REFERENCES

1. System Design Report for Omega Position Location Equipment Control Center, NASA Document U8-815800-8, Texas Instruments Incorporated, Dallas, Texas, February 1967.

2. Design Study Report for Omega Position Location Equipment Control Center, NASA Document 3-815800-3, Texas Instruments Incorporated, Dallas, Texas, September 1966.

3. P. M. Woodward, Probability and Information Theory with Applications to Radar, McGraw Hill Book Company, New York, 1953.

4. M. I. Skolnik, Introduction to Radar Systems, McGraw Hill Book Company, New York, 1962.

5. L. A. Wainstein and V. D. Zubakov, Extraction of Signals from Noise, Prentice Hall Incorporated, New Jersey, 1962.

6. F. E. Croxton, Elementary Statistics with Applications in Medicine, Prentice-Hall Incorporated, New Jersey, 1962.

7. G. T. Bergemann and H. L. Kucera, Signal Characteristics of a VHF Satellite-to-Aircraft Communications Link for 30-to-70 Degree Elevation Angles, Collins Engineering Report 523-0759781-00181m, Collins Radio Company, Cedar Rapids, Iowa, October 1967.

8. G. T. Bergemann and H. L. Kucera, "Signal Characteristics of a Very-High-Frequency Satellite-to-Aircraft Communications Link," IEEE Transactions on Communication Technology, Volume COM-17, No. 6, December 1969, pp 677-687.

9. H. L. Kucera, Fading Spectra of Ground, Satellite, Aircraft ATS Propagation Tests, Collins Working Paper 3550, Collins Radio Company, Cedar Rapids, Iowa, January 1968.

10. J. Aarons and J. P. Mullen, "The Relationship of High Latitude Scintillations to VHF Synchronous Satellite Communications," Conference Record, IEEE 1970 International Conference on Communications San Francisco, June 8-10, 1970, pp 48-13 to 48-22.

11. J. Aarons and H. E. Whitney, "Ionospheric Scintillation at 135 MHz from a Synchronous Satellite," Planetary and Space Science, Vol. 16, 1968, pp 21-28.

12. B. R. Bean and E. J. Dutton, Radio Meteorology, NBS Monograph 92, United States Government Printing Office, Washington, D.C., 1966.

13. A. G. McNish, "Velocity of Light," Appendix A to Report of Ad Hoc Panel On Basic Measurements, National Academy of Sciences, December 1961.

14. Frequency and Time Standards, Hewlett-Packard Application Note 52, Hewlett Packard Company, Palo Alto, California, 1965.

15. System Study Report for the Position Location and Aircraft Communications Equipment (PLACE) Ground Equipment, Report No. DR973000-2 Volume I, Texas Instruments Incorporated, Dallas, Texas, 1970, p.13.

16. OPLE Maintenance Manual, No. HB53-A67, Volume III, Texas Instruments Incorporated, Dallas, Texas, 1968.

17. JPL Technical Report No. 32-564.

18. Design Study Report for OMEGA Position Location Equipment Control Center, Report to NASA/GSFC under Contract No. NAS 5-10248, Texas Instruments Incorporated, Dallas, Texas, 1966.

19. D. E. Nelson, Technical Data for Dorne and Margolin, Inc., Satcom Antennas DM C33-2 and DM C34-1, Report 300.115, Dorne and Margolin, Incorporated, Bohemia, N.Y., May 1968.

20. Maritime Mobile Satellite Communications Test Performed on S.S. Santa Lucia, Final Report, prepared by Space and and Defense Center, Westinghouse Electric Corp., Baltimore, Md., for Office of Research and Development, U.S. Department of Commerce Maritime Administration under contract MA-4329.

21. D. C. Hogg and W.W. Mumford, "The Effective Noise Temperature of the Sky," The Microwave Journal, vol. 3, No. 3, March 1960, pp.80-84.

22. Reference Data for Radio Engineers, 4th Ed., International Telephone and Telegraph Corp., New York, 1956, p.753

23. G. T. Bergemann and H. L. Kucera, "Signal Characteristics of a Very-High-Frequency Satellite-to-Aircraft Communications Link," IEEE Trans. Communication Technology, Vol. COM-17, No. 6, December 1969, pp.677-685.

24. S. Charton, "Radar System Sensitivity," Modern Radar, R.S. Berkowitz, ed. New York: John Wiley, 1965.

25. R.S. Lawrence, G.C. Little, and H.J.A. Chivers, "A Survey of Ionospheric Effects Upon Earth-Space Radio Propogation," Proc. of the IEEE, Vol. 52, No. 1, January 1964, pp.4-27.

26. T. Murakami and G. S. Wickizer, "Ionospheric Phase Distortion and Faraday Rotation of Radio Waves," RCA Review, Vol. 30, No. 3, September 1969, pp.475-503.

27. C.R. Laughlin, R.C. Hollenbaugh, E. Hirschmann, and W. K. Allen, Position Location and Aircraft Communication Equipment (PLACE), NASA Document X-731-67-159, Goddard Space Flight Center, Greenbelt, Maryland, April 1967.

28. Phase Difference Navigation Study, Interim Scientific Report, prepared by RCA Defense Electronics Products; Systems Engineering, Evaluation, and Research, Moorestown, N.J., for NASA Electronics Research Center, Cambridge, Mass., under Contract NAS 12-509, Sect. 6.3.2.2.

29. A. V. Da Rosa, "Propagation Errors in VHF Satellite-to-Aircraft Ranging," IEEE Trans. Antennas and Propagation, Vol. AP-17, No. 5, September 1969, pp.628-634.

30. O.K. Garriott, A.V. Da Rosa, and W.J. Ross "Electron content obtained from Faraday rotation and phase path length variations," Journal of Atmospheric and Terrestrial Physics, Vol. 32, 1970, pp.705-727.

31. Anon, Meteorological Balloon Location Experiment Using Geosynchronous Satellites, NASA, Goddard Space Flight Center, Greenbelt, Maryland, March 1968.

32. O.K. Garriott, F.L. Smith, III, and P.C. Yven, "Observations of Ionospheric Electron Content Using a Geostationary Satellite," Planetary and Space Science, Vol. 13, pp.829-838.

33. Joint Satellite Studies Group, "Ionospheric Electron Content and Scintillation Studies at Widely-Spaced Low-Latitude Stations," Planetary and Space Science, Vol. 16, pp.1277-1289.

34. P. Bandyopadhyay, "Measurement of Total Electron Content at Huaneayo, Peru," Planetary and Space Science, Vol. 18, No. 2, February 1970, pp.129-135.

35. J.W. King, E.O. Olatunji, D. Eccles, and W.S. Neroman, "The Integrated Electron Content in the Equatorial Ionospheric," Journal of Atmospheric and Terrestrial Physics, Vol. 29, No. 11, November 1967, pp.1391-1396.

36. L. Liszka, "The High-Latitude Trough in Ionospheric Electron Content", Journal of Atmospheric and Terrestrial Physics, Vol. 29, No. 10, October 1967, pp.1243-1259.

37. A. N. Hunter "Total Electron Content Studies in Equatorial Regions," Radio Science, Vol. 5, No. 6, June 1970, pp. 869-880.

38. H. R. Reed and C. M. Russell, Ultra High Frequency Propagation, sec. ed., Boston Tech. Pub. Inc., Cambridge, Mass., 1966, Chapter 4.

39. K. L. Jordan, Jr., "Measurement of Multipath Effects in a Satellite-Aircraft VHF Link," Proc. of the IEEE, Vol. 55, No. 6, June 1967, pp.1117-1118.

40. K. A. Norton, L. E. Vogler, W. V. Mansfield, and P. J. Short, "The Probability Density of a Constant Vector Plus a Raylein-Distributed Vector," Proc. of the IRE, Vol. 43, No. 10, October 1955, pp. 1354-1361.

41. S. O. Rice, "Mathematical Analysis of Random Noise," Bell System Technical Journal, Vol. 23, pp. 282-332, July 1944; Vol. 24, pp. 44-156, January 1945.

42. M. Nakaganmi, "On the Intensity Distribution

$$\frac{2R}{\sqrt{\alpha\beta}} \exp\left[-\frac{R^2}{2}\left(\frac{1}{\alpha}+\frac{1}{\beta}\right)\right] I_o\left[\frac{R^2}{2}\left(\frac{1}{\beta}-\frac{1}{\alpha}\right)\right]$$

and Its Application to Signal Statistics," NBS Journal of Research - D. Radio Science, Vol. 680, September 1964, pp. 945-1003.

43. P. Beckmann, Probability in Communication Engineering, Harcourt, Brace & World, New York, 1967, Chapter 4.

44. J. P. Aasterud, Technical Memorandum, Texas Instruments Incorporated, Dallas, Texas, 24 August 1970.

APPENDIX A

VHF LINK PARAMETERS

A1. INTRODUCTION

This appendix summarizes the calculations performed to characterize the VHF links associated with the ATS-I and ATS-III satellites. It covers the VHF link calculations, satellite power sharing, and signal-to-noise (SNR) ratios, and the developments presented are sufficiently general to be applicable to both the VHF Satellite Navigation Experiment configuration and the Dual Satellite Navigation configuration discussed in this report.

A2. LINK CALCULATION

The link loss-to-noise power density ratios (L/N_o) for the various VHF links are summarized in Table A-1. The parameters used to obtain these values for the 135.6-MHz links are presented in Table A-2, and those for the 149.22-MHz link are presented in Table A-3. The aircraft antenna parameters were taken from [19], and the satellite parameters were obtained from [20]. The multipath fade margins on the aircraft/satellite links are derived in Appendix C; the fade margins on the ground-to-satellite links are derived from the ionospheric scintillation data in Appendix B; the antenna temperatures are derived in Section A5; and the various noise-power densities (N_o) are derived from the material presented in Section A6.

Table A-1. L/N_o for the VHF Satellite Links

Link	Frequency	Nominal L/N_o	Worst-Case L/N_o	Units
GCC-to-ATS-I	149.22 MHz	41	25.9	Hz/dBw
ATS-I-to-A/C	135.6 MHz	28.3	14.5	Hz/dBw
A/C-to-ATS-I	149.22 MHz	26.5	12.2	Hz/dBw
ATS-I-to-GCC	135.6 MHz	43.1	27.2	Hz/dBw
GCC-to-ATS-III	149.22 MHz	41.5	26.2	Hz/dBw
ATS-III-to-A/C	135.6 MHz	30	16.2	Hz/dBw
A/C-to-ATS-III	149.22 MHz	27	12.5	Hz/dBw
ATS-III-to-GCC	135.6 MHz	44.8	28.9	Hz/dBw

Table A-2. Link Parameters for 135.6-MHz Down Links

Link Parameter	Nominal	Worst-Case	Units
Free Space Loss	-166	-167.3	dB
Polarization Loss	-3	-3	dB
Satellite-A/C Fade Margin	-2	-7	dB
Satellite-A/C Net Propagation Loss	-171	-177.3	dB
GCC-Satellite Fade Margin	-1.3	-9.4	dB
GCC-Satellite Net Propagation Loss	-170.3	-179.7	dB
ATS-I Transmit Antenna Gain	9.5	9.5	dB
ATS-I Transmit Losses	-2.4	-2.4	dB
A/C Antenna Gain	0	0	dB
A/C Antenna Ellipticity	-3	-4.3	dB
A/C Receiving Losses (estimate)	-1	-1.5	dB
ATS-I-to-A/C Net Link Loss (L_{1A})	-167.9	-175.4	dB
ATS-III Transmit Antenna Gain	10.5	10.5	dB
ATS-III Transmit Losses	-1.7	-1.7	dB
ATS-III-to-A/C Net Link Loss (L_{3A})	-166.2	-173.7	dB
GCC Antenna Gain	12	12	dB
GCC Antenna Ellipticity	-.7	-.7	dB
GCC Receiving Losses (estimate)	-1	-1.5	dB
ATS-I-to-GCC Net Link Loss (L_{1G})	-152.9	-162.8	dB
ATS-III-to-GCC Net Link Loss (L_{3G})	-151.2	-161.1	dB
Aircraft Antenna Effective Noise Temperature	1420	7100	°K
Aircraft Noise Figure (estimate)	2.5	3	dB

Table A-2. Link Parameters for 135.6-MHz Down Links (cont)

Link Parameter	Nominal	Worst-Case	Units
Aircraft Received Noise-Power Density (N_{0A})	-196.2	-189.9	dBw/Hz
L_{1A}/N_{0A}	28.3	14.5	Hz/dBw
L_{3A}/N_{0A}	30	16.2	Hz/dBw
GCC Antenna Temperature	1420	7100	°K
GCC Noise Figure	3	3.5	dB
GCC Received Noise-Power Density (N_{0G})	-196	-190	dBw/Hz
L_{1G}/N_{0G}	43.1	27.2	Hz/dBw
L_{3G}/N_{0G}	44.8	28.9	Hz/dBw

Table A-3. Link Parameters for 149.22-MHz Up Links

Link Parameter	Nominal	Worst-Case	Units
Free Space Loss	-166.9	-168.2	dB
Polarization Loss	-3	-3	dB
Satellite-A/C Fade Margin	-2	-7	dB
Satellite-A/C Net Link Loss	-171.9	-178.2	dB
GCC-Satellite Fade Margin	-1.3	-9.4	dB
GCC-Satellite Net Propagation Loss	-171.2	-180.6	dB
ATS-I Receive Antenna Gain	7.5	7.5	dB
ATS-I Receiving Losses	-1.4	-1.4	dB
A/C Antenna Gain	0	0	dB
A/C Antenna Ellipticity	-2	-4.3	dB
A/C Transmit Losses (estimate)	-1.5	-2	dB

Table A-3. Link Parameters for 149.22-MHz Up Links (cont)

Link Parameter	Nominal	Worst-Case	Units
A/C-to-ATS-I Net Link Loss (L_{A1})	-169.3	-178.4	dB
ATS-III Receive Antenna Gain	7.5	7.5	dB
ATS-III Receiving Losses	-1.3	-1.3	dB
A/C-to-ATS-III Net Link Loss (L_{A3})	-169.2	-178.3	dB
GCC Antenna Gain	12	12	dB
GCC Transmit Loss (estimate)	-1	-1.5	dB
GCC Antenna Ellipticity	-.7	-.7	dB
GCC-to-ATS-I Net Link Loss (L_{G1})	-159.8	-164.7	dB
GCC-to-ATS-III Net Link Loss (L_{G3})	-154.7	-164.6	dB
Satellite Antenna Noise Temperature	1120	5520	°K
ATS-I Noise Figure	4	4	dB
ATS-I Noise-Power Density (N_{01})	-195.8	-190.8	dBw/Hz
L_{A1}/N_{01}	26.5	12.9	Hz/dBw
L_{G1}/N_{01}	41	25.9	Hz/dBw
ATS-III Noise Figure	3.5	3.5	dB
ATS-III Noise-Power Density (N_{03})	-196.2	-190.8	dBw/Hz
L_{A3}/N_{03}	27	12.5	Hz/dBw
L_{G3}/N_{03}	41.5	26.2	Hz/dBw

Carrier-to-noise power density ratios (C/N_o) for the various links are presented in Table A-4 for a GCC transmitter power of 50 watts (17 dBw), ATS-I transmitter power of 40 watts (16 dBw) [20], ATS-III transmitter power of 50 watts (17 dBw) [20], and an aircraft transponder power of five watts (7 dBw). The weakest link is the aircraft-to-satellite link, which has a

C/N_o at least 10 dB lower than the other links for these power levels and will, therefore, determine the ultimate C/N_o that may be achieved in the transponding mode.

Table A-4. C/N_o for the VHF Satellite Links

Link	Frequency	Nominal C/N_o	Worst-Case C/N_o	Units
GCC-to-ATS-I	149.22 MHz	58	42.9	dB-Hz
ATS-I-to-A/C	135.6 MHz	44.3	30.5	dB-Hz
A/C-to-ATS-I	149.22 MHz	33.5	19.2	dB-Hz
ATS-I-to-GCC	135.6 MHz	59.1	43.2	dB-Hz
GCC-to-ATS-III	149.22 MHz	58.5	43.2	dB-Hz
ATS-III-to-A/C	135.6 MHz	47	33.2	dB-Hz
A/C-to-ATS-III	149.22 MHz	34	19.5	dB-Hz
ATS-III-to-GCC	135.6 MHz	61.8	45.9	dB-Hz

A3. SIGNAL-TO-NOISE RATIOS AND SATELLITE POWER SHARING

A3.1 Satellite Power Sharing

From Section A6, the satellite power allocated to the GCC signal (pilot tone plus ranging tones) is

$$P_{sg} = P_s/[1 + (P_t/P_g)(L_{ts}/L_{gs}) + (B_s/P_g)(N_{os}/L_{gs})] \qquad (A\text{-}1)$$

where the quantities are defined in Figure A-1. Utilizing the nominal values from Table A-3 for the aircraft-to-ATS-III and ATS-III-to-GCC links, together with the power levels specified in Section A2 and B_s = 100 kHz, the satellite power allocated to the GCC-transmitted signal is calculated as

$$P_{sg} \simeq 40/[1.142 + 3.55 \times 10^{-3} m] \qquad (A\text{-}2)$$

where m is the number of transponders using the system simultaneously. For m = 1, $P_{sg} \simeq 35$ watts; and for m = 5, $P_{sg} \simeq 34.4$ watts.

The satellite power allocated to the remote platforms is

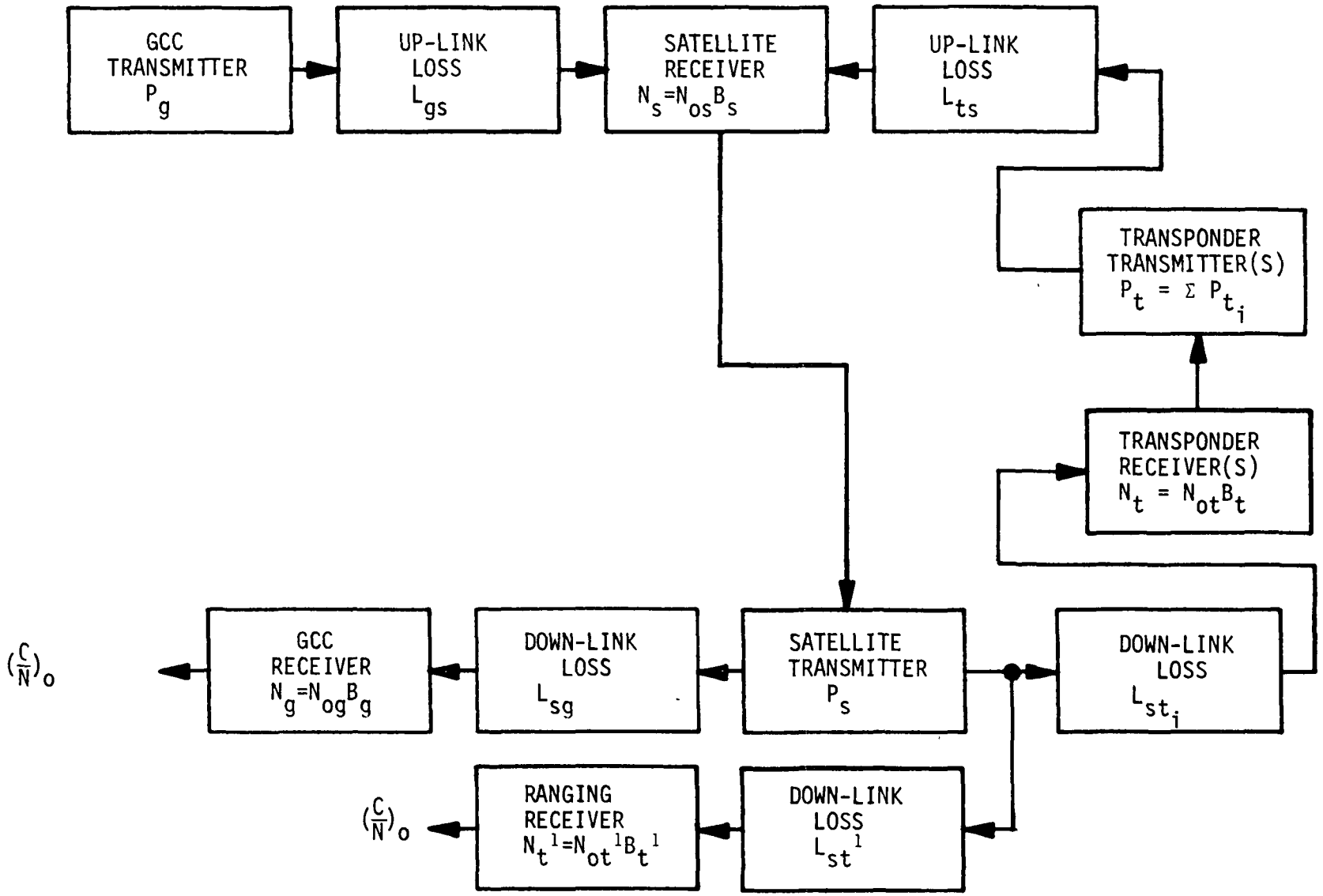

Figure A-1. Link Power Flow Diagram

$$P_{st} = P_s/[1 + (P_g/P_t)(L_{gs}/L_{ts}) + (B_s/P_t)(N_{os}/L_{ts})] \quad \text{(A-3)}$$

$$\simeq 40/[1 + 322/m] \quad \text{(A-4)}$$

For $m = 1$, $P_{st} \simeq 124$ mW; and for $m = 5$, $P_{st} \simeq 611$ mW.

The thermal noise power transmitted by the satellite is

$$P_{sn} = P_s/[1 + (P_g/B_s)(L_{gs}/N_{os}) + (P_t/B_s)(L_{ts}/N_{os})] \quad \text{(A-5)}$$

$$\simeq 40/[8.25 + .025\ m] \quad \text{(A-6)}$$

For $m = 1$, $P_{sn} \simeq 4.83$ watts; and for $m = 5$, $P_{sn} \simeq 4.77$ watts.

The satellite power allocated to the pilot tone is $K_{sj}P_s$, and the GCC pilot tone power is $K_{gj}P_g$. From Section A6

$$K_{gj}/K_{sj} = 1 + (P_t/P_g)(L_{ts}/L_{gs}) + (B_s/P_g)(N_{os}/L_{gs})] \quad \text{(A-7)}$$

$$\simeq 1.142 + 3.55 \times 10^{-3} m \quad \text{(A-8)}$$

For $K_{sj} = 0.25$ and $m = 1$, $K_{gj} \simeq 0.286$, and for $m = 5$, $K_{sj} \simeq 0.29$. The above equations illustrate that approximately 71 percent of the GCC transmitter power, or 35.5 watts, will be available for the ranging tones.

A3.2 Transponder Signal-to-Noise Ratios

For a pilot tone requiring 25 percent of the satellite transmitter power, the pilot tone carrier-to-noise power density ratio (C/N_o) is found from Section A6 to be

$$(C/N_o)_j = K_{gj}P_{sg}/[N_{ot}/L_{st} + P_{sn}/B_s] \quad \text{(A-9)}$$

$$\simeq 9.55 \times 10^3/\text{Hz or } 39.8 \text{ dB-Hz}$$

The tone package SNR is

$$(C/N_o)_{tones} = (1 - K_{gj})\ P_{sg}/[N_{ot}/L_{st} + P_{sn}/B_s] \quad \text{(A-10)}$$

$$\simeq 23.8 \times 10^3/\text{Hz or } 43.8 \text{ dB-Hz}.$$

A3.3 GCC Signal-to-Noise Ratios

The C/N_o for the pilot tone received at the GCC is

$$(C/N_o)_{gj} = K_{gj}P_{gs}/[N_{og}/L_{sg} + P_{sn}/B_s] \qquad \text{(A-11)}$$

$$\simeq 1.25 \times 10^5/\text{Hz or } 50.9 \text{ dB-Hz.}$$

If a transponder bandwidth of 5 kHz is assumed, then from Equation (A-9) the tone package C/N at the transponder is

$$(C/N)_t = (C/N_o)_{tj}/B_t = 39.8 - 37 = 2.8 \text{ dB}$$

The portion of the transponder power that is actually signal power is

$$P_{ts} = P_t[P_{sig}/(P_{sig} + 0.525\ P_{sig})] \qquad \text{(A-12)}$$

$$\simeq 0.656\ P_t \text{ or } 3.28 \text{ watts}$$

The tone package (C/N_o) at the GCC is

$$(C/N_o)_{tones} = .656\ P_{st}/[N_{og}/L_{sg} + P_{sn}/B_s] \qquad \text{(A-13)}$$

$$\simeq 10^3/\text{Hz or } 30 \text{ dB-Hz.}$$

A4. ANTENNA TEMPERATURES

A4.1 Satellite Antenna Temperature

If the satellite antenna beamwidth, θ_s, is greater than the angle subtended by the earth, θ_e, as shown in Figure A-2, then the satellite antenna thermal noise temperature will be a combination of both the earth and cosmic temperatures. To a first approximation, the satellite antenna noise temperature may be expressed by

$$T_a \simeq T_e(\theta_e/\theta_s)^2 + T_c(\theta_s^2 - \theta_e^2)/\theta_s^2$$

$$= kT_e + (1-k)T_c \qquad \text{(A-14)}$$

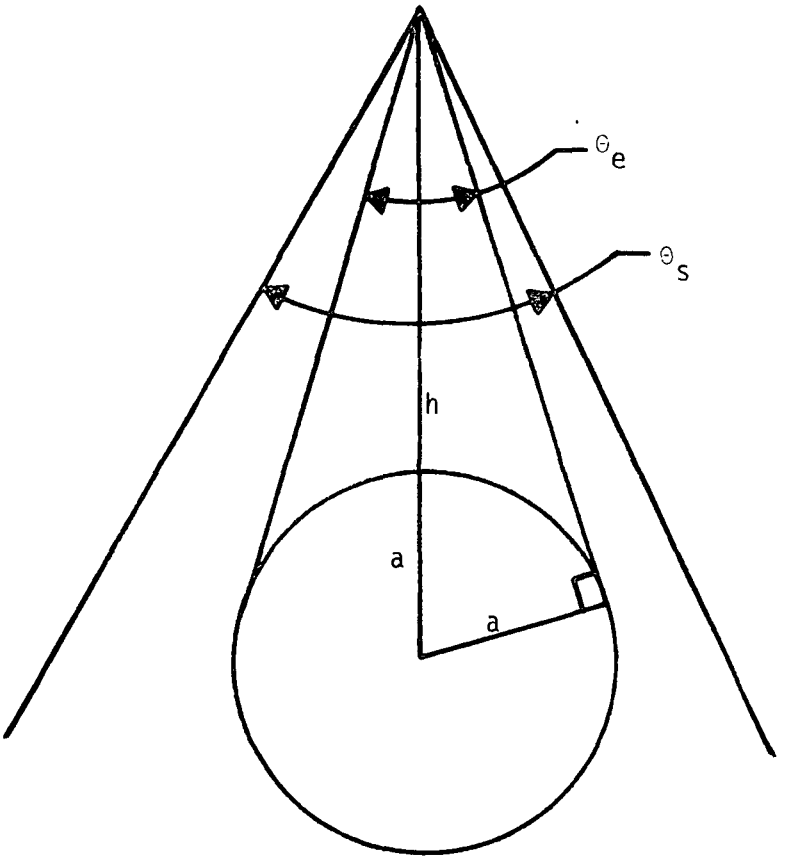

$$\Theta_e = 2 \sin^{-1}\left(\frac{a}{a+h}\right)$$

$$= 17.32°$$

Figure A-2. Satellite Antenna Coverage

where $T_e \simeq 290°K$

$$k = (\Theta_e/\Theta_s)^2 \quad \text{(A-15)}$$

and T_c, the nominal cosmic temperature, is given by [21]

$$T_c = 290\ \lambda^2$$

$$= 2.61 \times 10^7/f^2_{MHz}\ (°K) \quad \text{(A-16)}$$

The maximum value of T_c is five times the value given by Equation (A-16) [21].

An approximate expression for the beamwidth of the satellite antenna in terms of its gain relative to an isotropic antenna is [22]

$$\Theta_s^2 = 27000/\text{antilog}_{10}\ (G_{dB}/10) \quad \text{(A-17)}$$

When this expression is combined with the value for Θ_e given in Figure A-2, Equation (A-15) becomes

$$k = (17.32)^2/27000/\text{antilog}_{10}\ (G_{dB}/10)$$

$$= 0.0111\ \text{antilog}_{10}\ (G_{dB}/10) \quad \text{(A-18)}$$

For a satellite receiving antenna gain of 7.5 dB, k = 0.0624. Substitution of this value and $f_{MHz} = 149.22$ into Equation (A-14) gives a nominal satellite receiving antenna temperature of 1120°K and a maximum temperature of 5520°K.

A4.2 Aircraft Antenna Temperature

The nominal aircraft antenna temperature is given by Equation (A-16). For a receive frequency of 135.6 MHz, Equation (A-16) gives a nominal antenna temperature of 1420°K; and the maximum value will be 7100°K. Although the aircraft antenna temperature can reach almost 70000°K during precipitation static discharge [23], the 7100°K worst-case value will be used until a time distribution of the antenna temperature can be obtained.

A5. NOISE POWER DENSITY CALCULATIONS

A5.1 Receiver Input Noise Temperature

The thermal noise generated within the receiver along with that caused by transmission line losses may be referred back to the transmission line input in the form of the effective receiver input temperature, T_{eff}. This is expressed in terms of the transmission line and receiver parameters by [24]

$$T_{eff} = T_L\ (1/L - 1) + T_R\ (F - 1)/L \qquad \text{(A-19)}$$

where L is the transmission line loss ($L = P_{out}/P_{in}$), T_L is the transmission line temperature, F is the receiver noise factor, and T_R is the receiver temperature. If it is assumed that both T_L and T_R are at the "standard" temperature of 290°K, then Equation (A-19) reduces to

$$T_{eff} = 290\ (F/L - 1) \qquad \text{(A-20)}$$

This is plotted as a function of $F_{dB} - L_{dB}$ in Figure A-3.

The receiver noise temperature is the sum of Equation (A-19) and the antenna temperature. Thus,

$$\begin{aligned} T_r &= T_{ant} + T_{eff} \\ &= T_{ant} + 290\ (F/L - 1) \end{aligned} \qquad \text{(A-21)}$$

A5.2 Receiver Noise Power Density

The receiver noise power is given by

$$P_{rn} = KT_rB \quad \text{watts} \qquad \text{(A-22)}$$

where K is Boltzman's constant (1.38×10^{23} J/°K), T_r is the receiver noise temperature, and B is the receiver bandwidth. The receiver noise power density is given by

$$N_o = P_{rn}/B = KT_r \text{ watts/Hz (Joules)} \qquad \text{(A-23)}$$

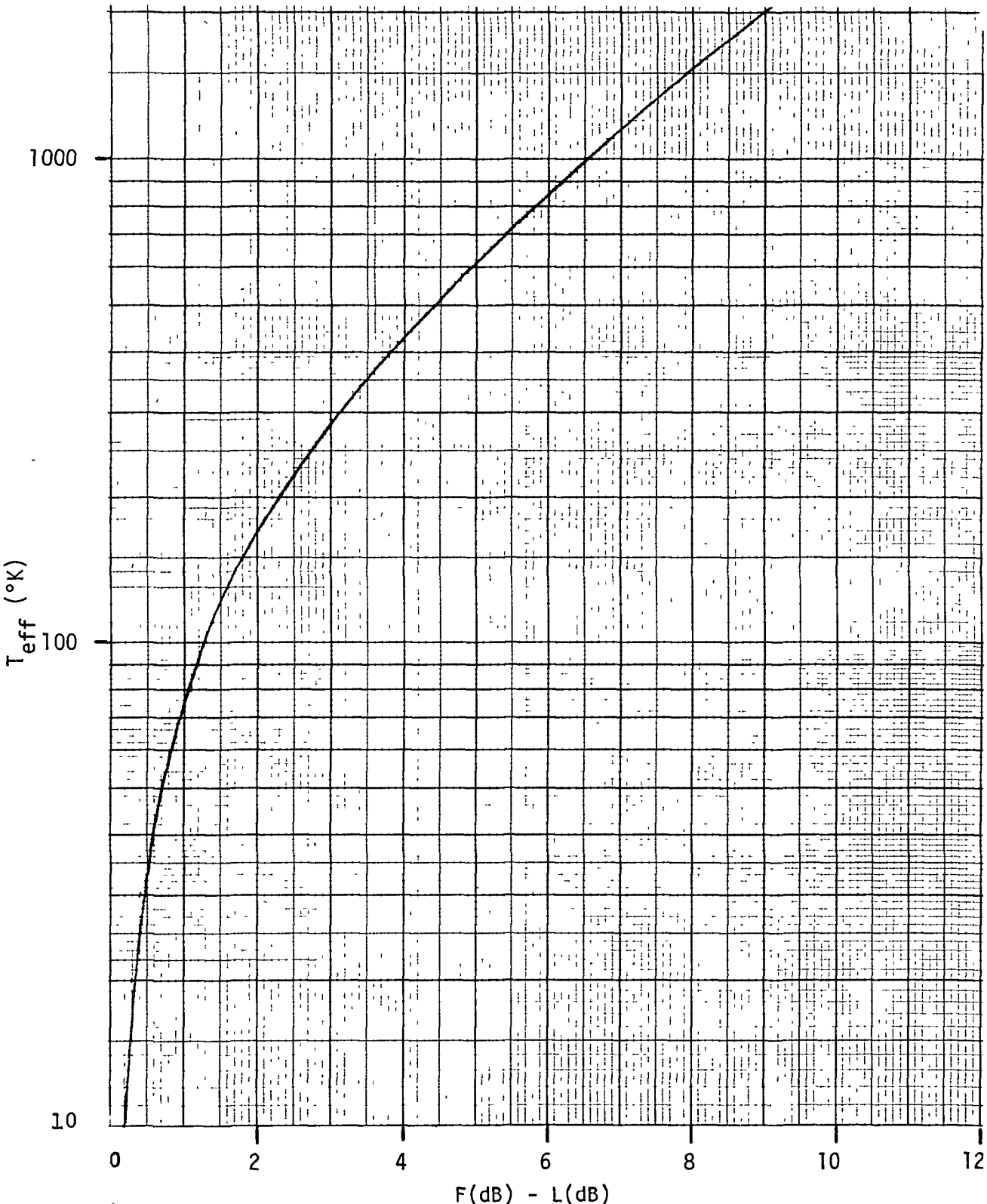

Figure A-3. Effective Input Noise Temperature vs. Product of Receiving Loss and Noise Figure

which is plotted in Figure A-4. N_o is plotted as a function of antenna temperature, receiver noise figure, and transmission line loss in Figure A-5.

A6. DERIVATION OF LINK EQUATIONS

A6.1 Introduction

The link equations will be derived from the power flow diagram shown in Figure A-1. Note that this diagram applies to both the VHF Satellite Navigation Experiment and the Dual Satellite configuration links. The satellite power sharing equations will be derived in Section A6.2, and the transponder and GCC receiver carrier-to-noise power density ratios (C/N_o) will be derived in Section A6.3.

A6.2. Satellite Power Sharing

Satellite Received Power

The total power received by the satellite is the sum of the thermal noise power plus the power received from the GCC and the remote platform(s). This may be expressed by

$$P_{sr} = P_g L_{gs} + P_t L_{ts} + N_s \qquad \text{(A-24)}$$

where the quantities are defined in Figure A-1. Note that the remote platform (transponder) power may be the power transmitted by several platforms, and that the "link loss" term is given by

$$L = \alpha\, G_T\, L_T'\, G_R\, L_R' \qquad \text{(A-25)}$$

where α is the free space attenuation; G_T and G_R are respectively, the transmitting and receiving antenna gains; and L_T' and L_R' are, respectively, the transmitting and receiving losses.

Basic Satellite Transmitter Power Allocation

The satellite power will be allocated to the various receiver inputs according to the fraction of the total received power that they represent. Thus, the satellite power allocated to the GCC signal is

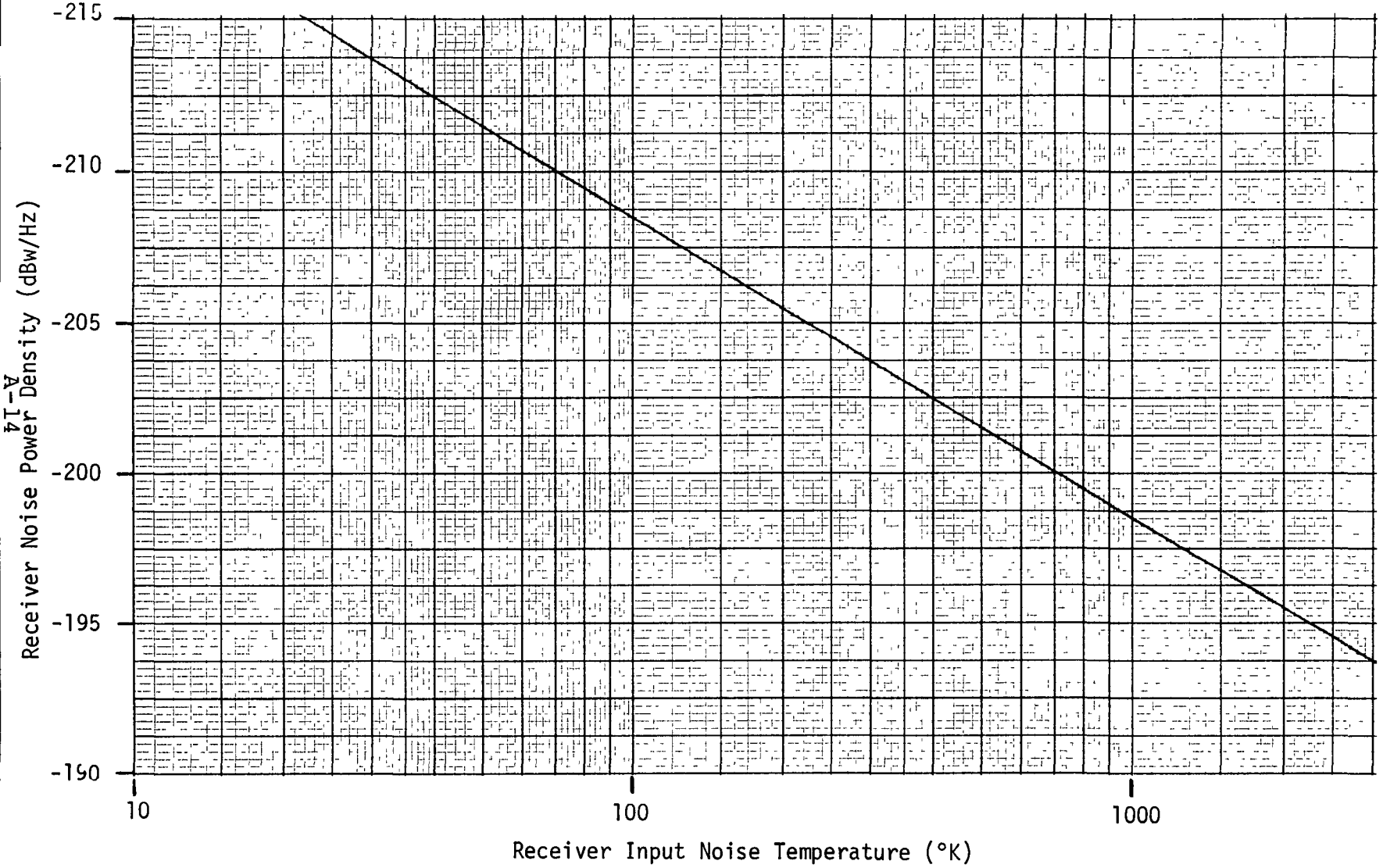

Figure A-4. Receiver Noise Power Density vs. Input Noise Temperature

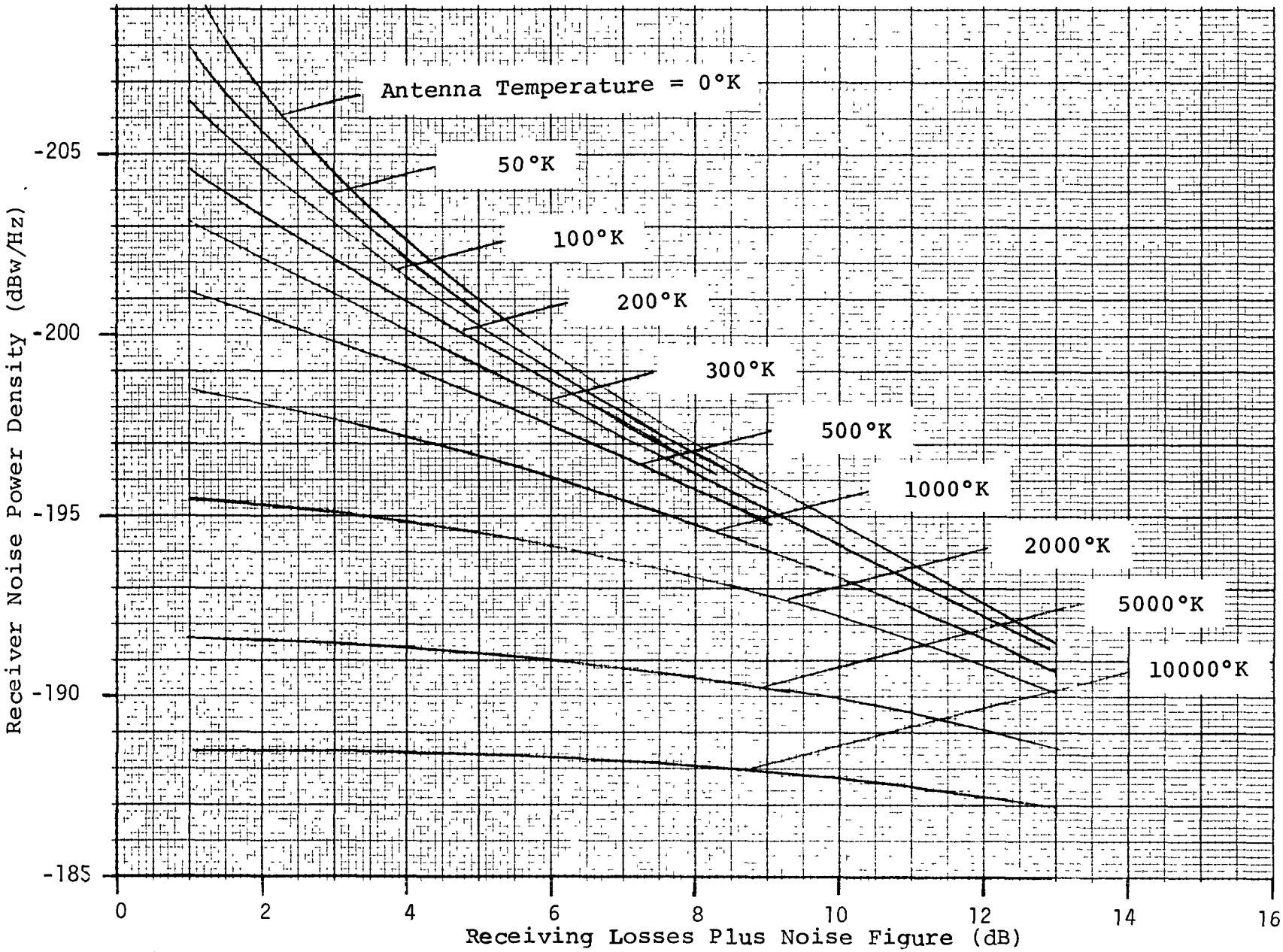

Figure A-5. Receiver Noise Power Density vs. Receiving Losses and Noise Figure

$$P_{sg} = (P_g L_{gs}/P_{sr})\ P_s$$

$$= P_s/[1 + (P_t/P_g)(L_{ts}/L_{gs}) + (B_s/P_g)(N_{os}/L_{gs})] \quad \text{(A-26)}$$

the power allocated to the remoted platform(s) is

$$P_{st} = (P_t L_{ts}/P_{sr})\ P_s$$

$$= P_s/[1 + (P_g/P_t)(L_{gs}/L_{ts}) + (B_s/P_t)(N_{os}/L_{ts})] \quad \text{(A-27)}$$

and the transmitted noise power (excluding intermodulation noise) is

$$P_{sn} = (N_s/P_{sr})\ P_s$$

$$= P_s/[1 + (P_g/B_s)(L_{gs}/N_{os}) + (P_t/B_s)(L_{ts}/N_{os})] \quad \text{(A-28)}$$

Pilot Tone Power Allocation

A tone is transmitted by the GCC to aid the system receivers in removing frequency jitter introduced by the ATS-III satellite. For a given pilot tone power transmitted by the satellite

$$P_{sj} = K_{sj}\ P_s, \qquad 0 \leq K_{sj} \leq 1 \quad \text{(A-29)}$$

the GCC will be required to transmit a pilot tone power of

$$P_{gj} = K_{gj}\ P_g, \qquad 0 \leq K_{gj} \leq 1 \quad \text{(A-30)}$$

Substituting (A-29) and (A-30) into Equation (A-26) and solving for K_{gj} gives

$$K_{gj} = K_{sj}[1 + (P_t/P_g)(L_{ts}/L_{gs}) + (B_s/P_g)(N_{os}/L_{gs})] \quad \text{(A-31)}$$

A6.3 Signal-to-Noise Ratio Derivations

Transponder Signal-to-Noise Ratio

The power received by the transponder is

$$P_{tr} = [P_{sg} + (B_t/B_s)\ P_{sn}]\ L_{st} + N_t \qquad \text{(A-32)}$$

The carrier-to-noise ratio (C/N) is

$$(C/N)_t = P_{sg}/[B_t(N_{ot}/L_{st}) + B_t/B_s)\ P_{sn}] \qquad \text{(A-33)}$$

Multiplying both sides of Equation (A-33) by B_t gives the carrier-to-noise power density ratio

$$(C/N_o)_t = P_{sg}/[N_{ot}/L_{st} + P_{sn}/B_s] \qquad \text{(A-34)}$$

$$\simeq P_{sg}/(N_{ot}/L_{st}),\ N_{ot}/L_{st} >> P_{sn}/B_s \qquad \text{(A-35)}$$

GCC Signal-to-Noise Ratios

The pilot tone C/N_o can be derived in a manner similar to that used to obtain Equation (A-34) and is given by

$$(C/N_o)_{jg} = K_{gj}P_{gs}/[N_o/L_{sg} + P_{sn}/B_s] \qquad \text{(A-36)}$$

$$\simeq K_{gj}P_{gs}\ (L_{sg}/N_{og}),\ N_{og}L_{sg} >> P_{sn}/B_s \qquad \text{(A-37)}$$

The tone package C/N_o is given by

$$(C/N_o)_{tone} = (1-K_{gj})\ P_{gs}/N_{og}/L_{sg} + P_{sn}/B_s] \qquad \text{(A-38)}$$

$$\simeq (1-K_{gj})\ P_{gs}\ (L_{sg}/N_{og}),\ N_{og}/L_{sg} >> P_{sn}/B_s \qquad \text{(A-39)}$$

The tone power transponded by a remote terminal is a function of the CNR at the transponder. For a given CNR the ratio of signal-to-signal plus noise is

$$R = S/(S + S/CNR)$$

$$= 1/(1 + 1/CNR \qquad \text{(A-40)}$$

The actual ranging tone power transmitted by the transponder is

$$P_{trt} = RP_t \qquad \text{(A-41)}$$

The power received at the GCC in the i-th ranging tone channel is

$$P_{gr} = (R/m)\ P_{st}L_{sg} + (B_g/B_s)\ P_{sn}L_{gs} + N_g \qquad \text{(A-42)}$$

and the i-th ranging tone channel C/N_o is

$$(C/N_o)_{rt} = (R/m)\ P_{st}/[N_{og}/L_{sg} + P_{sn}/B_s] \qquad \text{(A-43)}$$

$$\simeq (R/m)\ P_{st}\ (L_{sg}/N_{og}),\ N_{og}/L_{sg} >> P_{sn}/B_s \qquad \text{(A-44)}$$

where m is the number of platforms transmitting simultaneously.

APPENDIX B

IONOSPHERIC EFFECTS

B1. INTRODUCTION

The net effect of the ionospheric electrons is to reduce the group velocity of an electromagnetic wave that passes through the ionosphere. This effectively increases the path-length relative to free space by [25]

$$\Delta R = (1600/\omega^2) \int_L N_e \, d\ell \quad \text{meters} \tag{B-1}$$

where $\omega = 2\pi f$ and N_e is the electron density in electrons/m^3 along the wave path. ΔR is a minimum when the satellite is nearly overhead, and it increases as the satellite elevation decreases because the radio wave then traverses a greater portion of the ionosphere. One may account for this by expressing Equation (B-1) in the more convenient form

$$\Delta R = 4.06 \times 10^{-11} K_\varepsilon I / f_{MHz}^2 \tag{B-2}$$

where K_ε is the satellite elevation factor, f_{MHz} is the frequency of the radio tone in MHz, and $I = \int_h N_e dh$ (sometimes referred to as the total electron content) is the integrated electron density (i.e., the number of electrons in a column of the ionosphere that has a cross-section of one m^2).

There is some difference among the satellite elevation factors used by various authors [26,27,28] as shown by the curves in Figure B-1 where the biggest difference occurs for elevations less than 30 degrees. An average of these curves, as plotted in Figure B-1, will be used for the calculations in this appendix.

The range error for a one-way path through the ionosphere at 0 degree satellite elevation is plotted as a function of frequency in Figure B-2 for three values of I. The curves show that the ionospheric range error at VHF frequencies is 100 times

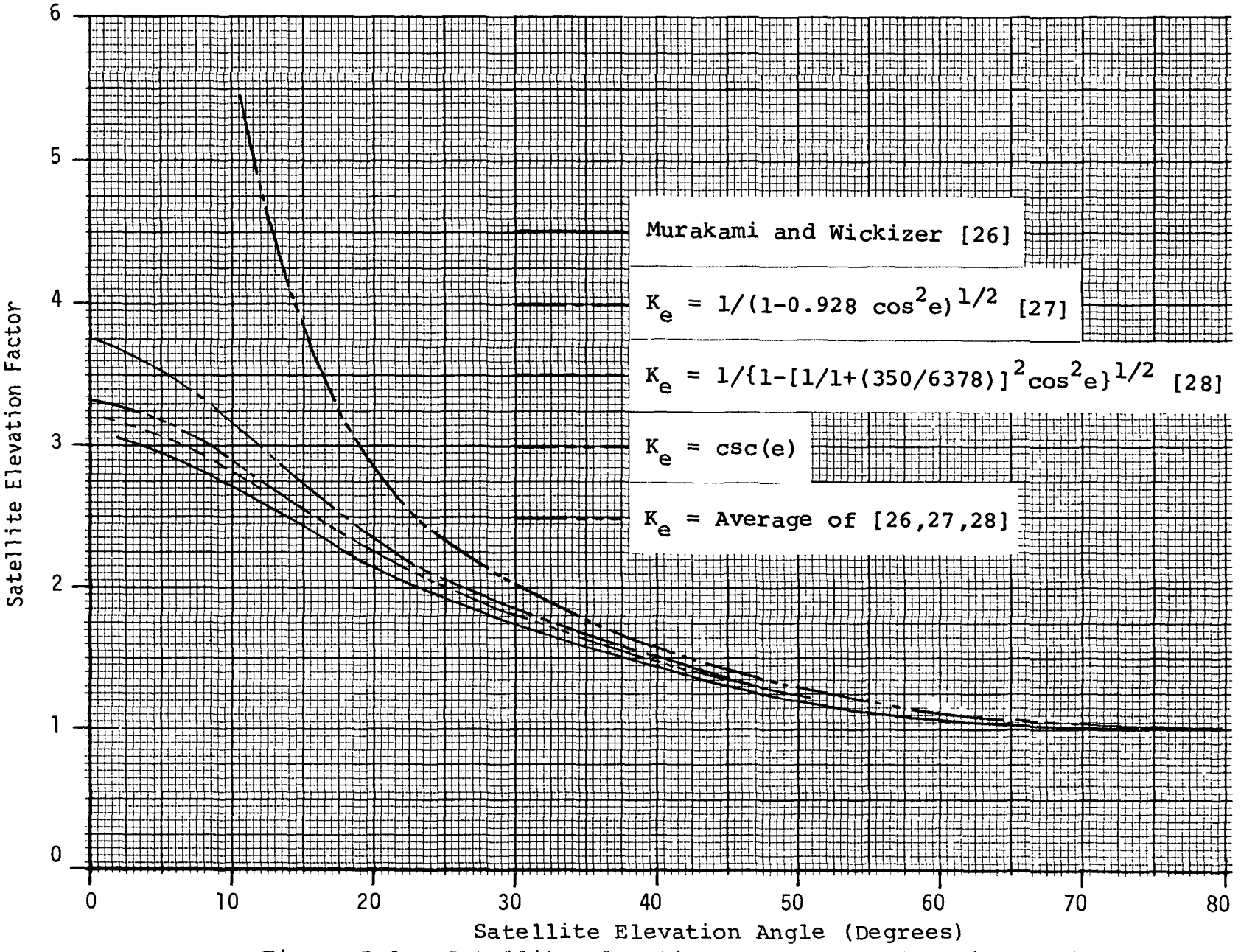

Figure B-1. Satellite Elevation Factor vs. Elevation Angle

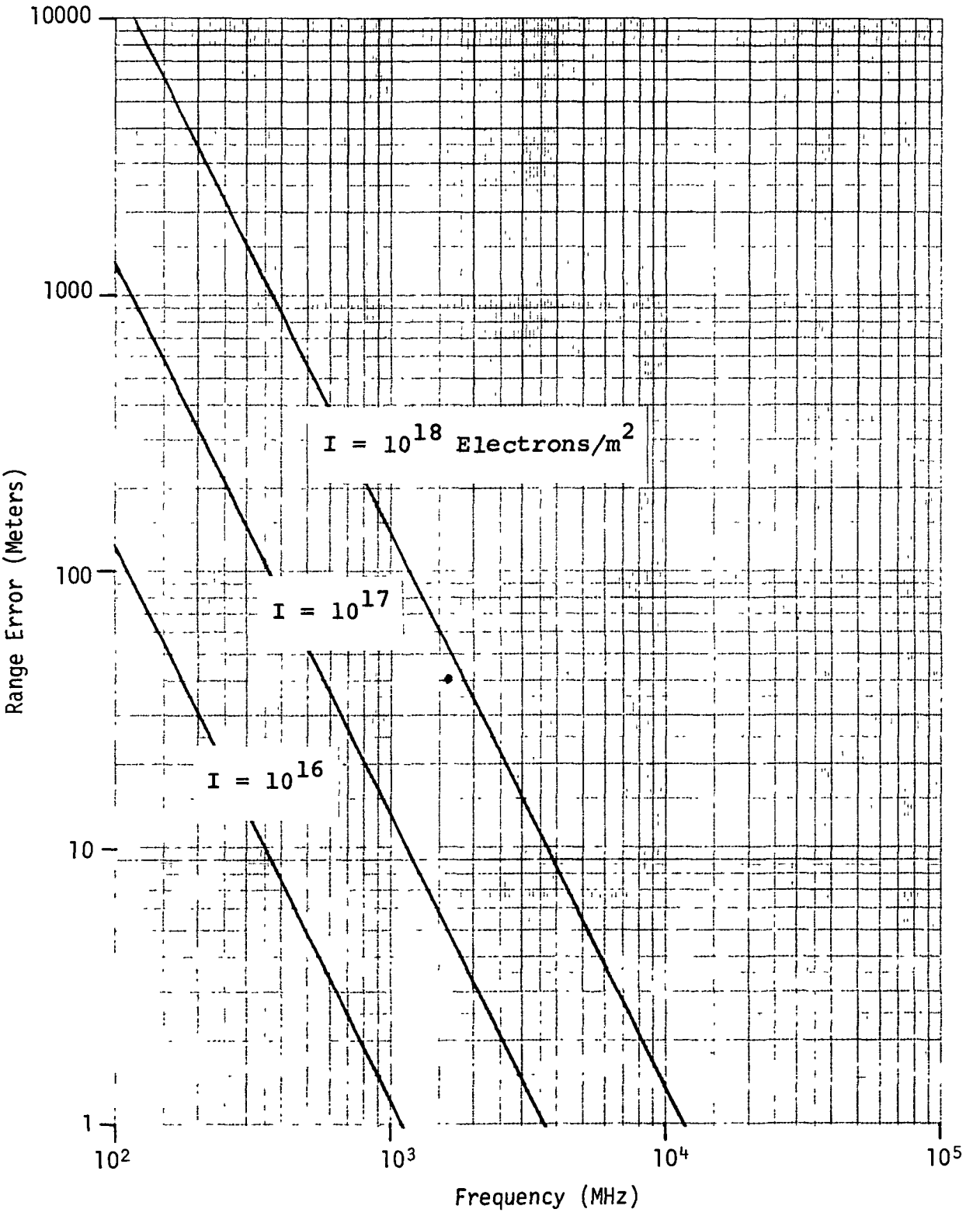

Figure B-2. Ionospheric Range Error for 0° Satellite Elevation Angle

greater than that at L-Band frequencies, and the magnitude is such that it must be examined closely.

B2. DIFFERENTIAL PHASE ERROR

The ionospheric phase delay on the GCC-satellite-aircraft link is given by

$$\theta_{ion} = -(2\pi/\lambda_{up})\ \Delta R_{up} - (2\pi/\lambda_{down})\ \Delta R_{down}$$

$$= -(2\pi f_u/c)\ (K_{ion}/f_u^2) - (2\pi f_d/c)\ (K_{ion}/f_d^2)$$

$$= -(2\pi K_{ion}/c)\ (1/f_u + 1/f_d) \qquad \text{(B-3)}$$

where $K_{ion} = 4.06 \times 10^{-11}\ K_\varepsilon I$ and the negative sign indicates phase delay.

The differential phase error between the i-th ranging tone and the A/R tone is given by

$$\Delta\theta_{ion} = \theta_i - \theta_{ar}$$

$$= -(2\ K_{ion}/c)\,[(1/f_{iu} + 1/f_{id}) - 1/f_{aru} + 1/f_{ard})] \qquad \text{(B-4)}$$

Let $f_{io} = f_o + f_{ar} + f_i$ and $f_{aro} = f_o + f_{ar}$. Substituting these into Equation (B-4)

$$\Delta\theta_{ion} \simeq -(2\pi K_{ion}/c)\,[f_i/f_{iu}^2 + f_i/f_{id}^2]$$

$$= -(\omega_i/c)\,[K_{ion}/f_{iu}^2 + K_{ion}/f_{id}^2] \qquad \text{(B-5)}$$

since $f_{iu}f_{aru} = f_{iu}^2 - f_i/f_{iu} \simeq f_i^2$ and $f_{id}f_{ard} \simeq f_{id}^2$. Thus, the differential ranging tone phase error caused by the ionosphere represents a decrease in the total path length by an amount given by Equation (B-2).

The mean ionospheric range error given by Equation (B-2) with K_ε average taken from Figure B-1 is plotted as a function of I and ε in Figure B-3 for f = 135.6 MHz. The range errors for f = 149.22 MHz can also be obtained from Figure B-3 by multiplying the ordinate by 0.823. Figure B-3 was used to obtain the GCC-satellite-aircraft ionosphere range errors that are given in Table B-1 for a night-time minimum of 2×10^{16} electrons/m^2, a "typical" day-time maximum I of 3×10^{17} electrons/m^2, and a maximum day-time I of 8.6×10^{17} electrons/m^2. Values for a two-way link are also given which show that the two-way ranging error can be somewhat greater than twice the one-way ranging error, although it generally is less.

The ionospheric range/range errors in Table 1 are sufficiently large that compensation must be introduced. This topic will be discussed in the next subsection.

Table B-1. Mean Ionospheric Range Error*

Satellite Elevation at A/C	$I = 2 \times 10^{16}$		$I = 3 \times 10^{17}$		$I = 8.6 \times 10^{17}$	
	One-way Path Error	Two-way Path Error	One-way Path Error	Two-way Path Error	One-way Path Error	Two-way Path Error
$\varepsilon = 20°$	-0.16km	-0.32km	-2.6km	-5.1km	-6.5km	-13km
$\varepsilon = 45°$	-0.12km	-0.25km	-2km	-4km	-5.3km	-10.7km
$\varepsilon = 60°$	-0.11km	-0.23km	-1.8km	-3.8km	-4.9km	-10km

* Satellite Elevation at GCC = 25°

B3. IONOSPHERIC RANGE ERROR COMPENSATION

B3.1 Introduction

One of the major problems in compensating for ionospheric range error is that I is subject to diurnal, seasonal, solar cycle, and random day-to-day variations as well

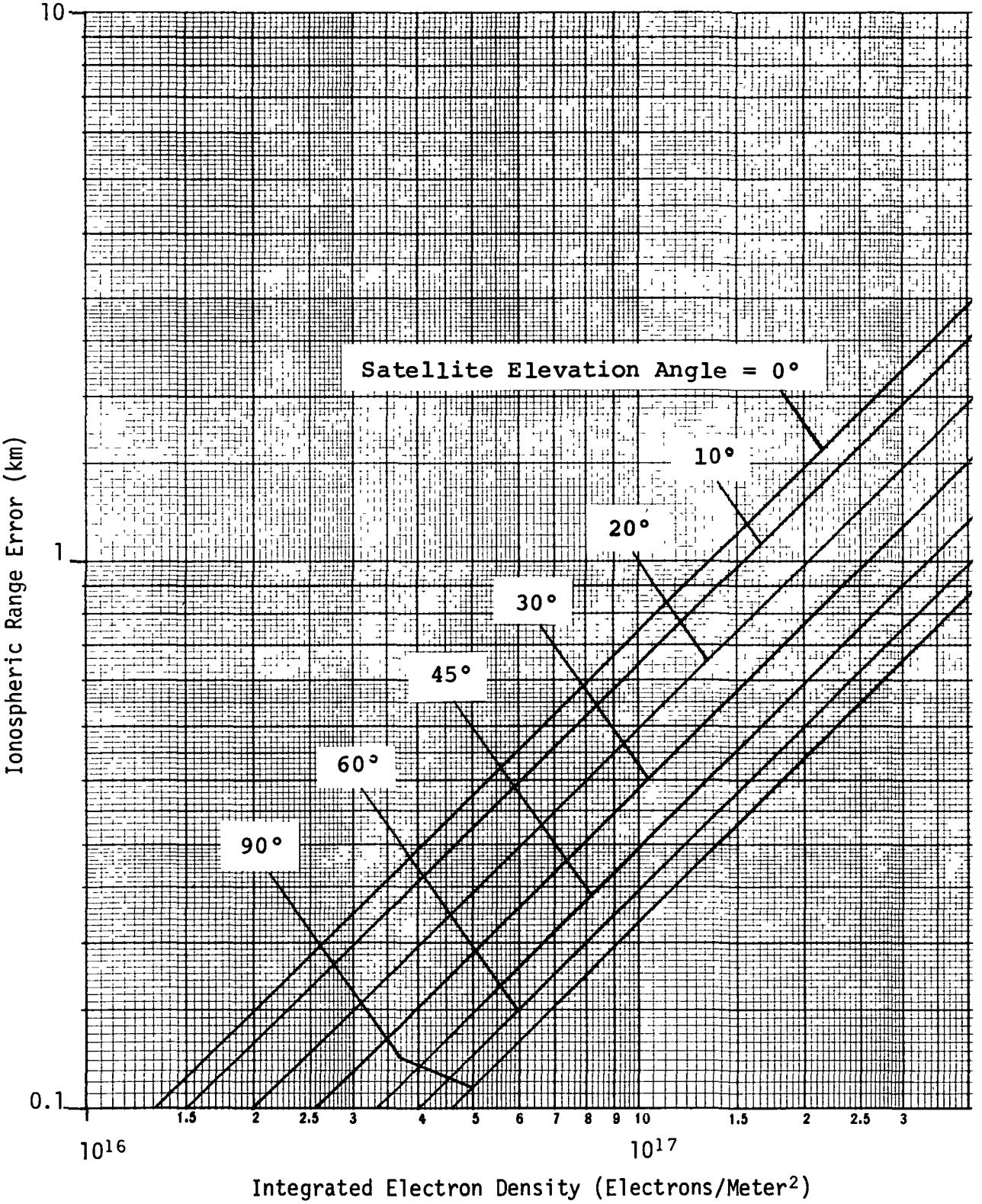

Figure B-3. One-Way Ionospheric Range Error

as latitudinal and longitudinal variations. DaRosa [29] cites an example where the predicted value of I was 3×10^{17} electrons/m^2, the measured value was 8×10^{17} electrons/m^2, and the following day it was 1.4×10^{17} electrons/m^2. A summary by RCA [28] of the range of variation of I due to various effects is given in Table B-2. These figures demonstrate that real-time measurements are required especially, as DaRosa states [29], if VHF navigation precision better than 5 km is desired.

Either Faraday rotation or phase-path measurements can be made to provide the ionospheric path corrections. The absolute accuracy of Faraday rotation measurements is about 1×10^{16} electrons/m^2 [30], which corresponds to a maximum range uncertainty of 135 meters for the VHF frequencies that will be used. Since additional equipment is required to make the Faraday rotation measurements, measurement of phase-path variations using the ranging equipment are preferable.

Table B-2. Summary of Ionospheric Variability Factors [28]

Factor	Range of Variation
Diurnal Variation	3:1 to 13:1
Seasonal Variation	2:1, variable
Solar Variation	12:1 (11-year cycle)
Day-to-Day Variation	±20%, variable
Latitudinal Variation	2:1/10°, quite variable
Short-term rms Variation	1-2%

B3.2 GCC-to-Satellite Range Compensation

The ionospheric ranging error for the GCC-to-satellite link can be measured at the GCC from the phase variations of the 135.6-MHz satellite signal. As described previously [31], independent measurements of range (including ionospheric range

errors) and electron density could be used to establish the GCC-to-satellite range, and the ionospheric range error would be measured with respect to this reference value. This relative error measurement would afford somewhat higher accuracy [30], but the absolute ranging accuracy would depend on the accuracy of the electron content measurement technique that was used. Day-time measurements of I with an absolute value of 1 percent have been reported [30], but if the ionospheric measurements are made at night when the ranging errors are smallest, the absolute accuracy of the measurements will also decrease.

This basic technique can be extended to additional locations by placing a transponder at the desired location and making an additional electron density measurement during a calibration period. However, before determining how many additional remote stations are required in order to provide ionospheric range compensation over the satellite's area of coverage, the spatial and temporal variation of I will first be discussed.

B3.3 Spatial and Temporal Variations of Integrated Electron Density

The temporal variation of I, considering short-term, diurnal, and day-to-day variations, as well as diurnal variation measured at different locations have been studied by many investigators. From their studies it is evident that individual measurements during the same period may be compared directly; but day-to-day, seasonal, and yearly fluctuations in I are great enough so that relative, rather than absolute, variations must be compared for different measurement periods.

Investigators have shown [30 through 37] that the daily increase in I begins approximately 0500 local mean time and continues to approximately 1200 LMT, although the time when the peak is reached varies from day-to-day. The initial rate of increase is rough 0.5×10^{17} electrons/m^2/h, which corresponds to a "one way" (GCC-to-satellite and return) VHF ranging error of 445 m/h for satellite elevations of 20 degrees. Garriott, et al [30], note that a sudden change in this initial rate of increase occurs sometime in the morning in all seasons and all phases of solar activity. This change may be either an increase or decrease in the rate of growth of I, and the data shows a variation in growth rate ranging from approximately 0.16×10^{17} electrons/m^2/h to somewhat greater than 2×10^{17} electrons/m^2/h. These figures correspond to increases in one-way ranging errors

of 190 m/h to 1.7 km/h.

The electron content begins a rapid decrease between 1600 and 1800 LMT, and reaches a minimum by 1900 LMT at mid-latitudes and sometime after midnight at low latitudes. At high latitudes, a nocturnal maximum occurs during the winter at local midnight at 50°N, but this effect disappears beyond 55°N [36]. The rate of decay of I is variable, but is generally somewhat higher than the growth rate. Decay rates as high as 2.5×10^{17} electrons/m^2/h have been noted, which corresponds to a one-way ranging error decrease of approximately 2.25 km/h.

One relative number that can be used as a basis of comparison is the diurnal ratio I_{max}/I_{min} because it does exhibit a latitudinal variation. Garriott, et al [30], report that it is relatively constant at approximately 4 during the summer months at all mid-latitudes (20-40 degrees) and for all phases of the solar cycle, but it does vary seasonally and can reach much higher values in winter. At high latitudes the diurnal ratio ranges from approximately 1.5 in summer to 3 in winter. At equatorial latitudes (0-20°) the diurnal ratio exceeds 10 [37], and it has been noted as high as 20 [34]; however, as Table B-3 shows, the high equatorial diurnal ratios are due more to low night-time values of I, for which the greatest measurement uncertainty exists, than to extremely high day-time maxima.

The model for the variation of I with latitude that is presented in Table B-4 was developed from References 28, 30, and 32 through 37. Although this variation is more properly expressed in terms of geomagnetic latitude, the geographic variation of I is required for the ranging calculations. Also, the data presently available does not justify a more detailed model. The diurnal ratios and values of I_{max} were chosen to reflect the upper limits of the corresponding values described in the references in order to obtain estimates of the upper limits of the differences in ionospheric ranging error between widely separated stations.

Table B-3. Equatorial Diurnal Ratios [34]

Station	Period of Measurements	I_{min} Before Ground Sunrise (m^{-2})	I_{max} Around Midday (m^{-2})	Ratio I_{max}/I_{min}
Zaria, Nigeria	11/14/64 - 2/13/65	2×10^{16}	26×10^{16}	13
Bangkok, Thailand	June '64 - Sept '64	1×10^{16}	20×10^{16}	20
Huancayo, Peru	8/15/61 - 10/31/61	5×10^{16}	40×10^{16}	8
Huancayo, Peru	1/1/67 - 3/31/67	8×10^{16}	70×10^{16}	8.7

Table B-4. Model for Latitude Variation of I

Latitude	I (10^{17} electrons/m^2)		Ratio
	I_{max}	I_{min}	I_{max}/I_{min}
0°	8	0.67	12
20°N	5	0.6	8
30°N	3	0.6	5
40°N	2	0.5	4
50°N	1.6	0.4	4
60°N	1	0.33	3

The longitude variation of I will be based upon the earth's rate of rotation of 15 deg/h. Thus, for two stations separated by 90 degrees (6 hours in time), the value of the integrated electron density at one station could be I_{max}, and the value at the other station could be I_{min}. The values of I

from Table B-4 that will be used to calculate the ionospheric ranging error to geographically separated stations are given in Table B-5.

Table B-5. I vs Longitude for Ionospheric Error Model

Station Longitude	Longitude of I_{max}				
	8°W	53°W			98°W
	(Model A)	(Model B)	(Model C)	(Model D)	(Model E)
8°W	I_{max}	I_{max}	0.5 I_{max}	0.5 I_{max}	I_{min}
53°W	0.5 I_{max}	I_{max}	I_{max}	I_{max}	0.5 I_{max}
98°W	I_{min}	0.5 I_{max}	0.5 I_{max}	I_{max}	I_{max}

The values of I given in Table B-5 were used to calculate the ionospheric range error from the GCC located at 33°N, 98°W to stations at 0°, 20°N, 30°N, 40°N, 50°N, and 60°N at longitudes of 8°W, 53°W, and 98°W. The satellite elevations used were obtained from an assumed position of 50°W for the satellite.

The ranging errors that were calculated from the model in Table B-5 are given in Tables B-6 through B-10, in which ΔR_1 is the one-way (GCC-to-satellite-to-remote station) ionospheric range error, ΔR_2 is the two-way (one-way plus return) ionospheric range error, and ΔG is the GCC-to-satellite-to-GCC ionospheric range error. The one-way error ranges in value from -0.4 km to -4.1 km and has a mean value of -1.7 km and a standard deviation of 0.8 km. The two-way error ranges in value from -0.8 to -7.4 km and has a mean value of -3.35 km and a standard deviation of 1.6 km.

One possible compensation method is to subtract ΔG from ΔR_1, since this may be readily measured at the GCC. The resultant error decreases to a range of 0 to 2.8 km and has a mean of -0.2 km and a standard deviation of about 0.8 km.

Table B-6. Ionospheric Ranging Errors Predicted by Model A

Longitude	Latitude	ΔR_1	$\Delta R_1 - \Delta G$	ΔR_2	$0.5\Delta R_2$	$\Delta R_1 - 0.5\Delta R_2$	$\Delta R_1 - 0.5\Delta R_2 (50°)$
	0	-2.76km	-2.29km	-5.12km	-2.56km	-0.2km	
8°W	20°N	-1.91km	-1.44km	-3.57km	-1.79km	-0.12km	
$I = I_{max}$	30°N	-1.31km	-0.89km	-2.48km	-1.24km	-0.07km	
	40°N	-1.06km	-0.59km	-2.02km	-1.01km	-0.01km	-0.43km
	50°N	-1 .km	-0.53km	-1.91km	-0.96km	-0.04km	-0.37km
	60°N	-0.79km	-0.32km	-1.53km	-0.77km	-0.02km	-0.16km
	0°	-1.01km	-0.62km	-2.08km	-1.04km	-0.05km	
53°W	20°N	-0.81km	-0.34km	-1.56km	-0.78km	-0.02km	
$I = 0.5\ I_{max}$	30°N	-0.62km	-0.15km	-1.22km	-0.61km	-0.01km	
	40°N	-0.52km	-0.05km	-1.03km	-0.52km	0 km	0.11km
	50°N	-0.51km	-0.04km	-1.02km	-0.51km	0 km	0.12km
	60°N	-0.45km	0.02km	-0.91km	-0.46km	0.01km	0.18km
	0°	-0.41km	.06km	-0.83km	-0.42km	0.01km	
98°W	20°N	-0.44km	.03km	-0.89km	-0.45km	0.01km	
$I = I_{min}$	30°N	-0.46km	.01km	-0.93km	-0.47km	0.01km	
	40°N	-0.44km	.03km	-0.89km	-0.45km	0.01km	0.19km
	50°N	-0.43km	.04km	-0.87km	-0.44km	0.01km	0.2 km
	60°N	-0.42km	.05km	-0.85km	-0.43km	0.01km	0.21km

Table B-7. Ionospheric Ranging Errors Predicted by Model B

Longitude	Latitude	ΔR_1	$\Delta R_1 - \Delta G$	ΔR_2	$0.5\Delta R_2$	$\Delta R_1 - 0.5\Delta R_2$	$\Delta R_1 - \overline{0.5\Delta R_2(50°)}$
	0°	-3.25km	-1.6 km	-6.2 km	-3.1 km	-0.15km	
8°W	20°N	-2.4 km	-0.85km	-4.65km	-2.33km	-0.07km	
$I = I_{max}$	30°N	-1.8 km	-0.25km	-3.56km	-1.78km	-0.02km	
	40°N	-1.55km	0	-3.1 km	-1.52km	-0.03km	-0.22km
	50°N	-1.44km	0.06km	-2.99km	-1.5 km	0.01km	-0.16km
	60°N	-1.28km	0.27km	-2.61km	-1.32km	0.04km	-0.05km
	0°	-2.46km	-0.91km	-4.76km	-2.38km	-0.08km	
53°W	20°N	-1.9 km	-0.35km	-3.74km	-1.87km	-0.03km	
$I = I_{max}$	30°N	-1.52km	0.03km	-3.05km	-1.53km	0.01km	
	40°N	-1.31km	0.24km	-2.66km	-1.33km	0.02km	0.02km
	50°N	-1.29km	0.26km	-2.63km	-1.32km	0.04km	0.04km
	60°N	-1.17km	0.38km	-2.41km	-1.21km	0.04km	0.16km
	0°	-1.89km	-0.34km	-3.72km	-1.86km	-0.03km	
98°W	20°N	-1.66km	-0.11km	-3.3 km	-1.65km	-0.01km	
$I = 0.5\ I_{max}$	30°N	-1.32km	0.13km	-2.68km	-1.34km	0.02km	
	40°N	-1.17km	0.38km	-2.41km	-1.21km	0.04km	0.16km
	50°N	-1.13km	0.42km	-2.33km	-1.17km	0.04km	0.2 km
	60°N	-1.02km	0.43km	-2.13km	-1.07km	-0.05km	0.31km

Table B-8. Ionospheric Ranging Errors Predicted by Model C

Longitude	Latitude	ΔR_1	$\Delta R_1 - \Delta G_1$	ΔR_2	$0.5\Delta R_2$	$\Delta R_1 - 0.5\Delta R_2$	$\Delta R_1 - \overline{.5\Delta R_2(50°)}$
	0°	-1.98km	-0.43km	-3.78km	-1.89km	-0.09km	
8°W	20°N	-1.55km	0	-3.1 km	-1.55km	0 km	
$I = 0.5\ I_{min}$	30°N	-1.25km	0.3 km	-2.55km	-1.23km	-0.02km	
	40°N	-1.12km	0.43km	-2.32km	-1.16km	0.04km	0.01km
	50°N	-1.1 km	0.45km	-2.32km	-1.16km	0.06km	0.03km
	60°N	-0.99km	0.56km	-2.08km	-1.04km	0.05km	0.14km
	0°	-2.46km	-0.91km	-4.76km	-2.38km	-0.08km	
53°W	20°N	-1.9 km	-0.35km	-3.74km	-1.87km	-0.03km	
$I = I_{max}$	30°N	-1.52km	0.03km	-3.05km	-1.52km	0	
	40°N	-1.01km	0.54km	-2.11km	-1.06km	0.05km	0.12km
	50°N	-1 km	0.55km	-2.1 km	-1.05km	0.05km	0.13km
	60°N	-0.86km	0.69km	-1.84km	-0.92km	0.06km	0.27km
	0°	-1.89km	-0.34km	-3.72km	-1.86km	-0.03km	
98°W	20°N	-1.66km	-0.11km	-3.3 km	-1.65km	-0.01km	
$I = 0.5\ I_{max}$	30°N	-1.32km	0.23km	-2.68km	-1.34km	0.02km	
	40°N	-1.17km	0.38km	-2.41km	-1.21km	0.04km	-0.04km
	50°N	-1.13km	0.42km	-2.33km	-1.17km	0.04km	0
	60°N	-1.02km	0.53km	-2.18km	-1.09km	0.07km	0.11km

Table B-9. Ionospheric Ranging Errors Predicted by Model D

Longitude	Latitude	ΔR_1	$\Delta R_1 - \Delta G_1$	ΔR_2	$0.5\Delta R_2$	$\Delta R_1 - 0.5\Delta R_2$	$\Delta R_1 - .5\overline{\Delta R_2(50°)}$
	0°	-2.98km	0.12km	-5.33km	-2.67km	-0.31km	
8°W	20°N	-2.55km	0.55km	-4.65km	-2.33km	-0.22km	
$I = .5\ I_{max}$	30°N	-2.25km	0.85km	-4.1 km	-2.05km	-0.2 km	
	40°N	-2.12km	0.98km	-3.87km	-1.94km	-0.18km	-0.09km
	50°N	-2.1 km	1 km	-3.87km	-1.94km	-0.16km	-0.07km
	60°N	-1.99km	1.41km	-3.63km	-1.82km	-0.17km	0.04km
	0°	-3.46km	-0.36km	-6.31km	-3.16km	-0.3 km	
53°W	20°N	-2.9 km	0.2km	-5.29km	-2.65km	-0.35km	
$I = I_{max}$	30°N	-2.52km	0.58km	-4.6 km	-2.3 km	-0.22km	
	40°N	-2.01km	1.09km	-3.66km	-1.83km	-0.18km	0.02km
	50°N	-2 km	1.1 km	-3.65km	-1.83km	-0.17km	0.03km
	60°N	-1.86km	1.24km	-3.39km	-1.7 km	-0.16km	0.17km
	0°	-4.08km	-0.98km	-7.44km	-3.72km	-0.36km	
98°W	20°N	-3.62km	-0.52km	-6.6 km	-3.3 km	-0.32km	
$I = I_{max}$	30°N	-2.93km	0.17km	-5.34km	-2.67km	-0.26km	
	40°N	-2.63km	0.47km	-4.8 km	-2.4 km	-0.23km	-0.6 km
	50°N	-2.56km	0.54km	-4.67km	-2.34km	-0.22km	-0.53km
	60°N	-2.34km	0.76km	-4.27km	-2.14km	-0.2 km	-0.31km

Table B-10. Ionospheric Ranging Errors Predicted by Model E

Longitude	Latitude	ΔR_1	$\Delta R_1 - \Delta G$	ΔR_2	$0.5\Delta R_2$	$\Delta R_1 - 0.5\Delta R_2$	$\overline{\Delta R_1 - 0.5\Delta R_2(50°)}$
	0°	-1.62km	1.48km	-3.5 km	-1.75km	0.13km	
8°W	20°N	-1.61km	1.49km	-3.48km	-1.74km	0.13km	
$I = I_{min}$	30°N	-1.62km	1.48km	-3.5 km	-1.75km	0.13km	
	40°N	-1.61km	1.49km	-3.49km	-1.75km	0.14km	0.35km
	50°N	-1.6 km	1.5 km	-3.46km	-1.73km	0.13km	0.36km
	60°N	-1.59km	1.51km	-3.45km	-1.73km	0.14km	0.37km
	0°	-2.32km	0.78km	-4.71km	-2.36km	0.04km	
53°W	20°N	-2 km	1.1 km	-4.19km	-2.7 km	0.1 km	
$I = 0.5\ I_{min}$	30°N	-1.81km	1.29km	-3.85km	-1.93km	0.12km	
	40°N	-1.71km	1.39km	-3.66km	-1.83km	0.12km	0.25km
	50°N	-1.7 km	1.4km	-3.45km	-1.83km	0.13km	0.26km
	60°N	-1.64km	1.46km	-3.54km	-1.77km	0.13km	0.32km
	0°	-3.78km	-0.68km	-7.44km	-3.72km	-0.04km	
98°W	20°N	-3.32km	-0.22km	-6.6 km	-3.3 km	-0.02km	
$I = I_{max}$	30°N	-2.63km	0.47km	-5.34km	-2.67km	0.04km	
	40°N	-2.33km	0.77km	-4.8 km	-2.4 km	0.07km	-0.37km
	50°N	-2.26km	0.84km	-4.67km	-2.34km	0.08km	-0.3 km
	60°N	-2.04km	1.06km	-4.27km	-2.14km	0.1 km	-0.08km

Although this procedure does decrease the error and its mean value, the standard deviation remains the same so the uncertainty in the error value is unchanged.

Another possible compensation method is to measure the two-way ionospheric path error to a given location and subtract half this value from the one-way error. This procedure can reduce the magnitude of the maximum ionospheric error to less than 0.4 km. The mean error is -0.03 km, and the standard deviation is 0.12 km so a substantial improvement has been made. However, this improvement comes at the expense of the large number of remote stations required to obtain accurate ionospheric range error estimates at points within the satellite's region of coverage.

The maximum value, mean value, and standard deviation of ΔR_1 and ΔR_2 is tabulated in Table B-11 for various regions to see if regional coverage with a single compensation value appears feasible. The figures show that the higher latitudes might provide the largest region in which a single ionospheric range error estimate might apply. The mean value of $0.5\Delta R_2$ at 50°N in Table B-6 was subtracted from the ΔR_1 values for 40°N, 50°N and 60°N in Table B-6, and a similar procedure was followed in Tables B-7 through B-10. The maximum resultant error was -0.6 km, and except for the GCC longitude the resultant error was substantially less than that obtained by subtracting ΔG from ΔR_1.

Since the mean ionospheric range errors can be several kilometers, a compensation method is necessary. The most promising scheme is to obtain real-time measurements from remote stations and retard the phase of the ranging tones by the amount derived from the ionospheric range error measurements. A number of different phase delays will be required because a single value cannot serve all regions. The number of different phase delays that will be required depends upon the spatial variation of I at a given moment, the satellite elevation at the receiving station, and the desired ranging accuracy. One or two compensation values might suffice for the period during which I_{min} applies for the entire satellite region of coverage, but several values will be necessary otherwise.

Since the ionosphere changes relatively slowly the phase compensations need not be updated continuously, but only every few minutes; the range error estimation system capacity need not be very large.

Table B-11. Ionospheric Range Errors for Various Regions

Latitude	Longitude	ΔR_1 (km)			ΔR_2 (km)		
		Max	Mean	Std.Dev.	Max	Mean	Std.Dev.
0°-60°N	8°W	-3.25	-1.74	0.61	-6.21	-3.41	1.07
0°-60°N	53°W	-3.46	-1.61	0.74	-6.31	-3.17	1.37
0°-60°N	98°W	-4.08	-1.78	1.07	-7.44	-3.49	1.98
0°-60°N	8°-98°W	-4.08	-1.71	0.82	-7.44	-3.35	1.58
0°N	8°-98°W	-4.08	-2.43	1	-7.44	-4.65	1.82
20°N	8°-98°W	-3.32	-2.02	0.85	-6.6	-3.91	1.52
30°N	8°-98°W	-2.93	-1.66	0.71	-5.34	-3.28	1.25
40°N	8°-98°W	-2.63	-1.4	0.63	-4.8	-2.88	1.18
50°N	8°-98°W	-2.56	-1.42	0.62	-4.67	-2.83	1.16
60°N	8°-98°W	-2.34	-1.3	0.59	-4.27	-2.61	1.11

B3.4 Ionospheric Scintillation

Irregularities in the ionospheric structure produce amplitude fluctuations, or scintillations. The fluctuations at mid-latitudes are not as large as those at equatorial and high latitudes [10] nor do they occur as frequently. To be consistent with the discussion of multipath effects presented in Appendix C, it is convenient to consider the scintillation fluctuation effect in terms ov the fade depth of the received signal, where

$$\text{Fade Depth} = 20 \log_{10} (1 - m_{si})$$

and

$$m_{si} = \text{Scintillation Index} = (P_{max} - P_{min})/(P_{max} + P_{min})$$

Aarons and Whitney [11] investigated scintillation fading distribution at mid-latitudes. They showed that 90 percent of the time the fade depth was less than 1.3 dB ($m_{si} = 0.14$), and the 99 percentile value was -9.4 dB ($m_{si} = 0.67$). Both the GCC-to-satellite and satellite-to-remote station links can experience ionospheric scintillations of these magnitudes, simultaneously, but it is possible that only one of the links might experience scientillation fading or that the fade values on the two links will differ because of the irregular boundary of the region of ionospheric irregularity [10].

The duration of the mid-latitude scintillations ranged from a few minutes to a few hours with scintillation bursts of 3 to 14 minutes duration occurring near the daytime ionization peaks [11]. The distribution of the fading periods is summarized in Table B-12.

Table B-12. Mid-Latitude Scintillation Fading Period [11]

Fading Period	Percentage of Occurrences
$T_s \leq 5$ seconds	43
6 sec $\leq T_s \leq$ 14 sec	29
15 sec $\leq T_s \leq$ 59 sec	28

The net effect of ionospheric scintillation is to produce an amplitude fading and a corresponding phase shift similar to that produced by specular multipath interference, as discussed in Appendix C. The phase shift in this case, however, will be a function of the change in I.

APPENDIX C

MULTIPATH EFFECTS

C1 INTRODUCTION

The multipath effects that will be considered for the satellite-to-aircraft links arise from interference between the direct path signal and an earth-reflected signal as shown in Figure C-1. As a result of this interference, the amplitude of the received signal will vary so that the effective link signal-to-noise ratio will be reduced at times, and the signal phase will vary so that a range error will be introduced.

Since the ranging information is transmitted on a set of spaced tones, which may be considered as separate unmodulated carriers, the multipath effects may be calculated by using the vector model in Figure C-2. Here the direct signal is represented by a unit vector, a specular (phase coherent) reflected signal is represented by a vector with an amplitude m_s ($0 \leq m_s \leq 1$) and a time-varying (caused by aircraft motion) phase ϕ_s, and a diffuse (random phase) reflected component is represented by a vector with an rms amplitude m_d ($0 \leq m_d \leq 1$). Both types of reflected signals will usually be present, although one may be sufficiently stronger than the other so that it will essentially determine the amplitude and phase variations of the received signal.

C2 REFLECTED SIGNAL PARAMETERS

The amplitude and phase of the reflected signal are functions of several factors such as signal polarization, reflecting surface characteristics, the antenna pattern, and satellite elevation angle. Since these factors will vary over any given flight path, a statistical description of the reflected signal is required. Bergemann and Kucera [7, 9, 23] have reported signal fading distributions and fading spectra obtained from 135.6 MHz-transmissions from ATS-I and ATS-III to aircraft equipped with a Dorne and Margolin SATCOM antenna.

The amplitude fading distribution obtained by Bergemann and Kucera were found to differ mainly with satellite elevation angle. Although some difference between overland and overwater fading was noted [7], the distribution obtained as a function

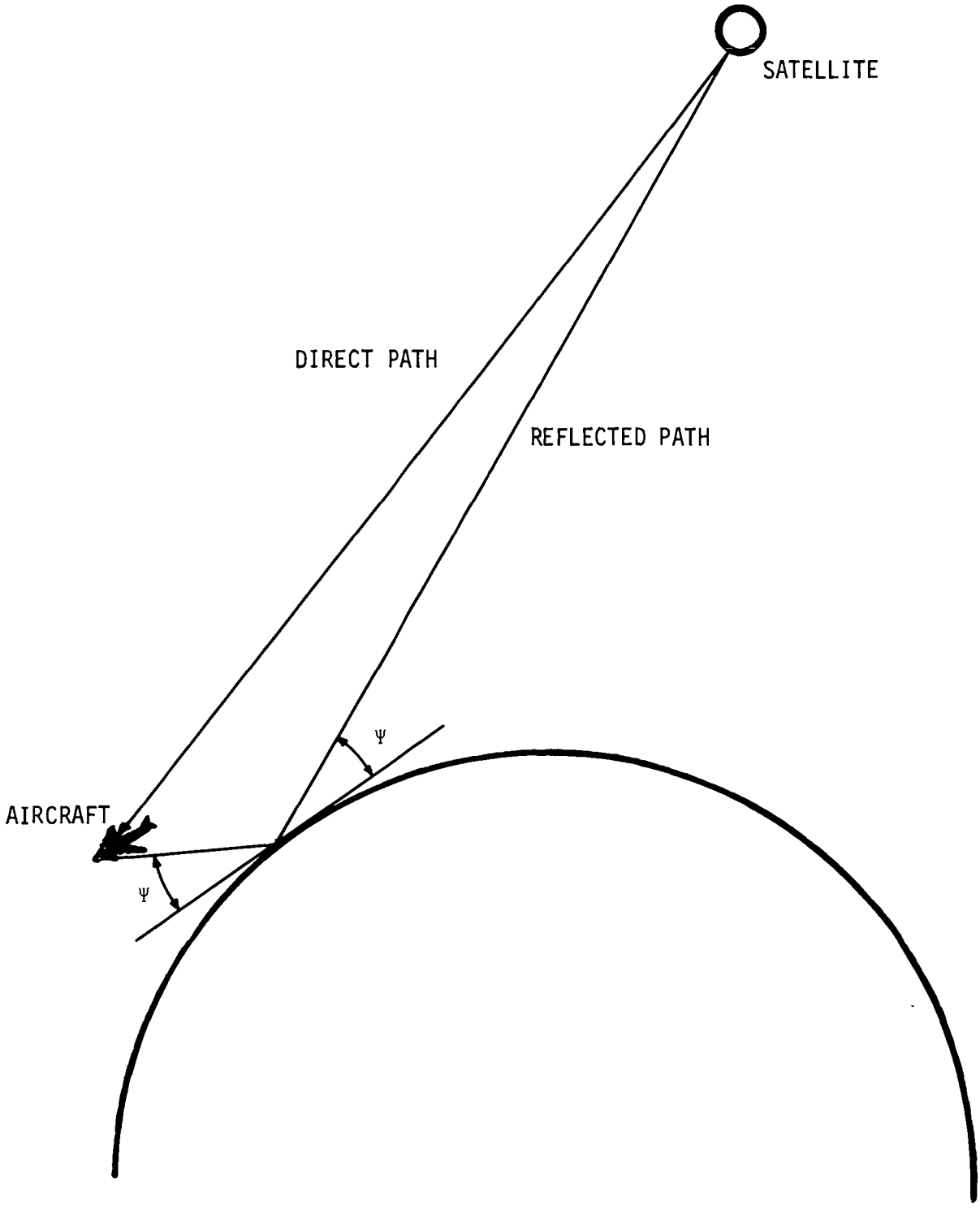

Figure C-1. Multipath On Satellite-To-Aircraft Link

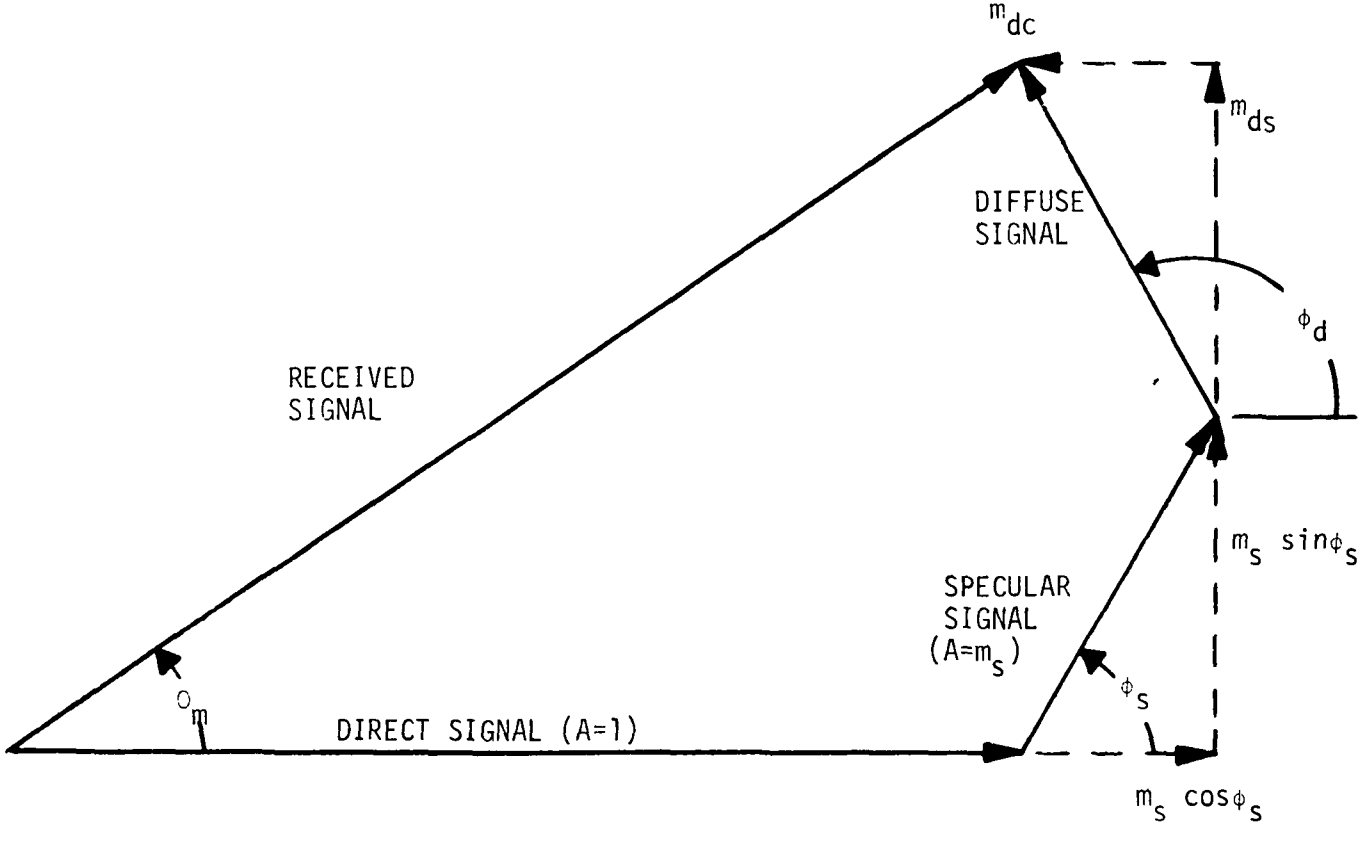

Figure C-2. Vector Multipath Model

of satellite elevation angle generally applied for all types of terrain. Bergemann and Kucera's data, as well as that of other investigators [38, 39] indicate that the fading is primarily due to specular multipath interference for satellite elevation angles less than 30 degrees, while diffuse fading is more common for higher satellite elevation angles.

Kucera [9] and Jordan [39] have found the spectral components of specular fading to be generally less than 0.3 Hz, but their measurements differed on the bandwidth of the diffuse spectrum. Kucera noted that except for cases of very strong multipath interference or satellite spin modulation, the fading spectrum did not extend beyond 2.5 to 3 Hz while Jordon reported spectral components extending somewhat beyond 10 Hz. Kucera's data also showed that the diffuse signal was composed of relatively few components whose spectral envelope has approximately a gaussian shape; however, the sum of four to six randomly phase sine waves will closely approach the Rayleigh distribution [40] that is commonly used to describe the diffuse signal, and a narrow-band filter will give a uniform shape to the diffuse spectrum so that the Nakagami-Rice model [41, 42, 43] can be used to describe the amplitude and phase distributions of the received signal when diffuse multipath interference is present.

Bergemann and Kucera noted no evidence of selective fading on transmissions consisting of 25 tones spaced one kHz apart. The fading period was approximately the same for each tone, but the tone fades did not occur simultaneously in time because of the frequency difference between each tone.

The reflected signal parameters that will be used in subsequent analyses have been derived from Bergemann and Kucero's data [44] and are given in Table C-1, in which $M_d = 20 \log_{10} m_d$.

Table C-1. Reflected Signal Parameters

Satellite Elevation	Type of Fading	Amplitude	Fade Margin			Fading Bandwidth
			rms	P=.9	P=.99	
0°-30°	Specular	$m_s \simeq 0.2$	-2dB	-3dB	-7dB	<0.3 Hz
30°-50°	Diffuse	$M_d \simeq -14$dB	--	-1.6dB	-3.8dB	<5 Hz
50°-70°	Diffuse	$M_d \simeq -17$dB	--	-1.1dB	-2.3dB	<5 Hz

C3 DEMODULATION PROCESS

In the modulation process the ranging tones are translated from baseband to radio frequency with respect to a reference (A/R) tone. The demodulation process shown in Figure C-3 performs the inverse function by filtering the A/R tone from the received tones and using it to coherently translate the ranging tones back to baseband for phase comparison with the transmitted ranging tones.

From Figures C-2 and C-3 the input into the i-th phase comparator is

$$e_i(t) = A_i A_{ar} \sqrt{2P_i} \cos[\omega_i t + \Delta\Phi_i + \Delta\Theta_i] \qquad \text{(C-1)}$$

where

$$A = [(1 + m_s \cos\phi_s + m_{dc})^2 + (m_s \sin\phi_s + m_{ds})^2]^{1/2} \qquad \text{(C-2)}$$

$$\Delta\Phi_i = -2\pi(1/\lambda_i - 1/\lambda_{ar})d = \omega_i \tau_d \qquad \text{(C-3)}$$

$$\Delta\Theta_i = \arctan\left[\frac{m_s \sin\phi_{si} + m_{dsi}}{1 + m_s \cos\phi_{si} m_{dci}}\right] - \arctan\left[\frac{m_s \sin\phi_{sar} + m_{dsar}}{1 + m_s \cos\phi_{sar} + m_{dcsar}}\right] \qquad \text{(C-4)}$$

and P_i is the received power in the direct path signal, τ_d is the direct path time delay, and the in-phase and quadrature diffuse components have gaussian distributions with

$$\overline{m_{dc}} = \overline{m_{ds}} = \text{zero}$$

and

$$\overline{m_{dci}^2} = \overline{m_{dcar}^2} = \overline{m_{dsi}^2} = \overline{m_{dsar}^2} = \overline{m_d^2} \qquad \text{(C-5)}$$

From Equation (C-1) it can be seen that the filtered A/R tone input to the mixer should be limited ($A_{ar} = 1$) so additional multipath amplitude modulation of the ranging tone is not introduced. Considering only the specular multipath terms in Equation (C-4), it is seen that $\Delta\theta_{si}$ is minimized because

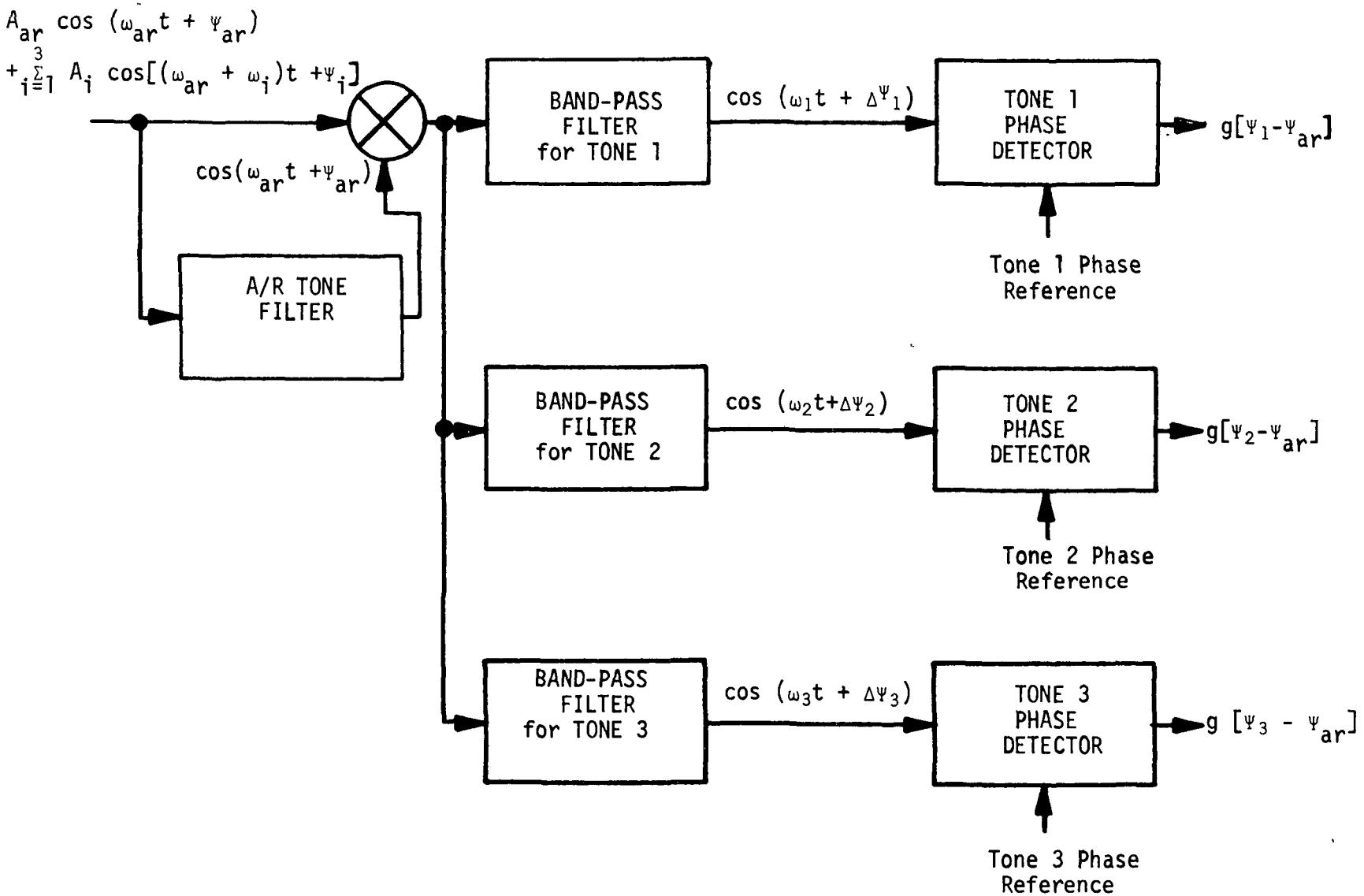

Figure C-3. Ranging Tone Detection Process

$|\theta_{si}| = |\theta_{sar}|$; however, when considering only the diffuse components in Equation (C-4), it is seen that the variance of the phase noise increases rather than decreases. This implies that if a phase-locked-loop (PLL) filter such as that in Figure C-4 is used to filter the A/R tone, the multipath phase error will be minimized if the PLL filter passes the slower specular phase variations and filters the diffuse phase variations.

Two types of phase detectors will be considered. The first is the linear phase detector shown in Figure C-5(a), and the second is the coherent phase detector shown in Figure C-5(b). The output of the linear phase detector will be

$$e_{lin} = \Delta\Phi_i + \Delta\theta_i \tag{C-6}$$

while the output of the coherent detector will be

$$e_c = \sin(\Delta\Phi_i + \Delta\theta_i) \tag{C-7}$$

In each case, the phase detector is preceded by a limiter to eliminate the amplitude fluctuation effects, and the output is filtered to reduce the multipath phase error.

C4 MULTIPATH RANGING ERRORS

The specular multipath phase error, although diminished because of the phase difference, presents the most difficult problem because it fluctuates at a rate (< 0.3 Hz) which is far less than the output filter bandwidth. By utilizing various trigonometric identities, the specular multipath phase error in Equation (C-4) can be expressed by [44]

$$\Delta\Theta_s = \tag{C-8}$$

$$\arctan\left\{\frac{-(m_s/2\ \sin(\pi\Delta\tau/T_i)\quad [\cos(\phi_{sar}-\pi\Delta\tau/T_i)+4m_s\cos(\pi\Delta\tau/T_i)]}{1-m_s^2+(m_s/2)\cos(\pi\Delta\tau/T_i)\,[\cos(\phi_{sar}-\pi\Delta\tau/T_i)+4m_s\cos(\pi\Delta\tau/T_i)]}\right\}$$

where $\Delta\tau$ is the differential delay between the direct and reflected signals and T_i is the period of the i-th ranging tone. Since ϕ_{sar} will vary over a 2π range due to aircraft motion, the magnitude of the maximum value of $\Delta\theta_s$ and the rms value were calculated for a 2π range of values for ϕ_{sar} and

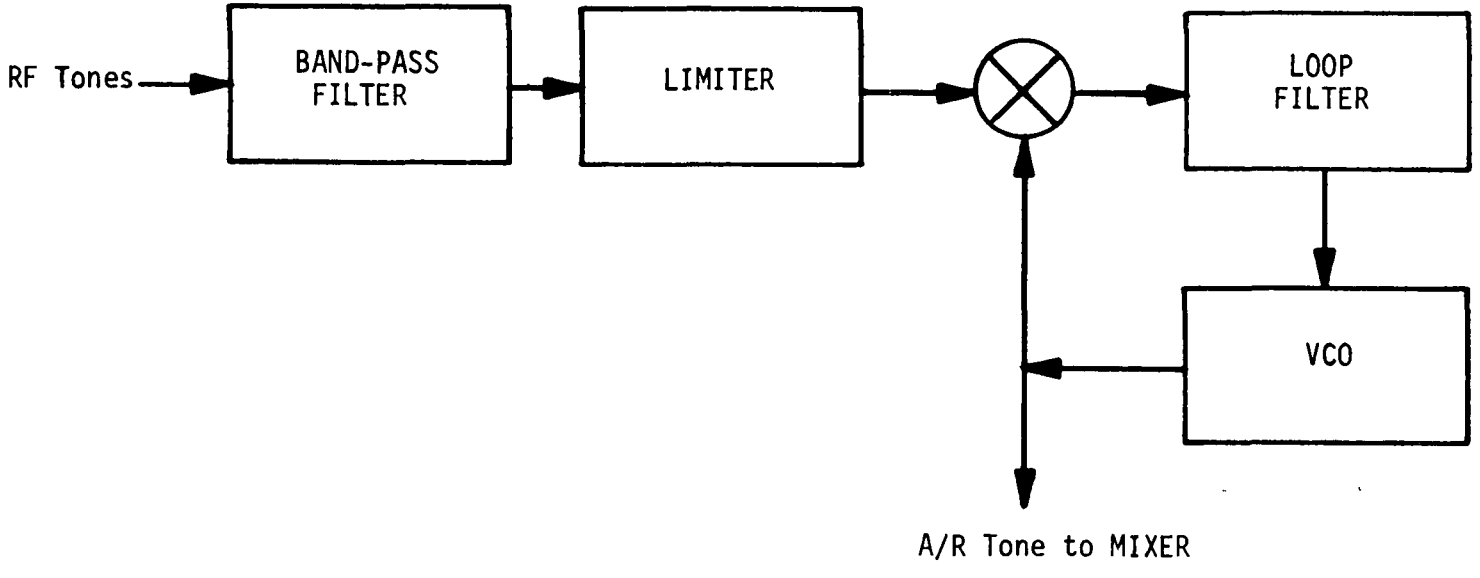

Figure C-4. A/R Tone Filter

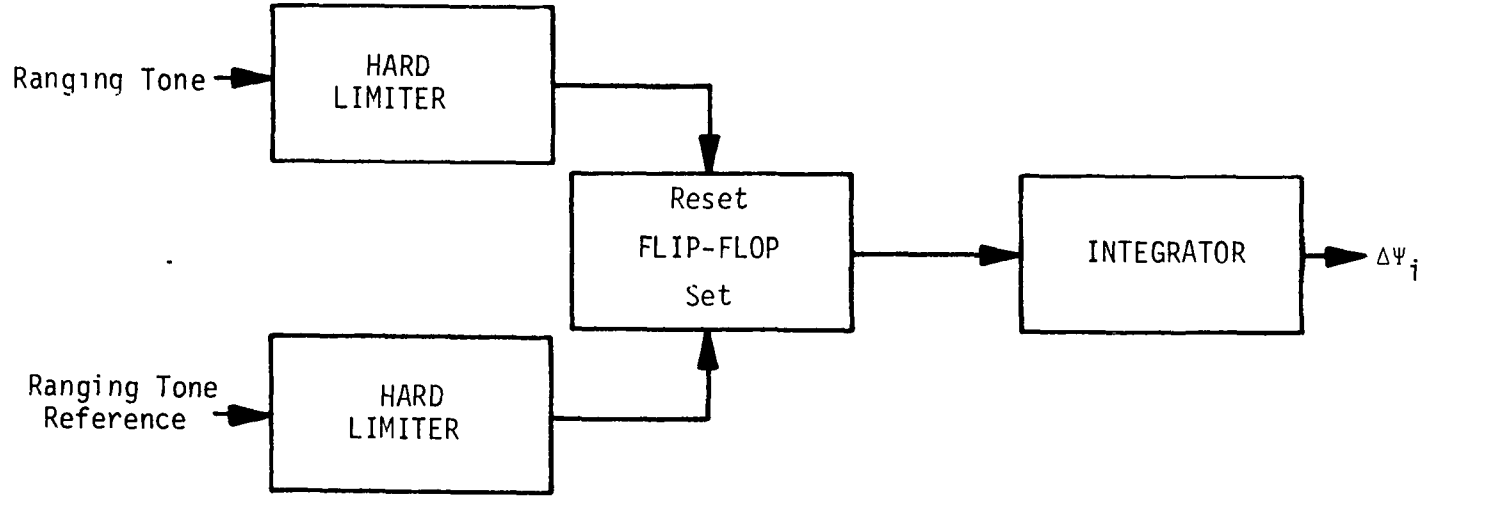

(a) LINEAR PHASE DETECTOR

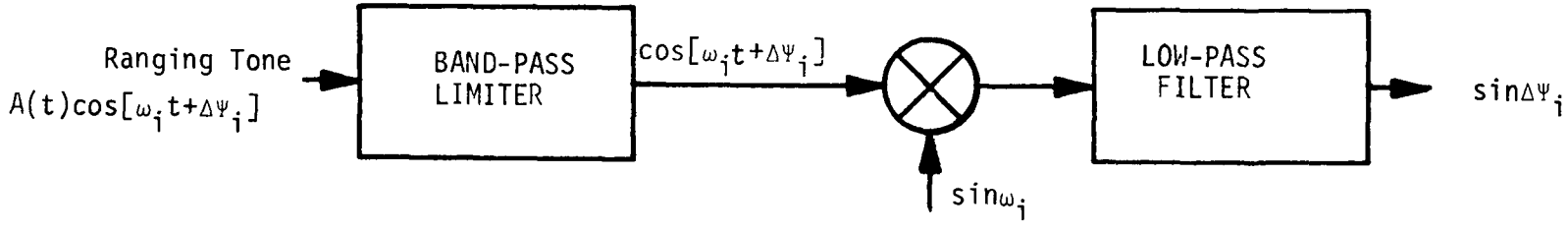

(b) COHERENT PHASE DETECTOR

Figure C-5. Phase Detector Configuration

plotted as functions of $\Delta\tau/T_i$ in Figures C-6 and C-7. The curves are repetitive over unit ranges (e.g., 0 to 1, 1 to 2, 20 to 21) of $\Delta\tau/T_i$.

The reduction in the magnitude of the maximum specular multipath phase error allowed by the differential process can be noted by comparing Figures C-6 and C-8. For M_s = -14 dB (where $M_s = 20_{\log_{10}} m_s$) the maximum error for a single tone is 11.5 degrees while the maximum differential error is 6.8 degrees. The maximum value of the corresponding rms differential error is 5.2 degrees.

For satellite elevation angles between 10 and 30 degrees, the differential multipath time delay will vary from 10 μs to 55 μs. The rms and maximum differential multipath phase errors for 426-Hz, 707-Hz, and 941-Hz ranging tones were obtained from figures C-6 and C-7 for an rms reflected signal amplitude of M_s = -14 dB and a "worst-case" (one percent) value of M_s = -5 dB. The corresponding range errors were determined from Figure C-9, and the results are given in Table C-2 for each ranging tone frequency (f_i). For subsequent calculations, a 1-km rms multipath ranging error will be assumed together with a "worst-case" value of 4 km.

Table C-2. Specular Multipath Ranging Errors

f_i	$\Delta\tau/T_i$	θ_s (rms)	R_s (rms)	$\lvert\theta_s\rvert$ (max)	R_s (max)
			$\Delta\tau$ = 10μs, M_s = -14 dB		
426 Hz	.00426	<0.1°	<190m	0.12°	235m
707 Hz	.00707	0.14°	162m	0.2°	235m
941 Hz	.00941	0.162°	145m	0.27°	240m
			$\Delta\tau$ = 55μs, M_s = -14 dB		
426 Hz	.0234	0.39°	760m	0.65°	1.27km
707 Hz	.0384	0.63°	730m	1.1°	1.28km
941 Hz	.0518	0.82°	720m	1.45°	1.28km

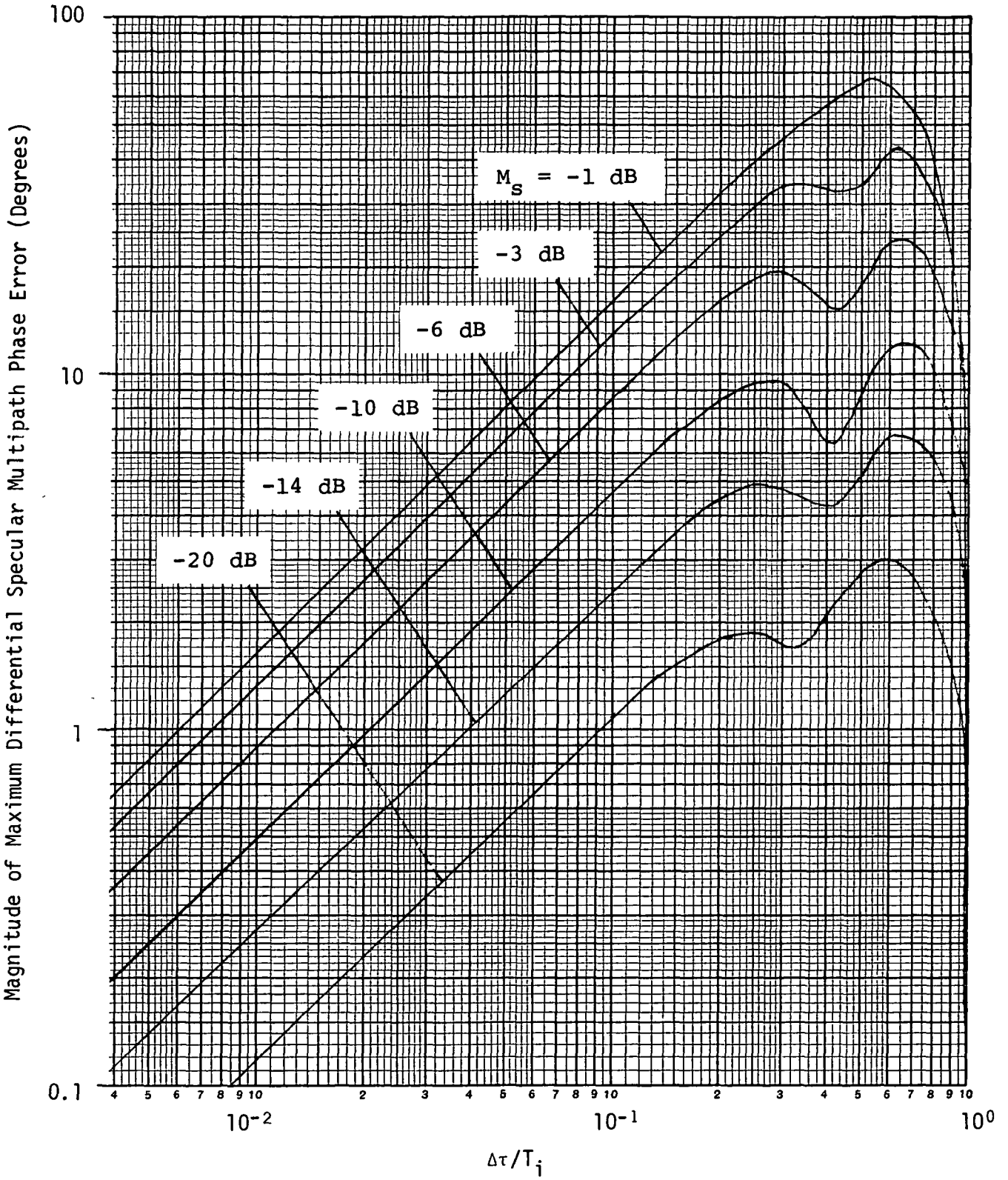

Figure C-6. Magnitude of Maximum Differential Specular Multipath Phase Error

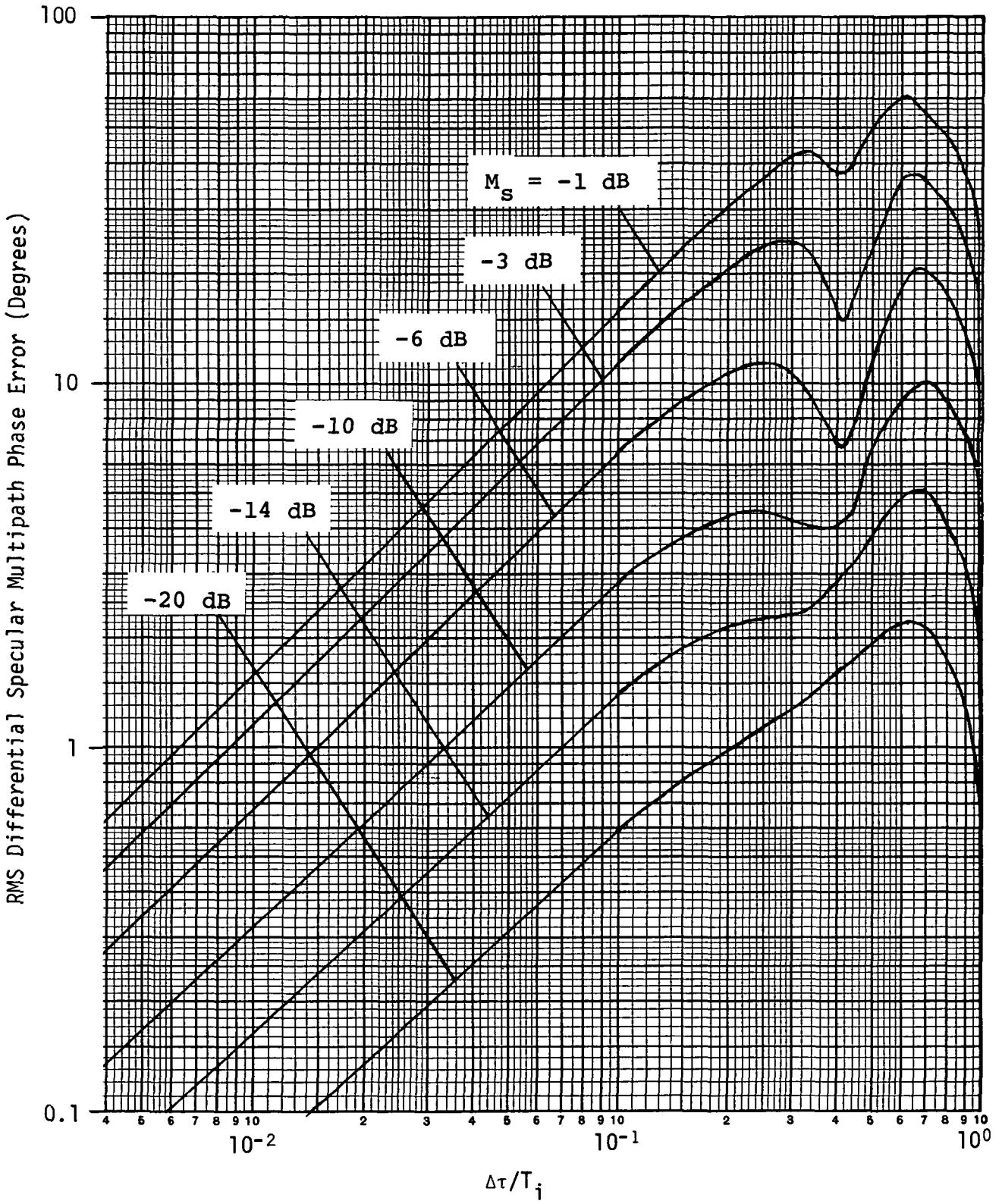

Figure C-7. RMS Differential Specular Multipath Phase Error

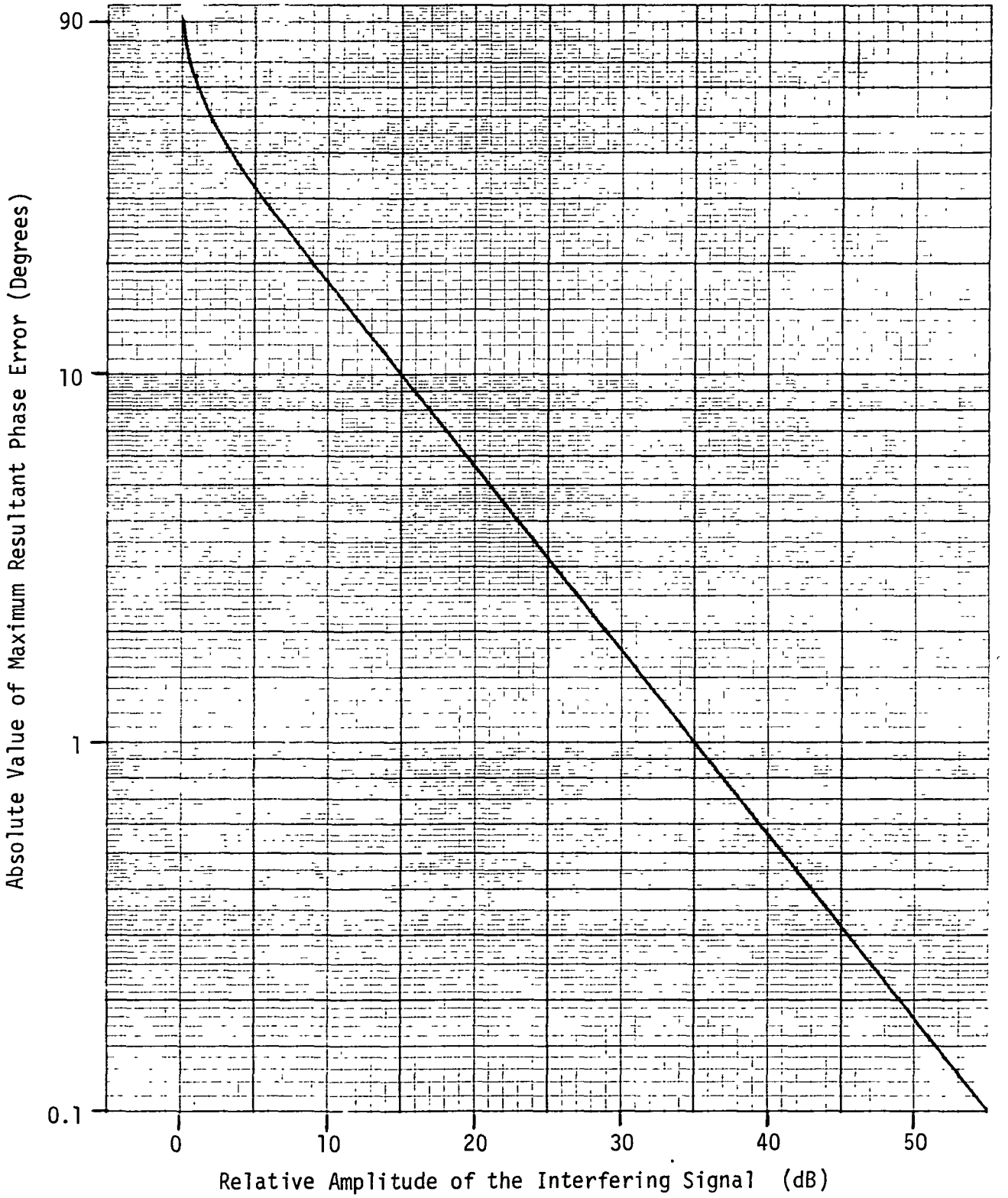

Figure C-8. Maximum Phase Error Due to an Interfering Signal

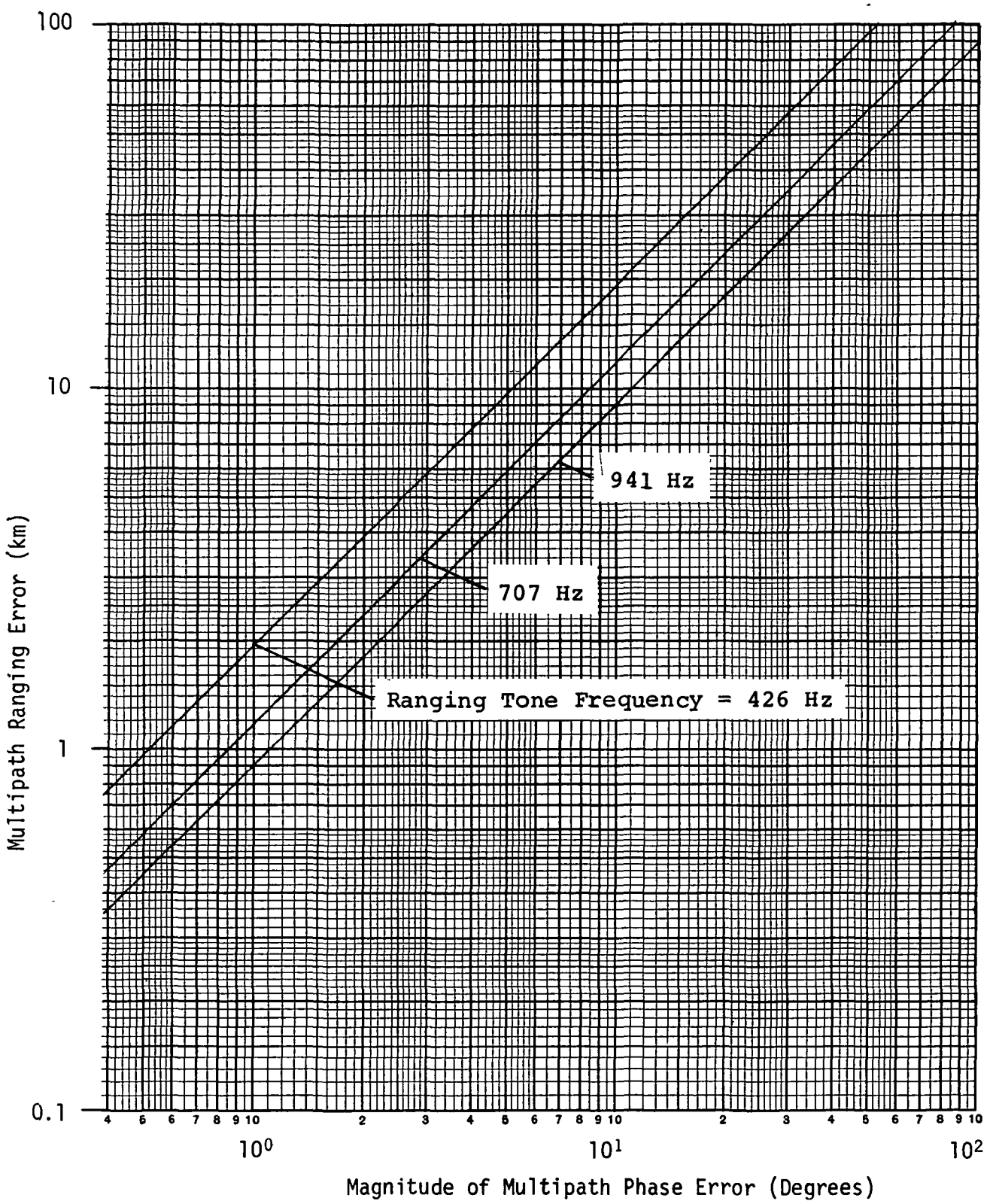

Figure C-9. Multipath Ranging Error

Table C-2. Specular Multipath Ranging Errors (Cont.)

f_i	$\Delta\tau/T_i$	θ_s (rms)	R_s (rms)	$\lvert\theta_s\rvert$ (max)	R_s (max)
		$\Delta\tau$ = 10μs, M_s = -5 dB			
426 Hz	.00426	0.35°	680m	0.43°	830m
707 Hz	.00707	0.58°	680m	0.7°	810m
941 Hz	.00941	0.78°	690m	0.95°	840m
		$\Delta\tau$ = 55μs, M_s = -5 dB			
426 Hz	.0234	1.95°	3.8km	2.4°	4.7km
707 Hz	.0389	3.1°	3.6km	3.9°	4.6km
941 Hz	.0518	4.2°	3.7km	5.2°	4.6km

For satellite elevation angles of 30 to 50 degrees and 50 to 70 degrees the reflected signal was assumed to be diffuse with relative rms amplitudes of -14 dB and -17 dB, respectively. The output signal-to-noise ratio (SNR) is given by

$$\Gamma = -M_d - 3\ \text{dB} + I_{dB} \qquad \text{(C-9)}$$

where the 3 dB factor accounts for the A/R tone diffuse noise and I_{dB} is an improvement factor due to filtering. If the A/R tone filter bandwidth is one Hz and the phase detector bandwidth is also one Hz, then the SNR will improve somewhat due to reduction in the diffuse noise at the filter outputs. If a gaussian shape is assumed for the diffuse noise spectrum, then I_{dB} = 4.4 dB if the diffuse bandwidth (94 percent of the power) is 3 Hz, and I_{dB} = 8.2 dB if the diffuse bandwidth (B_n) is 5 Hz [44]. When the SNR is determined from Equation (C-9), the rms diffuse phase error (θ_d) may be obtained from Figure C-10, and the ranging error (R_d) can be determined from Figure C-9, The results are tabulated in Table C-3 for each ranging tone frequency (f_i).

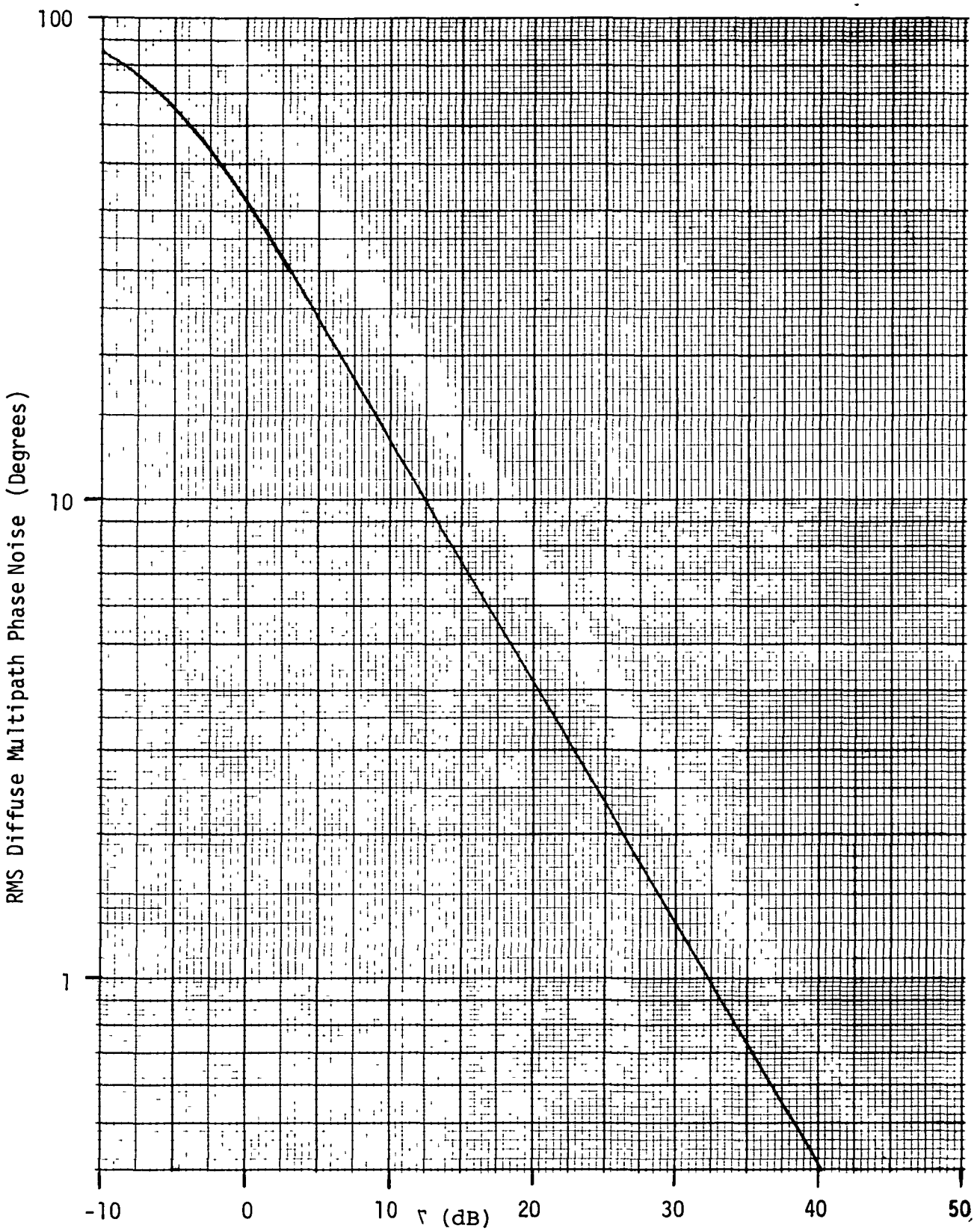

Figure C-10. RMS Phase Error For Nakagami-Rice Distribution

Table C-3. Diffuse Multipath Ranging Errors

	B_n = 3 H_z		B_n = 5 H_z	
f_i	Θ_d	R_d	Θ_d	R_d
		M_d = -14 dB		
426 Hz	7°	13.6km	4.4°	8.7km
707 Hz	7°	8.1km	4.4°	5.1km
941 Hz	7°	6.2km	4.4°	3.9km
		M_d = -17 dB		
426 Hz	4.9°	9.5km	3.3°	6.5km
707 Hz	4.9°	5.7km	3.3°	3.9km
941 Hz	4.9°	5.3km	3.3°	2.95km

From Table C-3 it is seen that the diffuse multipath ranging error will be less than the specular ranging error. The major factor that accounts for this somewhat unusual situation is the relatively narrow diffuse noise bandwidth indicated by the Collins spectral data [7, 8, 9]. Further multipath spectral measurements to verify this are needed.

Since the magnitude of the reflected signal depends directly upon that of the transmitted signal, any reduction of the magnitude of the reflected signal cannot occur through variation of the transmitter power, but rather through more attenuation of the reflected signal by the aircraft antenna.